2009

Desert varnish as an indicator of modern-day air pollution in southern Nevada

Piotr Nowinski
University of Nevada Las Vegas

DESERT VARNISH AS AN INDICATOR OF MODERN-DAY AIR POLLUTION IN SOUTHERN NEVADA

by

Piotr Nowinski

Bachelor of Science, Chemistry
University of Nevada, Las Vegas
1988

Master of Science, Chemistry
University of Nevada, Las Vegas
1993

A dissertation submitted in partial fulfillment
of the requirements for the

Doctor of Philosophy in Environmental Science
Department of Environmental Studies
Greenspun College of Urban Affairs

Graduate College
University of Nevada, Las Vegas
December 2009

UNIVERSITY OF NEVADA LAS VEGAS

THE GRADUATE COLLEGE

We recommend that the dissertation prepared under our supervision by

Piotr Nowinski

entitled

Desert Varnish as an Indicator of Modern-Day Air Pollution in Southern Nevada

be accepted in partial fulfillment of the requirements for the degree of

Doctor of Philosophy
Environmental Studies

Vernon F. Hodge, Committee Chair

Krystyna A. Stave, Committee Member

Shawn Gerstenberger, Committee Member

Moses Karakouzian, Graduate Faculty Representative

Ronald Smith, Ph. D., Vice President for Research and Graduate Studies
and Dean of the Graduate College

December 2009

ABSTRACT

Desert Varnish as an Indicator of Modern-Day Air Pollution in Southern Nevada

by

Piotr Nowinski

Dr. Vernon Hodge, Examination Committee Chair
Professor of Chemistry
University of Nevada, Las Vegas

Rock varnish, often called desert varnish, is a slow-growing, manganese-rich coating that accumulates on exposed rock surfaces. The mechanism of varnish formation is not fully understood, however, most authors agree that varnishes derive their components from the atmosphere. The main goal of this study was to demonstrate the potential use of desert varnish as a passive environmental monitor of present and past atmospheric pollution. Analysis of varnishes is a new field that can potentially provide records of pre-anthropogenic levels of atmospheric metals and other environmental pollutants. To evaluate the potential of desert varnish as an environmental monitoring tool, the following hypotheses were tested: (1) rock varnish accumulates and preserves a record of airborne heavy elements and can be used as a passive environmental monitor of relatively recent events; (2) anthropogenic pollutants are deposited in the varnish's outermost layers and can be traced to their sources, such as ore smelters or coal–fired power plants; and (3) heavy metals and radionuclides can be quantified in the varnish coatings using field portable X-ray fluorescence spectroscopy (FPXRF), inductively coupled plasma mass spectroscopy (ICPMS), laser ablation-inductively coupled plasma

mass spectroscopy (LA-ICPMS), and cold vapor atomic absorption spectrometry (CVAA).

Desert varnish samples were collected in the areas surrounding four point sources of air pollution: the Nevada Test Site (NTS), Nye County, NV; the Mohave Power Project (MPP), Laughlin, NV; the Reid Gardner Power Plant (RGPP), Moapa, NV; and the Titanium Metal Corporation (TIMET), Henderson, NV. The chemical composition of rock varnishes was examined with FPXRF, LA-ICPMS, ICPMS, and CVAA.

Both FPXRF and LA-ICPMS results show that many trace elements in the analyzed varnishes appear to be enriched relative to the upper continental crust (UCC). Notably, elements that show the highest levels of enrichment relative to the UCC are commonly found in atmospheric emissions from coal-fired power plants. Abundances of these elements plotted against the distance from the power plant show general patterns consistent with the predictions of the Gaussian Plume model for transport and diffusion of the pollutants. The model predicts that lower concentrations of pollutants will be observed at the point of origin followed by a maximum peak concentration and gradual decrease with distance from the source.

To confirm correlation of contamination to distance from the power plant, total concentrations of the elements in desert varnish films were determined. Varnishes collected in the downwind locations from MPP and RGPP were stripped from the base rock with concentrated HCl. The resulting solutions were analyzed by quantitative ICPMS for 27 isotopes (^{9}Be, ^{51}V, ^{52}Cr, ^{59}Co, ^{60}Ni, ^{63}Cu, ^{66}Zn, ^{75}As, ^{88}Sr, ^{98}Mo, ^{102}Ru, ^{103}Rh, ^{106}Pd, ^{111}Cd, ^{118}Sn, ^{121}Sb, ^{133}Cs, ^{184}W, ^{187}Re, ^{195}Pt, ^{205}Tl, ^{206}Pb, ^{207}Pb, ^{208}Pb, ^{209}Bi, ^{232}Th, and ^{238}U). Additionally, mercury was analyzed by CVAA. The average elemental

concentrations in the varnish samples were plotted as a function of the distance from each power plant. The ICPMS data confirm that many trace elements have a deposition patterns consistent with the Gaussian Plume model.

The results of this study provided basic knowledge of the chemical and radiochemical composition of varnish coatings and, thus, additional evidence to help understand the mechanism of varnish formation. In conclusion, the results of this study will have implications 1) for the mapping of the distribution of some of the components of air contamination, 2) for identifying the sources of air pollution, 3) for deciphering the history of atmospheric pollution, 4) for contributing to our understanding of desert varnish formation, and 5) for use as a prospecting tool.

TABLE OF CONTENTS

LIST OF TABLES

LIST OF FIGURES

ACKNOWLEDGMENTS

I would like to extend gratitude to my long time teacher and mentor Dr. Vernon F. Hodge for making my experience at the University of Nevada, Las Vegas both challenging and exciting. I would also like to thank the University of Nevada, Las Vegas Department of Public Health, Harry Reid Center for Environmental Studies, and Clark County Department of Air Quality and Environmental Management.

I wish to thank my committee members for their support, guidance, and advice. These great individuals include my committee chair Dr. Vernon F. Hodge, committee members Dr. Krystyna A. Stave, Dr. Shawn Gerstenberger, and Dr. Moses Karakouzian. I would also like to thank Dr. James Cizdziel who was a great guidance during the first few years of this project and while he served on my committee.

I also want to recognize and appreciate those who helped me to complete this dissertation. I would like to acknowledge Mr. Kazumasa Lindley for his aid with ICPMS and LA-ICPMS analyses, Ms. Ashley Phipps for her help with the XRF analyses, Ms. Joanna Kramer and Ms. Sarah Mueting for their help with the CVAA mercury analyses. I am especially thankful to Ms. Sandra Elkouz for her assistance with editing the manuscript and insightful comments. My superiors and co-workers at the Department of Air Quality extended sincere support and encouragement throughout the duration of this project, which are greatly appreciated.

Finally, I would like to thank those who are the closest to my heart and make living worthwhile. First, I need to thank my loving and supporting wife, Renata for all her love, help, patience and understanding. My children, Kasia, Magda, Magdalena, and Karol who have been a great inspiration and motivation, deserve special appreciation. My

parents, Wlodziemierz and Cecylia earn particular thanks for always believing in me and instilling in me love of science and curiosity of the world.

CHAPTER 1

INTRODUCTION AND PROBLEM STATEMENT

Rock surfaces are often covered with a dark coating called rock varnish or desert varnish. Many ancient peoples produced petroglyphs or primitive writings by scratching through this coating to expose the much lighter rock substrate. These thin films are thought to be slow-growing (~ 1μm/1000 yr) and consist of layers of clay minerals cemented together to the parent rock by Fe-Mn oxyhydroxides (Krinsley, 1998). Analytical results reveal that desert varnish consists of ~ 70% clay and 30% manganese and iron oxides (Liu and Broecker, 2000). Most evidence suggests that the ingredients of desert varnish are derived from the atmosphere (Potter and Rossman, 1977; Perry and Adams, 1978; Fleisher et al., 1999; Broecker and Liu, 2001; Moore et al., 2001; Bao et al., 2001; Hodge et al., 2005). There is strong indication that these coatings can effectively capture and retain relatively recent air pollutants, including heavy metals and radionuclides (Thiagarajan and Lee, 2004; Hodge et al., 2005; Wayne et al., 2006).

Statement of Problem

Industrial production and other anthropogenic activities require large quantities of various chemicals. Many of these substances have been released during industrial processes or have been disposed of as a waste that accumulates and pollutes the natural environment. Knowledge of the sources, transport, and fate of contaminants in the environment allows for the evaluation of anthropogenic impacts on the geochemical cycles found in nature (Jaffe, 1991). Extensive monitoring programs are required to establish the quality of different environmental compartments such as air, water, soil and

biota. However, continuous environmental monitoring over a period of many years is expensive and, in many locations, may be impractical. Additionally, putting together a history of past pollution is technically difficult and often fraught with uncertainties.

To address this problem, environmental archives such as lichens, mosses, sediment cores, and ice cores have been used as natural collectors of heavy metals and radioactivity in order to document the history, distribution, and major sources of air contamination (Bruggeman, 1982; Settle and Patterson, 1982; Boutron and Patterson, 1983; Hamelin et al., 1990; Boutron et al., 1994; Zachmann and Block, 1994; Candelone et al., 1995; Alcock and Jones, 1996; Moor et al., 1996; Christensen et al., 1997; Monna et al., 1997; Shotyk et al., 1998; Weiss et al., 1999; Shintu and Dagetto, 1999; Bargagli et al., 2002; Carignan et al., 2002; Turner et al., 2003; Arnuad et al., 2004; Augusto et al., 2004; Shotyk et al., 2004; Sun et al., 2006; Yin et al., 2006; Zheng et al., 2006; Kovalchuk and Kovalchuk, 2008). Use of lichens and mosses as natural air pollution monitors is limited in arid and semi-arid environments. An attractive alternative to these may be the naturally occurring patina – rock varnish.

Rock varnish accumulates on exposed rock surfaces in all terrestrial environments, including tropical and polar regions, but is most common in deserts (Krinsley, 1998). A small number of reports in the literature indicate that rock varnish can capture and preserve heavy metals and radionuclides from the atmosphere (Fleisher et al., 1999; Liu and Broecker, 2000; Diaz, 2003; Hodge et al., 2005). Wayne et al. (2006) suggest that elevated trace metal concentrations on the varnish surfaces may be directly attributed to metal-containing, atmospherically-deposited particulates and that these particulates probably originated at coal-fired power plants. The authors conclude that trace metals

can be retained in the rock varnish, and thus, provide a record of ambient airborne pollution. In another study, an exponential increase in Pb was observed in the outermost microlaminae of varnish coatings collected in eastern California (Broecker and Liu, 2001). This excess Pb was attributed to automobile exhaust.

Analysis of radionuclides in desert varnish revealed the presence of ^{137}Cs and ^{210}Pb (Fleisher et al., 1999). Cesium-137 was foreign to the environment prior to 1945, and was introduced to the atmosphere as a component of the fallout following atmospheric testing of nuclear weapons. Pb-210, a naturally occurring radionuclide, is present in the atmosphere from the decay of ^{222}Rn gas. Alpha particle counts of rock varnishes collected in the Great Basin showed activity from ^{210}Po, a decay product of ^{210}Pb (Hodge et al., 2005). The observed sharp peak suggested that most of the alpha ^{210}Po and its parent, if present, were adsorbed on the rock surfaces. Since these radionuclides were present in varnish coatings and were not present in the rock substrate, they were apparently adsorbed from the atmosphere. Providing that minerals in desert varnish adsorb and hold airborne radionuclides, such as ^{137}Cs, ^{210}Po, ^{210}Pb and $^{239,240}Pu$, analysis of varnish samples could be used to map radiological contamination (Wayne et al., 2006).

Tebo et al. (2004) and Thiagarajan and Lee (2004) noticed that the relative abundances of the elements in varnish coatings appear to reflect their solubilities in water or their tendency for being scavenged by Fe-Mn oxyhydroxides. Thiagarajan and Lee (2004) report the extreme relative depletions of rubidium and cesium in varnishes relative to the upper continental crust (UCC) in the samples collected in the Mojave Desert and Death Valley, California. They proposed that Rb and Cs are probably leached from the airborne dust particles before the particles are incorporated into the varnish films. The

authors also observed relative enrichments in rare-earth elements (REE), Co, Ni, and Pb in varnishes and suggested that these enrichments are consistent with the susceptibility of these elements for adsorption by Fe-Mn oxyhydroxides. Thiagarajan and Lee (2004) introduced a wet-atmospheric deposition model for varnish formation. The model states that varnishes form by direct chemical precipitation of atmospheric components dissolved in rainwater, fog, or aerosols. The authors suggest that concentrating and diluting elements during incorporation into varnish films could provide specific information about atmospheric levels of metals.

During coal combustion, many heavy metals such as Zn, As, Cd, Tl, Pb and others are introduced to the atmosphere with the fly ash and flue gases (Nodelman et al., 2000; Yan et al., 2001; Danihelka et al., 2003). Therefore, elevated levels of heavy metals in the varnish samples collected in the deposition areas from the coal-fired power plants could indicate possible contamination. Mines and metal ore smelters that operated in Nevada dispersed large amounts of heavy metals into the environment (Diaz, 2004). Consequently, elevated concentrations of V, Zn, Mo, and W in the varnish coatings could point to contamination from these sources (Wayne et al., 2006).

The presented results point to the potential value of rock varnish as a record keeper of atmospheric pollution. If trace metals and radioactive isotopes can be incorporated into varnish films, then these thin coatings could preserve a record of air pollution.

Purpose of the Research

The research reported in this dissertation tested the following hypotheses: (1) rock varnish accumulates and preserves a record of airborne heavy elements and can be used

as a passive environmental monitor of relatively recent events; (2) anthropogenic pollutants are deposited in the varnish's outermost layers and can be traced to their sources, such as ore smelters or coal–fired power plants; and (3) heavy metals can be quantified in the varnish coatings using energy dispersive X-ray fluorescence spectroscopy (EDXRF), inductively coupled plasma mass spectroscopy (ICPMS), and laser ablation-inductively coupled plasma mass spectroscopy (LA-ICPMS). Additionally, Hg was analyzed by cold vapor atomic absorption (CVAA).

Research Approach

My research strategy involved examination of the chemical composition of collected varnish samples. Concentrations of anthropogenic contaminants retained in the varnish coatings were determined at locations downwind from the selected point sources of air pollution. The elements of interest were measured by field portable EDXRF, LA-ICPMS, ICPMS and CVAA. Chapter 4 contains a description and discussion of the experimental methods used in this study.

To test hypothesis (1), that rock varnish accumulates and preserves a record of airborne heavy elements and can be used as a passive environmental monitor, I used field portable EDXRF and LA-ICPMS to analyze a set of rock varnish samples collected in Arizona, California, and Nevada. First, the collected samples were analyzed with field portable EDXRF to determine total concentration of 16 elements (Ti, Cr, Mn, Fe, Co, Ni, Cu, Zn, As, Se, Rb, Sr, Zr, Mo, Hg, and Pb). Both varnish-coated and unvarnished rock surfaces on the same sample were analyzed and the results were compared. The hypothesis would be supported upon finding elevated concentrations of the pollutants on

the varnished rock surfaces in comparison to the unvarnished surfaces exposed when chipping off the sample pieces of stable rocks or boulders. .

Secondly, magnetic sector ICPMS coupled with a laser ablation system was applied to measure concentrations of 11 low resolution elements (Be, Ag, Cd, Sn, Sb, Ba, W, Tl, Pb, Th and U) in two varnish samples collected in southern Nevada. To confirm that varnishes accumulate airborne heavy elements, the varnish-coated and exposed unvarnished rock plus the skyward-facing and ground-facing varnished surfaces were analyzed on the same sample. After the concentration of each element was determined, the results from the varnish-coated and unvarnished surfaces were compared, as well as from the skyward-facing and ground-facing surfaces. Elevated concentrations of the pollutants on the varnished and skyward-facing rock surfaces in comparison to the unvarnished surfaces would support hypothesis (1).

Hypothesis (2), that anthropogenic pollutants are deposited in the varnish's layers and can be traced to their sources, was tested by analyzing samples collected in the deposition areas of the selected point sources of air pollution. The selected point sources included four sites in southern Nevada: the Nevada Test Site (NTS), Nye County; the Mohave Power Project (MPP), Laughlin; the Reid Gardner Power Plant (RGPP), Moapa; and the Titanium Metal Corporation (TIMET), Henderson. These sources have a known history of emissions of air pollutants and documented deposition patterns of contamination. The contamination from the air pollution sources was identified by comparing concentrations of the specific elements in the samples collected in the source deposition area with the background samples, as well as with values reported in the upper continental crust (UCC). It was found that the samples collected in the deposition areas have higher

concentrations of the contaminants. In Chapter 5, the analytical results are discussed in detail.

After the initial analytical work, I selected sites around coal-fired power plants (MPP and RGPP) that showed the highest levels of contamination and re-sampled wider geographical areas around these sources. The contaminants are emitted during coal combustion as submicron-sized aerosol particles or as larger particles in the bottom ash (Nodelman et al., 2000; Yan et al., 2001; Danihelka et al., 2003). The most volatile trace elements (As, Se, and Hg) are emitted mostly with the flue gas (Seames and Wendt, 2000; Zeng et al., 2001; Yan et al., 2000; Lockwood and Yousef, 2000). Danihelka et al. (2003) noted that the most common trace metals in the particulate emissions from the stack include Cu, Zn, Cd, Sn, Sb, and Pb. Total concentrations of the elements in desert varnish were determined by acid leaching of varnish-covered rocks and analysis of the leached solutions by ICPMS. The following isotopes were analyzed: ^{9}Be, ^{47}Ti, ^{51}V, ^{52}Cr, ^{55}Mn, ^{56}Fe, ^{58}Ni, ^{59}Co, ^{65}Cu, ^{66}Zn, ^{75}As, ^{88}Sr, ^{98}Mo, ^{103}Rh, ^{106}Pd, ^{107}Ag, ^{114}Cd, ^{115}In, ^{120}Sn, ^{121}Sb, ^{133}Cs, ^{138}Ba, ^{184}W, ^{187}Re, ^{195}Pt, ^{197}Au, ^{205}Tl, ^{206,207,208}Pb, ^{209}Bi, ^{232}Th, and ^{238}U. Additionally, all the solutions were analyzed for Hg by cold vapor atomic absorption (CVAA). Chapter 5 gives a comprehensive description of the analytical results.

There are reports in the literature that support hypothesis (3), that heavy metals and radionuclides can be quantified in the varnish coatings using LA-ICPMS, and ICPMS (Thiagarajan and Lee, 2004; Hodge et al. 2005; Wayne et al., 2006). On the other hand, field portable EDXRF and Hg analysis by CVAA are not commonly used for analysis of rock varnish samples. Nevertheless, it seems that the XRF technique has a great potential for the rapid “screening” of areas of potential atmospheric contamination. Additionally,

applied analytical methods were fine-tuned during the course of this research to optimize the analysis of varnish samples. In Chapter 6, the analytical results are summarized and assessed, conclusions are drawn, and recommendations for future research are made.

CHAPTER 2

ENVIRONMENTAL ARCHIVES

Passive Sampling

Monitoring of environmental pollutants often involves collection of a large number of samples from a given location over a specified time period of active sampling. This approach is time-consuming and very costly. A solution to these problems is the method of passive sampling. Passive sampling can provide a representative picture of pollution levels over a period of time by measuring the average concentrations to which the samplers have been exposed. The concentration of the analyte is integrated over the entire exposure time, averaging the extreme variations of the pollutant concentrations. The collected data allow for a long-term overview of pollutant levels in the environment (Namiesnik et al., 2005; Namiesnik and Gorecki, 2000).

In contrast to dynamic techniques, active sampling devices such as pumps are not required in passive sampling. Passive sampling is based on the free flow of pollutant from the sampled medium to a collection medium. The samplers used for passive sampling usually rely on diffusion through a well-defined diffusion barrier or permeation through a membrane (Zabiegala et al., 2002; Zabiegala et al., 2003). The equipment used must be simple and reliable, since sampling sites often lie in remote locations. Additionally, only a few devices are necessary at a sampling site during sample collection. This is a great advantage over grab sampling, where the sample represents conditions at the site at a given moment in time, and a large number of samples need to be collected to obtain time-averaged data. Passive sampling seems to eliminate most of the disadvantages of active extraction and sample preparation techniques (Namiesnik et

al., 2005; Seethapathy et al., 2007). Additionally, passive sampling greatly simplifies the sampling and sample preparation process by eliminating power requirements, significantly reducing analysis cost (only a few analyses are required over the monitoring period), and minimizing decomposition/degradation of the sample during transport and storage. For example, a network of polyurethane foam (PUF) disks was successfully used to monitor the distribution of persistent organic pollutants (POPs) in the ambient air throughout Europe. A total of 71 samplers were placed for six weeks in 22 countries. After sampling was completed, the samplers were returned to the laboratory for extraction and analysis. The concentrations of POPs obtained during the study were comparable to previously reported results obtained with active sampling (Jaward et al., 2004; Beyer et al., 2000; Halsall et al., 1995; Stanley and Hites, 1991).

Passive sampling has a few disadvantages, such as a relatively low sampling rate that requires long sampling times at low concentrations. However, this can also be seen as an advantage of the technique, since it provides time-averaged concentrations of the pollutant. Factors affecting the analytical results obtained by passive sampling include environmental conditions such as temperature, humidity, and wind velocity. One major downside of passive samplers is their inability to monitor historical pollution patterns and paleo climatic cycles. Knowledge of historical climate changes is a prerequisite to the interpretation and projection of future climatic events (Shotyk et al., 2004). Fortunately, past pollution and paleo climatic data can be derived from natural environmental monitors or environmental archives such as ice cores, sediments, soils, and plants.

Environmental Archives

In their editorial, Shotyk et al. (2004) state that: "…'past is the key to the present'…it is sometimes helpful to have a window on the past to understand how things worked prior to significant intervention by Man. This is precisely where 'archives' can be useful: they provide us with quantitative insight into physical and chemical processes as they operated naturally, in historic or pre-historic times."

An environmental archive is defined as a geological, biological, or chemical medium that grows or accumulates over time, possibly preserving a record of some environmental condition, pollutant, or environmental change (Shotyk et al., 2004). Lake and marine sediments are examples of geological archives because they accumulate sedimentary material through erosion and aquatic transport (Kober et al., 1999; Monna et al., 1999; Renberg et al., 1994; Arnaud et al., 2004). Lichens, mosses, animal organs, hair, tree rings, and peat bogs are types of biological archives, or biomonitors (Frazen et al., 2004; Arnaud et al., 2004; Augusto et al., 2004; Sun and Xie, 2001; Sun et al., 2004; Sun et al., 2006). Examples of chemical archives include alpine and polar ice, marine corals, stalagmites, and stalactites (Vandal et al., 1993; Candelone et al., 1995; Planchon et al., 2002; Zheng et al., 2006). All of these have preserved some important environmental record, and each has its own inherent advantages and disadvantages. Some reports in the literature propose another environmental monitor: the naturally-occurring patina – or rock varnish (Thiagarajan and Lee, 2004; Wayne et al., 2006; Perry et al., 2006). In the following paragraphs, the properties and utilities of common environmental monitors such as ice cores, sediments, soils, peat bogs, biomonitors, lichens and desert varnish will be described and evaluated.

Ice Cores

Glaciers and snow pack are unique environmental monitors because they are directly linked to the atmosphere. The ice cores have provided valuable records of the concentrations and isotopic composition of elements in gases, soil dust, volcanic ash particles, marine aerosols, and trace metals extending back as far as 420,000 years (Koide et al., 1982; Koide and Goldberg, 1983; Petit et al., 1999; Vandal et al., 1993; Hong et al., 1994; Wolff and Suttie, 1994; Wolff et al., 1999; Candelone et al., 1995; Planchon et al., 2002; Zheng et al., 2006). Ice cores have also provided direct evidence of links between greenhouse gas concentrations and climate, providing many new insights into the Earth's climate (Shotyk et al., 2004; Spahni et al., 2005; Wolff et al., 2007; Brook, 2008).

Ice cores have been widely used to document past trends in the atmospheric deposition of trace elements. Information obtained from the analysis of ice cores aids in the identification of pollution sources, and contributes to the understanding of environmental biogeochemical cycles. The study of trace elements in dust is exceptionally useful in understanding past circulation systems and the contributions of pollutants from various sources. Additionally, analyses of ice cores established the natural background levels of pollutants and helped with the determination of the spread of pollutants around the world (Mayewski et al., 1990; Hinkley and Matsumoto, 2001; Wolff et al., 1999; Delmas and Petit, 1994; Bourton et al., 1991; Barbante et al., 2004). The ice core records have supplied valuable information about pollution on both the regional and global scales. Investigations of Antarctic ice cores provided evidence that volcanic gases are the major source of trace metals, while the continental dust is of minor importance (Matsumoto and Hinkley, 2001). Anthropogenic pollution detected in Antarctic and Arctic ice caps

provided evidence that lead pollution in the atmosphere in the 20th century was caused by gasoline additives (Candelone et al., 1995). Increase of platinum group metals in Greenland ice pointed to the pollution associated with the widespread use of automobile catalytic converters (Boutron et al., 1994). Ice-core records from regional glaciers provided records of heavy metal pollution in the Alps and Andes (Barbante et al., 2001).

However, collecting ice core samples requires substantial investment in the drilling equipment and the supporting operations such as transportation, fuel, maintenance, and personnel. Ice coring is often performed under extreme conditions, and is thus both costly and time consuming. Additionally, there are safety considerations both during collection of the ice cores and during their transportation to the laboratory for analysis. Concentrations of the deposited metals in the ice cores are extremely low and their accurate determination remains challenging. For example, the maximum concentrations of Pb and Cd reported in the ice cores were around tens of $pg \cdot g^{-1}$, and these concentrations could vary with annual deposition patterns (Zeng et al., 2006). Therefore, it is important to collect ice cores that are as free from contamination as possible. The analytical methods include tedious and time-consuming decontamination procedures that have to be performed under extremely clean conditions (Candelone et al., 1995).

Marine and Lake Sediments

The use of both marine and lake sediment records as an archive of environmental changes is well established in the journal literature (Kober et al., 1999; Monna et al., 1999; Renberg et al., 1994; Arnaud et al., 2004; Monna et al., 1997; Weiss et al., 1999). The Fe-Mn crusts and deep-sea sediments generally cannot be used to assess short-term

environmental changes due to their low accumulation rates. The lead isotopic composition of Fe-Mn crusts has remained uniform over the past 30 million years. However, the record of small variations in concentrations of Pb isotopes corresponds with other indicators of climate change, including weathering and glaciations. Christensen et al. (1997) suggest that the changes in Pb isotopic composition relate to ocean temperature and continental ice volume, and consequently to climate.

Coastal sediments have much higher accumulation rates and have been successfully used to establish regional pollution records, despite complications caused by biological and/or geological interferences (Battiston et al., 1989; Schintu and Degetto, 1999; Bettinetti et al., 2009; Di Leonardo et al., 2009). Significant heavy metal pollution has been documented in the sediments collected from the Atlantic shelf. Lead isotope measurements of the coastal sediments identified Europe and North America as the dominant sources of Pb in the northeastern and northwestern Atlantic (Hamelin et al., 1990).

Lake sediments have been widely investigated mainly as regional archives, and mostly covering a time period of the last 150 years (Monna et al., 1997). Study of sediments from Lake Zug, Switzerland showed the greatest Pb concentrations around 1970, which was the time of maximum lead emissions in Switzerland from the use of leaded gasoline (Moor et al., 1996; Goldberg et al., 1981). However, sources of pollutants in sediments are not only atmospheric in origin. Fluvial inputs and erosion of rocks add to the atmospheric deposition and make the sediment records more complex (Schintu and Degetto, 1999; Di Leonardo et al., 2009). Separating the “natural” fraction of the pollutant present in the sediment from atmospheric signals can be challenging (Arnaud et

al., 2004). For many chemical elements, the interpretation of data is complicated by physical or chemical transformations caused by variables such as pH, Eh, or other geochemical conditions prevalent during the sedimentation process.

Animal hair and excrement preserved in sediments have also been used to study past contamination in the animals' living environment. Mercury profiles in the hair of Antarctic seals revealed significant exposure to human activities for the past 2000 years (Sun et al., 2006). Lead concentrations in penguin droppings suggested that noticeable anthropogenic contamination on sub-Antarctic islands began at least 200 years ago (Yin et al., 2006).

Soils

The use of soils for monitoring of atmospheric pollution is limited by insufficient stratigraphic layering and by the mobility of the pollutants. There is also the possibility that high concentrations of contaminants in the topsoil can be derived from natural sources and do not reflect anthropogenic activities. Nevertheless, the study of soils has been successful in tracing the sources of atmospherically-derived lead contamination (Weiss et al., 1999). Following deposition of the radioactive global fallout, soils and sediments are the main reservoirs of radionuclides in the environment. For example, tests of soils collected around the Nevada Test Site (NTS) showed that 90% of the radioactive ^{137}Cs and 99% of the $^{239, 240}Pu$ reside in the upper 5 cm of the soil (Turner et al., 2003).

The collection of surface soil samples is much easier than the collection of sediment cores, but reconstruction of historical records is limited. Both soils and sediments are analyzed by well-established analytical methods.

Peat Bogs

The ombrotrophic peat bogs receive all their water and nutrients from precipitation. Their surface layers are hydrologically isolated from both groundwater and surface waters, and thus receive chemical compounds only from the atmosphere (Shotyk et al., 1998; Weiss et al., 1999; Weiss et al., 2007; Kylander et al., 2009). These bogs are well suited to the study of deposition patterns of air pollutants, especially heavy metals. The botanical composition of peat has been known to reflect changes in climate (Shotyk, 2004). The inorganic fraction of peat; derived from soil dust particles, volcanic ashes, cosmogenic dust, marine aerosols, and atmospheric contaminants; preserves the record of atmospheric deposition of airborne pollutants (Shotyk et al., 1998).

Ombrotrophic peats are one of the best continental archives of atmospheric Pb deposition, and allow for the quantification of temporal changes in worldwide atmospheric Pb contamination (Weiss et al., 1999). Using isotope analysis of peat cores, both the rate of atmospheric dust deposition and its predominant sources can be identified. For elements that are quantitatively retained in the peat column, the natural and anthropogenic geochemical cycles can be investigated (Glooschenko, 1986; Livett, 1988; Weiss et al., 1999; Franzen et al., 2004; Weiss et al., 2007; Kylander et al., 2009). For example, the decrease in Pb emissions following the decline of the Roman Empire, and the increase in Pb emissions at the onset of the Industrial Revolution are clearly

recorded in the layers of European peat bog deposits (Lee and Tallis, 1973; Shotyk at al., 1998; Van Geel et al., 1989).

One of the advantages offered by the study of peat bogs is that peat lands are distributed around the globe, covering around 5% of total land area and presenting the opportunity to study local pollution histories. Additionally, peat formation began after the retreat of glaciers, allowing peat bogs to record events occurring throughout the entire Holocene (~ 10,000 BC – present). Due to their proximity to pollution sources, peat bogs contain relatively high concentrations of pollutants, allowing for greater ease in the measurement of contamination levels. Finally, peat cores can be dated using ^{14}C methods and a detailed chronology of atmospheric deposition can be established in the spatially resolved samples (Weiss et al., 1999).

Biomonitors

Biomonitoring is based on the measurement of pollutant accumulation in the tissues of living organisms. The use of biomonitors in measuring environmental pollutants has advantages, since many pollutants are biomagnified in organisms. Biomonitors, such as vegetation, cow's milk, and mosses have been successfully used to monitor ambient air contamination in the proximity of potential point sources (Alcock and Jones, 1996; Wallberg and Moberg, 2002). They can also provide a measurement of integrated exposure over a period of time and reduce analytical uncertainty. Additionally, biomonitors enable a high density of sampling points and ensure representative spatial measurements (Alcock and Jones, 1996; Wallberg and Moberg, 2002).

The outer waxy surfaces of pine needles, kale and grasses absorb atmospheric lipophilic pollutants and have been used as monitors of dioxins (Augusto et al., 2004). Tree ring analyses have proved useful for monitoring and reconstructing heavy metals emissions. For example, a timeline of lead pollution in Sweden during the 20th century was reconstructed using core samples from oak trees (Weiss et al., 2003). However, the use of plants as biomonitors has some drawbacks. Plants have different mechanisms of uptake, distribution, storage, and metabolism of various pollutants. Numerous factors, such as wind, drought, and light intensity can influence the response of plants to the pollutant (Simonich and Hites, 1994; Czuczwa et al., 1984; Kovalchuk and Kovalchuk, 2008).

In bodies of water, hydrophobic pollutants such as pesticides and polychlorinated biphenyls (PCBs) accumulate mainly in the lipid fraction of fish and other aquatic organisms. Interestingly, the "contaminated" organism can be used as a monitor of environmental pollution. For example, the U.S. "Mussel Watch" program utilizes non-migratory aquatic organisms such as carp, suckers, catfish, mollusks, and others to monitor a variety of pollutants along the coastal areas. Bottom feeders efficiently accumulate sediment-adsorbed pollutants and have been used as site-specific pollution indicators (Bruggeman, 1982; Goldberg et al., 1983; Tripp et al., 1992; Goldberg and Bertine, 2000).

Lichens

Lichens are biomonitors with an exceptional accumulation capacity that allows the measurement of airborne contamination in terrestrial ecosystems. They have been

extensively used to monitor a variety of atmospheric pollutants including heavy metals, radionuclides, PCBs, polycyclic aromatic hydrocarbons (PAHs), and organochloride pesticides (Villeneuve et al., 1988; Calamari et al., 1991; Owczarek et al., 2001; Guidotti et al., 2003; Augusto et al., 2004; Monna et al., 1999; Doucet and Carignan, 2001; Carignan et al., 2002).

Lichens derive their moisture and nutrients solely from ambient air. The processes by which lichens intercept airborne particulates and gases include wet precipitation, dry deposition, and gaseous adsorption (Nash, 1996; Silberstein et al., 1996; Sarret et al., 1998). Lichens do not have a waxy cuticle like other plants, and elemental exchange takes place across their entire surface. An additional advantage of using lichens rather than other higher plants is that lichens lack a vascular root system, and thus are not subject to the complication of pollutants being absorbed by the roots from the soil. The sensitivity of lichens to airborne contamination is related to their biology (Nash and Gries, 1995; Nash, 1996; Scerbo et al., 2002; Cicek and Koparal, 2003).

The benefits of using lichens as environmental monitors of atmospheric pollution include: (1) widespread occurrence and ease of sampling, (2) biomagnification of some pollutants allowing for application of routine analyses, and (3) capacity to average the atmospheric signal over a period of a few years. Monitoring pollutant distributions on a continental scale is critical in order to minimize the effect of seasonal changes in atmospheric circulation, as well as interferences from forest fires and exceptional wind conditions (Carignan et al., 2002).

Lichens have been used as natural collectors of airborne Pb in order to map the distribution of atmospheric Pb contamination. For example, high Pb content (>1 ppm)

was reported in lichen samples collected in northeastern North America (Chiarenzelli et al., 2001). Additionally, lead isotopic ratios ($^{206}Pb/^{207}Pb$) present in the contamination are directly related to, and allow for the identification of, the sources of air pollution. Consequently, Pb contamination in the northeast was traced to coal-fired power plants and industrial facilities (Carignan et al., 2002).

Desert Varnish as an Environmental Monitor

Desert varnish has many potential advantages as an environmental monitor. The varnishes are distributed worldwide and in all climates, offering convenience of sampling and the possibility of studying local pollution. Desert varnish is directly linked to the atmosphere, since its ingredients are derived from it. Enhanced concentrations (around 5-60 times) of trace metals in comparison to the surrounding soils were reported in varnish samples (Wayne et al., 2006). An extremely high concentration ratio (about 10^{11}) of ^{210}Po over the air concentration of ^{210}Po was reported in varnish samples from Great Basin (Hodge et al., 2005). The high concentration ratios of pollutants greatly reduce analytical uncertainty. Additionally, varnish samples are stable, easy to handle, and the possibility of contamination is relatively low.

The main disadvantage of desert varnish as an environmental and paleo climatic monitor is the need for labor-intensive sample preparation techniques and advanced analytical methods. Analyses of varnish layers involve preparation of ultra thin sections (5-10 µm) of the sample, followed by electron microscopy (Liu and Broecker, 2007). The application of various analytical methods in the analysis of varnishes is relatively new and still under development. However, the techniques of inductively coupled

plasma mass spectroscopy (ICPMS) and laser ablation-inductively coupled plasma mass spectroscopy (LA-ICPMS) offer the most promise (Diaz, 2004; Wayne et al., 2006).

CHAPTER 3

DESERT VARNISH LITERATURE REVIEW

Introduction

Rock varnish has been a scientific marvel for over 200 years, dating back to the travels of Alexander von Humboldt in South America from 1799 to 1804, when he described varnish coatings on rocks in the Chilean deserts (von Humboldt, 1852). However, after two centuries of study, there are still unanswered questions regarding varnish's origin, chemical and physical nature, age, and growth rate.

Chemistry and Mineralogy of Desert Varnish

Rock varnish grows on exposed mineral surfaces where it usually forms a dark, thin (2-200 μm), metallic coating (Figure 3.1). The major elements in varnish coatings are O, H, Si, Al, Fe and Mn (Engel and Sharp, 1958). Typically, manganese and iron oxides make up about 25-35% of the varnish composition (Potter and Rossman, 1977; Krinsley, 1998). Abundances of trace elements correlate with those of Mn and Fe, due to the scavenging properties of Mn and Fe oxyhydroxides (Tebo et al., 2004; Thiagarajan and Lee, 2004). The abundances of minor elements vary widely (0.5 – 1.5 %), with B, Na, Mg, P, K, Ca, K, Sc, Ti, V, Cr, Co, Ni, Cu, Sr, Y, Zr, Ba, La, and Pb found in all varnishes (Engel and Sharp, 1958). Other elements such as Zn, Ga, Nb, Mo, Ag, Cd, Sn, and W are found only in some varnishes (Lakin et al., 1963).

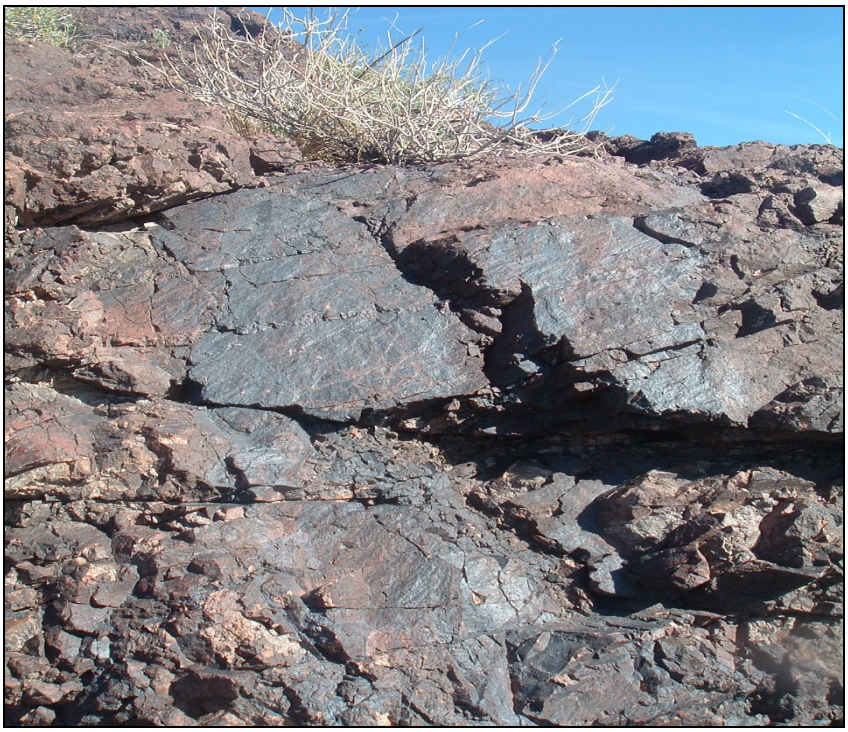

Figure 3.1. Dark, Mn-rich rock varnish covering the mountains near Searchlight, NV.

Manganese chemistry has long been recognized as a key to understanding varnish formation. While the ratio of Mn:Fe in varnishes may be as high as 50:1, this ratio in the Earth's crust is about 1:60 (Dorn, 1998). In nature, soluble Mn(II) is stable in the pH range of 6 – 8, which is the pH of natural waters (Morgan and Stumm, 1965). The activation energy of Mn(II) oxidation to Mn(III) and Mn(IV) is high, and the reaction is often catalyzed by bacteria and fungi (Tebo et al., 2004). In the desert environment, Mn(III) is thermodynamically unstable, and Mn(IV) is consequently the primary insoluble oxyhydroxide found in varnish (Potter and Rossman, 1979). Tebo et al. (2004) presented the Mn cycle of oxidation states found in nature (Figure 3.2).

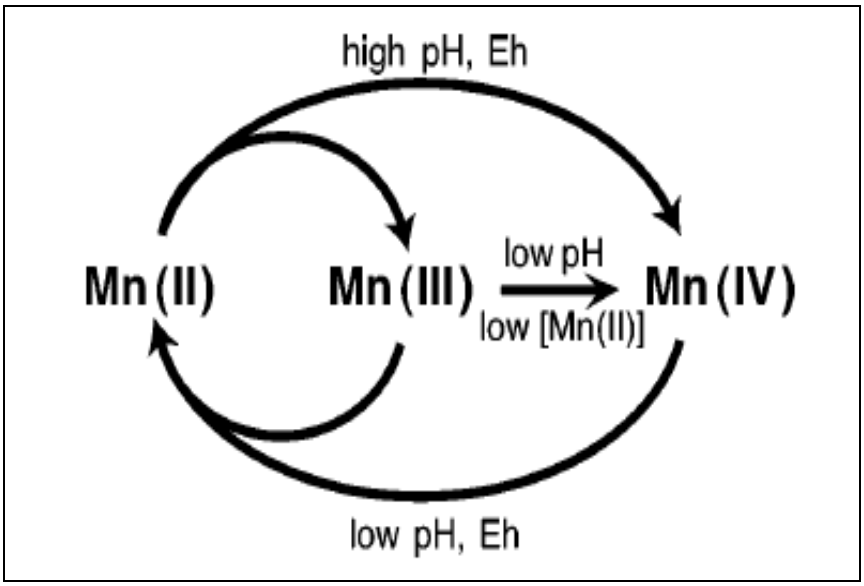

Figure 3.2. The Mn cycle of oxidation states found in nature. Mn(II) is thermodynamically stable at low pH and in the absence of O_2. In the presence of O_2 and higher pH, the formation of insoluble Mn(III) and Mn(IV) oxyhydroxides is favored (Tebo et al., 2004).

Potter and Rossman (1977) analyzed varnishes using infrared spectroscopy (IR), X-ray diffraction (XRD) and electron microscopy. Their analyses revealed that varnishes are composed mainly of clay minerals, such as illite ($(K, H_3O)(Al, Mn, Fe)_2(Si, Al)_4O_{10}[(OH)_2, (H_2O)]$), montmorillonite ($(Na, Ca)_{0.3}(Al, Mg)_2Si_4O_{10}[(OH)_2 \cdot (H_2O)]$), and mixed-layer illite-montmorillonite. These minerals are cemented to the substrate rock by Mn and Fe oxides. The manganese-rich minerals birnessite ($[Na, Ca]\ Mn_7O_{14} \cdot 2.8H_2O$) and todorokite ($(Mn, Mg, Ca, Ba, K, Na)_2Mn_3O_{12} \cdot 3H_2O$) are major components of the black varnish. Orange varnish, in contrast, contains mainly hematite (Fe_2O_3) (Potter and Rossman, 1977; McKeown and Post, 2001). Krinsley (1998) reported that the Mn and Fe oxides form layered structures in the varnish coatings.

The Mn(IV) oxides and the mixed Mn(III, IV) hydroxides, present in varnishes, are called manganates. Manganates have open crystal structures, large negatively-charged

surface areas, and easily-interchangeable cations. These Mn minerals can adsorb, undergo ion-exchange with, or precipitate many trace metals and radionuclides (Tebo et al., 2004). It has been reported in the literature that the presence of minute quantities of Mn oxides decreases by orders of magnitude, the concentrations of dissolved trace metals and radionuclides in natural waters (Bacon et al., 1980; Kay et al., 2001; Tebo et al., 2004). These "scavenging" properties of Mn oxides are presumed to be the main factor driving incorporation of trace elements into desert varnish films.

Desert Varnish and Microorganisms

A number of researchers have identified microorganisms growing on varnishes, or have reported organic compounds present within varnish films (Allen et al., 2004; Perry et al., 2002; Kuhlman et al., 2005, 2006). Kuhlman et al. (2006) reported relatively dense microbial populations on the varnish samples from the Whipple Mountains, AZ (10^8 microorganisms per gram of dry varnish). Schelbe et al. (2005) used fatty acid methyl ester (FAME) extraction to examine microbial organisms present on the varnished rocks. The study showed a diversity of microorganisms present, but failed to identify any microbes specific to desert varnish. The main bacterial species observed in the varnishes include: *Bacillus, Geodermatophilus, Arthrobacter, Micrococcus,* and *Curtobacterium* (Hungate et al., 1987; Kuhlman et al., 2005). Some of these bacteria are known to accumulate manganese oxides (Figure 3.3) (Palmer et al. 1985; Ehlrich, 1996; DiGregorio, 2005). It has been noted, however, that microcolonial fungi (MCF) are the predominant organisms observed on varnish films, and may be involved in varnish formation (Stanley, 1982; Taylor-George et al., 1983; Perry et al., 2002).

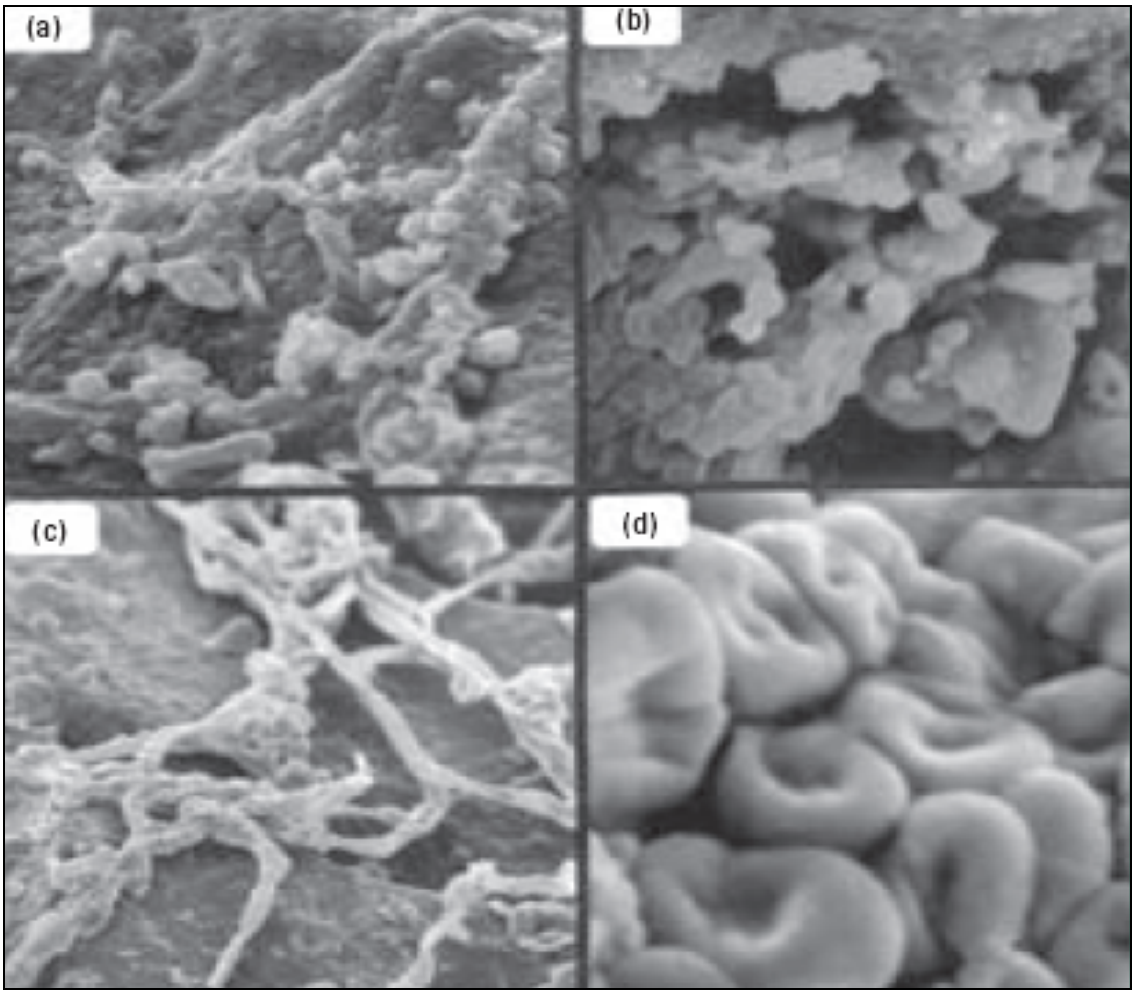

Figure 3.3. High-resolution transmission electron micrographs showing various Mn-enhanced bacterial forms: hyphae (a,c) and cocci (b,d) (all forms < 1 μm diameter) (DiGregorio, 2005).

McKeown and Post (2001) suggested that manganates (birnessite and todorokite) found in both rock varnish and ocean nodules indicate biogenic activity. NASA's Martian explorations discovered varnish-like materials and spherules, similar to the deep-sea nodules (DiGregorio, 2005). Some researchers have speculated that desert varnish could be a habitat for life forms on other planets (Perry and Kolb, 2004). Allen et al. (2001) applied scanning electron microscopy (SEM) to terrestrial hematite deposits and observed scale rods, spheres, and filaments consisting predominantly of iron and oxygen, with some carbon also present. The authors interpreted these objects as microbial cells

mineralized by iron oxide. They identified desert varnish as a potential analog to Martian hematite, and hypothesized that Martian hematite-rich samples may provide confirmation of ancient microbial life on Mars.

Genesis of Desert Varnish

There is substantial debate over the process of desert varnish formation. Originally, the formation of desert varnish was thought to be the result of simple chemical and physical processes consisting of direct leaching of the rock substrate followed by re-precipitation on the rock surface. This hypothesis proposed that the growth of varnish took place from the inside of the rock to the outside, as a result of a sequence of processes. These included internal decomposition, capillary migration of solutions to the surface, and evaporation resulting in re-deposition of minerals from the parent rock (Walther, 1891; Linck, 1900). However, this mechanism is flawed since desert varnish occurs on all kinds of rock including quartzites, which contain little or no Fe, Mn, or clays (Potter and Rossman, 1977; Krinsley, 1998). Varnishes also contain small amounts of sulfate, whose oxygen isotopic signature is uniquely atmospheric (Bao et al., 2001).

Recently, most authors subscribe to the idea that varnishes are extraneous to the parent rock on which they are deposited, and are of atmospheric origin. The clays present in the varnishes are widespread in terrestrial weathering environments, and require only simple wind deposition of dust on the rock surface. Minor and trace elements are absorbed into the clays by the scavenging properties of Mn-Fe oxyhydroxides (Tebo et al., 2004; Thiagarajan and Lee, 2004). Four general conceptual models for explaining the mechanism of rock varnish formation have been proposed.

These are: (1) abiotic enhancement of Mn, (2) biotic concentration of Fe-Mn oxyhydroxides, (3) polygenetic clay-bacteria interactions, and (4) silica binding (Figure 3.4)

Proponents of the abiotic, or physiochemical, model claim that varnish forms without the aid of biological enhancement of Mn (Hooke et al., 1969; Smith and Whalley, 1988). This model involves the formation of Fe-O-Si chemical bonds that attach the varnish film to the host rock (Scheidegger et al., 1993). These bonds are strong and their formation is irreversible, making the iron film strongly and permanently attached to the silica surface. The increase in Mn concentration in comparison to that of Fe is explained by the greater mobility of Mn(II) over Fe(II) (Krauskopf, 1957). Small amounts of divalent Fe and Mn cations are liberated to the rock surface by leaching/dissolution of airborne dust particles around which rain/fog droplets have nucleated. At the pH (~ 5.7) and Eh (~ 0.8 V) of rainwater, Mn is more soluble than Fe, resulting in an enhanced content of Mn relative to dissolved Fe (Thiagarajan and Lee, 2004). Precipitation of Fe and Mn on rock substrates requires that these ions be oxidized to their insoluble trivalent states (Dorn, 1998; Tebo et al., 2004). This cycle of dissolution-precipitation of Fe and Mn repeats, leading over time to varnish formation (Dorn, 2007).

In the biotic or biological model, microorganisms and their organic remains play the major role in binding varnish and concentrating Fe-Mn oxyhydroxides. Fine particles, mainly clays, accumulate on the surface of the rocks, where microorganisms develop and concentrate Fe and Mn (Dorn, 2007). Fe(III) found on rock and grain surfaces in deserts is dissolved by the siderophores produced by microorganisms (Adams et al., 1992).

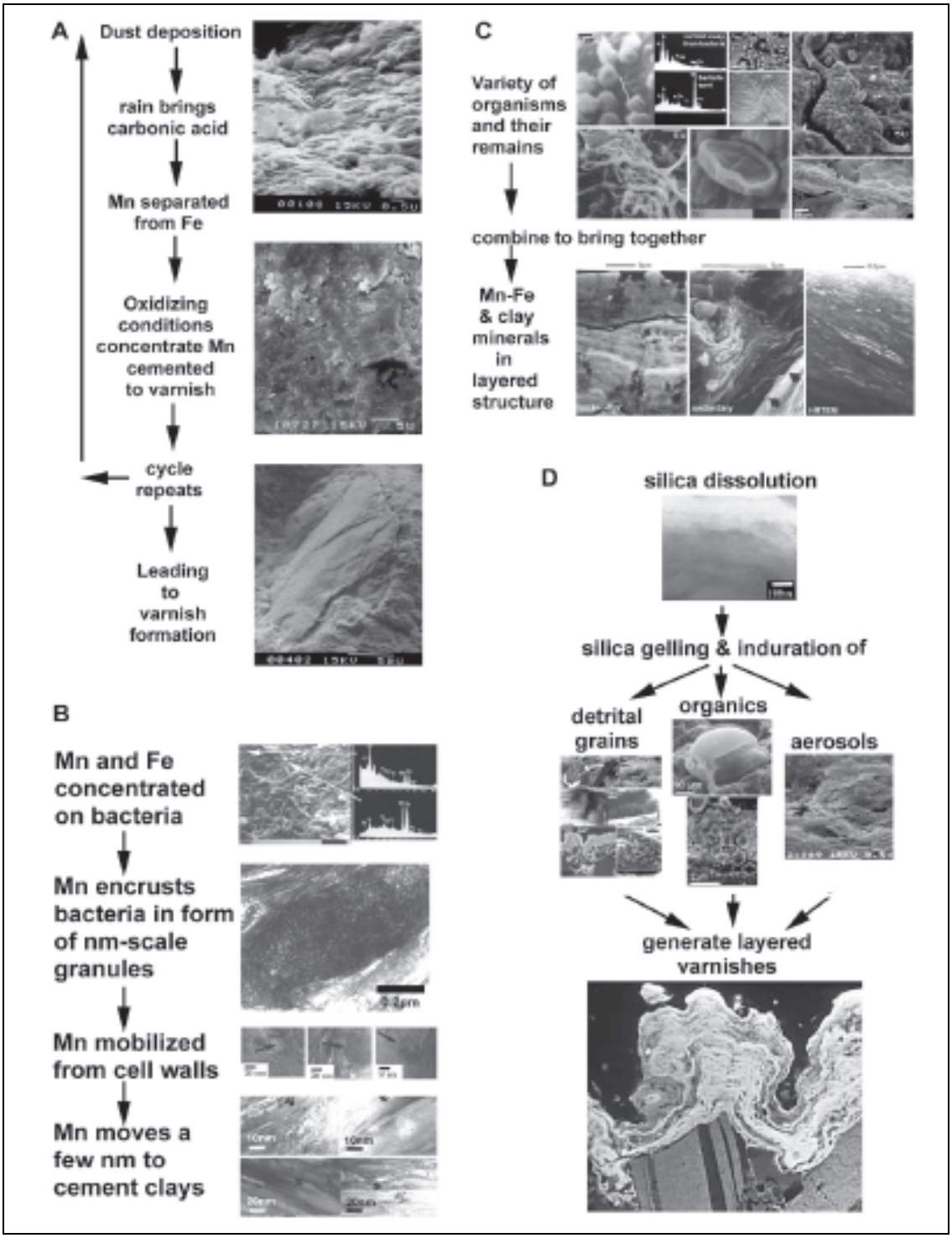

Figure 3.4. Conceptual models of desert varnish formation (Dorn, 2007). (A) Physiochemical model of Mn enhancement (Hooke et al., 1969; Smith and Whalley, 1988). (B) Polygenetic model clay-bacteria interactions (Dorn, 2007). (C) Microorganisms play a role in binding varnish and concentrating Mn and Fe oxides (Dorn and Meek, 1995; Dorn, 1998; Krinsley, 1998). (D) Silica binding detrital grains, organics and aerosols (Perry and Kolb, 2003; Perry et al., 2006).

Siderophores are biochemical chelating agents that microorganisms secrete in order to obtain Fe from their environment for metabolic purposes (Schwyn and Neilands, 1987). The deposited iron forms a continuous film on the rock surface where silica and other elements, including Mn displaced during wetting-drying cycles, can accumulate. Iron causes this film to adhere to the siliceous surface (Scheidegger et al., 1993). When concentrations of silica (SiO_2) are high in the associated waters, silica will also bind to the film (Urrutia and Beveridge, 1994).

The polygenetic hypothesis of rock varnish development merges the biotic enhancement of Mn with abiotic processes. In short, Mn-containing remnants of microorganisms fix dust particles to the rock surfaces (Dorn, 1998). Varnish formation begins with the deposition of clay dusts on the rock surfaces, followed by the active concentration of Mn and Fe by bacteria and fungi (Dorn and Oberlander, 1982). Some of these microorganisms become microfossils that decay and become incorporated into the varnish coatings (Krinsley, 1998). A significant advantage of the polygenetic model is that it explains both very slow processes of Mn enhancement, as well as Fe-Mn interactions with clays (Dorn, 2007).

The most recent model of varnish genesis centers on silica (SiO_2) as the key factor in varnish formation (Perry et al., 2006). This model implies that varnish and silica glazes are closely related since they both contain primarily silicon, with other oxides present in smaller quantities. Consequently, silica glaze formation may provide a simplified model of varnish formation. The hypothesis begins with the dissolution of SiO_2 and the formation of anhydrous and hydrous minerals; followed by the SiO_2 gelling, condensing, and then hardening. Detrital minerals, organics, and dust are incorporated into the

varnish films during the process of SiO_2 binding (Perry et al., 2006). Laboratory experiments based on this model successfully achieved the formation of *in vitro* silica coatings (Perry et al., 2005).

Dating Desert Varnish

Different techniques for dating desert varnish have been proposed in the last 50 years, but none of them have allowed for decisive age determination. Characteristics of rock varnish such as its darkness (Hooke, 1967), thickness (Hayden, 1976), and Mn content (Bard, 1979) have been used as estimates of the relative ages of lithic surfaces. However, these properties are dependent not only on time, but are also greatly influenced by environmental factors.

Bard (1979) proposed a method of dating varnish coatings based on the total Mn concentration relative to that of Fe. However, chemical analyses of varnish at different sites, compared to the relative-age controls, indicated that the bulk of the Fe:Mn ratios were not related to the underlying surface (Dorn, 1983).

Dorn (1983) introduced cation ratio dating for the age determination of desert varnish, and applied this technique to dating samples from Death Valley and the Nagev Desert. The principle of cation ratio dating is based on the differences in solubility of minor elements in the varnish. Over time, leachable cations in the varnish, such as Na, Mg, K, and Ca are gradually replaced or depleted relative to less mobile cations, such as Ti, Al, or Fe. The decreasing cation ratios of Na^{+}, Mg^{2+}, K^{+}, and Ca^{2+} to Ti^{4+} provide an indication of the duration of varnish exposure to the leaching process. The premise of this technique is that varnishes from similar micro environmental settings at a given site

should indicate a relative-age sequence. Dorn (1983) analyzed subaerial varnish samples by backscatter scanning electron microscopy (SEM) and empirically determined that the concentration ratio of (K + Ca)/Ti decreases with time, due to preferential leaching of K and Ca. Based on analytical results, a series of cation-leaching curves was constructed for the sampled areas. The limitation of cation-ratio dating is that several theoretical assumptions such as sources of the varnish constituents, cation ratios of airborne particles, cation-exchange capacity of varnishes, and the rates of leaching of varnish cations have to be verified by field-sampling and laboratory analysis (Dorn, 1983).

Reneau et al. (1992) observed that the minor elements used in cation ratio dating reflect varnish stratigraphy as defined by the major constituents Mn, Fe, and Si. They also noticed that K is associated with Si, Ca, and Mn; and that Ti is associated with Fe. Therefore, cation ratios reflect the variations in major element composition that are associated with varnish stratigraphy. The authors also demonstrated that there were no changes as a result of depth or age in the ratios of K:Si or Ca:Mn, as would be expected if K and Ca were preferentially leached from the varnish.

Accelerator mass spectrometry radiocarbon dating (AMS ^{14}C) is another method used for dating rock varnish (Francis et al., 1993; Watchman, 2000). This technique was applied under the assumption that any organic matter in rock varnish was deposited simultaneously with inorganic substances, and that organic matter in rock varnish is the main source of any carbon present. The aim of this method is to analyze carbon substances at the interface between the varnish and the substrate rock in order to determine when the varnish began to form. The authors were able to determine the minimum time for varnish to start accumulating at the base, resulting in an estimated age

of the varnish (Francis et al., 1993; Sowers, 2001; Watchman, 2000). This technique is controversial because the source of carbon is often unknown, and the incidence of carbon before the formation of varnish cannot be determined.

Desert Varnish Accumulation

Fleisher et al. (1999) demonstrated that varnish accumulates short-lived radioisotopes (^{210}Pb and ^{137}Cs) and other cosmogenic materials (^{7}Be and ^{10}Be) from the atmosphere. Based on this study, Moore et al. (2001) moved varnish-coated rocks from McDowell Mountain, AZ and Panamint Valley, CA to an area adjacent to Biosphere 2. Some rocks were shielded during times of precipitation, and the others were continuously exposed to the environmental elements. Results from this study showed that rocks exposed to precipitation accumulated more ^{7}Be than those shielded. The study concluded that ~ 62% of the accumulated Be was supplied by precipitation and that the remainder was provided by a combination of aerosols, dew, and dust. Varnish is greatly affected by wind abrasion and heavy rainfall, making it difficult to determine the length of time required for the accumulation to take place. The accumulation of varnish on the rock surfaces is inconsistent and it is difficult to obtain reliable growth rates for desert varnish. Based on exposed rock surfaces found on the shorelines of pluvial lakes, it was deducted that varnish starts to accumulate within 25 years of subaerial exposure (Moore et al., 2001).

Rock varnish coatings become thicker, darker, and more continuous over time, leading to the use of varnish as a visual indicator of age. The dark color of varnish is attributed to the presence of manganese. Reneau et al. (1992) attempted to quantify the development of varnish over time by measuring the amount of Mn in varnish from rock

surfaces of different ages. The authors dissolved rock varnish from samples collected in the Mojave Desert, California. Samples were then analyzed for the presence of Mn by inductively coupled plasma emission spectroscopy (ICP-ES). The study was performed assuming that the amount of accumulated Mn in the varnish would increase from younger to older surfaces. The authors concluded that rock varnish can show significant growth difference on surfaces of similar age, and that the amount of Mn accumulated provides a quantitative means of comparing varnish development.

Desert Varnish and Climatic Data

Although there have been setbacks in dating varnish, and measuring its rate of accumulation, some scientists are still convinced that rock varnish is useful in evaluating paleoclimatic patterns (Broecker and Liu, 2001). Many authors conclude that the method with the most potential for deciphering the paleoenvironmental data is varnish microlaminations (VML). The VML technique is based on microscopic examination of the lamination patterns in ultra-thin sections of varnished rocks. These authors hypothesized that the different colors of layers in the varnish reflect regional climatic changes (Liu and Dorn, 1996; Zhou et al., 2000; Broecker and Liu, 2001; Liu, 2006; Liu and Broecker, 2007, 2008). Thus, black layers that are rich in Mn, record wet periods; while yellow and orange layers containing less Mn, record drier intervals (Jones, 1991). Temporal variations in Mn and Ba concentrations likely relate to variations of moisture in the atmosphere during climatic changes. Comparisons of mean MnO_2 content in varnish coatings from the Holocene to the present, in samples from the Mojave Desert and Death

Valley, demonstrated higher MnO_2 content due to an increase in precipitation (Liu and Broecker, 2007) (Figure 3.5).

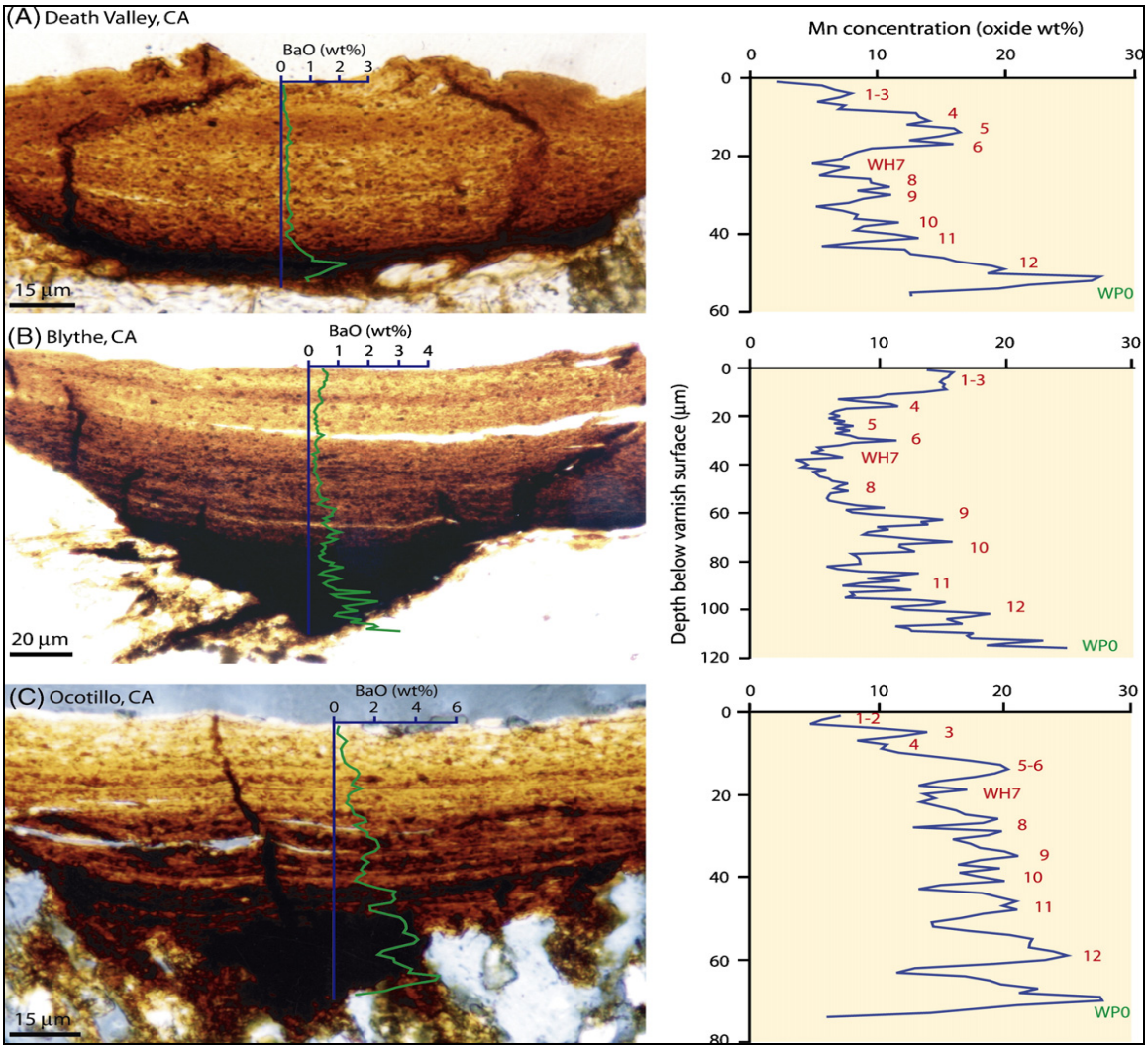

Figure 3.5. Optical (left) and chemical (right) microstratigraphies in rock varnish from three locations in the dry lands of the western US. The WH1-WH12 and WP0 on the right identify Mn-rich peaks that largely correspond to Holocene wet periods. WH = wet event in Holocene, and WP = wet event in Pleistocene (Liu and Broecker, 2007).

Moore et al. (2001) conducted an experiment to identify the sources of delivery of varnish constituents. In this experiment, they analyzed rock varnish for the presence of ^{7}Be, a radioisotope with a 53-day half-life, produced in the atmosphere by cosmic-ray

bombardment. The results indicated that varnish shielded from the rain accumulated 38% ± 10% the amount of ^{7}Be, relative to non-shielded varnish samples. The authors concluded that the experiment provided support for the idea that MnO_2 is delivered partly by atmospheric moisture. These results are consistent with the study relating MnO_2 content in the varnish layers with high precipitation (Broecker and Liu, 2001).

Bailley and Orndorff (2001) tested the null hypothesis that variations in chemical composition of microlaminations in rock varnish reflect climate change. Samples for this study were collected from undisturbed basalt boulders on the paleoshorelines of Paleolake Lahontan in central Nevada. The authors used scanning electron microscopy (SEM) and energy dispersive spectrometry (EDS) to develop varnish profiles, and conduct surface analyses. Profile analysis showed total varnish thickness ranging from 10 to 242 μm. Additionally, the authors identified elements that may reflect climate changes: Al, Si, Mn, and Fe. Surface analysis of the rock varnish revealed microbial communities concentrated mainly in pits on the surface of the rock. The EDS analysis of laminations found that there is a strong inverse correlation between the concentrations of Si and Mn, as well as between those of Al and Mn. Results supported the hypothesis that during humid climates, sparser microbial communities produce more MnO_2, while in dry conditions, greater quantities of dust, rich in Al and Si, are present in the air.

CHAPTER 4

RESEARCH DESIGN AND METHODOLOGY

My work entailed the sampling and analysis of desert varnish samples from several locations in Arizona, Nevada, and California. One of the analytical methods used was field-portable X-ray fluorescence (FPXRF) for the elemental analysis of Ti, Cr, Mn, Fe, Co, Ni, Cu, Zn, As, Se, Rb, Sr, Zr, Mo, Hg, and Pb. Other methods used included laser ablation – inductively coupled plasma mass spectroscopy (LA-ICPMS) and ICPMS for the determination of 31 isotopes: ^{9}Be, ^{51}V, ^{52}Cr, ^{59}Co, ^{60}Ni, ^{65}Cu, ^{66}Zn, ^{75}As, ^{88}Sr, ^{98}Mo, ^{102}Ru, ^{103}Rh, ^{106}Pd, ^{107}Ag, ^{114}Cd, ^{115}In, ^{120}Sn, ^{121}Sb, ^{133}Cs, ^{138}Ba, ^{184}W, ^{187}Re, ^{195}Pt, ^{197}Au, ^{205}Tl, ^{206,207,208}Pb, ^{209}Bi, ^{232}Th, and ^{238}U. Additionally, Hg was analyzed by cold vapor atomic absorption (CVAA). The analytical results were used to establish the chemical composition of varnish coatings and to evaluate the applicability of rock varnish as a passive environmental monitor.

Selected Point Sources of Air Pollution

The point sources of air pollution for this study were chosen because of: (1) their history of atmospheric emissions and (2) the availability of reports documenting geographic deposition patterns or dispersal of their contamination (U.S. Department of Energy, 1994; U.S. Environmental Protection Agency, 1999; U.S. Environmental Protection Agency, 2003). The selected point sources included: the Nevada Test Site (NTS); the Mohave Power Project (MPP), Laughlin, Nevada; the Reid Gardner Power Plant (RGPP), Moapa, Nevada; and the Titanium Metals Corporation, Inc. (TIMET),

Henderson, Nevada (Figure 4.3). Brief histories of each point source and their environmental impacts are presented below.

Nevada Test Site (NTS)

The NTS is a United States Department of Energy (USDOE) reservation in Nye County, Nevada, located about 65 miles (105 km) northwest of Las Vegas, Nevada. The site was established in 1951 for the testing of nuclear weapons, and is composed of approximately 1,350 square miles (3,500 km^2) of desert and mountainous terrain. The aboveground nuclear weapons tests at the NTS took place from January 1951 to October 1958 (U.S. Department of Energy, 1994).

More than 100 aboveground nuclear tests took place before atmospheric testing was banned in 1963. The prevailing weather patterns at the time of the testing dispersed most of the fallout to the north and east of the NTS. Little direct fallout has blown toward Las Vegas (U.S. Department of Energy, 1994). The regions considered to be most heavily affected by NTS fallout include Clark, Esmeralda, Lincoln, and Nye counties in Nevada, and Washington County in Utah. The DOE has conducted extensive monitoring of the radiation fallout from the NTS (U.S. Department of Energy, 1994).

Titanium Metal Corporation, Inc. (TIMET)

The TIMET facility, which is part of the Black Mountain Industrial (BMI) Complex, is located in the City of Henderson, Nevada, in the southeast margin of the Las Vegas Valley. The TIMET plant site comprises approximately 180 acres and is used mainly for the manufacture of titanium industrial products, including titanium sponge, ingot, and titanium tetrachloride (U.S. Environmental Protection Agency, 2003).

In 1941, the U.S. Government designated approximately 5,000 acres of the Las Vegas Valley for the location of the world's largest magnesium plant (Nevada Division of Environmental Protection, 2007). After magnesium production was halted in 1944, the U.S. Government worked to attract other industries to the site. In 1949, the State of Nevada, through the Colorado River Commission (CRC), purchased Basic Magnesium, Inc., and became the owner of the entire industrial complex (Nevada Division of Environmental Protection, 2007).

In 1952, the National Lead Company (now TIMET) purchased the existing plant site. Although the technology of titanium production has changed since 1952, the facility has been used exclusively for titanium production since that time. Presently, using vacuum arc re-melting (VAR) furnaces, the Henderson plant has the capacity to melt up to 13,636 tons of titanium ingot per year (U.S. Environmental Protection Agency, 2003).

Mohave Power Project (MPP)

The MPP was a 1580 megawatt (MW) coal-fired power plant located in Laughlin, Nevada, approximately 75 miles southwest of Grand Canyon National Park (GCNP) (Figure 4.1). The plant operated from 1971 to 2005 and emitted up to 40,000 tons of sulfur dioxide (SO_2) per year, making it the largest source of SO_2 in the Western United States (U.S. Environmental Protection Agency, 1999). In 1991, the Environmental Protection Agency (EPA), National Park Service (NPS) and the majority owners of the MPP, Southern California Edison, conducted a monitoring, modeling, and data assessment study designed to estimate the power plant's contributions to haze at the Grand Canyon (U.S. Environmental Protection Agency, 1999). This cooperative effort was named Project Measurement of Haze and Visibility Effects, referred to as Project

MOHAVE (U.S. Environmental Protection Agency, 1999). The findings of project MOHAVE caused closure of the MPP in December 2005 (Edwards, 2005).

Figure 4.1. Mohave Power Project, Laughlin, NV (Nevada Division of Environmental Protection, 2005).

Reid Gardner Power Plant (RGPP)

The RGPP is a 650 MW coal-fired electric generation facility operated by the Nevada Power Company (NPC), dba NV Energy, Las Vegas, Nevada (Nevada Division of Environmental Protection, 2005). The plant's construction was completed in 1983. The RGPP is located in the Muddy River Valley, Clark County, Nevada, approximately one mile southwest of the city of Moapa, Nevada, and approximately 60 miles northwest of Las Vegas. The facility consists of four coal-fired external combustion boilers that produce electricity for various locations in Nevada (Figure 4.2).

Figure 4.2. Reid Gardner Power Plant, Moapa, NV (Nevada Division of Environmental Protection, 2005).

Sampling Program Overview

A sampling program should follow a design process that considers the location of sampling points, as well as the number of samples and replicates, in order to satisfactorily address the program objectives (Kramer, 1994). Representativeness is the main goal of the sampling program, meaning that the sample should accurately reflect the origin environment, and that the sampling process should be under adequate control to prevent any degradation/decomposition/contamination of the samples between the time of sampling and that of analysis (U.S. Environmental Protection Agency, 2002).

The method of judgmental sampling was used in this study. In judgmental sampling, the selection of sampling units (i.e. the number and location and/or timing of collecting samples) is based on knowledge of the feature or condition under investigation and on professional judgment. Judgmental sampling is different from probability-based sampling in that inferences are based on professional judgment, not statistical scientific

theory. Therefore, statistical statements about parameters are not possible, and any conclusions regarding the target population are limited and depend entirely on the validity and accuracy of the judgment (U.S. Environmental Protection Agency, 2002).

Field Sampling

Sample collection was largely a matter of site selection, since the sampling methodology is well established (Diaz, 2004; Hodge et al., 2005). Desert varnish samples were collected from July 2007 to March 2009 in the areas surrounding the selected point sources of air pollution. The samples were collected from exposed rock faces, boulders, rocks, and pebbles that were dark in color with a metallic sheen and a smooth surface. To avoid interferences from any surface deposits and vegetation, rocks with extensive tufa deposits (calcium carbonate, $CaCO_3$) and lichen communities were not sampled. Small, varnished rocks and pebbles were gathered. Otherwise, sampled pieces of rock were chipped off of stable rock surfaces or exposed boulders using a geological hammer. Sets of 5 to10 replicates of rocks or pebbles were collected at each sampling point within the sampled area. The sampled area covered a circle with a radius of about 50 to 150 m, depending on terrain configuration and the location of the varnished rocks. The probability of rock sample contamination during transport and storage is very low (Kramer, 1994). Thus, field and container blanks were not used. All rock sample replicates were transported and stored in sealed polyethylene bags (Johnson & Sons, Inc., Racine, WI). Additionally, pictures of each sampling location and selected sampling points were taken. The geographical coordinates and the altitude of each sampling site were determined with a Global Positioning System (GPS) (eTerx, Garmin

International, Inc., Olathe, Kansas, USA). A list of sampling sites with their coordinates and altitude (Table 4.1), as well as a map showing locations of the sampling sites (Figure 4.3), are included.

Table 4.1 List of Sampling Sites.

Site	Geographical Name	Latitude	Longitude	Altitude (ft)
NTS 1	Queen City Summit, Rachel, NV	N 37° 45.905'	W 115° 57.940'	5,742
NTS 2	Hancock Summit, Crystal Springs, NV	N 37° 26.812'	W 115° 22.264'	5,305
NTS 3	Pahranagat Valley, Alamo, NV	N 37° 18.572'	W 115° 07.419'	3,404
TIMET 1	Henderson, NV	N 36° 02.895'	W 114° 59.361'	1,796
TIMET 2	Black Mountain, Henderson, NV	N 36° 01.257'	W 115° 00.792'	2,113
TIMET 3	Henderson, NV	N 36° 03.274'	W 115° 000.582'	1,699
TIMET 4	Henderson, NV	N 36° 04.308'	W 115° 20.393'	1,690
MPP 1	Las Vegas Wash, Henderson, NV	N 36° 04.432'	W 114° 55.603'	1,719
MPP 2	Cottonwood Cove, Searchlight, NV	N 35° 29.000'	W 114° 44.491'	1,504
MPP 3	Dolan Springs, AZ	N 35° 35.069'	W 114° 17.126'	3,270
MPP 4	Laughlin, NV	N 35° 09.074'	W 114° 38.251'	1,061
MPP 5	Lake Havasu, AZ	N 34° 37.612'	W 114° 19.525'	1,390
MPP 5a	Lake Havasu, AZ	N 34° 37.612'	W 114° 19.525'	1,390
MPP 6	Cattail Cove State Park, AZ	N 34° 21.564'	W 114° 09.597'	613
MPP 7	Chiquita Hills, NV	N 35° 09.629'	W 114° 50.099'	2,580
MPP 8	Chemehuei Valley, CA	N 34° 35.452'	W 114° 38.185'	1,950
MPP 9	Parker Dam, AZ	N 34° 17.498'	W 114° 07.782'	610
MPP 10	Earp, CA	N 34° 10.713'	W 114° 15.621'	417
RGPP 1	Elgin, NV	N 37° 22.723'	W 114° 32.993'	3,501
RGPP 2	Moapa, NV	N 36° 40.442'	W 114° 37.412'	1,671
RGPP 3	Valley of Fire, Overton, NV	N 36° 25.414'	W 114° 33.038'	2,206
RGPP 4	Gunsight Mountain, NV	N 36° 39.650'	W 114° 55.374'	2,620
RGPP 5	Coyote Springs, NV	N 36° 57.714'	W 114° 58.476'	2,560
RGPP 6	Kane Spring Wash, NV	N 37° 00.902'	W 114° 51.923'	2,980
BKG 1	Brian Head Peak, UT	N 37° 41.267'	W 112° 50.116'	11,020
BKG 2	Spring Mountains, NV	N 36° 24.552'	W 115° 33.918'	5,450

Figure 4.3. Map of the sampling sites (Google, Inc., Mountain View, CA). Note that locations of some sites (MPP7, RGPP 2, TIMET 1, TIMET 3, and TIMET 4) are not displayed because of the map scale. The sampling site MPP 7 is located close to site MPP 4, site RGPP 2 is located next to the RGPP, and the sites TIMET 1, TIMET 3, and TIMET 4 are located in the proximity of the sampling site TIMET 2.

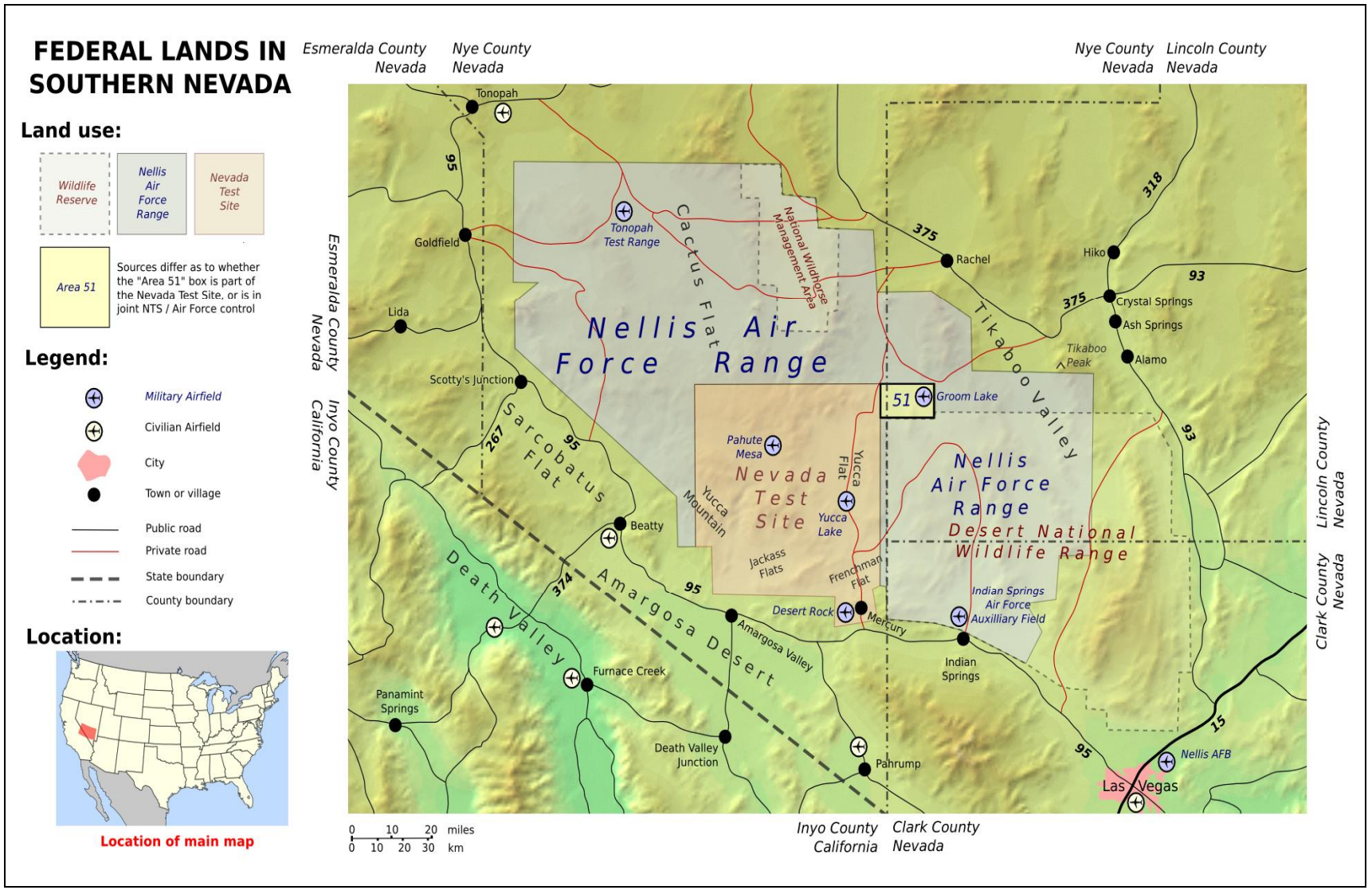

Figure 4.4. Map of federal lands in southern Nevada including Nevada Test Site (Wikipedia, the free encyclopedia, 2007).

NTS Sampling

Sampling around the NTS was performed at three locations to the north and northeast of the NTS (NTS 1, NTS 2, and NTS 3). All three sites are located in the predominant fallout deposition area for many of the atmospheric tests conducted at the NTS (Figures 4.3 and 4.4). NTS 1 was collected at Queen City Summit, Rachel, NV. The site is situated approximately 55 km north of the NTS and 190 km north of Las Vegas, near NV375. NTS 2 was collected at Hancock Summit, Crystal Springs, NV. The site is situated approximately 45 km northeast of the NTS and 150 km north of Las Vegas, near NV375. NTS 3 was collected in Pahranagat Valley, Alamo, NV. The site is situated approximately 60 km east of the NTS and 125 km north of Las Vegas, near US93. All samples were chipped off from stable varnished rock surfaces.

MPP Sampling

During Project MOHAVE, a perfluorocarbon tracer (PFT) was used to establish prevailing wind directions and deposition patterns of the contaminants (U.S. Environmental Protection Agency, 1999). At the MPP, the PFT was injected into the power plant stack at a height of 20 meters. The tracer, ambient particulate composition, and SO_2 concentrations were measured at about 30 locations in the four-state region of Arizona, California, Nevada, and Utah (Green, 1999).

The modeling of plume deposition patterns from the MPP resulted in the development of the influence functions. The influence functions are a direct measure of the average dispersion between the emission and monitoring locations. The assessment of average dispersion includes calculations of the range, average deviation, variance, and standard deviation of the measured values. The spatial patterns of the mean influence functions

illustrate the typical tracer distribution observed throughout each season. Summer wind flow is generally from the south, along the Colorado River, and from the west (or possible southwest), from the western edge of the Mojave Desert. This is consistent with the predominant summer surface wind flow patterns for California (U.S. Environmental Protection Agency, 1999).

Summer MPP average influence function values were highest at sites to the north of the plant. The average summer MPP influence function values at the Las Vegas Wash were comparable to the average value at Dolan Springs, in spite of the former being more than twice the distance from the MPP (Figure 4.5). This suggests that MPP emissions during the summer (April through September) consistently occur over most of the area of Lake Mead (north of the MPP along the Colorado River) with relatively little dilution (U.S. Environmental Protection Agency, 1999). Three sites were sampled in the summer deposition areas. All three sites were located to the north of the MPP along the Colorado River Canyon (MPP 1, MPP 2, and MPP 3)(Figure 4.3)

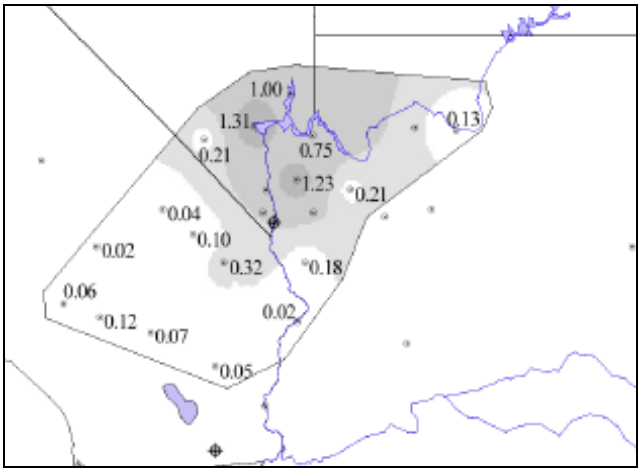

Figure 4.5. Map of average PFT influence functions measured at receptor sites during the summer (April – September) monitoring period (U.S. Environmental Protection Agency, 1999).

A predominant feature of winter airflow shown by the PFT data is drainage down the Colorado River. The largest values of the influence functions were observed during the winter intensive monitoring period (November – February) at sites along the Colorado River Canyon, which acts as a natural conduit for airflow in the winter (Figure 4.6). Winter airflow for the MPP also follows the Colorado River, with the greatest influence function values to the south of Parker, AZ (U.S. Environmental Protection Agency, 1999). The seven sites were sampled in the winter deposition areas. All sites were located to the south of the MPP along the Colorado River Canyon (MPP 4, MPP 5, MPP 5a, MPP 6, MPP 7, MPP 8, MPP 9, and MPP 10) (Figure 4.3).

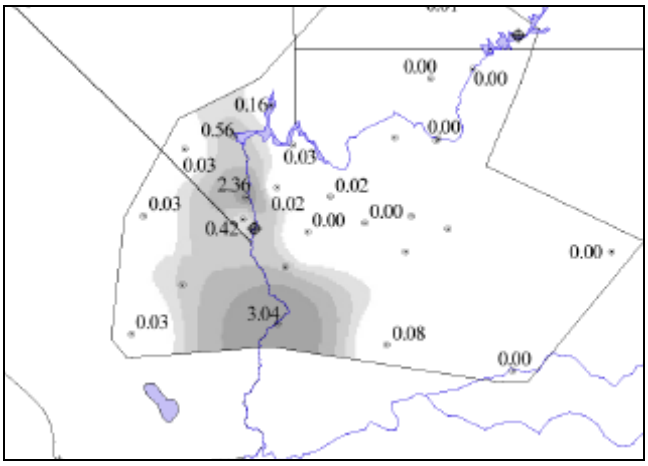

Figure 4.6. Map of average PFT influence functions measured at receptor sites during the winter (November - February) monitoring period (U.S. Environmental Protection Agency, 1999).

TIMET Sampling

Sampling was conducted at four sites located around the TIMET facility (TIMET 1, TIMET 2, TIMET 3, and TIMET 4) (Figure 4.3). TIMET 1 was collected from flat area to the northeast near the TIMET plant, next to Boulder Highway (NV582). These

samples consist of lose, rounded pebbles of volcanic rock (~ 5-15 cm diameter). TIMET 2 was collected on the western slopes of Black Mountain, about 1.5 km southeast of BMI Complex and US95. The site is characterized by volcanic boulders with the visible signs of erosion (1-3 m diameter). These samples were chipped off from the varnished surfaces of the volcanic boulders. TIMET 3 was collected at flat area southwest to the TIMET plant. The site is covered by small, sparsely spaced pebbles ~ 2-8 cm in diameter. TIMET 4 was collected on flat plane located about 1 km southwest to the plant. The site is situated near Pitman Wash. These samples consist of loose, pebbles ~ 10-30 cm in diameter.

RGPP Sampling

The RGPP sampling was performed at six sites located mainly to the north and northeast of the RGPP (RGPP 1, RGPP 2, RGPP 3, RGPP 4, RGPP 5, and RGPP 6) (Figure 4.3). RGPP 1 was collected in Rainbow Canyon, Elgin, NV. The site is situated approximately 75 km north of the RGPP and 140 km northeast of Las Vegas, near NV317. RGPP 2 was collected next to the RGPP, Moapa, NV. The site is situated 80 km northeast of Las Vegas, near I15 and NV168. RGPP 3 was collected in Valley of Fire, Overton, NV. The site is situated approximately 30 km south of the RGPP and 60 km northeast of Las Vegas, near NV169. These samples were collected from highly varnished red sandstone formations. RGPP 4, RGPP 5, and RGPP 6 were collected along US95 north 26 km, 46 km, and 56 km north of the RGPP. These samples consist of loose, pebbles ~ 10-20 cm in diameter.

Background Samples

Two background samples were collected outside the deposition areas of pollutants from the selected point sources (BKG 1 and BKG 2). The background sites were selected outside deposition areas based on the prevailing wind directions and high altitude (Figure 4.3)

Analytical Methods

The analytical techniques used to examine the chemical composition of rock varnish included: FPXRF, LA-ICPMS, ICPMS, and CVAA for total Hg analysis. The analytical work was performed at the Harry Reid Center for Environmental Studies (HRC) at UNLV, and the Environmental Health Laboratory at UNLV.

A Quality Assurance Plan (QAP) was designed to assure validity of the analytical data. Initially, the samples were screened with a portable XRF that allowed for the rapid determination of major elements. The XRF analysis was followed by LA-ICPMS. Although analysis by LA-ICPMS is accepted only as semi-quantitative, some elements in this study showed good agreement with standard reference materials (SRM). Finally, the total concentrations of elements in the varnishes were determined by stripping the varnish coatings from the base rock with concentrated HCl and analyzing the resulting solutions with ICPMS. The same solutions were analyzed separately for Hg by CVAA.

X-Ray Fluorescence Spectroscopy (XRF)

The XRF analysis is non-destructive, multi-elemental, and fast. Consequently, it is widely used for the analysis of environmental, geological, biological, and industrial samples. Depending on the element and on the sample matrix, detection limits vary between 10 and 100 ppm (Kalnicky and Singhvi, 2001).

In XRF, inner shell electrons are excited by incident X-ray photons. During the de-excitation process, electrons move from higher energy levels to fill the vacancy. The energy difference between the two shells is emitted by the atom as an X-ray. The emitted X-ray radiation has a spectrum with characteristic peaks. The energy of the peaks allows for identification of the elements present in the sample (qualitative analysis), while the peak intensity provides the basis for semi-quantitative or quantitative analysis. A technique that employs the energy spectra for XRF analysis is called energy dispersive X-ray fluorescence (EDXRF) and is commonly used in portable XRF instruments (Shefsky, 1997).

A typical XRF spectroscopy arrangement includes a source of primary radiation (usually a radioisotope or an X-ray tube) and a secondary X-ray detector. The energy of the primary radiation should be close to the binding energy of the K- and L-shell electrons of the excited atom. Quantitative XRF analyses require instrument calibrations, which may be performed either by the empirical or by the fundamental parameters (FP) method. The empirical calibration method is based on the analysis of standards with known elemental and geological compositions. The FP technique depends on built-in mathematical algorithms that describe the physics of the detector's response to pure elements. In this case, the calibration model should be verified and optimized using standard reference materials (SRM) (Kalnicky and Singhvi, 2001).

All XRF data were collected with a NITON XLt portable X-ray spectrometer equipped with a 10 mCi ^{109}Cd radioisotope source; a silicon PiN, Peltier cooled detector (750 eV resolution); and the NDT © PC analytical software with expanded multi-element capability (Thermo Fisher Scientific, Billerica, MA). A total of 16 elements were

determined: Ti, Cr, Mn, Fe, Co, Ni, Cu, Zn, As, Se, Rb, Sr, Zr, Mo, Hg, and Pb. Samples were measured for a duration of 60 seconds, and adjusted for source decay. Samples were measured both in bulk sample mode (up to 2 mm depth) and surface mode (surface only).

The XRF calibration was verified with standards obtained from the U.S. National Institute of Standards and Technology (NIST). Two NIST SRMs were used: SRM 2709, San Joaquin Soil (low-level) and SRM 2710, Montana Soil (high-level). For calibration purposes, the certified value for the SRM was used; when that information was unavailable, consensus values were used. SRM 2710 was used as a continuous calibration verification (CCV) standard to verify the validity of the calibration throughout the course of the analytical run (at least 10% of the sample frequency). A recovery of at least 80% for all elements was considered acceptable (conc. > 10 MDL).

In addition, method detection limits (MDLs) were estimated by analysis of a silica (SiO_2) blank material provided by the instrument manufacturer. The MDLs were calculated from the standard error of the blank measurements (n = 10).

Laser Ablation – Inductively Coupled Plasma Mass Spectroscopy (LA- ICPMS)

LA-ICPMS analysis of rock varnish is similar to the analyses of many geological materials, and was referenced in the literature (Wayne et al., 2006). Typical LA-ICPMS instrumentation consists of a laser, an ablation stage, and a detection system (Russo et al., 2002). The sample is irradiated by a pulsed, high-energy laser beam, which generates particulate aerosols from solid materials by an extremely rapid interaction between a high-energy laser pulse and the sample surface. The ablation is performed inside an enclosed chamber continuously purged with argon gas. The ablated material is removed

from the ablation chamber (sample cell) by the purge (carrier) gas and swept into the ICP torch where the particles are vaporized, atomized, and ionized in the plasma (Figure 4.7).

Currently, most laser ablation systems utilize either Nd:YAG (neodymium doped yttrium aluminum garnet: $Y_3Al_5O_{12}$) or excimer laser (Durrant, 1999). Neodymium ions in the Nd:YAG crystal are excited to metastable levels in the process of optical pumping, produced by the intense flash of white light from a flash lamp or diode. In this condition, the stimulated emission can take place and the Nd:YAG crystal can act as a laser or as an optical amplifier. For the Nd:YAG laser, the fundamental wavelength is 1064 nm. However, increases in optical frequency produced Nd:YAG laser wavelengths at 532, 355, 266, and 213 nm (Russo et al., 2002).

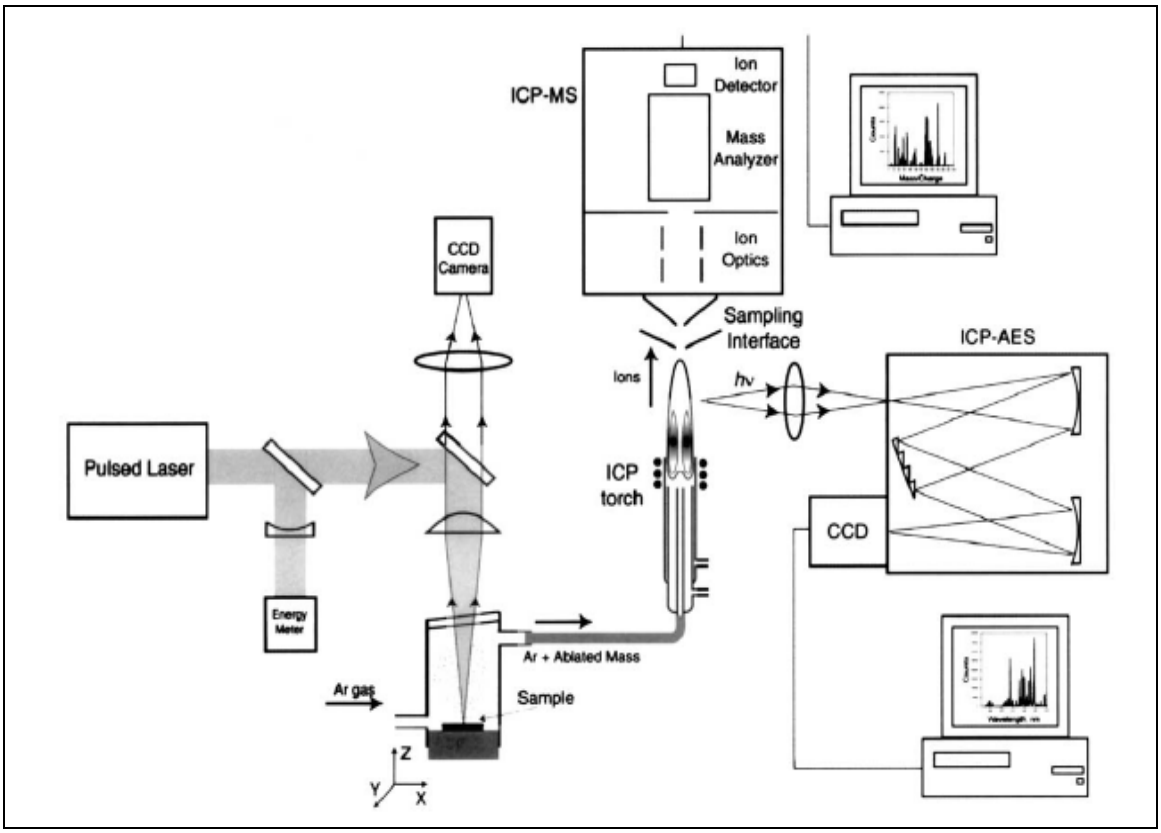

Figure 4.7. Schematic of a laser ablation system with ICP-AES and ICPMS (Russo et al., 2002).

Interactions between the laser radiation and the solid sample depend on laser wavelength, laser energy, and the geometry of the laser beam as well as the heat capacity, heat of vaporization, and thermal conductivity of the sample (Ditrich and Wennrich, 1990). Observations of laser ablation indicated that the ion signals recorded in ICPMS often did not represent the composition of the sample (Durrant, 1999). This phenomenon is called fractionation. Fractionation may occur during ablation, aerosol transport, or the atomization and ionization processes within the ICP. It is strongly dependent on the laser wavelength and irradiance. Fractionation effects are greatly reduced by using a laser wavelength of 213 nm or 193 nm (Russo et al., 2002).

Calibrations against external, well-characterized standards have been used for multi-element LA-ICPMS analysis. NIST produces a number of well-known glass standards that have wide use in geochemical analyses by LA-ICPMS (Russo et al., 2002; Durrant, 1999).

LA Coupled with Magnetic Sector ICPMS

Initially, laser ablation (LA) coupled with a double-focusing magnetic sector ICPMS was used for direct *(in situ)* elemental analysis of desert varnish samples. Magnetic sector ICPMS offers a high level of sensitivity and extremely low background noise, but the analyses are time consuming. In magnetic sector ICPMS, the ions from the ICP enter the instrument through a slit that produces a narrow beam of ions. The ion beam passes through an electrostatic analyzer (ESA) and is both focused and curved. The ESA acts as an effective energy filter, since only ions with a specific kinetic energy are able to pass through. Next, all ions travel into the sector magnet that creates a uniform magnetic field, causing the passing ions to have a similar kinetic energy. Finally, the ion beam

passes through the collector slit situated at the focal point of the magnet. High resolutions are thus achieved by making both of the slits very narrow, resulting in a beam that has a very narrow bandwidth of mass. The high-resolution mass analyzer is called a double focusing system because it is able to focus both energy and mass/charge (Halliday et al., 1998).

LA-ICPMS analysis was conducted using an LSX-213 laser ablation system (CETAC Technologies, Inc., Omaha, NE, USA) interfaced with an Axiom, double-focusing magnetic sector ICPMS which was originally manufactured by VG Elemental (now Thermo Scientific, Waltham, MA, USA). Thirteen isotopes (^{9}Be, ^{107}Ag, ^{111}Cd, ^{118}Sn, ^{121}Sb, ^{184}W, ^{205}Tl, ^{206}Pb, ^{207}Pb, ^{208}Pb, ^{209}Bi, ^{232}Th, ^{238}U) were determined at low mass resolution ($m/\Delta m \approx 400$). To remove any loose particulates from the analyzed surfaces all samples were rinsed with ultra pure water (18 MΩ-cm or better from a Nanopure water system (Barnstead Corporation, Dubuque, IA)) and dried with lint-free paper towels prior to analysis.

The LSX-213 employs a frequency quintupled Nd:YAG laser with a resulting wavelength of 213 nm. The LA-ICPMS system was optimized for sensitivity (e.g. gas flows, torch position) prior to sample analysis using NIST glass SRM 614. Instrumental settings are summarized in Table 4.2. Briefly, the LA unit was operated at its full energy setting (100%), with a repetition rate of 20 Hz, a spot size of 100 µm, and a scan rate of 25 $\mu m \cdot sec^{-1}$, whereas the ICP-MS was operated in low resolution ($m/\Delta m \approx 400$) and magnetic scanning mode (10 ms dwell time, 0.2 peak widths).

The ICPMS was calibrated with a set of multi-element NIST SRM glass standards (NIST SRM 61X series) (Figure 4.8). These standards have been well characterized in

LA-ICPMS studies and provide reliable calibrations for analysis of geological materials (Flem et al., 2002; Wayne et al., 2006). The certified values for the SRMs were used; and when that information was unavailable, consensus values were used. Aluminum-27 was used as an internal standard (IS).

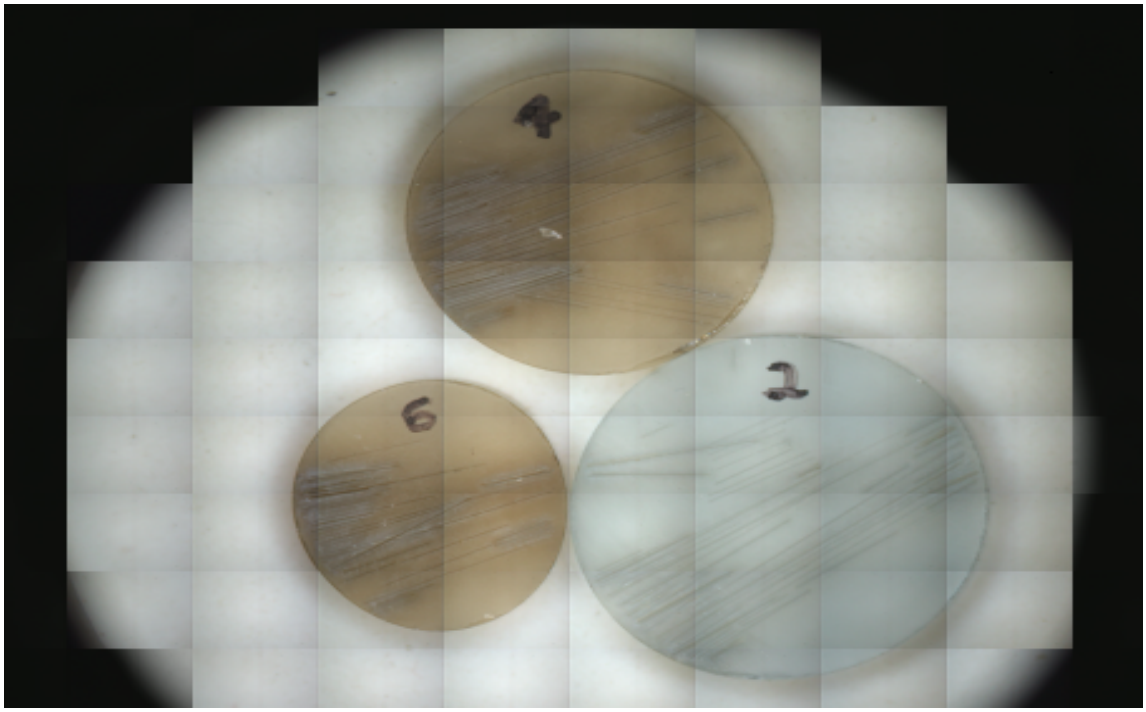

Figure 4.8. Overhead image of NIST glass reference materials situated in the laser ablation chamber: (6) NIST SRM 616; (4) NIST SRM 614; (2) NIST SRM 612. Note that ablation scans are visible on the surface of the glass wafers.

Data were collected for three ablation scans using continuous-line ablations to average the sample variability. Site selection, laser focusing, and ablation parameters were monitored in real time by a camera aimed down the laser axis. Within each line scan were ten analytical runs, each consisting of 10 ms of signal collection per mass, plus the time it took the ICP-MS to move between the masses, plus the time required for the software to "process" the data at the end of the run. Combined, the data collection and

peak jumping time was relatively fast (~5 s), corresponding to <125 µm in varnished rock distance (at a scan rate of 25 µm·sec^{-1}). Thus, the data were collected from essentially the same location on the rock surface, increasing the appropriateness of using an internal standard for the correction of varying mass transport. This process was repeated three times for each rock sample (Figure 4.9). Argon gas blanks were analyzed between each sample to prevent sample cross-contamination and to assess the memory effects.

Figure 4.9. Image of a varnished rock sample showing ablation tracks.

SRM 612 was used to verify the validity of the calibration curve and instrument memory effects (10% of the sample frequency). Argon gas blanks were used as continuous calibration blanks (CCB). A minimum recovery of 80% for all elements was considered acceptable. The MDLs were calculated based on replicate measurements (n=10) of argon gas blanks and the slope of the calibration curve (3σ).

Table 4.2 Laser and Axiom ICPMS operating conditions.

Laser ablation parameters	
Laser type	Nd:YAG
Wavelength	213 nm
Pulse Width	5 ns
Laser energy	>4.0 mJ/pulse
Pulse Rate	20 Hz
Spot size	100 μm
Scan rate	25 $\mu m \cdot s^{-1}$
Energy setting	100%
Plasma parameters	
RF power	1.2 kW
Cooling gas flow	14 $L \cdot min^{-1}$
Auxiliary gas flow	1.2 $L \cdot min^{-1}$
Nebulizer gas flow	1.2 $L \cdot min^{-1}$
Data acquisition	
Masses monitored	9, 27, 107, 111, 118, 121, 138, 184, 205, 206, 207, 208, 232, 238
Dwell time	10 ms
Points/peak	1
Sweeps	1
Runs	10
Total acquisition time per run	0.9 s
Mass spectrometer settings	
Mass resolution	400 ($m/\Delta m$)
Ion Energy	4970
Transfer 1	4123
Transfer 2	4200
X deflection 1	-6
X deflection 2	38
Curve lens	21
X lens	-1740
Multiplier	-2251

LA-Quadrupole ICPMS

After magnetic sector ICPMS analysis, the LA system was coupled with a quadrupole ICPMS. The quadrupole ICPMS instrument can scan the mass spectrum efficiently, allowing for fast and reliable multi-element analysis. The quadrupole mass analyzer

consists of two pairs of cylindrical rods onto which RF and DC electrical fields are applied. The RF and DC fields are carefully matched so that only ions of a particular mass are able to resonate at the correct frequency and pass through the system. The instrument is able to move from mass to mass quickly and precisely; that allows for the "peak hopping" technique, an acquisition of a single point of data at the top of the mass peak. Quadrupole systems are able to detect trace elements consistently in the low-ppb range (Cottingham, 2004).

LA-ICPMS analysis was conducted using an LSX-213 laser ablation system (CETAC Technologies, Inc., Omaha, NE, USA) interfaced with an ELAN 6100 DRC, quadrupole ICPMS (PerkinElmerSCIEX Instruments, Concord, Ontario, Canada). Concentrations of 25 isotopes (^{9}Be, ^{51}V, ^{52}Cr, ^{59}Co, ^{60}Ni, ^{65}Cu, ^{66}Zn, ^{88}Sr, ^{98}Mo, ^{107}Ag, ^{111}Cd, ^{115}In, ^{118}Sn, ^{121}Sb, ^{133}Cs, ^{138}Ba, ^{184}W, ^{197}Au, ^{205}Tl, ^{206}Pb, ^{207}Pb, ^{208}Pb, ^{209}Bi, ^{232}Th, and ^{238}U) were determined in the varnish samples.

The same LSX-213 laser settings were used as in the varnish analysis with the Axiom ICPMS. The LA-ICPMS system was optimized for sensitivity (e.g. gas flows, torch position) prior to sample analysis using NIST glass SRM 614. Instrumental settings are summarized in Table 4.3. The ICPMS was calibrated with a set of multi-element NIST SRM glass standards (NIST SRM 61X series). The certified values for the SRMs were used; and when that information was unavailable, consensus values were used.

Table 4.3 Laser and Elan DRC 6100 ICPMS operating conditions.

Laser ablation parameters	
Laser type	Nd:YAG
Wavelength	213 nm
Pulse Width	5 ns
Laser energy	>4.0 mJ/pulse
Pulse Rate	20 Hz
Spot size	100 μm
Scan rate	25 $\mu m \cdot s^{-1}$
Energy setting	100%
Plasma parameters	
RF power	1.3 kW
Cooling gas flow	15 $L \cdot min^{-1}$
Auxiliary gas flow	0.95 $L \cdot min^{-1}$
Nebulizer gas flow	1.2 $L \cdot min^{-1}$
Data acquisition	
Masses monitored	9, 51, 52, 59, 60, 65, 66, 88, 98, 107, 111, 118, 121, 133, 138, 197, 205, 206, 207, 208, 209, 232, 238
Scan mode	Peak hopping
Dwell time	100 ms
Integration time	1500 ms
Sweeps/Reading	15
Replicates	3
Dead Time	70 ns
Total acquisition time per run	42 s
Mass spectrometer settings	
Mass resolution	0.7
Lens Voltage	9
Analog stage voltage	-2150
Pulse stage voltage	2100
Detector	Dual

Data were collected for three ablation scans using continuous-line ablations to average the sample variability. Site selection, laser focusing, and ablation parameters were monitored in real time by a camera aimed down the laser axis. Within each line scan were three analytical runs, each consisting of 15 sweeps with 100 ms of signal

collection per mass. Each analytical run lasted about 42 s, corresponding to a total distance of 1.05 mm in varnished rock distance (at a scan rate of 25 $\mu m \cdot sec^{-1}$). Overall, about 3.15 mm of the rock surface were ablated (3 runs). This process was repeated three times for each rock sample.

Inductively Coupled Plasma Mass Spectroscopy (ICPMS)

The ICPMS determination of total metal content in the rock varnish required dissolution of the varnish coatings. The varnish samples were stripped from the base rock with high purity 12 M HCl (Seastar Chemicals, Inc., Sidney, BC, Canada) and diluted five-fold with 2% high purity nitric acid (EM Science, Gibbstown, NJ) prepared with ultra pure water (18 MΩ-cm or better from a Nanopure water system (Barnstead Corporation, Dubuque, IA)). All varnish samples were prepared and analyzed in triplicate.

Moisture content of the varnished rocks was determined as the average weight loss after heating the samples at 145ºC in a laboratory oven (Cole-Parmer, Vernon Hills, IL) until a constant weight was obtained (~ 80 min.). The mass of the rocks was determined using a certified analytical balance (Sartorius, Goettingen, Germany).

Each dried rock sample was placed in a 250-mL Teflon® beaker, with the varnished surface facing the bottom. A 10-mL aliquot of concentrated HCl was added and the beaker was heated on a hotplate (Thermo Fisher Scientific, Rochester, NY) until all of the particulates were dissolved (~ 5 min). The beaker was rinsed with three 10-mL aliquots of 2% nitric acid. The rinsate was transferred to a pre-weighed, 50-mL plastic vial (Thermo Fisher Scientific, Rochester, NY) and diluted to approximately 50g with 2% nitric acid. The stripped rock samples were dried at 145°C to constant weight. The mass

of the removed varnish material was determined as the weight loss after stripping and drying.

The ICPMS instrument used was an ELAN 6100 DRC (PerkinElmerSCIEX Instruments, Concord, Ontario, Canada), with a CETAC U-5000 AT^{+} ultrasonic nebulizer (CETAC Technologies, Inc., Omaha, NE) and an AS-90 Plus autosampler. ELAN 2.3.2 was the software used.

The ELAN 6100 DRC was optimized daily with a tuning solution containing 1 $\mu g \cdot L^{-1}$ of the following elements in 0.5% nitric acid: Be, Mg, Co, In, Ba, Ce, and Pb. The nebulizer gas flow was adjusted so that the CeO^{+}/Ce^{+} ratio was < 3%. Next, the lens was optimized for In^{+}. The minimum conditions for acceptable performance were: In^{+} counts/s = 130000 with CeO^{+}/Ce^{+} and Ba^{++}/Ba^{+} < 3%.

Standard stock solutions (10 $mg \cdot L^{-1}$) were purchased from SPEX CertiPrep (Metuchen, NJ). High purity nitric acid was purchased from EM Science (Gibbstown, NJ). All standards were prepared by a dilution of the stock standard with 2% nitric acid.

The ELAN software provides a semi-quantitative (TotalQuant®) method for the rapid analysis of total unknowns. The technique allows for analysis of 81 elements in a single measurement. The software automatically corrects for isotopic interferences. The following mass ranges were scanned by the ELAN instrument: 6-15, 19-39, 42-210, and 230-240. The instrument was mass calibrated with a 1 $\mu g \cdot L^{-1}$ multi-element standard (SPEX CertiPrep, Metuchen, NJ). The TotalQuant® calibration uses stored responses to correlate measured ion intensities with known concentration values.

Data were collected in the peak hopping mode in a single analytical run, consisting of 25 sweeps with 50 ms of signal collection per mass. The analytical run lasted for about 60 s. Instrumental settings are summarized in Table 4.4.

Table 4.4 Elan DRC 6100 ICPMS TotalQuant® operating conditions.

Nebulizer parameters	
Nebulizer type	CETAC ultrasonic
Pump tubing	0.45 mm i.d.
Pump speed	45 rev./min
Plasma parameters	
RF power	1.3 kW
Plasma gas flow	15 $L \cdot min^{-1}$
Auxiliary gas flow	1.25 $L \cdot min^{-1}$
Nebulizer gas flow	0.92 $L \cdot min^{-1}$
Data acquisition	
Masses monitored	6-15; 19-39; 42-210; 230-240
Scan mode	Peak hopping
Dwell time	50 ms
Points/Peak	1
Sweeps/reading	1
Replicates	1
Total acquisition time per run	60 s
Mass spectrometer settings	
Mass resolution	0.7
Lens voltage	9
Analog stage voltage	-2150
Pulse stage voltage	2100
Detector	Dual

Following the semi-quantitative analysis, twenty-seven isotopes were determined quantitatively. The HCl solutions were filtered through a 0.45-µm syringe filter prior to ICPMS analysis and were analyzed for 25 elements (27 isotopes): ^{9}Be, ^{51}V, ^{52}Cr, ^{58}Ni, ^{59}Co, ^{63}Cu, ^{66}Zn, ^{75}As, ^{88}Sr, ^{98}Mo, ^{102}Ru, ^{103}Rh, ^{106}Pd, ^{111}Cd, ^{118}Sn, ^{121}Sb, ^{133}Cs, ^{184}W,

^{187}Re, ^{195}Pt, ^{205}Tl, ^{206}Pb, ^{207}Pb, ^{208}Pb, ^{209}Bi, ^{232}Th, and ^{238}U. Data were collected in peak hopping mode with three analytical runs, each consisting of 20 sweeps with 50 ms of signal collection per mass. Each analytical run lasted about 30 s. Instrumental settings are summarized in Table 4.5.

The ICPMS instrument was calibrated with a calibration blank and a set of five standards (0.5 -15 $\mu g \cdot L^{-1}$) (SPEX CertiPrep, Metuchen, NJ), to achieve a linear correlation coefficient $r^2 \geq 0.995$. The initial calibration verification (ICV) solution was prepared from a different source (High Purity, Charleston, SC, USA) than the calibration standards. Two different types of blanks were used. The calibration blanks (ICB/CCB) were used to establish the analytical curve, while the preparation blank (PB) was used to monitor for possible contamination. The PB contained all of the reagents used during sample preparation and was carried through the complete procedure. Additionally, initial rinse blanks were used to assess memory effects and the baseline. Replicate samples were used to verify the analytical method precision. The QA/QC sample frequency was 10%, with at least 90% recovery for all elements. MDLs were calculated based on replicate measurements (n=10) of water blanks and the slope of the calibration curve ($3\sigma/m$).

Table 4.5 Elan DRC 6100 ICPMS operating conditions.

Nebulizer parameters	
Nebulizer type	CETAC ultrasonic
Pump tubing	0.45 mm i.d.
Pump speed	45 rev./min
Plasma parameters	
RF power	1.3 kW
Plasma gas flow	15 $L \cdot min^{-1}$
Auxiliary gas flow	1.25 $L \cdot min^{-1}$
Nebulizer gas flow	0.92 $L \cdot min^{-1}$
Data acquisition	
Masses monitored	48, 51, 52, 55, 57, 59, 60, 65, 66, 75, 88, 98, 107, 114, 115, 118, 121, 133, 138, 184, 187, 193, 197, 199, 200, 202, 205, 206, 207, 208, 209, 232, 238
Scan mode	Peak hopping
Dwell time	50 ms
Integration time	1250 ms
Sweeps/reading	20
Replicates	3
Dead Time	70 ns
Total acquisition time per run	30 s
Mass spectrometer settings	
Mass resolution	0.7
Lens voltage	9
Analog stage voltage	-2150
Pulse stage voltage	2100
Detector	Dual

Mercury Analysis by Cold Vapor Atomic Absorption (CVAA)

Mercury analysis of the stripped solutions was performed by flow injection CVAA. In the CVAA mercury technique, mercury is chemically reduced to its free atomic state (Hg^0) by reaction with a strong reducing agent in a closed reaction system. The volatile Hg^0 is driven from the solution with argon gas. Mercury atoms are carried by the gas to

the absorption cell of the AA spectrometer. The entire CVAA analysis can be automated using flow injection techniques (Caroli et al., 2000).

The sensitivity of the cold vapor technique is far greater than that of conventional AA. This improved sensitivity is achieved through a 100% sampling efficiency. All of the mercury in the sample solution is chemically atomized and transported to the sample cell for measurement (Beaty and Kerber, 2002).

Mercury analyses were performed using a Flow Injection Mercury System FIMS-100 connected to an AS-91 autosampler (PerkinElmer, Norwalk, CT). The instrument was calibrated daily with a set of five Hg standards (0.5 - 10 $\mu g \cdot L^{-1}$) prepared daily from the 1000 $\mu g \cdot L^{-1}$ Hg stock solution (Ultra Scientific, North Kingstown, RI). The standards were prepared with 2% nitric acid and preserved with 1-2 drops of 5% $KMnO_4$ (EM Science, Gibbstown, NJ). To improve measurement sensitivity, the reducing agent solution was prepared fresh daily by dissolving 25 g of $SnCl_2 \cdot H_2O$ (EM Science, Gibbstown, NJ) in 15 mL of concentrated HCl and diluting to 500 mL with ultra pure water (18 MΩ-cm or better from a Nanopure water system (Barnstead Corporation, Dubuque, IA)). The carrier solution was prepared by dilution of 30 mL of concentrated HCl (J.T. Baker, Philipsburg, NJ) in 1000 mL of ultra pure water. Data were collected in the peak height mode with three analytical runs, each consisting of 20 s of signal collection. The instrument settings are summarized in Table 4.6.

ICV and CCV solutions were analyzed to verify the validity of the calibration curve. The calibration blanks (ICB/CCB) were used to establish the analytical curve, while the preparation blank (PB) was used to monitor for possible contamination. Method accuracy was verified with the NIST SRM 1946, Lake Superior Fish Tissue prepared

along with the samples. Replicate samples were used to verify the analytical method precision. The QA/QC sample frequency was 10%, with at least 90% recovery. The MDLs were calculated based on replicate measurements (n=10) of reagent blanks and the slope of the calibration curve ($3\sigma/m$). All reagents and QA/QC solutions were prepared with ultra pure water (18 MΩ-cm or better from a Nanopure water system (Barnstead Corporation, Dubuque, IA)).

Table 4.6 FIMS-100 Hg CVAA instrument settings.

Lamp	Hg EDL (Electrodeless Discharge Lamp)
Slit (nm)	0.7
Hg wavelength (nm)	253.7
Argon flow ($mL \cdot min^{-1}$)	70
Signal mode	Peak height, Smoothing, 0.5 s, 19 points
Read time	20 s
Reducing Agent	4.1% $SnCl_2$ in 3%(v/v) HCl
Carrier solution	3.0% (v/v) HCl
Loop volume	200 µL
Cell temperature (^oC)	100
Sample dilution	1:1 3.0% (v/v) HCl

CHAPTER 5

DATA ANALYSIS AND DISCUSSION

Introduction

The first purpose of this research, as stated in Chapter 1, was to establish that rock varnish accumulates and preserves a record of airborne heavy elements, and can be used as a passive environmental monitor of relatively recent events. The second purpose of this study was to determine if anthropogenic pollutants are deposited in the varnish's outermost layers and can be traced to their sources, such as coal–fired power plants. The third purpose of this research was to determine whether heavy metals can be quantified in the varnish coatings using field portable X-ray fluorescence spectroscopy (FPXRF), laser ablation-inductively coupled plasma mass spectroscopy (LA-ICPMS), inductively coupled plasma mass spectroscopy (ICPMS), and cold vapor atomic absorption (CVAA) for Hg analysis. These techniques are listed in order of increasing sensitivity. In an attempt to better understand rock varnish properties, the chemical composition of the varnish samples was determined. This chapter presents the analytical results and findings.

XRF Results

All XRF data were collected with a NITON XLi 700 portable X-ray spectrometer (Thermo Fisher Scientific, Billerica, MA). The rock varnish samples were analyzed in two different instrument testing modes: 1) bulk sample, standard soil mode (bulk analysis); and 2) thin sample, standard filter mode (thin surface analysis). The results are reported in $\mu g \cdot g^{-1}$ for bulk analysis and in $\mu g \cdot cm^{-2}$ for thin surface analysis. A total of 16

elements (Ti, Cr, Mn, Fe, Co, Ni, Cu, Zn, As, Se, Rb, Sr, Zr, Mo, Hg, and Pb) were analyzed. Zirconium was analyzed only by bulk analysis and Ti was analyzed only by thin surface analysis.

Method Detection Limit (MDL)

Method detection limits (MDLs) for field portable X-ray fluorescence (FPXRF) analysis are both element and matrix dependent. Generally, XRF detection limits are inversely proportional to analysis time, i.e. longer analysis times give lower detection limits (Kalnicky and Singhvi, 2001). The FPXRF MDLs were calculated from the replicate measurements (n=10) and the standard error (3σ) of the silica (SiO_2) blank material. Estimated MDLs for bulk analyses range from 6.9 $\mu g \cdot g^{-1}$ for Mo to 180 $\mu g \cdot g^{-1}$ for Cr (Figure 5.1). Estimated MDLs for surface analyses range from 0.73 $\mu g \cdot cm^{-2}$ for Rb to 8.3 $\mu g \cdot cm^{-2}$ for Hg (Figure 5.2).

XRF Calibration Check and Quality Assurance

The FPXRF instrument was calibrated by the manufacturer using built-in mathematical algorithms (FP technique). The instrument automatically performs an internal calibration check after each start up. Accuracy and precision of the FPXRF measurements were verified by analysis of duplicates of NIST SRM 2709 San Joaquin Soil (low-level) and SRM 2710 Montana Soil (high-level). For XRF environmental applications, analysis of these soil standards should produce results that are within ± 20% of the certified values for target elements that have concentrations of more than 10 times the MDL (Shefsky, 1997; Kalnicky and Singhvi, 2001).

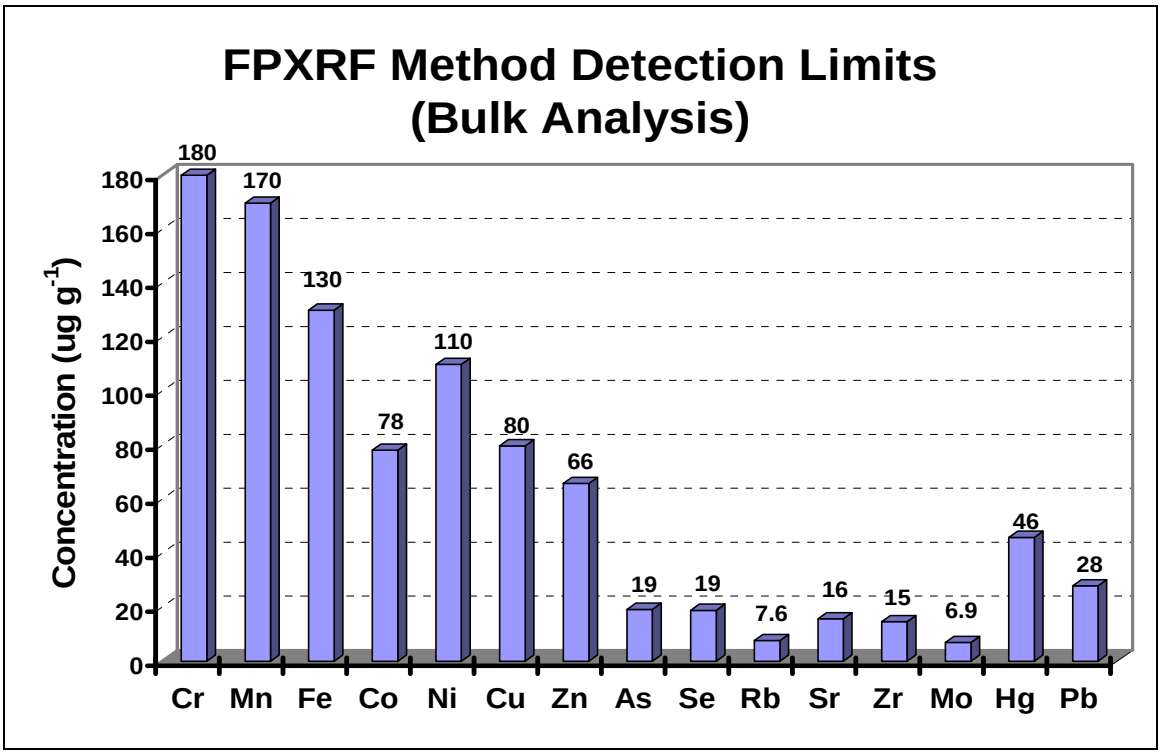

Figure 5.1. Estimated detection limits for FPXRF analysis (bulk analysis) of desert varnish samples.

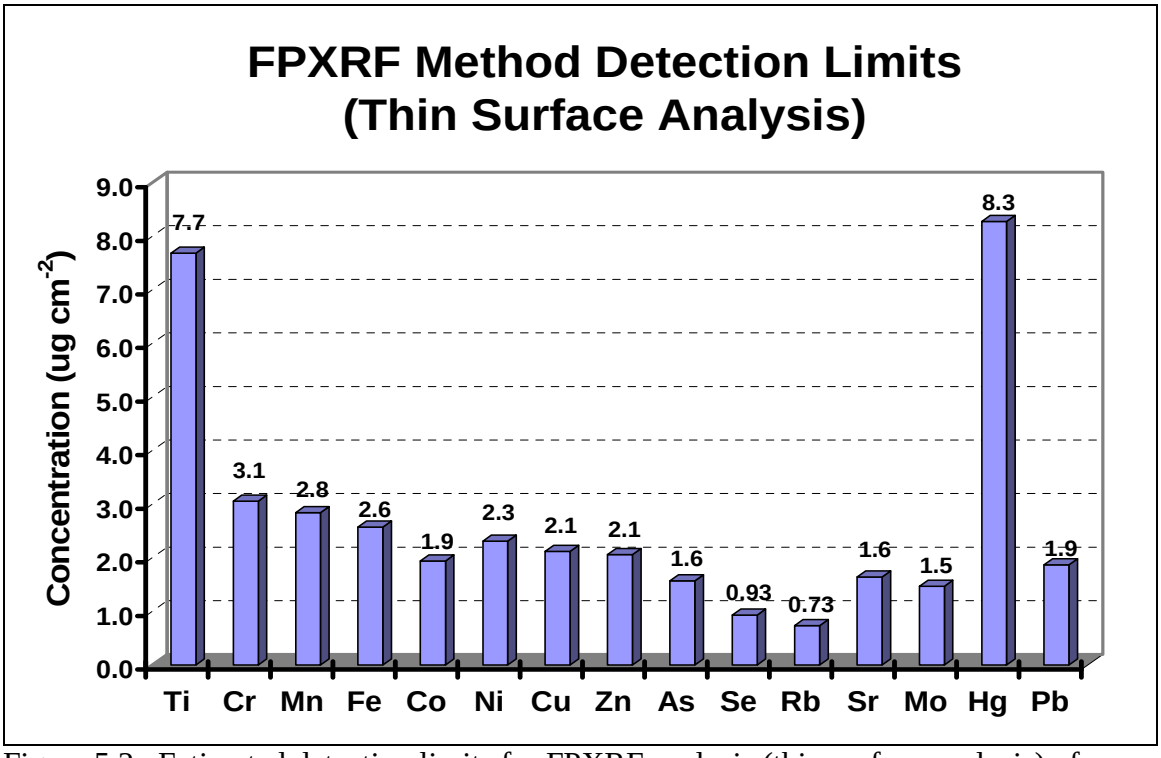

Figure 5.2. Estimated detection limits for FPXRF analysis (thin surface analysis) of desert varnish samples.

To examine the validity of the XRF method, elemental concentrations were obtained for each SRM using the desired SRM as an unknown. Five elements (Fe, Mn, Sr, Zr, and Rb) in low-level SRM 2709 San Joaquin Soil show good agreement with certified or consensus values and their percent recoveries range from 78% for Fe to 118% for Zr (Table 5.1). The certified values for 10 elements in SRM 2709 are reported below the estimated FPXRF MDLs (Cr, Co, Ni, Cu, Zn, As, Se, Mo, Hg, and Pb). Consequently, the percent recoveries for some analytes are outside the acceptable range of 80 to 120 %: Cr (111% and 77%); Co (999% and 562%), Ni (67% and 70%), Cu (75% and 118%), Zn (64% and 56%), As (125% and 82%); Se (306% and 172%), Pb (60 % and 132%), Mo and Hg are undetected. On the other hand, excellent agreement with certified or consensus values is obtained for high-level SRM 2710 Montana Soil (Table 5.1). Recoveries for eight analytes (Mn, Fe, Cu, Zn, As, Rb, Sr, and Pb) range from 79% for Rb to 105% for As. The certified values for six elements in SRM 2710 (Cr, Co, Ni, Se, Mo, and Hg) are reported below the FPXRF MDLs. As a result, Cr and Mo values are outside the acceptable range (80 to 120 %), and four elements (Co, Ni, Se, and Hg) are undetected. No certified values are available for Zr.

The precision of the XRF method was verified by calculating a relative percent difference (RPD) between duplicate measurements of SRM 2709 San Joaquin Soil and SRM 2710 Montana Soil (Table 5.1). An RPD below 20% is considered acceptable for environmental analysis (Taylor, 1987). Seven elements in SRM 2709 San Joaquin Soil (Mn, Fe, Ni, Zn, Rb, Sr, and Zr) have RPDs below the acceptable limit of 20%. The RPDs are outside the acceptable limit for: Cr (36%), Co (56%), Cu (46%), As (41%), Se (56%), Pb (74%), Mo and Hg are undetected so their RPDs are not available.

Conversely, the majority of the elements in SRM 2710 Montana Soil have RPDs within the acceptable limit, except for Cr (149%). Four elements (Co, Ni, Se, and Hg) are undetected and the RPDs cannot be determined. This gives confidence that the method is suitable for elements with concentrations above the MDL and provides reasonably accurate and precise results.

Table 5.1. FPXRF results for NIST SRM 2709 and 2710 soil reference materials. Concentrations are reported in $\mu g \cdot g^{-1}$.

Element	NIST SRM 2709 San Joaquin Soil					
	Found	Found	Certified or ref value	% Rec.	% Rec.	RPD
Fe	27000 ± 370	27000 ± 370	35000 ± 1100	78	78	0
Mn	430 ± 180	490 ± 180	538 ± 17	80	91	13
Sr	210 ± 9	200 ± 9	231 ± 2	92	87	5
Zr	180 ± 11	190 ± 11	(160)	111	118	6
Pb	11 ± 9	25 ± 10	18.9 ± 0.5	60	132	74
Zn	68 ± 22	59 ± 22	106 ± 3	64	56	14
Rb	80 ± 6	83 ± 6	(160)	83	86	4
Ni	59 ± 47	62 ± 47	88 ± 5	67	70	4
Co	130 ± 110	75 ± 110	13.4 ± 0.7	999	562	56
As	22 ± 7	15 ± 7	17.7 ± 0.8	125	82	41
Cr	140 ± 92	100 ± 90	130 ± 0.4	111	77	36
Se	4.8 ± 5.6	2.7 ± 5.4	1.57 ± 0.08	306	172	56
Hg	NA	NA	1.40 ± 0.08	NA	NA	NA
Mo	0.74 ± 2.3	NA	(2.0)	35	NA	NA
Cu	26 ± 25	41 ± 25	34.6 ± 0.7	75	118	46

Element	NIST SRM 2710 Montana Soil					
	Found	Found	Certified or ref value	% Rec.	% Rec.	RPD
Fe	3300 ± 480	3300 ± 490	33800 ± 1000	99	99	0
Mn	10000 ± 390	9700 ± 390	10100 ± 400	99	96	3
Sr	290 ± 13	300 ± 13	(330)	89	90	1
Zr	160 ± 14	160 ± 14	NA	NA	NA	0
Pb	5300 ± 97	5300 ± 98	5532 ± 80	96	96	0
Zn	6700 ± 120	6700 ± 120	6952 ± 91	96	97	0
Rb	95 ± 9	100 ± 10	(120)	79	87	10
Ni	NA	38 ± 67	14.3 ± 1.0	NA	268	NA
Co	NA	NA	(10)	NA	NA	NA
As	600 ± 68	660 ± 69	626 ± 38	96	105	8
Cr	15 ± 169	100 ± 173	(39)	38	264	149
Se	NA	NA	NA	NA	NA	NA
Hg	NA	NA	32.6 ± 1.8	NA	NA	NA
Mo	11 ± 3	10 ± 3	(19)	59	51	15
Cu	2800 ± 94	2800 ± 96	2950 ± 91	96	97	0

Values in parentheses are "informational" values and do not have uncertainties associated with them. Found values are ± 1 SD. Certified or consensus values are ± 95% confidence limit. NA = Not Available.

Sample Data

Bulk analysis concentrations of 15 elements (Cr, Mn, Fe, Co, Ni, Cu, Zn, As, Se, Rb, Sr, Zr, Mo, Hg, and Pb) in 26 samples of desert varnish are found in Table 5.2. Both varnished and unvarnished surfaces of the same sample were analyzed and the concentration ratios are calculated for each element. As expected, the highest concentrations are observed for Fe (3.9 x 10^3 to 3.5 x 10^5 $\mu g \cdot g^{-1}$) and Mn (ND to 3.0 x 10^4 $\mu g \cdot g^{-1}$) in varnished rocks. Three elements: Fe, Sr, and Zr are detected in every varnished sample. Manganese is not detected in sample NTS 1, but the Fe concentration in this sample is extremely high (3.5 x 10^5 $\mu g \cdot g^{-1}$), and the high Fe signal probably interfered with the Mn peak (Figure 5.3). Mercury is not detected in any sample. Molybdenum is detected only in sample NTS 1, and Se is detected only in sample TIMET 4.

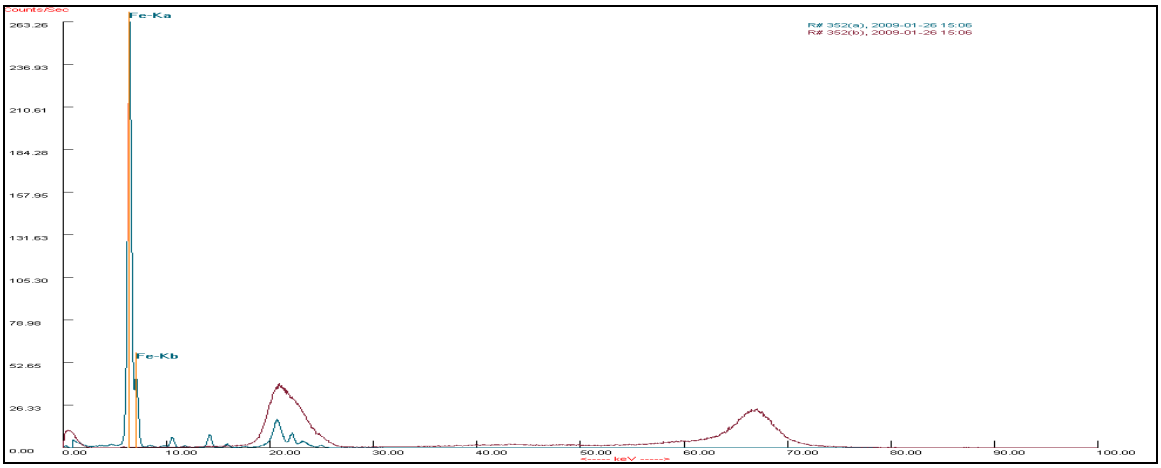

Figure 5.3. EDXRF spectra for sample NTS 1. The high narrow peak represents the Fe signal.

From Table 5.2 and the graphs of the elemental ratios (Figures in Exhibit 1), it is apparent that the concentration ratios of Zn, As and Pb are consistently higher for most of

the varnishes when compared to the unvarnished surface. For example, in the set of 26 varnish samples, Zn is found to be higher in 16 samples, As is higher in 12 samples, and Pb is found to be higher in 24 samples of the varnished rocks. Higher ratios of these elements in the skyward facing varnished surfaces may point to trace element deposition from the atmosphere. Ratios of strontium and zirconium are generally close to one, showing no enrichment of these elements in the varnishes. In 12 of the samples, Rb ratios have a value of less than 1, which could indicate depletion from the varnishes of this highly soluble element by precipitation, as suggested by Thiagarajan and Lee (2004).

Thin surface analysis generally confirmed results of the bulk analysis, but the MDLs are higher and some elements are undetected (Ni, As, Se, Mo, and Hg). Thin surface analysis concentrations of 15 elements (Ti, Cr, Mn, Fe, Co, Ni, Cu, Zn, As, Se, Rb, Sr, Mo, Hg, and Pb) in 15 samples of desert varnish are presented in Table 5.3.

Again, the highest concentrations are observed for Fe (97 to 1.8 x 10^3 $\mu g \cdot cm^{-2}$) and Mn (16 to 480 $\mu g \cdot cm^{-2}$) in varnished rocks. Three elements: Ti, Fe, and Sr are detected in every varnished sample. Manganese is not detected in seven unvarnished rocks. Copper is detected only in sample RGPP 5 and Co is detected only in sample BKG 1.

From Table 5.3 and the graphs of the elemental ratios (Figures in Exhibit 1), it is clear that the concentration of Pb is consistently higher in most of the varnishes. In the set of 15 samples, Pb is higher in 14 samples, Zn is found to be higher only in three samples, and As is undetected. Ratios of Ti and Sr are generally close to 1, showing no substantial enrichment or depletion of these elements in the varnishes. Rubidium ratios are mixed and no apparent trend is observed.

Table 5.2. FPXRF results for bulk analysis of desert varnish samples. Concentrations are reported in $\mu g \cdot g^{-1}$.

Element	Sample	NTS 1			NTS 2			NTS 3		
	MDL	Varnished	Unvarnished	Ratio	Varnished	Unvarnished	Ratio	Varnished	Unvarnished	Ratio
Mo	6.9	28	4.5	6.1	ND	ND	NA	ND	ND	NA
Sr	16	860	800	1.1	170	160	1.1	50	45	1.1
Rb	7.6	ND	12	0.64	160	170	1.0	150	140	1.1
Pb	28	ND	ND	NA	58	34	1.7	100	ND	3.6
Se	19	ND	ND	NA	ND	ND	NA	ND	ND	NA
As	19	1100	59	19	16	ND	0.83	28	ND	1.0
Hg	46	ND	ND	NA	ND	ND	NA	ND	ND	NA
Zn	66	ND	ND	NA	63	33	1.9	76	42	1.8
Cu	80	ND	ND	NA	ND	ND	NA	ND	ND	NA
Ni	110	ND	ND	NA	ND	ND	NA	ND	ND	NA
Co	78	ND	ND	NA	ND	ND	NA	ND	ND	NA
Fe	130	350000	5900	59	8200	6200	1.3	11000	5400	2.1
Mn	170	ND	ND	NA	4900	190	26	6300	200	32
Cr	180	ND	ND	NA	ND	ND	NA	ND	ND	NA
Zr	15	93	120	0.76	160	190	0.84	340	300	1.1

Element	Sample	TIMET 1			TIMET 2			TIMET 3		
	MDL	Varnished	Unvarnished	Ratio	Varnished	Unvarnished	Ratio	Varnished	Unvarnished	Ratio
Mo	6.9	ND	ND	NA	ND	ND	NA	ND	ND	NA
Sr	16	820	500	1.7	492	489	1.0	460	610	0.8
Rb	7.6	90	100	0.9	94	89	1.1	110	85	1.2
Pb	28	120	200	0.6	192	29	6.5	110	29	3.9
Se	19	ND	ND	NA	ND	ND	NA	ND	ND	NA
As	19	21	46	0.5	35	11	3.3	ND	ND	NA
Hg	46	ND	ND	NA	ND	ND	NA	ND	ND	NA
Zn	66	96	84	1.2	74	64	1.2	130	71	1.8
Cu	80	81	48	1.7	ND	ND	NA	45	47	1.0
Ni	110	ND	ND	NA	ND	ND	NA	ND	ND	NA
Co	78	ND	ND	NA	ND	ND	NA	62	36	1.7
Fe	130	42000	17000	2.4	17000	11000	1.5	13000	6600	2.0
Mn	170	13000	8300	1.6	8200	370	22	6300	170	36
Cr	180	130	270	0.5	110	130	0.8	110	120	0.9
Zr	15	580	610	0.9	600	530	1.1	510	380	1.3

Element	Sample	TIMET 4			BKG 1			BKG 2		
	MDL	Varnished	Unvarnished	Ratio	Varnished	Unvarnished	Ratio	Varnished	Unvarnished	Ratio
Mo	6.9	ND	ND	NA	ND	ND	NA	ND	ND	NA
Sr	16	1200	1200	1.0	460	430	1.1	66	140	0.5
Rb	7.6	50	73	0.7	150	150	1.0	40	19	2.1
Pb	28	163	37	4.4	67	43	1.6	41	18	2.2
Se	19	1.4	3.1	0.4	ND	ND	NA	ND	ND	NA
As	19	51	0.73	2.6	ND	ND	NA	12	ND	0.6
Hg	46	ND	ND	NA	ND	ND	NA	ND	ND	NA
Zn	66	150	140	1.1	58	ND	0.9	89	ND	1.4
Cu	80	33	44	0.8	ND	ND	NA	40	ND	0.5
Ni	110	ND	ND	NA	ND	ND	NA	54	ND	0.5
Co	78	ND	97	0.8	ND	ND	NA	ND	ND	NA
Fe	130	37000	31000	1.2	26000	18000	1.4	14000	2500	5.7
Mn	170	7500	700	11	1700	ND	10	2000	ND	12
Cr	180	290	200	1.5	ND	ND	NA	200	ND	1.1
Zr	15	460	480	0.9	660	560	1.2	840	330	2.6

ND = Not Detected. NA = Not Available.

Table 5.2. (cont.). FPXRF results for bulk analysis of desert varnish samples. Concentrations are reported in $\mu g \cdot g^{-1}$.

Element	Sample	MPP 1			MPP 2			MPP 3		
	MDL	Varnished	Unvarnished	Ratio	Varnished	Unvarnished	Ratio	Varnished	Unvarnished	Ratio
Mo	6.9	ND	ND	NA	ND	ND	NA	ND	ND	NA
Sr	16	1200	1100	1.2	260	240	1.1	1500	1500	1.0
Rb	7.6	65	77	0.8	260	310	0.8	54	65	0.8
Pb	28	310	26	11.7	84	ND	3.0	93	68	1.4
Se	19	ND	ND	NA	ND	ND	NA	ND	ND	NA
As	19	84	ND	4.4	37	15	2.6	ND	ND	NA
Hg	46	ND	ND	NA	ND	ND	NA	ND	ND	NA
Zn	66	92	ND	4.8	ND	ND	NA	134	147	0.9
Cu	80	ND	ND	NA	60	84	0.7	62	85	0.7
Ni	110	ND	ND	NA	52	ND	0.5	105	1.2	90
Co	78	ND	ND	NA	ND	ND	NA	ND	ND	NA
Fe	130	31000	19000	1.7	68000	16000	4.3	40000	34000	1.2
Mn	170	7900	440	18	6900	ND	41	21000	4900	4.3
Cr	180	ND	ND	NA	770	ND	4.3	280	410	0.7
Zr	15	540	480	1.1	280	250	1.1	780	830	0.9

Element	Sample	MPP 4			MPP 5			MPP 6		
	MDL	Varnished	Unvarnished	Ratio	Varnished	Unvarnished	Ratio	Varnished	Unvarnished	Ratio
Mo	6.9	ND	ND	NA	ND	ND	NA	ND	ND	NA
Sr	16	490	370	1.3	430	350	1.2	150	140	1.1
Rb	7.6	78	25	3.1	75	120	0.6	180	90	2.0
Pb	28	49	ND	1.8	520	56	9.3	92	33	2.8
Se	19	ND	ND	NA	ND	ND	NA	ND	ND	NA
As	19	18	ND	0.9	135	ND	7.0	ND	ND	NA
Hg	46	ND	ND	NA	ND	ND	NA	ND	ND	NA
Zn	66	ND	ND	NA	42	ND	0.6	230	ND	3.5
Cu	80	65	ND	0.8	59	ND	0.7	53	ND	0.7
Ni	110	ND	ND	NA	64	ND	0.6	ND	ND	NA
Co	78	ND	ND	NA	ND	ND	NA	ND	ND	NA
Fe	130	66000	61000	1.1	37000	14000	2.6	78000	23000	3.3
Mn	170	8700	630	14	13000	340	37	1800	ND	11
Cr	180	ND	ND	NA	550	ND	3.1	ND	ND	NA
Zr	15	160	160	1.0	330	400	0.8	240	500	0.5

Element	Sample	RGPP 1			RGPP 2			RGPP 3		
	MDL	Varnished	Unvarnished	Ratio	Varnished	Unvarnished	Ratio	Varnished	Unvarnished	Ratio
Mo	6.9	ND	ND	NA	ND	ND	NA	ND	ND	NA
Sr	16	48	35	1.4	56	70	0.8	80	42	1.9
Rb	7.6	240	230	1.1	82	86	1.0	31	40	0.8
Pb	28	180	34	5.4	45	14	3.1	22	12	1.9
Se	19	ND	ND	NA	ND	ND	NA	ND	ND	NA
As	19	ND	ND	NA	ND	ND	NA	ND	ND	NA
Hg	46	ND	ND	NA	ND	ND	NA	ND	ND	NA
Zn	66	98	39	2.5	ND	ND	NA	69	48	1.4
Cu	80	30	93	0.3	ND	ND	NA	ND	ND	NA
Ni	110	ND	ND	NA	ND	ND	NA	ND	ND	NA
Co	78	ND	ND	NA	ND	ND	NA	ND	ND	NA
Fe	130	15000	8200	1.8	3900	1600	2.5	6300	3600	1.8
Mn	170	6800	410	17	4200	230	18	3300	ND	19
Cr	180	120	ND	0.6	ND	ND	NA	ND	ND	NA
Zr	15	350	330	1.1	140	210	0.7	81	130	0.6

ND = Not Detected. NA = Not Available.

Table 5.2. (cont.). FPXRF results for bulk analysis of desert varnish samples. Concentrations are reported in $\mu g \cdot g^{-1}$.

Element	Sample	MPP 5a			MPP 7			MPP 8		
	MDL	Varnished	Unvarnished	Ratio	Varnished	Unvarnished	Ratio	Varnished	Unvarnished	Ratio
Mo	6.9	ND	ND	NA	ND	ND	NA	ND	ND	NA
Sr	16	180	160	1.1	270	250	1.1	570	470	1.2
Rb	7.6	250	260	1.0	35	54	0.6	78	120	0.7
Pb	28	140	39	3.7	130	31	4.3	100	36	2.8
Se	19	ND	ND	NA	ND	ND	NA	ND	ND	NA
As	19	33	ND	1.7	35	ND	1.8	31	ND	1.6
Hg	46	ND	ND	NA	ND	ND	NA	ND	ND	NA
Zn	66	130	ND	2.0	140	95	1.4	87	ND	1.3
Cu	80	66	ND	0.8	ND	ND	NA	65	ND	0.8
Ni	110	ND	ND	NA	ND	ND	NA	76	ND	0.7
Co	78	ND	ND	NA	ND	ND	NA	ND	ND	NA
Fe	130	45000	27000	1.7	120000	85000	1.5	28000	13000	2.1
Mn	170	19000	370	52	9600	950	10	25000	ND	148
Cr	180	ND	ND	NA	ND	ND	NA	360	ND	2.0
Zr	15	910	800	1.1	22	93	0.2	380	450	0.8

Element	Sample	MPP 9			MPP 10			RGPP 4		
	MDL	Varnished	Unvarnished	Ratio	Varnished	Unvarnished	Ratio	Varnished	Unvarnished	Ratio
Mo	6.9	ND	ND	NA	ND	ND	NA	ND	ND	NA
Sr	16	86	170	0.5	130	98	1.3	19	10	1.9
Rb	7.6	35	47	0.7	170	200	0.9	11	4.2	2.5
Pb	28	3300	41	80	84	ND	3.0	35	ND	1.2
Se	19	ND	ND	NA	ND	ND	NA	ND	ND	NA
As	19	490	ND	26	24	20	1.2	ND	ND	NA
Hg	46	ND	ND	NA	ND	ND	NA	ND	ND	NA
Zn	66	190	56	3.4	ND	ND	NA	ND	ND	NA
Cu	80	190	ND	2.4	140	47	3.0	ND	ND	NA
Ni	110	ND	ND	NA	ND	ND	NA	ND	ND	NA
Co	78	ND	ND	NA	ND	ND	NA	ND	ND	NA
Fe	130	340000	59000	5.7	26000	13000	2.0	12000	740	16
Mn	170	30000	ND	179	4300	ND	25	11000	ND	62
Cr	180	1100	ND	6.1	ND	170	1.1	ND	ND	NA
Zr	15	200	630	0.3	210	260	0.8	33	ND	2.3

Element	Sample	RGPP 5			RGPP 6		
	MDL	Varnished	Unvarnished	Ratio	Varnished	Unvarnished	Ratio
Mo	6.9	ND	ND	NA	ND	ND	NA
Sr	16	41	44	0.9	12	ND	0.7
Rb	7.6	230	120	2.0	10	2.9	3.4
Pb	28	130	25	5.3	63	ND	2.3
Se	19	ND	ND	NA	ND	ND	NA
As	19	28	ND	1.5	20	ND	1.0
Hg	46	ND	ND	NA	ND	ND	NA
Zn	66	190	68	2.8	ND	ND	NA
Cu	80	51	ND	0.6	ND	ND	NA
Ni	110	110	ND	1.0	ND	ND	NA
Co	78	ND	ND	NA	ND	ND	NA
Fe	130	21000	5900	3.5	7200	260	28
Mn	170	17000	2800	6.2	3700	ND	22
Cr	180	ND	ND	NA	140	ND	0.8
Zr	15	1700	290	6.0	45	42	1.1

ND = Not Detected. NA = Not Available.

Table 5.3. FPXRF results for thin surface analysis of desert varnish samples. Concentrations are reported in $\mu g \cdot cm^{-2}$.

Element	Sample	MPP 2			MPP 3			MPP 5		
	MDL	Varnished	Unvarnished	Ratio	Varnished	Unvarnished	Ratio	Varnished	Unvarnished	Ratio
Mo	1.5	ND	ND	NA	ND	ND	NA	ND	ND	NA
Sr	1.6	13	11	1.2	76	65	1.2	9.4	9.3	1.0
Rb	0.73	12	10	1.3	2.4	2.5	1.0	12	14	0.9
Pb	1.9	3.3	ND	1.8	2.9	2.2	1.3	5.3	1.6	3.3
Se	0.93	ND	ND	NA	ND	ND	NA	ND	ND	NA
As	1.6	ND	ND	NA	ND	ND	NA	ND	ND	NA
Hg	8.3	ND	ND	NA	ND	ND	NA	ND	ND	NA
Zn	2.1	ND	ND	NA	2.0	1.9	1.1	2.0	ND	1.0
Cu	2.1	ND	ND	NA	ND	ND	NA	ND	ND	0.5
Ni	2.3	ND	ND	NA	ND	ND	NA	ND	ND	NA
Co	1.9	ND	ND	NA	ND	ND	NA	ND	ND	NA
Fe	2.6	650	120	5.5	390	280	1.4	460	300	1.5
Mn	2.8	45	1.7	26	180	32	5.6	170	4.1	42
Cr	3.1	4.0	ND	1.3	3.2	ND	1.0	ND	ND	NA
Ti	7.7	31	23	1.3	42	31	1.4	56	45	1.2

Element	Sample	MPP 6			MPP7			MPP 8		
	MDL	Varnished	Unvarnished	Ratio	Varnished	Unvarnished	Ratio	Varnished	Unvarnished	Ratio
Mo	1.5	ND	ND	NA	ND	ND	NA	ND	ND	NA
Sr	1.6	9.7	4.7	2.1	8.7	11	0.8	60	31	1.9
Rb	0.73	8.8	2.3	3.8	1.8	1.5	1.2	3.5	6.4	0.5
Pb	1.9	3.3	ND	1.8	2.7	ND	1.4	2.8	1.2	2.3
Se	0.93	ND	ND	NA	ND	ND	NA	ND	ND	NA
As	1.6	ND	ND	NA	ND	ND	NA	ND	ND	NA
Hg	8.3	ND	ND	NA	ND	ND	NA	ND	ND	NA
Zn	2.1	4.4	ND	2.2	1.3	ND	0.6	ND	ND	NA
Cu	2.1	ND	ND	NA	ND	ND	NA	ND	ND	NA
Ni	2.3	ND	ND	NA	ND	ND	NA	ND	ND	NA
Co	1.9	ND	ND	NA	ND	ND	NA	ND	ND	NA
Fe	2.6	870	130	6.9	1000	670	1.5	250	160	1.6
Mn	2.8	16	ND	5.6	77	8.3	9.3	110	ND	40
Cr	3.1	ND	ND	NA	3.0	ND	1.0	4.1	ND	1.3
Ti	7.7	15	18	0.8	73	42	1.7	56	20	2.8

Element	Sample	MPP 9			MPP 10			BKG 1		
	MDL	Varnished	Unvarnished	Ratio	Varnished	Unvarnished	Ratio	Varnished	Unvarnished	Ratio
Mo	1.5	ND	ND	NA	ND	ND	NA	ND	ND	NA
Sr	1.6	4.6	5.1	0.9	14	7.0	2.0	27	28	1.0
Rb	0.73	2.8	1.9	1.4	9.2	11	0.8	7.4	8.2	0.9
Pb	1.9	63	1.4	46	3.7	0.83	4.4	2.1	1.9	1.1
Se	0.93	ND	ND	NA	ND	ND	NA	ND	ND	NA
As	1.6	ND	ND	NA	ND	ND	NA	ND	ND	NA
Hg	8.3	ND	ND	NA	ND	ND	NA	ND	ND	NA
Zn	2.1	1.1	1.3	0.8	ND	ND	NA	0.71	0.98	0.7
Cu	2.1	ND	ND	NA	ND	ND	NA	ND	ND	NA
Ni	2.3	ND	ND	NA	ND	ND	NA	ND	ND	NA
Co	1.9	ND	ND	NA	ND	ND	NA	2.7	ND	1.4
Fe	2.6	1800	620	2.9	220	170	1.3	260	230	1.2
Mn	2.8	130	5.4	24	33	ND	12	17	ND	6.1
Cr	3.1	ND	ND	NA	ND	ND	NA	ND	ND	NA
Ti	7.7	23	71	0.3	19	19	1.0	29	31	0.9

ND = Not Detected. NA = Not Available.

Table 5.3 (cont.). FPXRF results for thin surface analysis of desert varnish samples. Concentrations are reported in $\mu g \cdot cm^{-2}$.

Element	Sample	TIMET 2			TIMET 4			RGPP 3		
	MDL	Varnished	Unvarnished	Ratio	Varnished	Unvarnished	Ratio	Varnished	Unvarnished	Ratio
Mo	1.5	ND	ND	NA	ND	ND	NA	ND	ND	NA
Sr	1.6	35	28	1.3	66	65	1.0	6.4	3.7	1.7
Rb	0.73	5.6	4.4	1.3	2.3	3.4	0.7	2.2	2.9	0.7
Pb	1.9	10.1	ND	5.4	7.0	ND	3.8	ND	ND	NA
Se	0.93	ND	ND	NA	ND	ND	NA	ND	ND	NA
As	1.6	ND	ND	NA	ND	ND	NA	ND	ND	NA
Hg	8.3	ND	ND	NA	ND	ND	NA	ND	ND	NA
Zn	2.1	ND	ND	NA	ND	ND	NA	ND	ND	NA
Cu	2.1	ND	ND	NA	ND	ND	NA	ND	ND	NA
Ni	2.3	ND	ND	NA	ND	ND	NA	ND	ND	NA
Co	1.9	ND	ND	NA	ND	ND	NA	ND	ND	NA
Fe	2.6	200	120	1.6	380	310	1.2	97	57	1.7
Mn	2.8	100	ND	37	68	5.1	13	41	ND	14
Cr	3.1	ND	ND	NA	ND	ND	NA	ND	ND	NA
Ti	7.7	26	19	1.4	33	25	1.3	15	9.2	1.6

Element	Sample	RGPP 4			RGPP 5			RGPP 6		
	MDL	Varnished	Unvarnished	Ratio	Varnished	Unvarnished	Ratio	Varnished	Unvarnished	Ratio
Mo	1.5	ND	ND	NA	ND	ND	NA	ND	ND	NA
Sr	1.6	1.9	0.92	2.1	3.5	2.5	1.4	0.68	0.39	1.7
Rb	0.73	0.89	0.40	2.2	7.6	6.9	1.1	0.53	ND	0.7
Pb	1.9	2.2	ND	1.2	8.8	1.1	7.7	3.2	ND	1.7
Se	0.93	ND	ND	NA	ND	ND	NA	ND	ND	NA
As	1.6	ND	ND	NA	ND	ND	NA	ND	ND	NA
Hg	8.3	ND	ND	NA	ND	ND	NA	ND	ND	NA
Zn	2.1	1.2	ND	0.6	3.9	1.2	3.3	ND	ND	NA
Cu	2.1	ND	ND	NA	2.2	ND	1.0	ND	ND	NA
Ni	2.3	ND	ND	NA	ND	ND	NA	ND	ND	NA
Co	1.9	ND	ND	NA	ND	ND	NA	ND	ND	NA
Fe	2.6	190	25	7.5	210	73	2.9	210	4.0	52
Mn	2.8	150	5.0	29	480	11	43	240	ND	50
Cr	3.1	ND	ND	NA	6.4	ND	2.1	ND	ND	NA
Ti	7.7	15	4.6	3.3	87	6.4	14	15	ND	2.0

ND = Not Detected. NA = Not Available.

Many trace elements in the analyzed varnishes appear to be enriched relative to the upper continental crust (UCC) (Condie, 1993; Hu and Gao, 2008). Selected elemental abundances (Cr, Co, Ni, Cu, Zn, As, Rb, Sr, Zr, Mo, and Pb), normalized to estimates of the average composition of the UCC, are plotted for each point source (Figures 5.4 to 5.7). Graphs of the same elements plotted in order of their relative enrichment are found in Exhibit 2.

In all NTS samples, As shows the highest enrichment ranging from 3 to 200 times that of the UCC. Pb is enriched in both NTS 2 and NTS 3; and Mo is highly enriched in NTS 1, to about 46 times more than in the UCC. Sr, Rb, and Zr show variable enrichments and depletions. Other elements (Cr, Co, Ni, Cu, and Zn) are undetected.

The TIMET samples show enrichment of Pb > As > Zr > Sr ≈ Cr > Cu > Zn, ranging from 7 to11 times more than in the UCC for Pb, to less than 2 times for Zn. Co is enriched only in TIMET 3 and undetected in other samples. Rubidium shows variable enrichment and depletion, Ni and Mo are undetected in all TIMET samples.

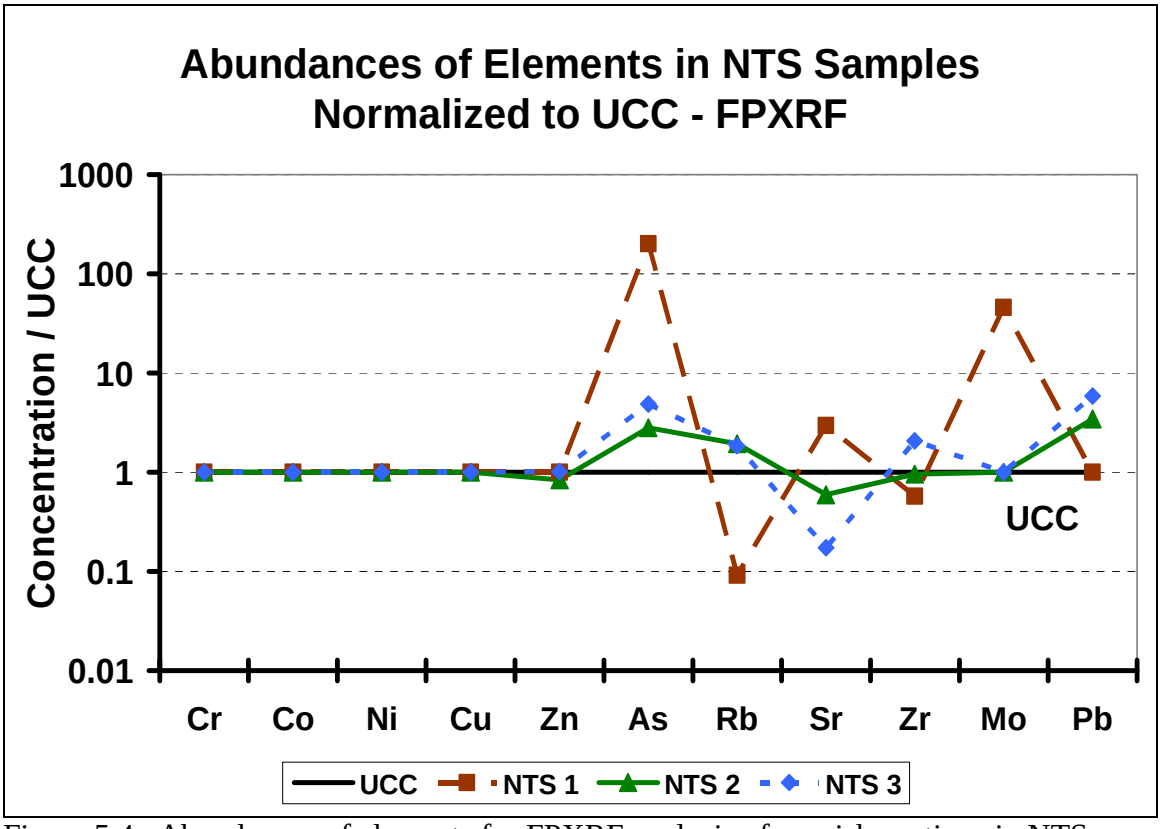

Figure 5.4. Abundances of elements for FPXRF analysis of varnish coatings in NTS samples normalized to the UCC. The thick black line represents the average UCC abundance (Ratio=1).

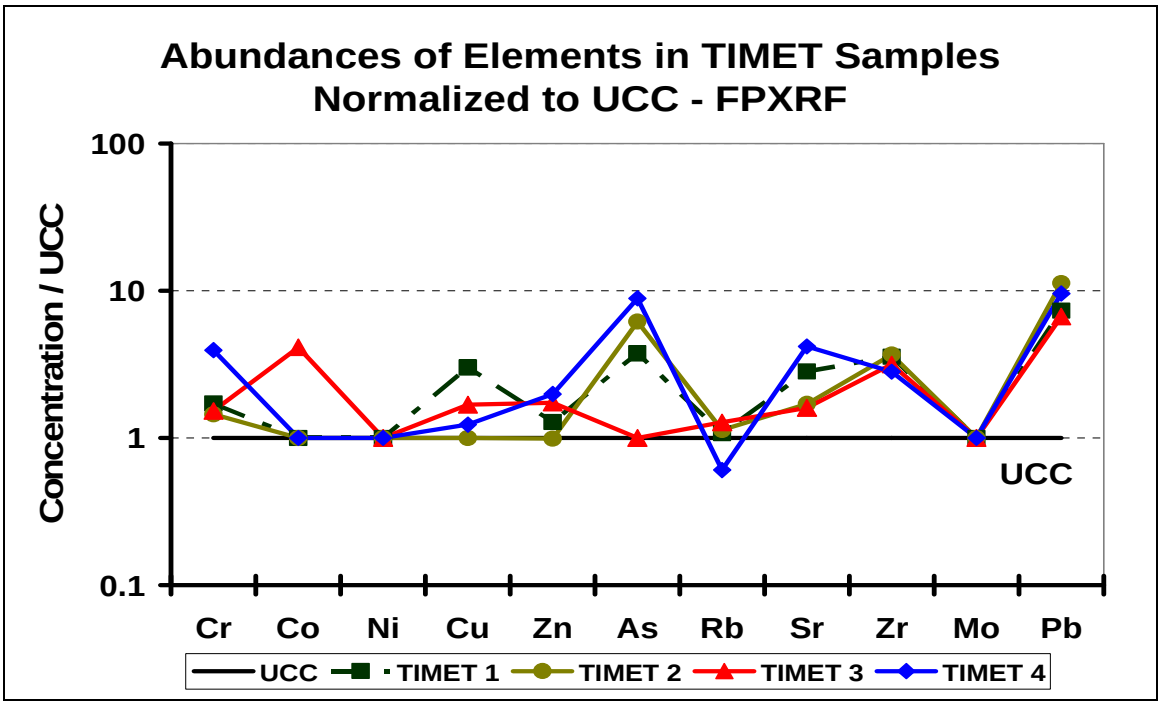

Figure 5.5. Abundances of elements for FPXRF analysis of varnish coatings in TIMET samples normalized to the UCC. The thick black line represents the average UCC abundance (Ratio=1).

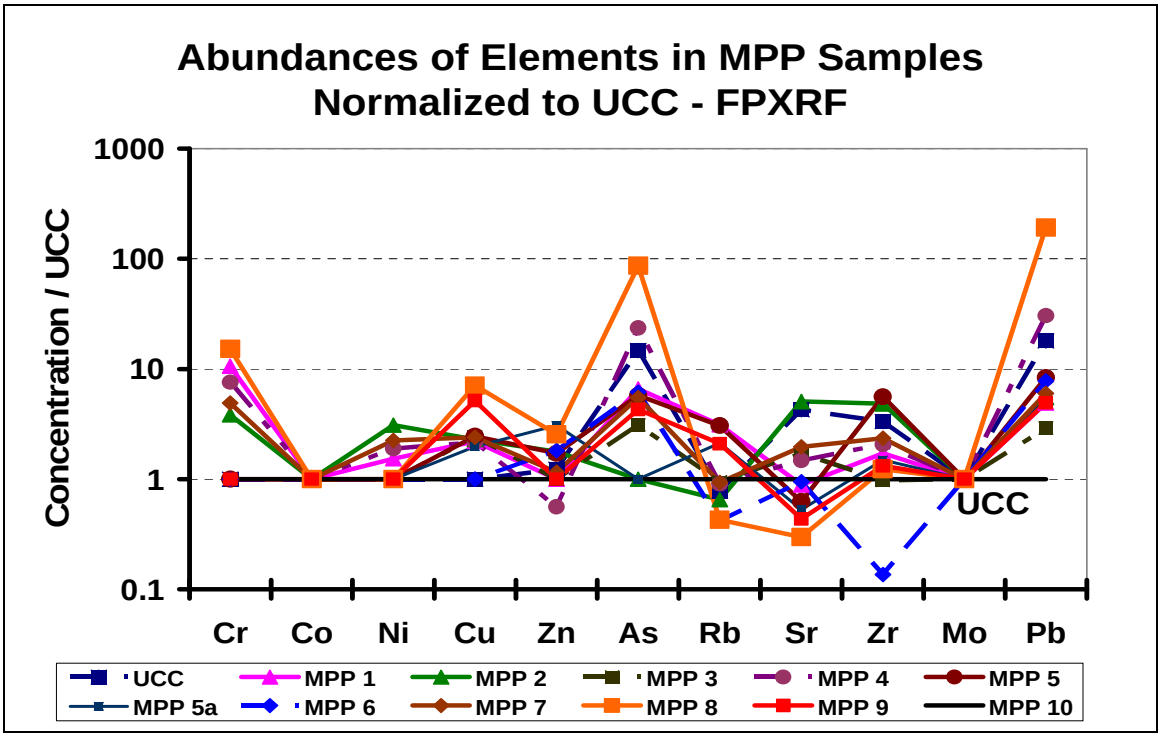

Figure 5.6. Abundances of elements for FPXRF analysis of varnish coatings in MPP samples normalized to the UCC. The thick black line represents the average UCC abundance (Ratio=1).

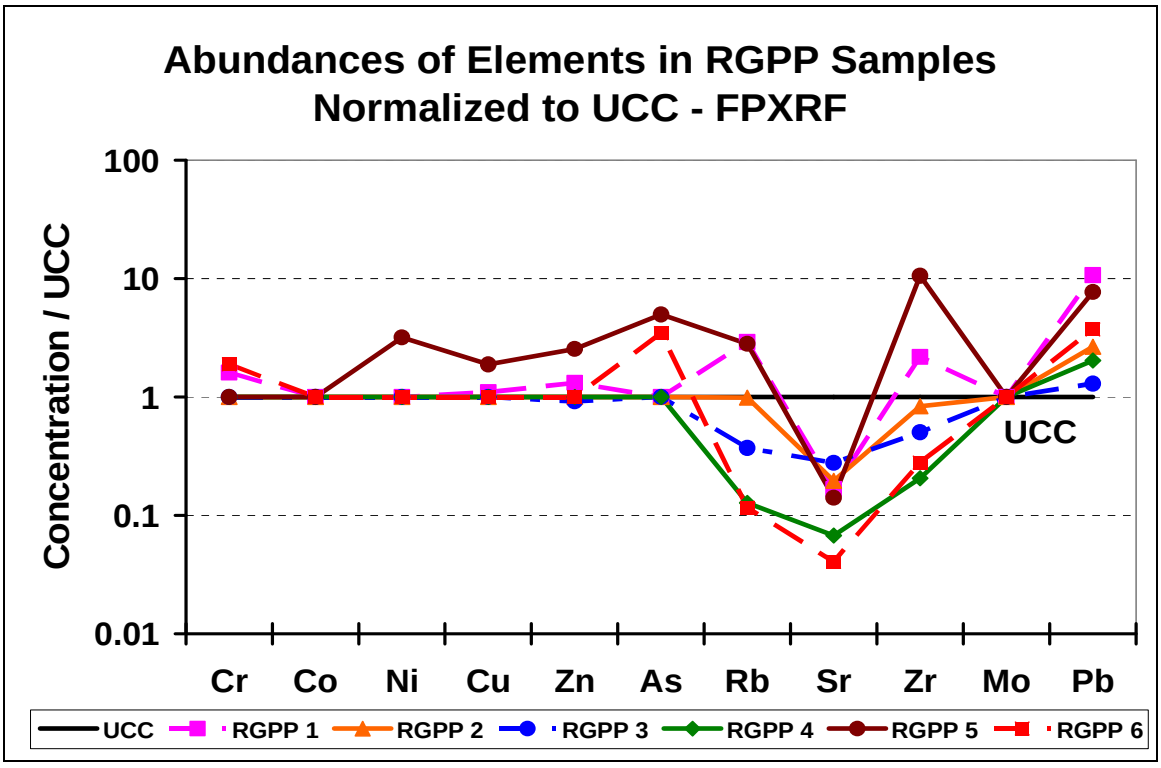

Figure 5.7. Abundances of elements for FPXRF analysis of varnish coatings in RGPP samples normalized to the UCC. The thick black line represents the average UCC abundance (Ratio=1).

Pb has the highest enrichment in all MPP samples, ranging from 3 to 193 times its concentration in the UCC. The majority of the MPP samples also show an enrichment in As > Cr > Cu > Zr > Zn > Ni of 3 to 87 times more than their UCC values. Zr is depleted in MPP 6, and Zn is depleted in MPP 4. Rb and Sr show variable enrichment and depletion, Co and Mo were undetected in all MPP samples.

The RGPP samples show enrichment of Pb > As > Zn > Ni > Cr > Cu, ranging from 2-11 times more than the UCC value for Pb, to about 2 times the UCC value for Cr and Cu. Ni and Cu are enriched only in RGPP 5 and undetected in the other samples. Rb and Zr show variable enrichment and depletion, while Co and Mo are not detected in any samples. Sr is depleted in all of the samples.

Notably, elements (Zn, As, and Pb) that have the highest concentrations in the analyzed varnish samples, and show the highest levels of enrichment relative to the UCC, are commonly found in atmospheric emissions from coal-fired power plants (Seames and Wendt, 2000; Furimski, 2000; Martines-Tarazona and Spears, 1996; Zeng et al., 2001; Danihelka et al., 2003). Indeed, two pollution sources in this study are coal-fired power plants. The behavior of trace metals during coal combustion is important because of their environmental and toxicological effects. Trace metals exit the coal combustion process in the vapor phase, with submicron-sized aerosol particles, or as a part of larger particles in the bottom ash (Nodelman et al., 2000; Yan et al., 2001; Danihelka et al., 2003). The most volatile trace elements (Hg, Se, and As) remain mainly in gaseous forms and are emitted mostly with the flue gas (Seames and Wendt, 2000; Zeng et al., 2001; Yan et al., 2001; Lockwood and Yousef, 2000). Danihelka et al. (2003) noted that many heavy metals (Cr, Co, Ni, Cu, Zn, As, Se, Cd, Sn, Sb, Tl, and Pb) are enriched in the fly ash. Consequently, the most common trace metals in the particulate emissions from the stack include Cu, Zn, Cd, Sn, Sb, and Pb. Mn and Fe have similar distributions in bottom and fly ash, and are depleted in the particulate flue emissions.

The abundances of three elements (Zn, As, and Pb) in the varnish coatings are plotted as a function of the distance from the coal-fired power plants (Tables 5.4 and 5.5). The distances north of the plant are entered as positive numbers and the distances south of the plant are entered as negatives. The resulting graphs show a general pattern for all three elements. However, there are possible contributions of Pb and As from other sources. Lower concentrations are observed at the source followed by a maximum peak concentration and gradual decrease with the distance from the source (Figures 5.8 and

5.9). The observed patterns are consistent with the predictions of the Gaussian Plume atmospheric transport and diffusion model used to calculate average ground level concentrations of the deposited pollutants (Wangen and Williams, 1978). The plume deposition model assumes that beyond the distance of maximum deposition, trace element concentrations in soils should decrease with increasing distance from the power plant if the power plant is a significant source of that element. An area of low deposition near the power plant is expected as a result of pollutant release from elevated stacks (Anderson et al., 1975; Connor et al., 1976; Keith et al., 1974; Wangen and Williams, 1978).

Table 5.4. Sampling sites and the distance in kilometers from the Mohave Power Project (MPP).

Site	Distance (km)	Geographical Name	Latitude	Longitude	Altitude (ft)
RGPP 3	138 km North	Valley of Fire, Overton, NV	N 36° 25.414'	W 114° 33.038'	2,206
TIMET 2	112 km North	Black Mountain, Henderson, NV	N 36° 01.257'	W 115° 00.792'	2,113
MPP 1	107 km North	Las Vegas Wash, Henderson, NV	N 36° 04.432'	W 114° 55.603'	1,719
MPP 3	53 km North	Dolan Springs, AZ	N 35° 35.069'	W 114° 17.126'	3,270
MPP 2	43 km North	Cottonwood Cove, Searchlight, NV	N 35° 29.000'	W 114° 44.491'	1,504
MPP7	22 km North	Chiquita Hills, NV	N 35° 09.629'	W 114° 50.099'	2,580
MPP 4	3 km North	Laughlin, NV	N 35° 09.074'	W 114° 38.251'	1,061
MPP 5	58 km South	Lake Havasu, AZ	N 34° 37.612'	W 114° 19.525'	1,390
MPP 5a	58 km South	Lake Havasu, AZ	N 34° 37.612'	W 114° 19.525'	1,340
MPP 8	70 km South	Chemehuei Valley, CA	N 34° 35.452'	W 114° 38.185'	1,950
MPP 6	92 km South	Cattail Cove State Park, AZ	N 34° 21.564'	W 114° 09.597'	613
MPP 9	123 km South	Parker Dam, AZ	N 34° 17.498'	W 114° 07.782'	610
MPP 10	126 km South	Earp, CA	N 34° 10.713'	W 114° 15.621'	417
BKG 1	322 km North	Brian Head Peak, UT	N 37° 41.267'	W 112° 50.116'	11,020
BKG 2	168 km North	Spring Mountains, NV	N 36° 24.552'	W 115° 33.918'	5,450

Table 5.5. Sampling sites and the distance in kilometers from the Reid Gardner Power Plant (RGPP).

Site	Distance (km)	Geograhical Name	Latitude	Longitude	Altitude (ft)
NTS 1	171 km North	Queen City Summit, Rachel, NV	N 37° 45.905'	W 115° 57.940'	5,742
NTS 2	109 km North	Hancock Summit, Crystal Springs, NV	N 37° 26.812'	W 115° 22.264'	5,305
NTS 3	83 km North	Pahranagat Valley, Alamo, NV	N 37° 18.572'	W 115° 07.419'	3,404
RGPP 1	80 km North	Elgin, NV	N 37° 22.723'	W 114° 32.993'	3,501
RGPP 6	56 km North	Kane Spring Wash, NV	N 37° 00.902'	W 114° 51.923'	2,980
RGPP 5	46 km North	Coyote Springs, NV	N 36° 57.714'	W 114° 58.476'	2,560
RGPP 4	27 km North	Gunsight Mountain, NV	N 36° 39.650'	W 114° 22.374'	2,620
RGPP 2	2 km North	Moapa, NV	N 36° 40.442'	W 114° 37.412'	1,671
RGPP 3	27 km South	Valley of Fire, Overton, NV	N 36° 25.414'	W 114° 33.038'	2,206
MPP 1	66 km South	Las Vegas Wash, Henderson, NV	N 36° 04.432'	W 114° 55.603'	1,719
TIMET 2	78 km South	Black Mountain, Henderson, NV	N 36° 01.257'	W 115° 00.792'	2,113
MPP 2	124 km South	Cottonwood Cove, Searchlight, NV	N 35° 29.000'	W 114° 44.491'	1,504
BKG 1	194 km North	Brian Head Peak, UT	N 37° 41.267'	W 112° 50.116'	11,020
BKG 2	88 km West	Spring Mountains, NV	N 36° 24.552'	W 115° 33.918'	5,450

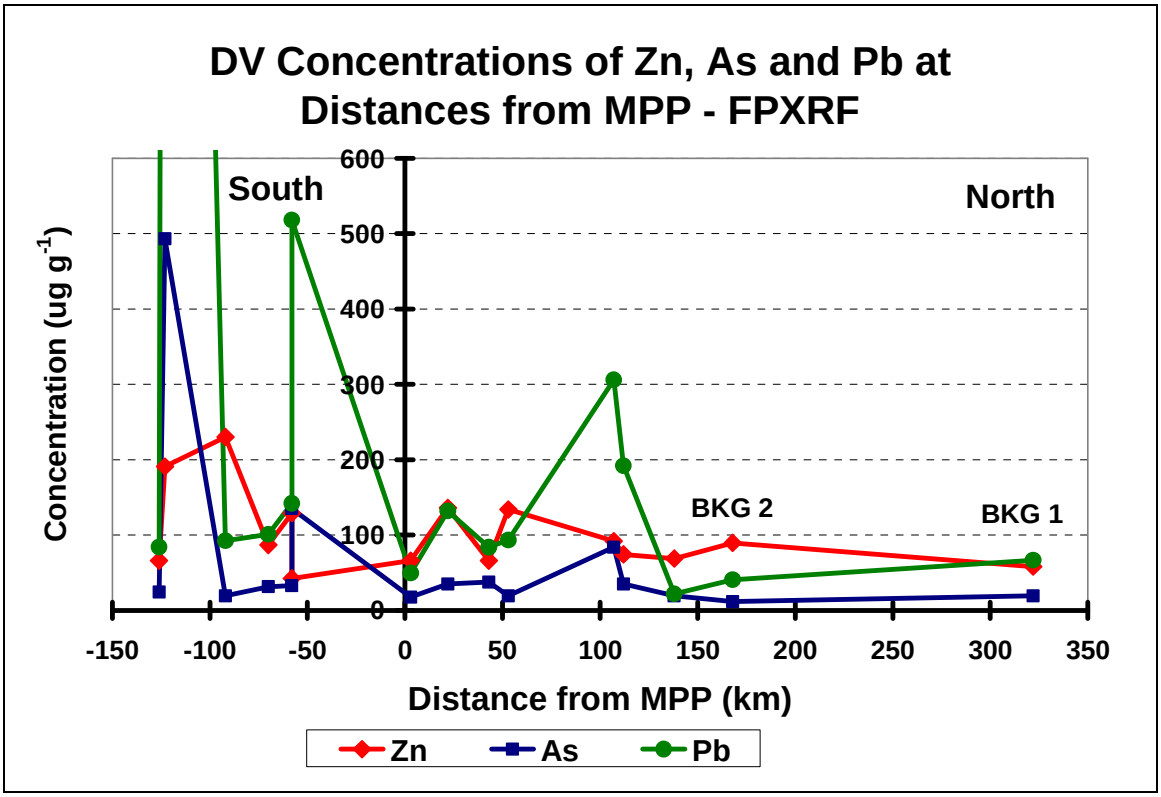

Figure 5.8. FPXRF analysis of Zn, As, and Pb in desert varnish samples as a function of distance from the Mohave Power Project (MPP). The off-scale Pb peak at 123 km south of the MPP shows the result for MPP 9 at 3.3 x 10^3 $\mu g \cdot g^{-1}$.

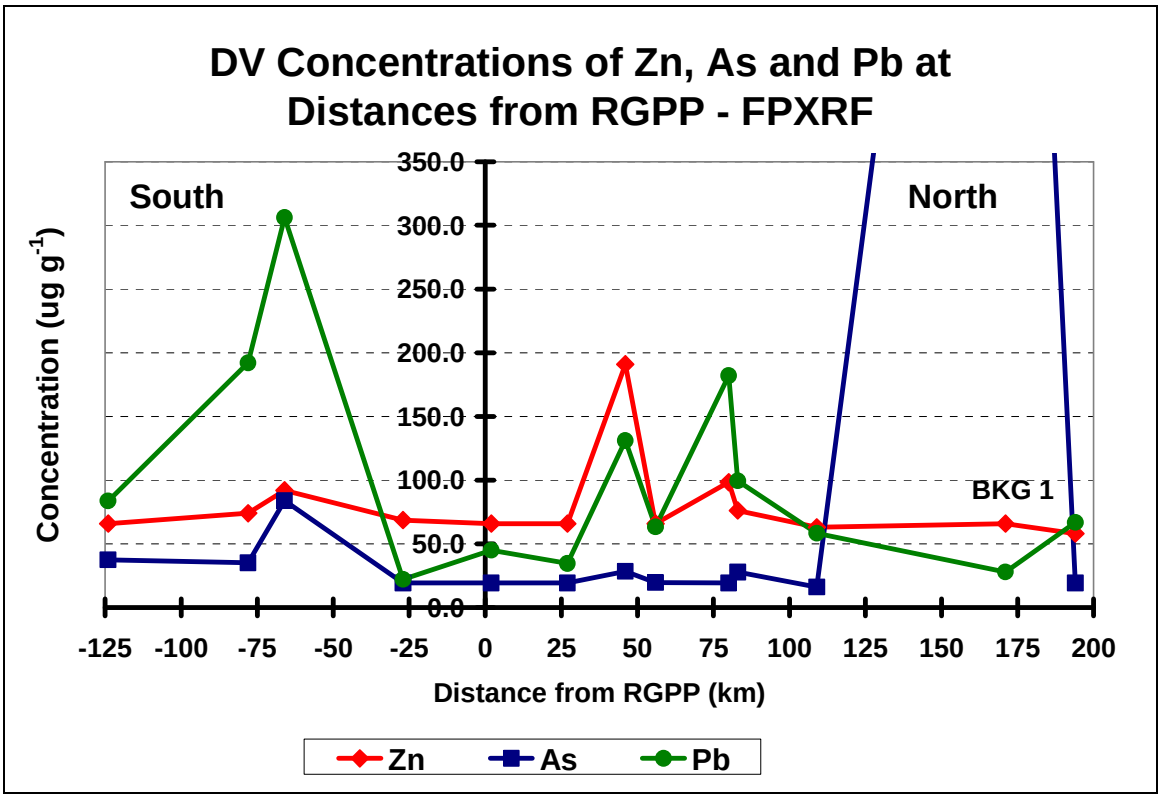

Figure 5.9. FPXRF analysis of Zn, As, and Pb in desert varnish samples as a function of distance from the Reid Gardner Power Plant (RGPP). The off-scale As peak at 171 km north of the RGPP shows the result for NTS 1 at 1.1 x 10^3 $\mu g \cdot g^{-1}$.

Magnetic Sector LA-ICPMS Results

The applicability of magnetic sector LA-ICPMS for the analysis of desert varnish samples was evaluated. Eleven elements (Be, Ag, Cd, Sn, Sb, Ba, W, Tl, Pb, Th and U) are determined at low mass resolution ($m/\Delta m \approx 400$) in two varnish samples from southern Nevada. Aluminum-27 is used as an internal standard (IS).

Method Detection Limit (MDL)

Method detection limits (MDLs) are calculated based on replicate measurements (n=90) of argon gas blanks and the slope of the calibration curve (3σ). The MDLs range from 0.001 $\mu g \cdot g^{-1}$ for Be, U, and Th to 0.501$\mu g \cdot g^{-1}$ for Ag (Figure 5.10).

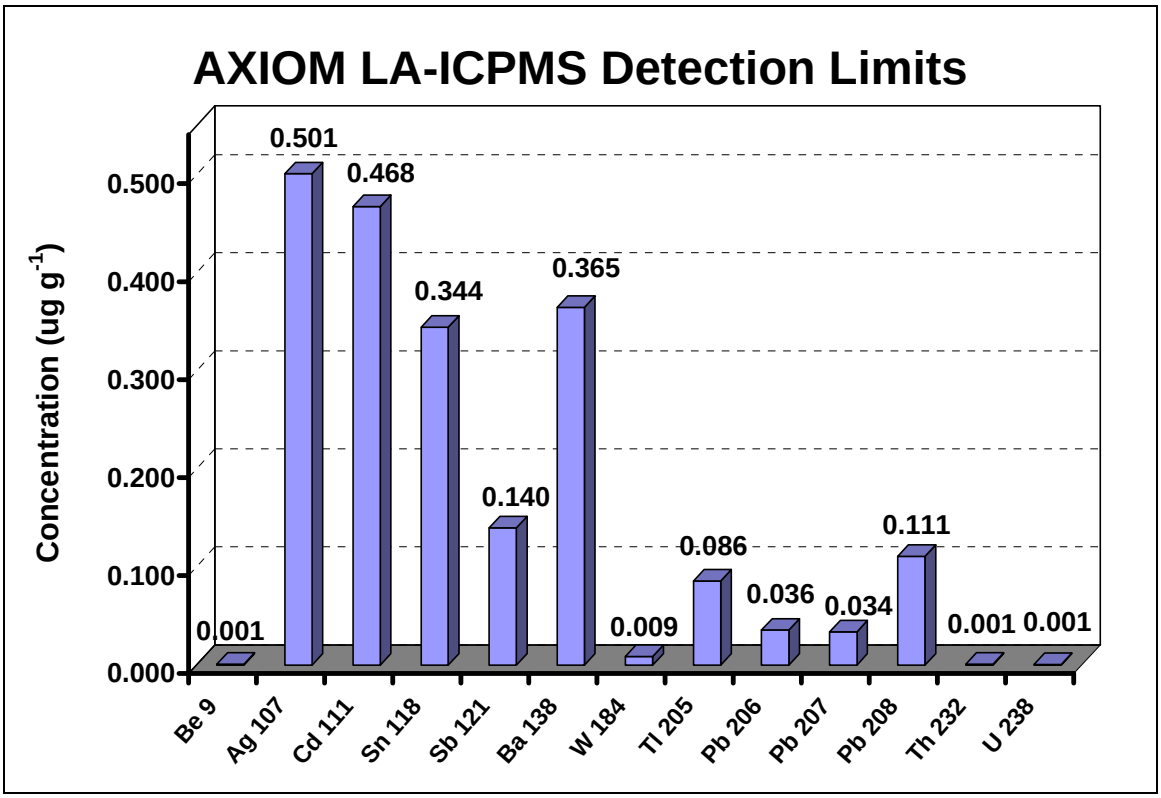

Figure 5.10. Estimated detection limits for the Axiom LA-ICPMS analysis of desert varnish samples.

Calibration Curves and QA/QC

Three NIST SRM 612, 614, and 616 glass standards (n=3) were used for calibration and quality assurance. Calibration curves using the NIST reference glass materials yield good linearity for all elements. Correlation coefficients for instrumental response (in counts-per-second) vs. concentration are ≥ 0.999 for eight elements (Be, Ag, Sn, Sb, Ba, W, Tl, and U); equal to 1.00 for Cd (only one standard value was available) and Th; and 0.996 for Pb (Figure 5.11).

To examine the accuracy and precision of the method, elemental concentrations were obtained for SRMs 612 and 614 using all three SRMs as standards and the desired SRM as an unknown.

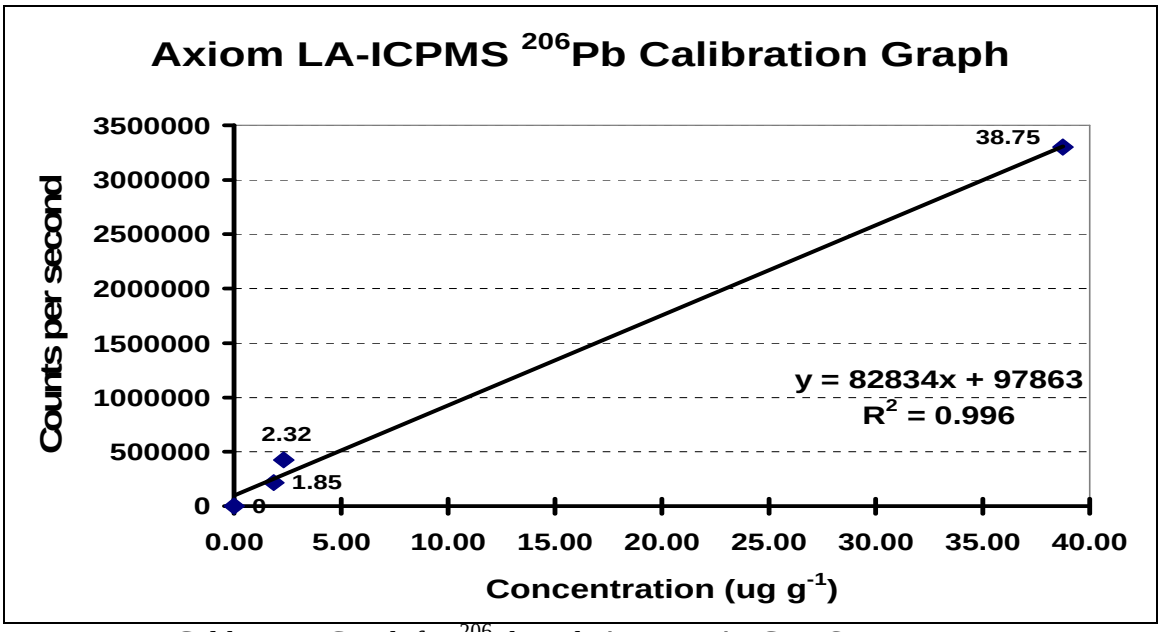

Figure 5.11. Calibration Graph for ^{206}Pb with Axiom LA-ICPMS.

The results are generally in acceptable agreement with certified or consensus values, with a few outliers, usually for Sn or U in the lower concentration standard (SRM 614). The analyte recoveries in SRM 614 range from 65% for Cd to 610% for U (Table 5.6). The percent recoveries for seven analytes are outside the acceptable range of 80 to 120 %: Cd (65%), Sn (605%), W (142%), Tl (167%), Pb (160%); Th (128%); and U (610%). Conversely, excellent agreement with certified or consensus values is obtained for SRM 612 (Table 5.6), with only the results for Pb (131%) and U (78%) falling outside of the acceptable range.

Precision of the analytical method is verified by calculating a relative percent difference (RPD) between duplicate measurements of SRM 612 (Table 5.6). Most of the elements have RPDs within the acceptable limit (< 20%), except for Pb (32%) and U (22%). This gives confidence that the method is suitable for the analysis of rock varnish samples, and that it provides quite accurate and precise results.

Table 5.6. Axiom LA-ICPMS results for glass reference materials NIST SRM 612 and 614 using three glass reference materials for calibration (concentrations given in $\mu g \cdot g^{-1}$).

Element	SRM 614			SRM 612					RPD
	Found	Certified or ref value	% Rec.	Found	Found	Certified or ref value	% Rec.	% Rec.	
Be	0.63 ± 0.09	0.73	86	33.5 ± 2.2	23.5 ± 1.5	37.15	90	90	0
Ag	0.46 ± 0.05	0.42 ± 0.04	110	21.9 ± 1.6	22.1 ± 2.2	22.0 ± 0.3	100	101	1
Cd	0.36 ± 0.08	0.55	65	11.2 ± 0.7	10.9 ± 0.9	NA	NA	NA	3
Sn	2.54 ± 0.13	0.42 ± 0.04	605	35.4 ± 2.1	33.9 ± 3.5	38.98	91	87	4
Sb	1.19 ± 0.10	1.06	112	33.7 ± 2.6	31.1 ± 3.5	36.22	93	86	8
Ba	5.19 ± 0.63	4.70 ± 0.14	110	40.4 ± 2.6	40.4 ± 4.5	41	99	99	0
W	1.05 ± 0.08	0.74	142	43.7 ± 2.2	34.0 ± 5.9	NA	NA	NA	NA
Tl	0.45 ± 0.07	0.269 ± 0.005	167	14.3 ± 1.3	15.9 ± 1.2	15.7 ± 0.3	91	101	10
Pb	3.72 ± 0.27	2.32 ± 0.046	160	36.7 ± 2.3	50.6 ± 18.3	38.57 ± 0.2	95	131	32
Th	1.00 ± 0.06	0.784 ± 0.006	128	38.8 ± 1.3	32.0 ± 5.3	37.79 ± 0.08	103	85	19
U	5.02 ± 1.03	0.823 ± 0.002	610	36.5 ± 18.6	29.3 ± 5.9	37.38 ± 0.08	98	78	22

The "informational" values do not have uncertainties associated with them. Found values are ± 1 SD.
Certified or consensus values are ± 95% confidence limit. NA = Not Available.

Sample Data

The Axiom LA-ICPMS analysis concentrations of 11 elements (Be, Ag, Cd, Sn, Sb, Ba, W, Tl, Pb, Th, and U) in two samples of desert varnish (RGPP 3 and TIMET 2) are found in Table 5.7. Each mean of the results represents the average of 30 individual analyses (3 lines, 10 runs), and was obtained using continuous-line ablations. Varnish coatings are not uniformly thick and possibly have different chemical compositions over the ablated area. Thus, the LA-ICPMS analysis represents an average bulk analysis of the varnish material with some rock substrate ablated during the line scans. These variations in varnish films combined with the errors of the analytical method account for higher relative standard deviations (up to 74% RSD) of the means of the individual results.

Both varnish samples have varied concentrations of trace elements (Table 5.7). Barium (271 to 1.83 x 10^3 $\mu g \cdot g^{-1}$) and Pb (34.2 to 814 $\mu g \cdot g^{-1}$) are by far the most

abundant, and Th is highly enriched (12.4 to 15.4 $\mu g \cdot g^{-1}$) in the varnished surfaces of both samples. The varnished surface of RGPP 3 has trace element concentrations that range from 1.27 x 10^3 $\mu g \cdot g^{-1}$ for Ba to 0.890 $\mu g \cdot g^{-1}$ for Ag. Both Cd (7.99 $\mu g \cdot g^{-1}$) and W (4.30 $\mu g \cdot g^{-1}$) are present at higher levels (Figure 5.12). Elements in RGPP 3 are listed (in order of abundance): Ba > Pb > Th > Cd > W > Tl > Be > Sb > Sn ≈ U > Ag.

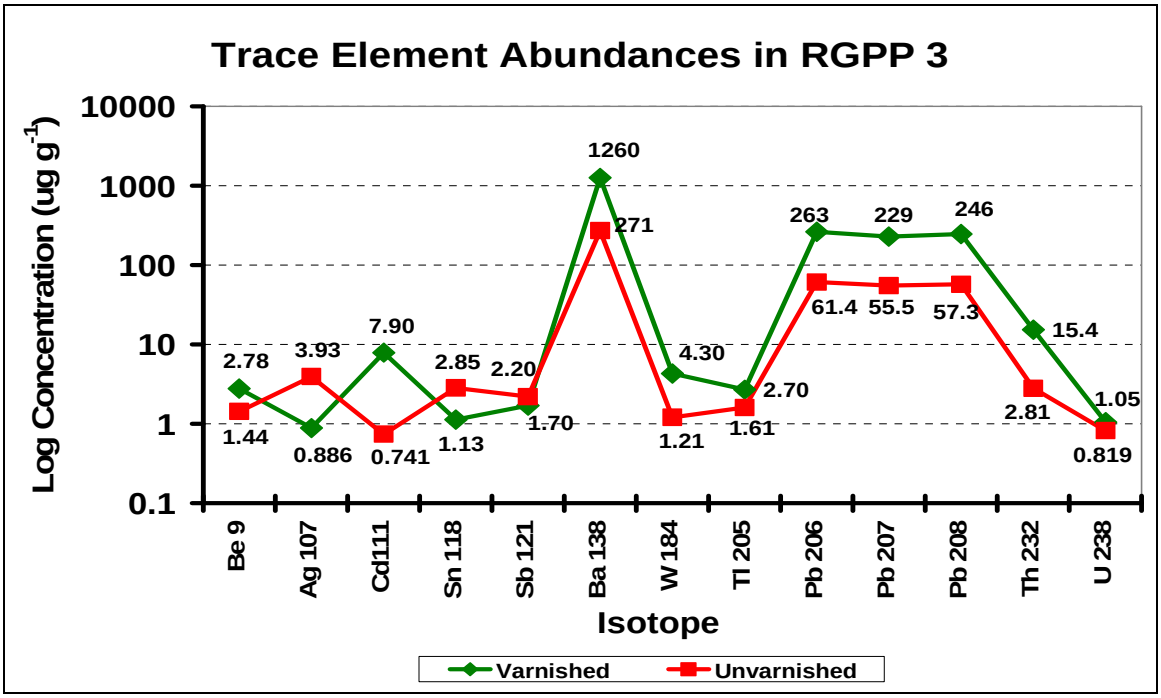

Figure 5.12. Trace element abundances from the Axiom LA-ICPMS analysis of an unvarnished surface, and a skyward-facing varnished surface of the same sample (RGPP 3).

To confirm that varnished surfaces are chemically distinct from unvarnished surfaces, both surfaces were analyzed on the same sample and the concentration ratio was calculated for each element (Table 5.8). In RGPP 3, eight elements (Cd > Th > Ba > Pb > W> Be > Tl > U) have concentration ratios greater than one, indicating higher concentrations of these elements in the varnished surface than in the unvarnished substrate rock (Figure 5.13).

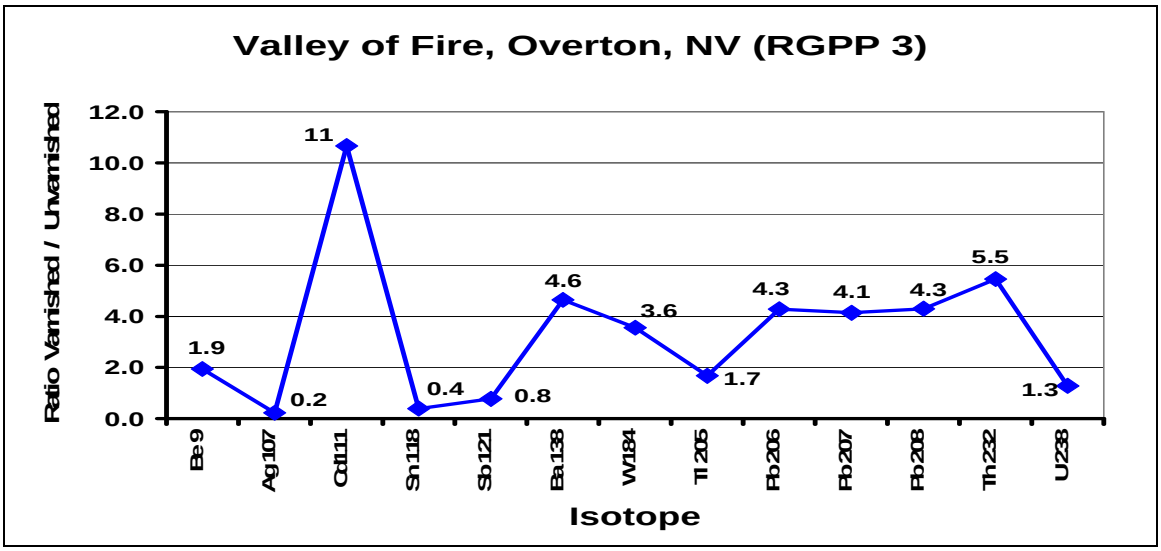

Figure 5.13. Ratio of the elements in the varnished and unvarnished surfaces of the desert varnish sample RGPP 3 by Axiom LA-ICPMS analysis.

The skyward-facing varnished surface of TIMET 2 has trace element concentrations that range from 1.83 x 10^3 $\mu g \cdot g^{-1}$ for Ba to 1.85 $\mu g \cdot g^{-1}$ for U, with enriched Cd, Sn, Sb, W, Tl, Pb, and Th (Figure 5.14). Elements in sample TIMET 2 are listed (in order of abundance): Ba > Pb > Tl > Th > Sn ≈ Cd ≈ Sb > W > Ag > Be > U.

In contrast, concentrations of Ag, Sn, and Sb were higher in the unvarnished surface. This could be caused by the limited absorption of these low solubility elements into the varnish films. Tebo et al. (2004) reported that Mn oxide minerals can adsorb or incorporate from solutions substantial amounts of Ca, Fe, Co, Ni, Cu, Zn, As, Se, Cd, Sn, Hg, Pb, Po, Ra, Th, U, and Pu. However, adsorption, ion exchange, and precipitation of metals by Mn oxides are affected by multiple factors (Tebo et al., 2004). Solubility in rain or fog droplets during wet deposition is a main factor that influences enrichment of the metal in the varnish coatings (Thiagarajan and Lee, 2004).

Table 5.7. Comparison of elements ($\mu g \cdot g^{-1}$) in desert varnish using Axiom LA-ICPMS.

Sample	Analyte	Line 1	Line 2	Line 3	Mean	RSD (%)
RGPP 3	Be	2.46 ± 1.29	2.94 ± 1.51	2.76 ± 1.73	2.72 ± 0.24	9
Varnished	Ag	0.80 ± 0.13	0.78 ± 0.25	1.07 ± 0.56	0.89 ± 0.16	18
	Cd	7.03 ± 4.01	9.64 ± 6.52	7.03 ± 3.83	7.99 ± 1.51	19
	Sn	1.00 ± 0.30	1.11 ± 0.37	1.28 ± 0.40	1.13 ± 0.14	13
	Sb	1.65 ± 0.63	1.74 ± 0.58	1.70 ± 0.60	1.70 ± 0.05	3
	Ba	1250 ± 600	1290 ± 600	NA	1270 ± 230	2
	W	4.02 ± 1.49	3.83 ± 0.98	5.04 ± 2.38	4.30 ± 0.66	15
	Tl	2.83 ± 1.51	2.81 ± 1.23	2.47 ± 1.03	2.70 ± 0.20	8
	Pb	268 ± 52	251 ± 53	270 ± 103	263 ± 10	4
	Th	13.8 ± 7.1	14.7 ± 6.1	17.6 ± 9.8	15.4 ± 2.0	13
	U	0.89 ± 0.39	1.00 ± 0.36	1.25 ± 0.61	1.05 ± 0.18	18
RGPP 3	Be	1.06 ± 0.35	1.38 ± 0.56	1.86 ± 0.59	1.46 ± 0.40	28
Unvarnished	Ag	3.67 ± 8.37	NA	4.20 ± 8.27	3.93 ± 0.37	10
	Cd	0.51 ± 0.14	0.64 ± 0.17	1.08 ± 0.33	0.74 ± 0.30	40
	Sn	2.36 ± 0.87	2.61 ± 0.53	3.57 ± 0.78	2.85 ± 0.64	22
	Sb	1.88 ± 0.40	2.03 ± 0.35	2.69 ± 0.70	2.20 ± 0.43	20
	Ba	251 ± 311	265 ± 162	297 ± 151	271 ± 24	9
	W	1.13 ± 0.57	1.05 ± 0.17	1.45 ± 0.43	1.21 ± 0.21	18
	Tl	1.17 ± 0.52	1.89 ± 0.96	1.79 ± 0.53	1.61 ± 0.39	24
	Pb	50.1 ± 13.3	61.4 ± 9.2	72.8 ± 12.8	61.4 ± 11.4	19
	Th	2.09 ± 0.50	2.45 ± 0.54	3.91 ± 0.99	2.81 ± 0.96	34
	U	0.57 ± 0.26	0.63 ± 0.17	1.26 ± 0.32	0.82 ± 0.38	47
TIMET 2	Be	1.33 ± 0.71	3.29 ± 0.64	2.27 ± 0.62	2.30 ± 0.98	43
Varnished Skyward-Facing	Ag	3.77 ± 1.28	NA	6.02 ± 0.46	4.85 ± 1.59	33
	Cd	7.97 ± 2.75	9.30 ± 3.27	5.66 ± 0.92	7.64 ± 1.84	24
	Sn	7.42 ± 1.48	9.42 ± 2.95	6.98 ± 1.23	7.94 ± 1.30	16
	Sb	9.38 ± 4.09	6.59 ± 1.50	6.38 ± 3.09	7.45 ± 1.68	23
	Ba	1600 ± 525	2250 ± 400	1630 ± 290	1830 ± 360	20
	W	6.85 ± 2.50	6.77 ± 1.80	5.65 ± 2.78	6.42 ± 0.67	11
	Tl	25.2 ± 8.9	29.2 ± 9.0	21.6 ± 6.5	25.3 ± 3.7	15
	Pb	771 ± 314	1072 ± 581	599 ± 407	814 ± 239	29
	Th	9.83 ± 5.42	17.9 ± 4.8	17.2 ± 7.1	15.0 ± 4.5	30
	U	1.21 ± 0.64	2.23 ± 0.67	2.11 ± 0.80	1.85 ± 0.56	30
TIMET 2	Be	1.58 ± 0.71	1.54 ± 0.64	1.51 ± 0.42	1.55 ± 0.04	3
Unvarnished	Ag	2.75 ± 1.15	2.57 ± 1.40	NA	2.66 ± 0.13	5
	Cd	0.17 ± 0.07	0.17 ± 0.06	0.20 ± 0.05	0.18 ± 0.02	10
	Sn	0.93 ± 0.18	0.65 ± 0.20	0.86 ± 0.35	0.81 ± 0.14	18
	Sb	0.82 ± 0.19	0.84 ± 0.33	0.99 ± 0.60	0.88 ± 0.09	10
	Ba	500 ± 170	566 ± 213	527 ± 317	532 ± 32	6
	W	0.86 ± 0.27	0.92 ± 0.62	1.17 ± 1.06	0.99 ± 0.16	17
	Tl	0.55 ± 0.18	0.43 ± 0.21	0.57 ± 0.36	0.52 ± 0.08	15
	Pb	23.8 ± 8.9	NA	44.7 ± 39	34.2 ± 14.8	43
	Th	5.51 ± 2.72	5.68 ± 3.63	5.98 ± 4.16	5.72 ± 0.24	4
	U	0.55 ± 0.26	0.61 ± 0.37	0.72 ± 0.57	0.63 ± 0.08	13
TIMET 2	Be	2.31 ± 0.47	2.55 ± 0.65	2.59 ± 0.70	2.48 ± 0.15	6
Varnished Ground-Facing	Ag	4.27 ± 0.52	3.86 ± 0.99	5.80 ± 3.89	4.61 ± 1.02	22
	Cd	1.82 ± 0.56	4.09 ± 1.71	5.09 ± 2.28	3.67 ± 1.68	46
	Sn	2.96 ± 0.62	3.63 ± 0.85	3.40 ± 1.25	3.33 ± 0.34	10
	Sb	2.22 ± 0.70	4.12 ± 1.81	4.49 ± 1.21	3.61 ± 1.22	34
	Ba	975 ± 193	1800 ± 1100	NA	1390 ± 590	42
	W	5.03 ± 3.07	13.3 ± 7.9	19.3 ± 18.1	12.5 ± 7.1	57
	Tl	2.36 ± 0.49	5.84 ± 2.87	12.35 ± 11.35	6.85 ± 5.07	74
	Pb	278 ± 163	578 ± 304	568 ± 181	475 ± 170	36
	Th	11.04 ± 2.43	11.40 ± 3.27	14.7 ± 7.5	12.38 ± 2.0	16
	U	1.33 ± 0.20	1.35 ± 0.29	2.00 ± 0.91	1.56 ± 0.38	24

NA = Not Available; data for each line consisted of 10 analytical runs (see experimental), the mean is for the averages of line scans.

Trace element concentrations are consistently higher in the varnished surfaces in TIMET 2 (Table 5.8 and Figure 5.14). The concentration ratios of the elements in the skyward-facing varnished surface to the unvarnished surface in TIMET 2 range from 1.5 for Be to 49 for Tl. The elemental concentration ratios in descending order are: Tl > Cd > Pb > Sn > Sb > W > Ba > U > Th > Ag > Be. The ratios of the ground-facing varnished surface to the unvarnished surface of TIMET 2 range from 1.6 for Be to 21 for Cd (Table 5.8 and Figure 5.15). The elemental concentration ratios in descending order are: Cd > Pb > Tl ≈ W > Sn ≈ Sb > Ba > U > Th > Ag > Be.

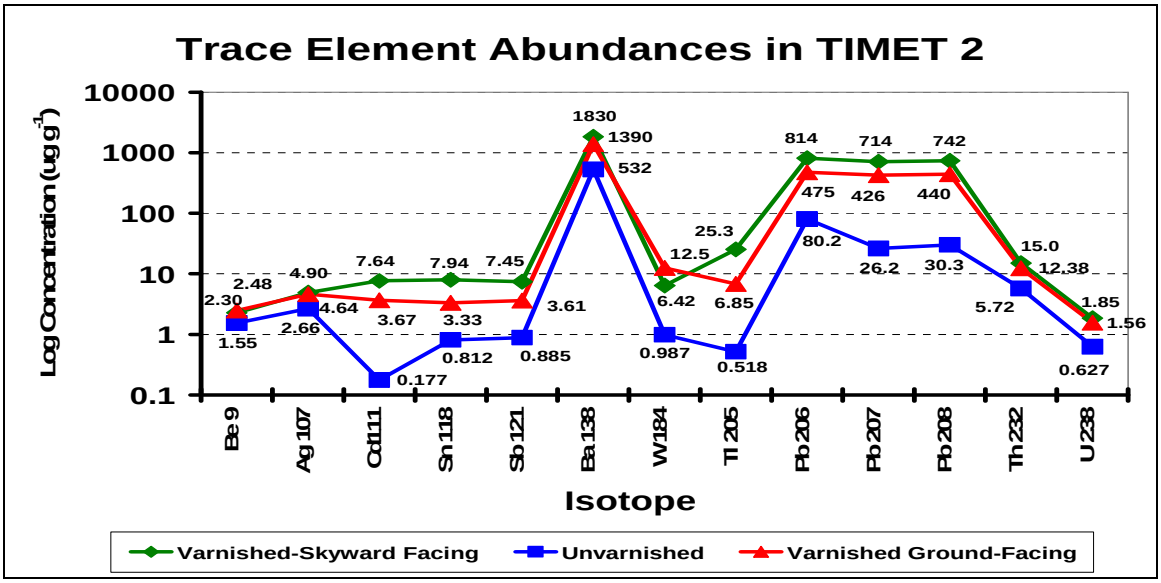

Figure 5.14. Trace element abundances from the Axiom LA-ICPMS analysis of an unvarnished surface, a ground-facing varnished surface, and a skyward-facing varnished surface of the same sample (TIMET 2).

To estimate atmospheric deposition of trace elements in the varnished surfaces, concentration ratios of the elements in the skyward-facing and ground-facing varnished surfaces were calculated for sample TIMET 2 (Table 5.9 and Figure 5.16). The elemental concentration ratios in the skyward- and ground-facing varnished surfaces

range from 0.5 to 3.7 (Table 5.8 and Figure 5.16). The ratios in descending order are: Tl > Sn > Cd ≈ Sb > Pb > Ba > Th ≈ U > Ag > Be > W.

Table 5.8. Comparison of elements ($\mu g \cdot g^{-1}$) in desert varnish using Axiom LA-ICPMS.

Isotope	Sample	RGPP 3			TIMET 2					
	MDL	Varnished	Unvarnished	Ratio	Varnished Skyward-Facing	Varnished Ground-Facing	Unvarnished	Ratio Sky./Unvar.	Ratio Ground./Unvar.	Ratio Sky./Ground.
^{9}Be	0.001	2.78	1.44	1.9	2.30	2.48	1.55	1.5	1.6	0.9
^{107}Ag	0.501	0.886	3.93	0.2	4.90	4.64	2.66	1.8	1.7	1.1
^{111}Cd	0.468	7.90	0.741	11	7.64	3.67	0.177	43	21	2.1
^{118}Sn	0.344	1.13	2.85	0.4	7.94	3.33	0.812	9.8	4.1	2.4
^{121}Sb	0.140	1.70	2.20	0.8	7.45	3.61	0.885	8.4	4.1	2.1
^{138}Ba	0.365	1260	271	4.7	1830	1390	532	3.4	2.6	1.3
^{184}W	0.009	4.30	1.21	3.6	6.42	12.5	0.99	6.5	13	0.5
^{205}Tl	0.086	2.70	1.61	1.7	25.3	6.85	0.52	49	13	3.7
^{206}Pb	0.034	263	61.4	4.3	814	475	80.2	10	5.9	1.7
^{207}Pb	0.036	230	55.5	4.1	714	426	26.2	27	16	1.7
^{208}Pb	0.111	246	57.3	4.3	742	440	30.3	24	15	1.7
^{232}Th	0.001	15.4	2.81	5.5	15.0	12.4	5.72	2.6	2.2	1.2
^{238}U	0.001	1.05	0.819	1.3	1.85	1.56	0.627	3.0	2.5	1.2

Each column represents data from 3 separate 10-run analyses using 100 um laser beam. Sky. = Skyward-Facing Varnished surface; Ground. = Ground-Facing Varnished surface; Unvar. = Unvarnished surface.

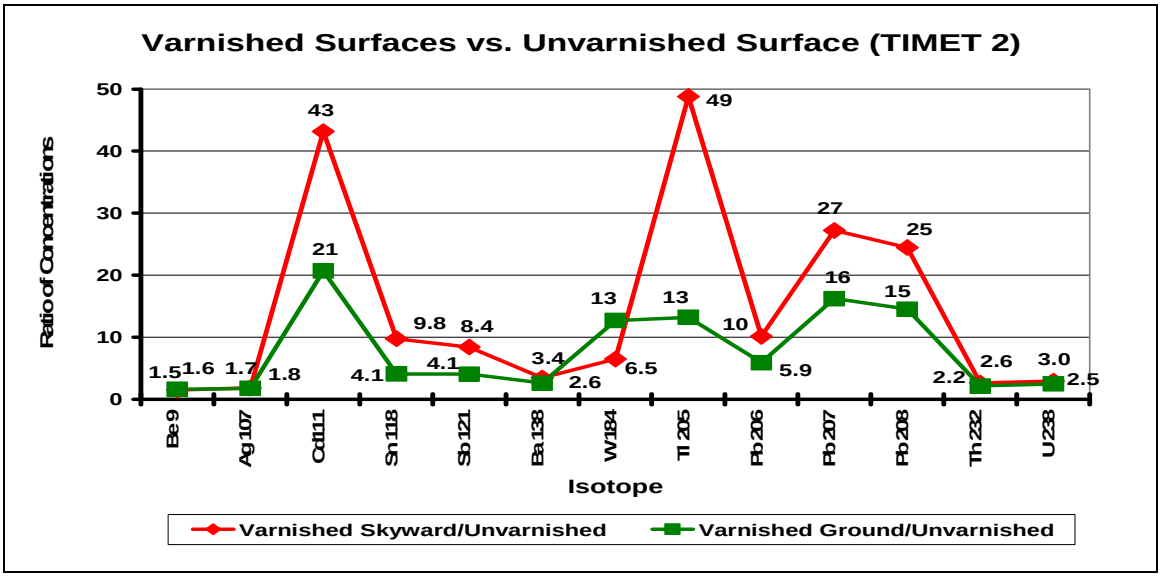

Figure 5.15. Ratio of the elements in the skyward-facing varnished surface, ground-facing varnished surface and unvarnished surface of the desert varnish sample TIMET 2 by Axiom LA-ICPMS analysis.

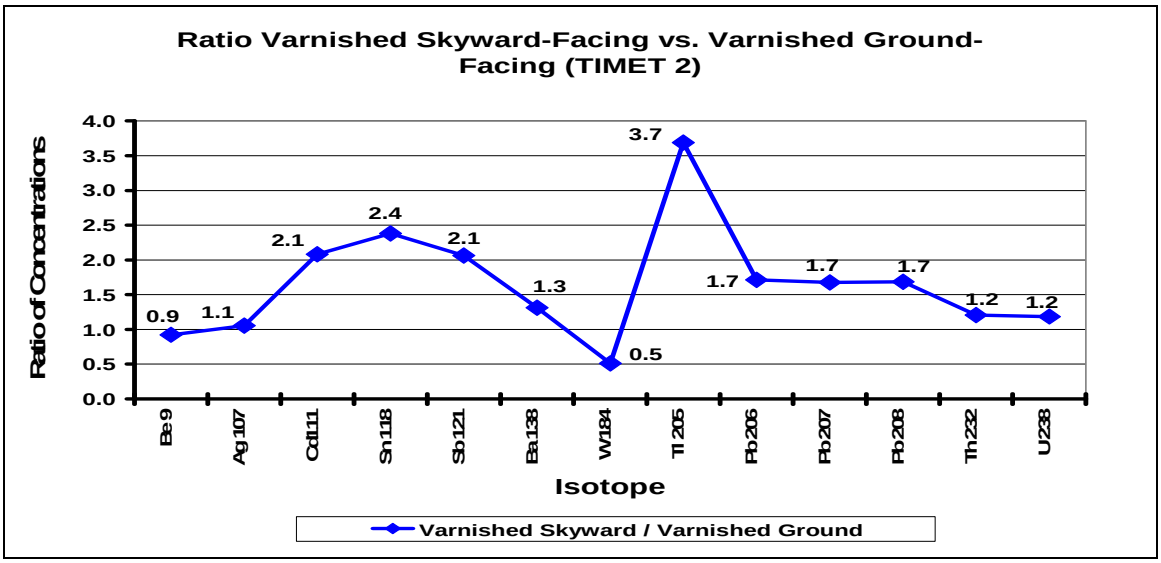

Figure 5.16. Ratio of the elements in the skyward-facing varnished surface vs. the ground-facing varnished surface of the desert varnish sample (TIMET 2) by Axiom LA-ICPMS analysis.

Interestingly, W and Be concentrations are higher in the ground-facing surfaces and may indicate incorporation of these elements in the rock surfaces from other sources. The difference in the atmospheric deposition of trace metals in the skyward-facing varnishes is illustrated by the Pb signals obtained during analysis of TIMET 2. The Pb signal from the skyward-facing varnished surface is orders of magnitude higher than the Pb signal from the varnished ground-facing surface (Figures 5.17 and 5.18).

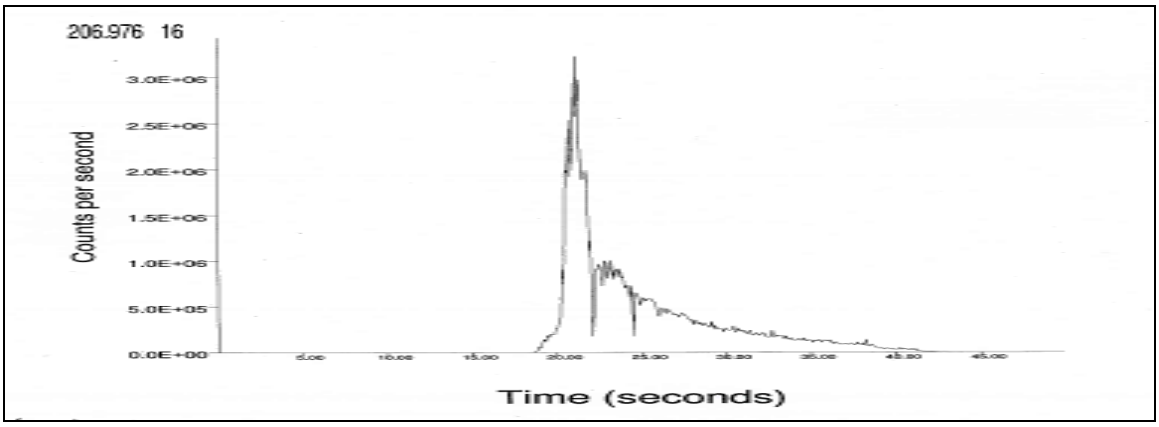

Figure 5.17. Axiom LA-ICPMS single point ablation signal for Pb from a scan of a varnished skyward-facing surface of the TIMET 2 sample.

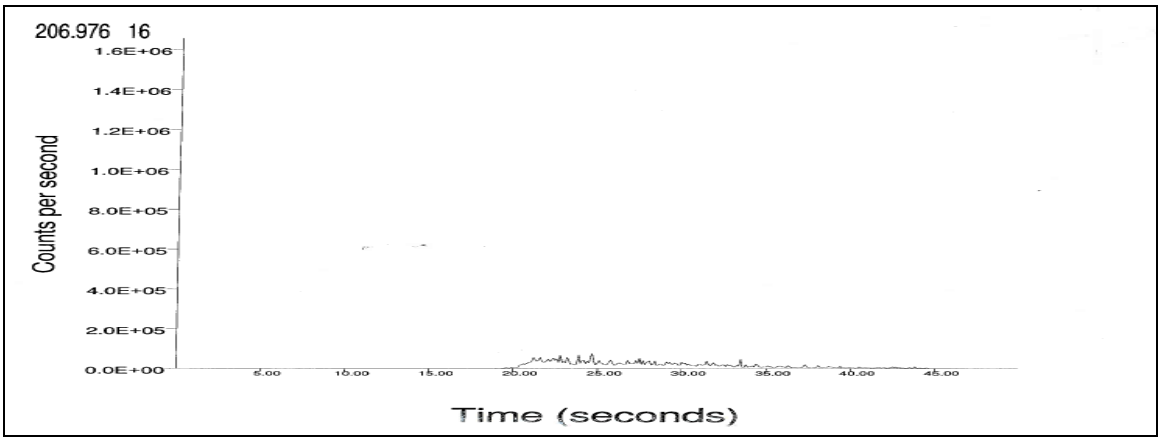

Figure 5.18. Axiom LA-ICPMS single point ablation signal for Pb from a scan of a varnished ground-facing surface of the TIMET 2 sample.

To evaluate the difference between varnished and unvarnished surfaces in RGPP 3, the null hypothesis, that the means of the results from analysis of both surfaces are equal, was tested (Table 5.9) (Miller and Miller, 1984). The comparison of the experimental | *t* | values with the critical values of | *t* | (P = 0.05) shows significant difference in the concentrations of seven elements (Be, Cd, Ba, W, Tl, Pb, and Th). There is no significant difference in the concentrations of Ag, Sn, Sb, and U.

The difference between the skyward-facing varnished surface and the unvarnished surface of sample TIMET 2 was tested by comparing the means of the results from analysis of both surfaces (Table 5.10). The comparison of the experimental | *t* | values with the critical values of | *t* | (P = 0.05) demonstrate significant differences in the concentrations of nine elements (Cd, Sn, Sb, Ba, W, Tl, Pb, Th, and U). There is no significant difference in the concentrations of Be and Ag.

The ground-facing varnished and unvarnished surfaces in sample TIMET 2 were compared by analyzing the means of the analytical results (Table 5.11). The comparison of the experimental | *t* | values with the critical values of | *t* | (P = 0.05) show significant

differences in the concentrations of eight elements (Be, Ag, Cd, Sn, Sb, Pb, Th, and U).

There is no significant difference in the concentrations of Ba, W, and Tl.

Table 5.9. Comparison of means of the results from Axiom analysis of varnished and unvarnished surfaces in sample RGPP 3.

Analyte	Mean Varnished	Mean Unvarnished	*t exper.*	*t critical one-tail*	*t critical two-tail*	*df*	Significantly Different (P=0.05)
Be	2.72 ± 0.24	1.06 ± 0.35	4.74	2.35	3.18	3	Yes
Ag	0.89 ± 0.16	3.67 ± 8.37	-10.86	6.31	12.71	1	No
Cd	7.99 ± 1.51	0.51 ± 0.14	8.07	2.92	4.30	2	Yes
Sn	1.13 ± 0.14	2.36 ± 0.87	-4.55	2.92	4.30	2	No
Sb	1.70 ± 0.05	1.88 ± 0.40	-2.01	2.92	4.30	2	No
Ba	1269 ± 23	251 ± 311	46.63	2.92	4.30	2	Yes
W	4.30 ± 0.66	1.13 ± 0.57	7.81	2.92	4.30	2	Yes
Tl	2.70 ± 0.20	1.17 ± 0.52	4.28	2.35	3.18	3	Yes
Pb	263 ± 10	50.1 ± 13.3	22.64	2.13	2.78	4	Yes
Th	15.4 ± 2.0	2.09 ± 0.50	9.85	2.35	3.18	3	Yes
U	1.05 ± 0.18	0.57 ± 0.26	0.93	2.35	3.18	3	No

The experimental and critical t values calculated at P=0.05; t exper.= t experimental; df =degrees of freedom.

Table 5.10. Comparison of means of the results from Axiom analysis of skyward-facing varnished and unvarnished surfaces in sample TIMET 2.

Analyte	Mean Varnished Skyward-facing	Mean Unvarnished	*t exper.*	*t critical one-tail*	*t critical two-tail*	*df*	Significantly Different (P=0.05)
Be	2.30 ± 0.98	1.55 ± 0.04	1.32	2.92	4.30	2	No
Ag	4.85 ± 1.59	2.66 ± 0.13	1.98	6.31	12.71	1	No
Cd	7.64 ± 1.84	0.18 ± 0.02	7.03	2.92	4.30	2	Yes
Sn	7.94 ± 1.30	0.81 ± 0.14	9.43	2.92	4.30	2	Yes
Sb	7.45 ± 1.68	0.88 ± 0.09	6.77	2.92	4.30	2	Yes
Ba	1828 ± 361	532 ± 32	6.19	2.92	4.30	2	Yes
W	6.42 ± 0.67	0.99 ± 0.16	13.60	2.92	4.30	2	Yes
Tl	25.3 ± 3.7	0.52 ± 0.08	11.45	2.92	4.30	3	Yes
Pb	814 ± 239	34.2 ± 14.8	6.26	2.92	4.30	2	Yes
Th	15.0 ± 4.5	5.72 ± 0.24	3.59	2.92	4.30	3	Yes
U	1.85 ± 0.56	0.63 ± 0.08	3.77	2.92	4.30	3	Yes

The experimental and critical t values calculated at P=0.05; t exper.= t experimental; df =degrees of freedom.

Table 5.11. Comparison of means of the results from Axiom analysis of ground-facing varnished and unvarnished surfaces in sample TIMET 2.

Analyte	Mean Varnished Ground-facing	Mean Unvarnished	*t exper.*	*t critical one-tail*	*t critical two-tail*	*df*	Significantly Different (P=0.05)
Be	2.30 ± 0.98	2.48 ± 0.15	10.57	2.92	4.30	2	Yes
Ag	4.61 ± 1.02	2.66 ± 0.13	3.32	2.92	4.30	2	Yes
Cd	3.67 ± 1.68	0.18 ± 0.02	3.61	2.92	4.30	2	Yes
Sn	3.33 ± 0.34	0.81 ± 0.14	11.86	2.92	4.30	2	Yes
Sb	3.61 ± 1.22	0.88 ± 0.09	3.87	2.35	3.18	3	Yes
Ba	1390 ± 586	532 ± 32	2.07	6.31	12.71	1	No
W	12.5 ± 7.1	0.99 ± 0.16	2.80	2.92	4.30	2	No
Tl	6.85 ± 5.07	0.52 ± 0.08	2.16	2.92	4.30	2	No
Pb	475 ± 170	34.2 ± 14.8	4.68	2.92	4.30	2	Yes
Th	12.38 ± 2.0	5.72 ± 0.24	5.67	2.92	4.30	2	Yes
U	1.56 ± 0.38	0.63 ± 0.08	4.17	2.92	4.30	2	Yes

The experimental and critical t values calculated at P=0.05; t exper.= t experimental; df =degrees of freedom.

Both skyward-facing and ground-facing varnished surfaces in sample TIMET 2 were compared by analyzing the means of the analytical results (Table 5.12). The comparison of the experimental $| t |$ values with the critical values of $| t |$ ($P = 0.05$) show significant differences in the concentrations of Cd, Sn, Sb, and Tl. There is no significant difference in concentrations of Be, Ag, Ba, W, Pb, Th, and U.

The statistical comparison of varnished and unvarnished surfaces of samples RGPP 3 and TIMET 2 confirms the differences in their chemical composition. Elements that have higher concentrations in varnish coatings (Cd, Sn, Sb, Ba, W, Tl, Pb, and Th) are frequently found in fly ash emitted from coal-fired power plants (Seames and Wendt, 2000; Furimski, 2000; Martines-Tarazona and Spears, 1996; Zeng et al., 2001; Danihelka et al., 2003). Additionally, the varnishes in RGPP3 and TIMET 2 show variations that can be attributed to the near sources of air pollution. TIMET 2 varnishes have significantly higher concentrations of Sn and Sb. There are also significant differences in the concentrations of Cd, Sn, Sb, and Tl between skyward-facing and ground-facing

varnished surfaces in TIMET 2. These elements could be emitted with particulates from the nearby titanium processing plant (Jacko and Nevendorf, 1977).

Table 5.12. Comparison of means of the results from Axiom analysis of skyward-facing and ground-facing varnished surfaces in sample TIMET 2.

Analyte	Mean Varnished Skyward-facing	Mean Varnished Ground-facing	*t exper.*	*t critical one-tail*	*t critical two-tail*	*df*	Significantly Different (P=0.05)
Be	2.30 ± 0.98	2.30 ± 0.98	-0.32	2.92	4.30	2	No
Ag	4.85 ± 1.59	4.61 ± 1.02	0.20	2.92	4.30	2	No
Cd	7.64 ± 1.84	3.67 ± 1.68	2.77	2.13	2.78	4	Yes
Sn	7.94 ± 1.30	3.33 ± 0.34	5.93	2.92	4.30	2	Yes
Sb	7.45 ± 1.68	3.61 ± 1.22	3.21	2.13	2.78	4	Yes
Ba	1828 ± 361	1390 ± 586	0.94	2.92	4.30	2	No
W	6.42 ± 0.67	12.5 ± 7.1	-1.48	2.92	4.30	2	No
Tl	25.3 ± 3.7	6.85 ± 5.07	5.06	2.13	2.78	4	Yes
Pb	814 ± 239	475 ± 170	2.10	2.13	2.78	4	No
Th	15.0 ± 4.5	12.38 ± 2.0	0.91	2.35	3.18	3	No
U	1.85 ± 0.56	1.56 ± 0.38	0.75	2.13	2.78	4	No

The experimental and critical t values calculated at P=0.05; t exper.= t experimental; df =degrees of freedom.

Quadrupole LA-ICPMS Results

The quadrupole LA-ICPMS was used for analysis of desert varnish samples. Concentrations of 25 isotopes (^{9}Be, ^{51}V, ^{52}Cr, ^{59}Co, ^{60}Ni, ^{65}Cu, ^{66}Zn, ^{88}Sr, ^{98}Mo, ^{107}Ag, ^{111}Cd, ^{115}In, ^{118}Sn, ^{121}Sb, ^{133}Cs, ^{137}Ba, ^{184}W, ^{197}Au, ^{205}Tl, ^{206}Pb, ^{207}Pb, ^{208}Pb, ^{209}Bi, ^{232}Th, and ^{238}U) were determined in the varnish samples collected in Arizona, California, and Nevada.

Method Detection Limit (MDL)

Method detection limits (MDLs) were calculated based on replicate measurements (n=42) of argon gas blanks and the slope of the calibration curve (3σ). The MDLs range from 0.001 $\mu g \cdot g^{-1}$ for Bi to 47.6$\mu g \cdot g^{-1}$ for Sr (Figure 5.19).

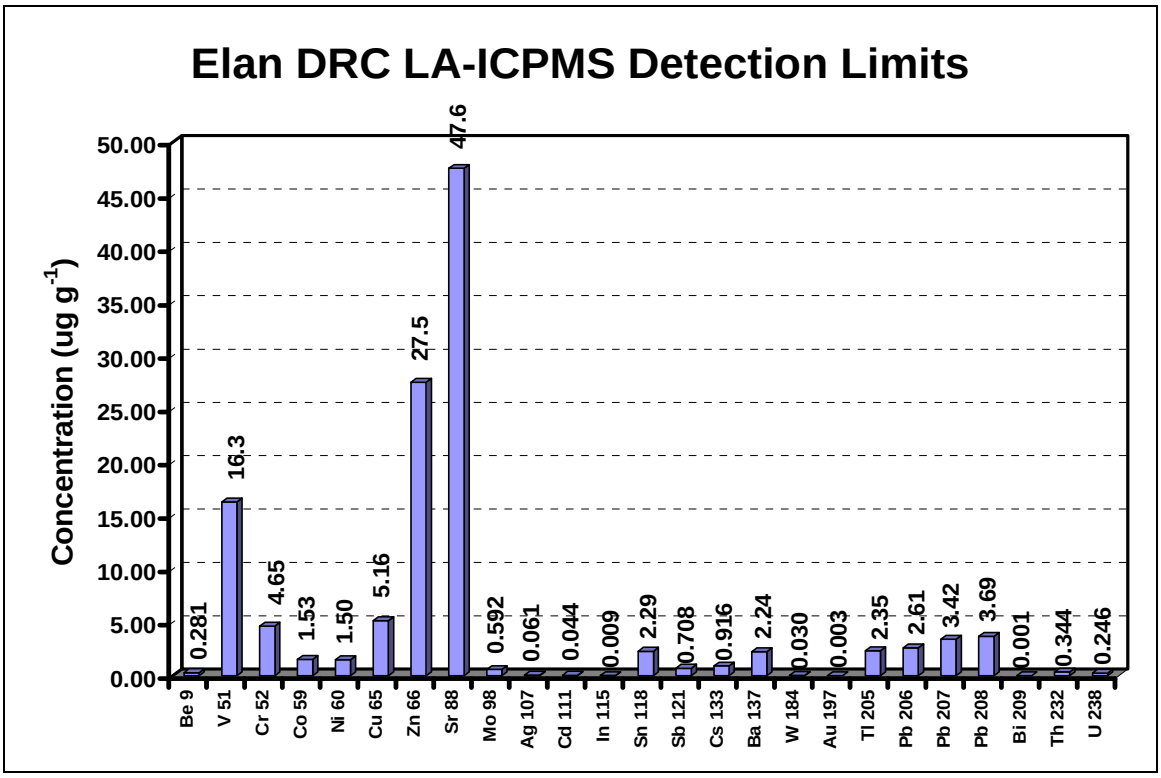

Figure 5.19. Estimated detection limits for Elan 6100 DRC LA-ICPMS analysis of desert varnish samples.

Calibration Curves and QA/QC

Three NIST SRM 612, 614, and 616 glass standards (n=3) were used for calibration and quality assurance. Calibration curves using the NIST reference glass materials yield good linearity for all elements. Correlation coefficients for instrumental response (in counts-per-second) vs. concentration are ≥ 0.995 for 21 elements (Be, V, Cr, Co, Ni, Cu, Zn, Sr, Mo, Ag, Cd, In, Sn, Sb, Cs, Ba, W, Tl, Pb, Th, and U); and equal to 1.000 for Bi (only one standard value was available) and Au.

To examine the accuracy and precision of the method, elemental concentrations were acquired for SRMs 612 and 614 using all three SRMs as standards and the desired SRM as an unknown. The recoveries for SRM 614 had many outliers, mostly for elements with concentrations near the MDL. The analyte recoveries in SRM 614 range from 59%

for Cd to 276% for Co (no values were available for Bi) (Table 5.13). Out of 23 elements, the percent recoveries for 13 analytes are outside the acceptable range of 80 to120 %: Be (69%), V (79%), Co (276%), Sr (73%), Ag (130%), Cd (59%), In (75%), Sn (124%), Sb (62%), Cs (78%), Au (63%), Tl (65%), and Pb (164%); four elements (Cr, Ni, Zn, and U) are undetected. Conversely, excellent agreement with certified or consensus values is obtained for SRM 612, with only two results falling outside of the acceptable range: Zn (69%) and Sr (77%) (no values were available for Cd, In, W, and Bi) (Table 5.13).

Precision of the analytical method is verified by calculating the relative percent difference (RPD) between duplicate measurements of SRM 612 (Table 5.13). The majority of the elements have RPDs within the acceptable limit (< 20%), except for Cd (30%) and Zn (21%). This gives confidence that the method is suitable for the analysis of rock varnish samples with concentrations above the MDLs, and that it provides quite accurate and precise results.

Sample Data

Analytical results for the Elan DRC 6100 LA-ICPMS analyses of desert varnish samples are found in Table 5.14. Each result represents the average of 9 individual analyses (3 lines, 3 runs), and was obtained using continuous-line ablations. Only varnished rock surfaces were analyzed. The irregularities of varnish coatings account for variations in %RSD (up to 304 %) of the means of the individual results (Table 5.14).

As previously observed, Ba (408 to 3.86 x 10^4 $\mu g \cdot g^{-1}$) and Pb (245 to 9.38 x 10^3 $\mu g \cdot g^{-1}$) are the most abundant, Zn (101 to 1.45 x 10^3 $\mu g \cdot g^{-1}$) and Sr (78.9 to 3.63 x 10^3 $\mu g \cdot g^{-1}$) are also enriched in all samples.

Table 5.13. Elan DRC 6100 LA-ICPMS results for glass reference materials NIST SRM 612 and 614 using three glass reference materials for calibration. Concentrations are reported in $\mu g \cdot g^{-1}$.

Element	SRM 614			SRM 612					RPD
	Found	Certified or ref value	% Rec.	Found	Found	Certified or ref value	% Rec.	% Rec.	
Be	0.50 ± 0.19	0.73	69	31.6 ± 1.8	35.0 ± 3.6	37.15	85	94	10
V	0.79 ± 0.10	1.01	79	32.7 ± 3.8	37.2 ± 4.3	38.76	84	96	13
Cr	ND	1.84	NA	32.3 ± 3.7	38.1 ± 3.8	39.59	82	96	17
Co	2.01 ± 0.71	0.73 ± 0.02	276	29.7 ± 3.0	32.9 ± 3.6	35.5 ± 1.2	81	93	14
Ni	ND	0.95	NA	31.1 ± 3.1	34.3 ± 4.5	38.8 ± 0.2	80	88	10
Cu	1.64 ± 0.71	1.37 ± 0.07	120	30.6 ± 3.5	33.5 ± 3.2	37.7 ± 0.9	81	89	9
Zn	ND	2.03	NA	26.2 ± 9.5	32.4 ± 6.4	37.96	69	85	21
Sr	33.3 ± 4.6	45.8 ± 0.1	73	60.2 ± 9.9	70.2 ± 9.7	78.4 ± 0.2	77	90	15
Mo	0.61 ± 0.08	0.74	83	30.5 ± 2.5	33.1 ± 2.6	35.99	85	92	8
Ag	0.55 ± 0.04	0.42 ± 0.04	130	24.0 ± 3.6	24.0 ± 2.7	22.0 ± 0.3	109	109	0
Cd	0.33 ± 0.04	0.55	59	20.0 ± 4.0	14.8 ± 1.7	NA	NA	NA	30
In	0.59 ± 0.04	0.79	75	30.5 ± 3.8	28.1 ± 2.5	NA	NA	NA	8
Sn	1.96 ± 0.40	0.42 ± 0.04	124	31.4 ± 3.3	32.8 ± 2.5	38.98	87	90	4
Sb	0.66 ± 0.07	1.06	62	31.6 ± 4.7	29.3 ± 2.7	36.22	87	81	8
Cs	0.51 ± 0.02	0.65	78	34.7 ± 3.6	38.0 ± 3.3	41.51	84	92	9
Ba	2.59 ± 0.21	4.70 ± 0.14	80	33.9 ± 3.4	40.6 ± 3.3	41	83	99	18
W	0.62 ± 0.08	0.74	84	27.0 ± 2.5	27.9 ± 2.1	NA	NA	NA	3
Au	0.32 ± 0.08	0.5	63	5.6 ± 0.6	5.7 ± 0.5	5	113	113	0
Tl	0.18 ± 0.03	0.269 ± 0.005	65	16.2 ± 2.4	14.5 ± 1.9	15.7 ± 0.3	103	92	12
Pb	3.81 ± 3.92	2.32 ± 0.04	164	32.8 ± 6.0	34.7 ± 2.4	38.57 ± 0.2	85	89	5
Bi	0.06 ± 0.01	NA	NA	3.0 ± 0.5	2.5 ± 0.3	NA	NA	NA	16
Th	0.62 ± 0.03	0.784 ± 0.006	83	32.7 ± 3.5	33.7 ± 2.7	37.79 ± 0.08	87	89	3
U	ND	0.823 ± 0.002	NA	31.7 ± 2.8	34.2 ± 2.5	37.38 ± 0.08	85	91	8

The "informational" values do not have uncertainties associated with them. Found values are ± 1 SD.
Certified or consensus values are ± 95% confidence limit. NA = Not Available; ND = Not Detected.

Some samples (MPP 9, RGPP4, RGPP 5, and RGPP 6) have a very high Pb signal and analyses had to be repeated due to exceedance of the upper sensitivity limit of the detector. Indium is not detected in samples TIMET 2, TIMET 3, MPP 1, MPP 4, MPP 8, and RGPP 3; and Sn is not detected in samples MPP 5a, MPP 7, MPP 8, MPP 9, and RGPP 4. Sample NTS 1 has very high concentrations of V (800 $\mu g \cdot g^{-1}$), Mo (614 $\mu g \cdot g^{-1}$), and Sb (2.07×10^3 $\mu g \cdot g^{-1}$). The concentration of U (50.3 $\mu g \cdot g^{-1}$) in NTS 1 is the highest value for U in any of the samples.

Table 5.14. Elan DRC 6100 LA-ICPMS data from desert varnish samples.

	NTS 1			NTS 2			NTS 3			TIMET 1			TIMET 2		
Isotope	ppm	SD	%RSD	ppm	SD	%RSD	ppm	SD	%RSD	ppm	SD	%RSD	ppm	SD	%RSD
^{9}Be	13.6	2.5	18	7.19	0.62	9	8.52	1.02	12	5.90	0.69	12	5.87	0.69	12
^{51}V	800	88	11	67.8	6.6	10	61.8	9.5	15	303	19	6	57.9	9.0	16
^{52}Cr	223	95	42	18.2	1.0	6	9.77	1.45	15	169	71	42	33.9	6.5	19
^{59}Co	3.79	1.72	45	213	32	15	125	13	10	171	56	33	36.4	22.7	62
^{60}Ni	14.3	3.7	26	47.1	4.1	9	58.1	3.8	7	130	26	20	25.3	11.6	46
^{65}Cu	24.7	6.7	27	62.6	9.9	16	59.5	6.3	11	239	62	26	31.3	16.2	52
^{66}Zn	305	113	37	387	50	13	388	20	5	1020	268	26	189	60	32
^{88}Sr	646	33	5	188	23	12	78.9	4.8	6	2770	202	7	1100	246	22
^{98}Mo	614	162	26	11.3	3.9	34	10.9	3.2	30	49.3	11.0	22	5.49	1.76	32
^{107}Ag	0.14	0.13	90	0.58	0.18	32	0.876	0.062	7	1.95	0.28	15	1.21	0.18	15
^{111}Cd	3.70	0.76	21	14.1	4.1	29	13.0	2.0	15	11.5	7.7	67	1.69	1.30	77
^{115}In	0.336	0.092	27	0.053	0.038	73	0.05	0.02	36	0.010	0.009	90	NA		
^{118}Sn	1.17	0.42	36	5.46	0.66	12	9.94	1.70	17	12.7	2.8	22	4.36	0.51	12
^{121}Sb	2070	317	15	4.74	0.83	17	2.33	0.03	1	8.41	1.85	22	2.33	0.70	30
^{133}Cs	1.02	0.81	80	9.87	1.73	18	7.64	2.18	28	7.14	0.34	5	3.76	0.37	10
^{137}Ba	408	87	21	2190	377	17	2590	236	9	5850	1300	22	5150	1560	30
^{184}W	19.1	4.0	21	21.9	6.5	29	10.8	1.8	16	31.5	8.5	27	6.33	2.00	32
^{197}Au	0.058	0.015	25	0.15	0.00	1	0.33	0.06	18	0.433	0.057	13	0.328	0.049	15
^{205}Tl	0.356	0.336	94	16.8	7.2	43	27.7	6.0	22	14.9	7.7	52	3.05	1.32	43
^{206}Pb	375	59	16	1300	312	24	1770	169	10	631	324	51	425	212	50
^{207}Pb	350	53	15	1220	296	24	1670	152	9	655	411	63	388	197	51
^{208}Pb	358	55	15	1250	295	24	1930	151	9	725	306	42	405	203	50
^{209}Bi	0.097	0.015	15	0.48	0.11	24	0.525	0.061	12	0.229	0.063	28	0.226	0.063	28
^{232}Th	33.5	4.2	13	158	23	14	113	7	6	64.7	8.5	13	66.0	11.1	17
^{238}U	50.3	8.6	17	14.5	0.3	2	12.1	0.9	7	13.2	2.6	19	8.44	1.58	19

Each column represents data from 3 separate 3-run analyses using 100 μm beam; NA = Not Available; ND = Not Detected.

Table 5.14 (cont.). Elan DRC 6100 LA-ICPMS data from desert varnish samples.

	TIMET 3			TIMET 4			MPP 1			MPP 2			MPP 3		
Isotope	ppm	SD	%RSD	ppm	SD	%RSD	ppm	SD	%RSD	ppm	SD	%RSD	ppm	SD	%RSD
^{9}Be	4.05	0.66	16	2.30	0.73	32	4.67	0.81	17	5.14	0.92	18	17.6	3.3	18
^{51}V	83.4	47.6	57	74.8	13.4	18	139	32	23	138	40	29	176	22	12
^{52}Cr	238	76	32	4.38	0.93	21	28.2	10.8	39	83.4	21.7	26	46.6	15.6	33
^{59}Co	35.3	22.5	64	55.6	6.2	11	130	18	14	309	108	35	457	118	26
^{60}Ni	34.7	24.8	71	27.0	5.4	20	89.9	13.4	15	132	66	50	160	40	25
^{65}Cu	63.4	28.4	45	33.0	3.2	10	93.5	14.1	15	232	129	56	238	82	35
^{66}Zn	373	143	38	200	31	15	578	92	16	812	406	50	523	162	31
^{88}Sr	2100	869	41	908	316	35	3630	661	18	1420	478	34	1230	246	20
^{98}Mo	9.12	5.18	57	2.11	0.34	16	5.20	0.84	16	17.5	2.8	16	13.8	1.7	12
^{107}Ag	0.994	0.310	31	0.623	0.100	16	1.27	0.37	29	2.84	1.41	50	1.87	0.28	15
^{111}Cd	2.27	1.49	66	3.59	0.80	22	9.55	0.70	7	27.9	20.0	72	16.2	7.5	46
^{115}In	ND			0.012	0.010	88	ND			0.131	0.036	28	0.041	0.027	65
^{118}Sn	8.03	0.77	10	4.75	0.19	4	3.45	0.65	19	9.70	1.03	11	4.21	0.68	16
^{121}Sb	7.49	3.12	42	1.85	0.26	14	3.10	0.41	13	17.5	2.1	12	3.81	0.48	13
^{133}Cs	4.43	2.79	63	1.08	0.21	19	12.3	3.2	26	7.80	3.05	39	4.13	1.29	31
^{137}Ba	5470	1400	26	1750	486	28	13500	1270	9	38600	18700	34	13600	4300	32
^{184}W	12.1	6.0	49	3.10	0.40	13	5.24	0.63	12	13.3	2.5	19	5.41	0.75	14
^{197}Au	0.330	0.069	21	0.085	0.014	16	0.171	0.044	26	0.110	0.033	30	0.248	0.051	21
^{205}Tl	5.43	2.76	51	3.68	0.85	23	6.63	1.37	21	31.0	24.1	78	17.7	8.7	49
^{206}Pb	315	150	48	753	63	8	5120	749	15	4720	2300	49	1980	338	17
^{207}Pb	287	137	48	691	59	9	6610	927	14	5970	2950	49	1580	269	17
^{208}Pb	301	143	48	715	60	8	5850	839	14	5400	2700	50	2070	337	16
^{209}Bi	0.136	0.055	40	0.550	0.076	14	0.313	0.045	14	0.759	0.104	14	0.472	0.077	16
^{232}Th	50.4	13.7	27	22.3	2.8	12	46.4	7.5	16	92.2	12.5	14	107	10	10
^{238}U	8.67	3.17	37	5.07	1.14	23	8.69	2.16	25	7.88	1.57	20	7.01	1.02	15

Each column represents data from 3 separate 3-run analyses using 100 μm beam; NA = Not Available; ND = Not Detected.

Table 5.14 (cont.). Elan DRC 6100 LA-ICPMS data from desert varnish samples.

	MPP 4			MPP 5			MPP 5a			MPP 6			MPP 7		
Isotope	ppm	SD	%RSD	ppm	SD	%RSD	ppm	SD	%RSD	ppm	SD	%RSD	ppm	SD	%RSD
^{9}Be	1.96	0.53	27	5.33	0.79	15	16.4	5.0	31	9.16	1.75	19	5.11	1.30	25
^{51}V	135	26	19	152	38	25	245	114	46	154	27	18	241	84	35
^{52}Cr	112	58	52	30.0	8.6	29	61.4	36.2	59	12.8	3.7	29	21.0	8.8	42
^{59}Co	94.9	5.8	6	166	26	16	506	255	50	110	16	15	345	177	51
^{60}Ni	98.4	12.1	12	60.4	14.7	24	204	115	57	52.5	9.2	18	336	86	26
^{65}Cu	81.9	24.3	30	85.1	31.7	37	NA			157	12	7	NA		
^{66}Zn	182	38	21	365	75	20	572	280	49	1450	39	3	299	136	45
^{88}Sr	1050	504	48	424	141	33	758	61	8	350	169	48	808	374	46
^{98}Mo	1.52	1.12	74	6.45	1.31	20	8.18	2.92	36	4.29	2.06	48	3.48	1.61	46
^{107}Ag	0.279	0.110	39	1.33	0.15	22	1.60	0.34	21	0.143	0.041	29	0.360	0.225	63
^{111}Cd	4.62	2.73	59	9.50	1.09	12	24.7	21.3	86	2.35	0.95	41	6.94	6.74	97
^{115}In	NA			0.118	0.035	29	0.151	0.146	97	1.87	0.58	31	0.074	0.095	128
^{118}Sn	1.80	0.48	26	10.0	2.1	21	ND			1.16	0.69	60	ND		
^{121}Sb	0.680	0.165	24	28.1	4.6	16	4.62	2.84	61	1.60	0.30	19	1.83	0.82	45
^{133}Cs	0.730	0.353	48	4.27	0.86	20	19.9	11.9	60	7.30	0.80	11	1.56	0.99	63
^{137}Ba	1950	774	40	1810	279	15	9470	490	5	10000	7050	70	4140	2800	68
^{184}W	2.24	0.32	14	8.40	1.69	20	9.42	3.51	37	1.53	0.17	11	6.80	2.69	40
^{197}Au	0.04	0.02	49	0.254	0.038	15	0.045	0.028	62	0.037	0.014	37	0.009	0.006	67
^{205}Tl	1.39	0.66	47	3.15	0.51	16	36.1	32.3	89	1.07	0.65	61	2.96	1.04	35
^{206}Pb	283	19	7	5870	4580	78	1220	440	36	691	161	23	956	413	43
^{207}Pb	258	16	6	9380	5260	56	1120	403	36	652	152	23	891	382	43
^{208}Pb	275	19	7	8700	4870	56	1100	391	35	670	157	23	NA		
^{209}Bi	0.187	0.035	19	0.759	0.155	20	0.692	0.255	37	0.257	0.078	30	0.632	0.281	44
^{232}Th	9.03	2.70	30	57.1	9.1	16	63.3	13.4	21	15.7	4.6	29	21.9	10.1	46
^{238}U	1.52	0.48	31	11.4	3.2	28	14.4	7.7	53	0.711	0.251	35	4.12	2.63	64

Each column represents data from 3 separate 3-run analyses using 100 μm beam; NA = Not Available; ND = Not Detected.

Table 5.14 (cont.). Elan DRC 6100 LA-ICPMS data from desert varnish samples.

	MPP 8			MPP 9			MPP 10			RGPP 1			RGPP 2		
Isotope	ppm	SD	%RSD	ppm	SD	%RSD	ppm	SD	%RSD	ppm	SD	%RSD	ppm	SD	%RSD
^{9}Be	11.2	3.5	31	2.93	0.68	23	3.72	0.84	23	12.3	1.8	15	2.47	0.80	32
^{51}V	25.8	13.3	51	76.7	14.5	19	244	51	21	74.7	12.0	16	76.0	25.2	33
^{52}Cr	ND			16.8	6.4	38	38.1	7.0	18	13.3	0.2	1	18.8	6.5	35
^{59}Co	135	81	60	57.9	11.4	20	159	29	18	204	17	8	123	45	37
^{60}Ni	71.3	29.2	41	60.3	12.3	20	71.7	16.1	22	37.6	10.7	29	70.7	36.2	51
^{65}Cu	NA			NA			NA			68.2	15.9	23	55.1	24.9	45
^{66}Zn	101	73	72	213	34	16	205	46	23	869	143	17	375	170	45
^{88}Sr	211	22	10	340	210	62	1520	612	40	327	116.0	36	241	16	7
^{98}Mo	0.965	0.528	55	1.66	0.32	19	8.64	2.07	24	10.7	0.7	6	2.41	0.69	29
^{107}Ag	0.974	0.156	16	0.333	0.039	12	0.972	0.282	29	0.639	0.089	14	0.450	0.155	34
^{111}Cd	7.18	7.12	99	7.55	1.54	20	8.09	3.67	45	19.8	1.9	10	11.3	6.0	53
^{115}In	ND			0.206	0.021	10	0.169	0.040	24	0.028	0.021	73	0.010	0.031	304
^{118}Sn	ND			ND			1.15	1.25	109	11.3	1.1	10	4.46	0.86	19
^{121}Sb	0.470	0.282	60	3.45	0.26	7	4.17	0.56	13	2.97	0.98	33	4.44	1.11	25
^{133}Cs	1.71	1.19	70	4.52	0.81	18	3.93	0.22	6	5.40	0.42	8	2.25	0.65	29
^{137}Ba	852	254	30	4980	1850	37	16800	6960	42	3610	52	1	5300	1940	37
^{184}W	0.897	0.396	44	2.90	0.42	14	6.39	1.96	31	7.34	1.09	15	9.34	3.35	36
^{197}Au	0.016	0.006	38	0.011	0.004	40	0.329	0.524	159	0.334	0.069	21	0.079	0.060	76
^{205}Tl	9.11	10.69	117	5.47	1.44	26	14.7	1.2	8	13.1	1.0	8	2.24	1.57	70
^{206}Pb	262	99	38	1110	131	12	1360	223	16	4560	975	21	806	161	20
^{207}Pb	245	93	38	1050	126	12	1260	211	17	3610	758	21	898	0	0
^{208}Pb	245	92	38	NA			1150	201	17	4680	987	21	760	149	20
^{209}Bi	0.170	0.057	33	0.762	0.123	16	1.32	0.28	21	0.457	0.111	24	0.44	0.08	18
^{232}Th	4.09	2.24	55	27.1	3.3	12	60.9	6.1	10	78.3	8.9	11	37.8	8.5	22
^{238}U	0.638	0.433	68	5.09	0.83	16	18.3	3.8	21	7.20	1.51	21	1.97	0.88	45

Each column represents data from 3 separate 3-run analyses using 100 μm beam; NA = Not Available; ND = Not Detected.

Table 5.14 (cont.). Elan DRC 6100 LA-ICPMS data from desert varnish samples.

	RGPP 3			RGPP 4			RGPP 5			RGPP 6			BKG 2		
Isotope	ppm	SD	%RSD	ppm	SD	%RSD	ppm	SD	%RSD	ppm	SD	%RSD	ppm	SD	%RSD
^{9}Be	4.36	0.59	14	16.9	6.6	39	23.4	2.0	8	12.9	1.7	13	3.74	0.57	15
^{51}V	86.7	9.3	11	61.6	38.1	62	52.6	16.6	32	191	19	10	196	28	14
^{52}Cr	29.8	6.2	21	38.7	37.0	96	11.4	0.7	6	94.5	12.0	13	406	45	11
^{59}Co	169	0	0	296	226	77	149	9	6	479	109	23	79.7	37.3	47
^{60}Ni	74.6	6.4	9	198	132	66	122	19	15	206	31	15	202	36	18
^{65}Cu	40.1	0.9	2	NA			NA			NA			99.4	24.6	25
^{66}Zn	178	24	14	465	182	39	476	23	5	552	54	10	1290	207	16
^{88}Sr	906	74	8	216	175	81	154	27	17	197	26	13	121	15	13
^{98}Mo	10.9	1.2	11	1.84	1.23	67	3.29	0.77	23	12.8	2.8	22	8.63	1.85	21
^{107}Ag	0.416	0.396	95	1.63	0.63	39	1.92	0.28	15	1.29	0.38	29	2.04	0.14	7
^{111}Cd	2.12	0.24	11	20.7	12.4	60	14.4	1.0	7	39.8	4.7	12	14.6	4.4	30
^{115}In	NA			0.059	0.157	266	0.200	0.028	14	0.342	0.107	31	0.027	0.025	94
^{118}Sn	1.35	0.88	65	ND			12.2	1.3	11	9.21	3.58	39	7.71	1.92	25
^{121}Sb	1.62	0.70	43	2.88	1.52	53	6.33	3.56	56	9.02	1.58	17	5.96	1.12	19
^{133}Cs	6.54	1.69	26	8.54	4.16	49	8.50	0.05	1	21.1	1.4	6	11.6	2.0	17
^{137}Ba	32300	1280	4	3450	1880	55	4710	1560	33	5360	893	17	1900	608	32
^{184}W	4.67	0.97	21	13.2	16.5	125	72.3	70.6	98	18.5	2.9	16	5.00	1.48	30
^{197}Au	0.099	0.093	94	0.030	0.021	70	0.037	0.008	22	0.055	0.043	78	0.108	0.013	12
^{205}Tl	2.87	0.61	21	31.5	17.8	57	27.3	7.7	28	26.9	4.3	16	5.72	2.08	36
^{206}Pb	600	69	11	1230	863	70	2130	55	3	1770	449	25	668	174	26
^{207}Pb	552	60	11	1140	813	71	1990	54	3	NA			613	165	27
^{208}Pb	565	61	11	NA			NA			NA			626	160	26
^{209}Bi	0.101	0.008	7	0.799	0.669	84	1.49	0.05	3	1.06	0.28	26	0.19	0.05	25
^{232}Th	44.5	1.6	4	52.4	36.1	69	77.1	10.9	14	117	6	5	35.3	4.6	13
^{238}U	3.87	1.19	31	6.88	6.10	89	14.7	2.1	15	20.4	0.9	4	12.0	1.4	12

Each column represents data from 3 separate 3-run analyses using 100 μm beam; NA = Not Available; ND = Not Detected.

Figures 5.20 through 5.23 show selected elemental abundances for each point source normalized to estimates of the average composition of the UCC, and are plotted in order of the relative enrichment.

There is a noticeable difference in the chemical composition of sample NTS 1, and both NTS 2 and NTS 3 (Figure 5.20). The NTS 1 sample shows enrichment of Sb > Mo >> Cd > Pb > U > W > V > Be > In > Zn > Th > Cr > Sr; where Sb and Mo are extremely enriched at 2.76×10^3 and 1.02×10^3 times more than in the UCC, respectively. Cadmium and Pb are also highly enriched, about 62 and 22 times more than in the UCC. On the other hand, Cu, Tl, Ba, Sn, Bi, Ni, Co, and Cs are depleted. The NTS 1 sample also has a very low ratio of Th/U = 0.67, while the average UCC values range from 3.7 to 4.0 (Condie, 1993). The low ratio of Th/U could possibly be attributed to the radioactive fallout following nuclear testing, and the resulting elevated environmental levels of U, since the sampling site is located next to the NTS.

The samples NTS 2 and NTS 3 are enriched with Cd > Pb > Tl > Mo > Th > W > Co > Sb > U > Zn > Be > Ba > Sn > Cu > Bi > Cs > Ni. Both NTS 2 and NTS 3 are highly enriched in Cd, Tl, and Pb. Depleted elements include V, Cr, Sr, and In. All three NTS samples are enriched in Mo and W, which could be explained by their location in the W mineralization belt. Large quantities of W have been dispersed into the environment in central Nevada as a result of W mining and smelting operations (Diaz, 2003; Wayne et al. 2006).

The TIMET samples show enrichment of Cd > Pb > Mo > Tl > Co > Sr > Ba > Zn > Th > Sb > W > Sn > U > Cu > Be, ranging from 28 to 192 times more than in the UCC

for Cd, and from 1.2 to 3 times more for Be (Figure 5.21). Vanadium, Cr, Ni, In, Cs, and Bi show variable enrichment and depletion.

Cadmium and Pb have the highest enrichment in all MPP samples, ranging from 39 to 465 times that of the UCC for Cd, and from 15 to 345 times for Pb (Figure 5.22). All MPP samples also show an enrichment of 3 to 87 times more than the UCC values for Tl > Co > Mo > Ba > Zn > Ni > Sb. Antimony, W and Th are depleted only in MPP 8. Beryllium, V, Cr, Cu, Sr, In, Sn, Cs, Bi, and U show variable enrichment and depletion.

The RGPP samples show enrichment of Cd > Pb > Tl > > Co > Mo > W > Th > Ba > Sb > Zn > Be > Ni, ranging from 35 to 663 times more than the UCC for Cd, and from 1.1 to 6 times more for Ni (Figure 5.23). Cesium and U are depleted only in RGPP 2; Sn and Bi are depleted only in RGPP 3. Vanadium, Cr, Sr and In show variable enrichment and depletion.

The elements enriched in the fly ash from coal-fired power plants (V, Cr, Co, Ni, Cu, Zn, Cd, Sn, Sb, Tl and Pb) are often emitted into the atmosphere (Seames and Wendt, 2000; Furimski, 2000; Zeng et al., 2001; Danihelka et al., 2003). These elements have the highest enrichment relative to the UCC in the majority of the analyzed desert varnish samples. The elemental concentrations were plotted against the distance from each of the power plants and showed agreement with the predictions of the Gaussian Plume model (Figures 5.24 to 5.27)(Anderson et al., 1975; Connor et al., 1976; Wangen and Williams, 1978).

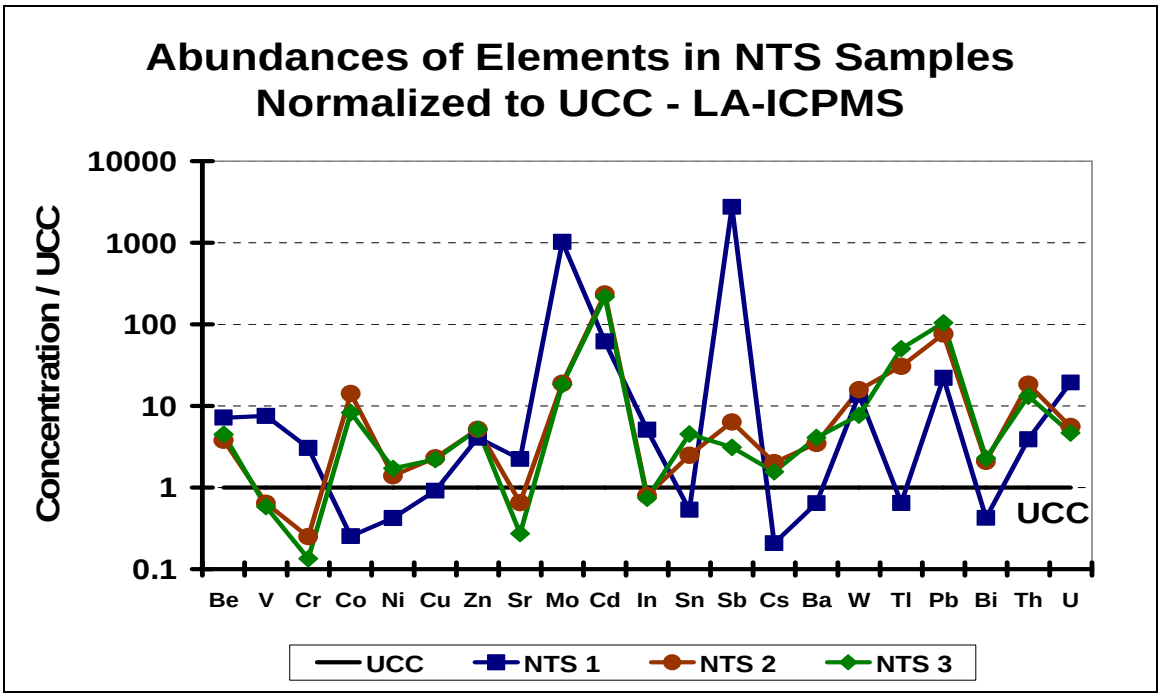

Figure 5.20. Abundances of elements in the varnish coatings of NTS samples analyzed by Elan LA-ICPMS and normalized to the UCC values. The thick black line represents the average UCC abundance (Ratio=1).

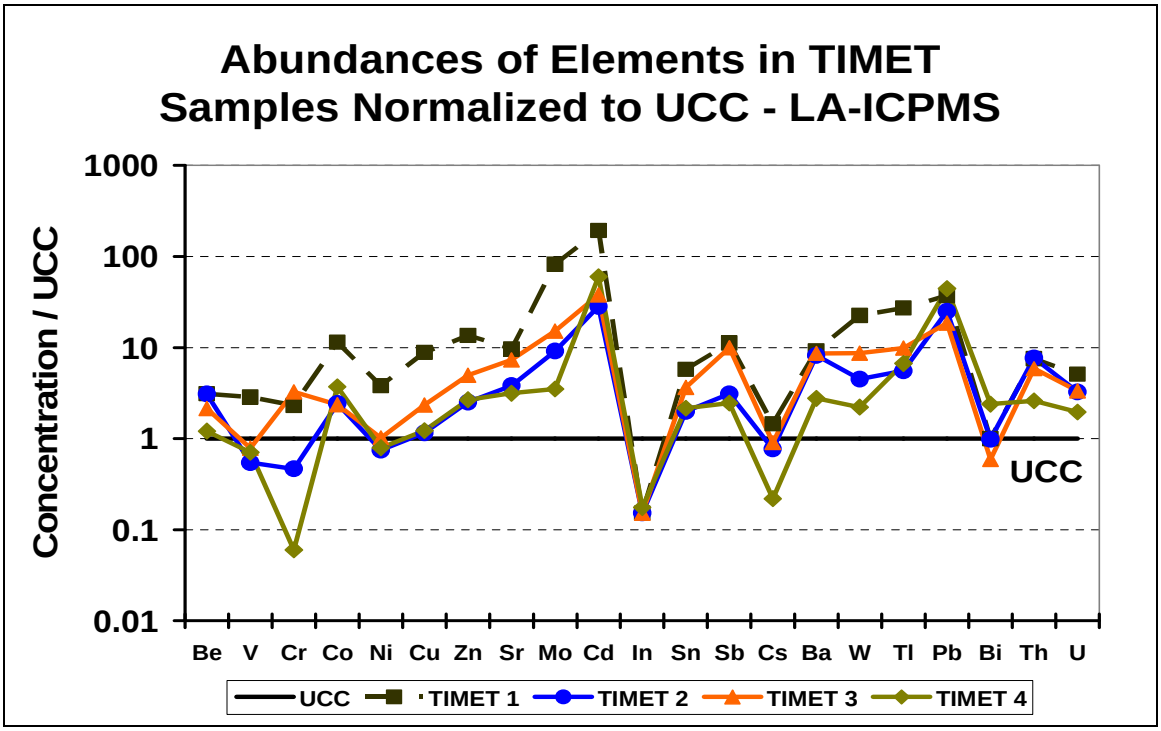

Figure 5.21. Abundances of elements in the varnish coatings of TIMET samples analyzed by Elan LA-ICPMS and normalized to the UCC values. The thick black line represents the average UCC abundance (Ratio=1).

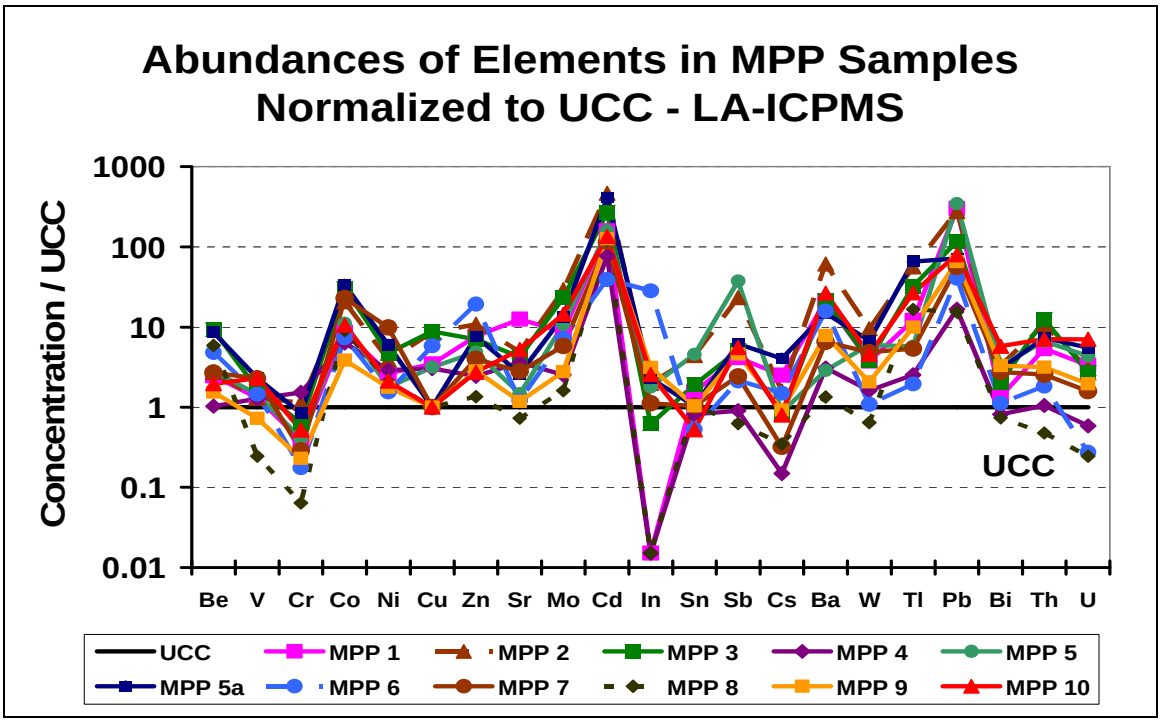

Figure 5.22. Abundances of elements in the varnish coatings of MPP samples analyzed by Elan LA-ICPMS and normalized to the UCC values. The thick black line represents the average UCC abundance (Ratio=1).

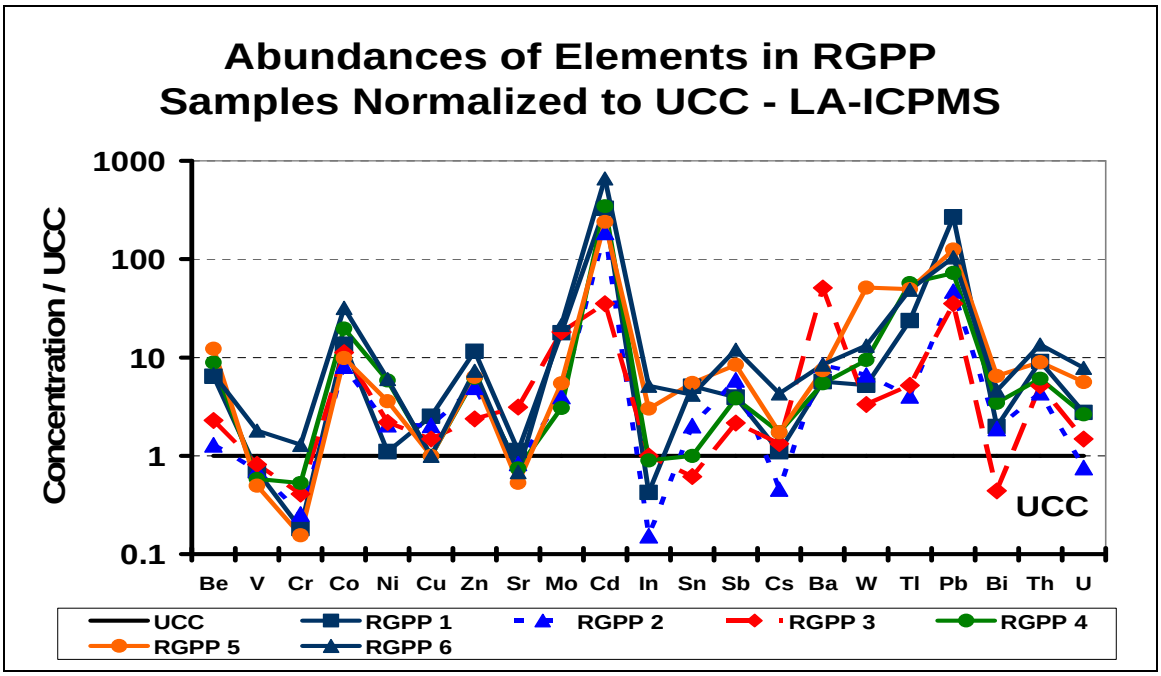

Figure 5.23. Abundances of elements in the varnish coatings of RGPP samples analyzed by Elan LA-ICPMS and normalized to the UCC values. The thick black line represents the average UCC abundance (Ratio=1).

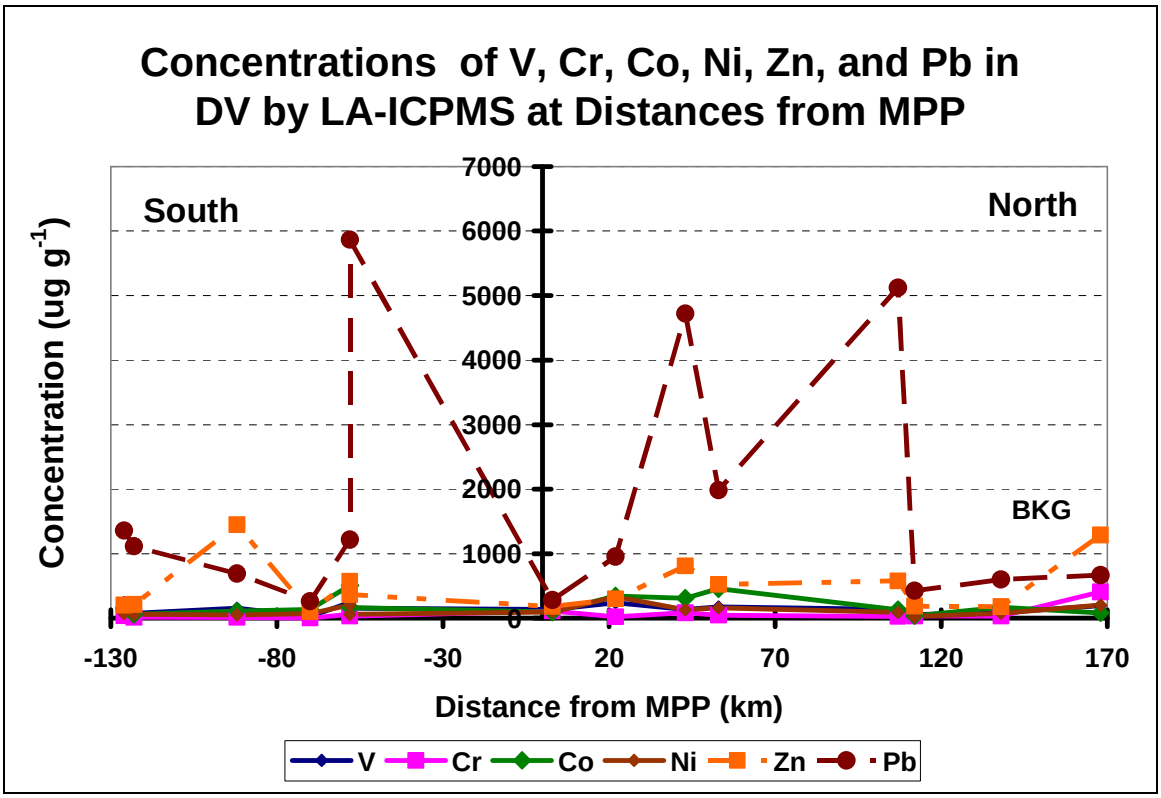

Figure 5.24. Concentrations of V, Cr, Co, Ni, Zn, and Pb by Elan LA-ICPMS analysis of desert varnish samples as a function of distance from the MPP.

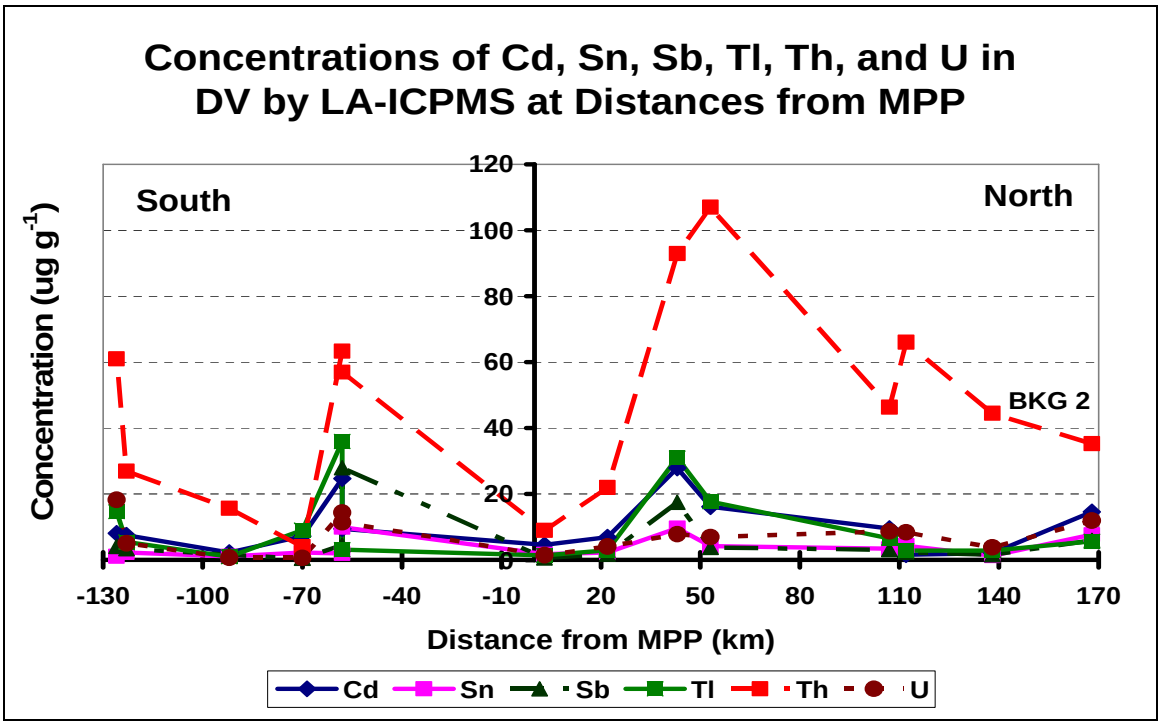

Figure 5.25. Concentrations of Cd, Sn, Sb, Tl, Th, and U by Elan LA-ICPMS analysis of desert varnish samples as a function of distance from the MPP.

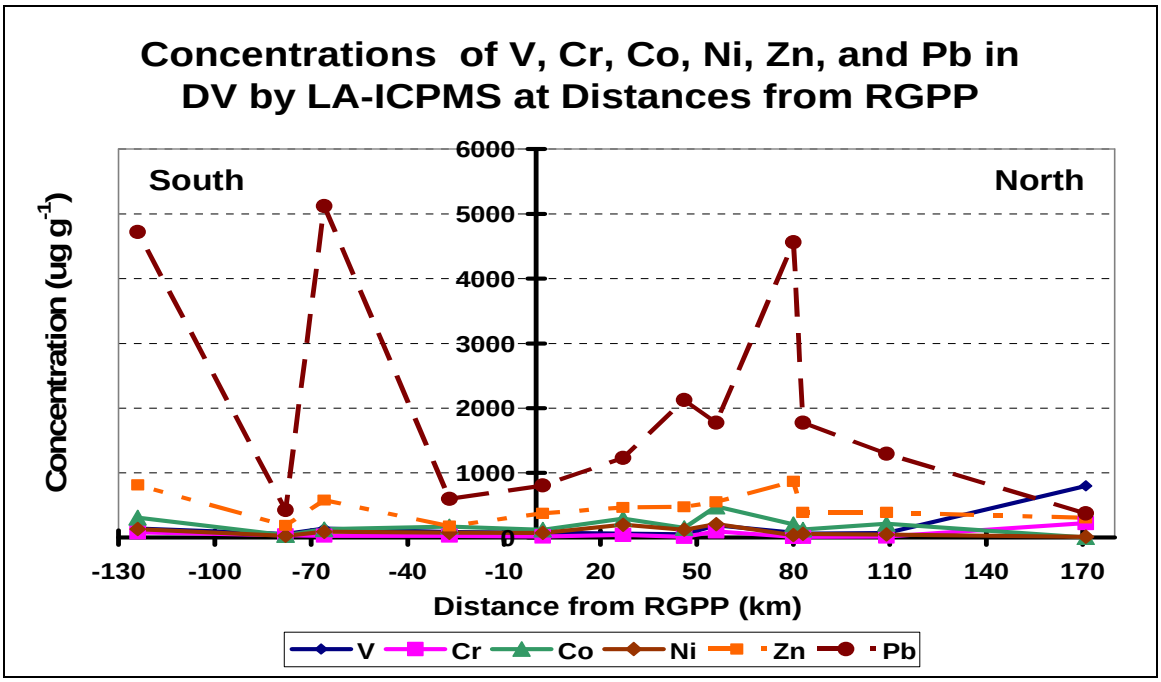

Figure 5.26. Concentrations of V, Cr, Co, Ni, Zn, and Pb by Elan LA-ICPMS analysis of desert varnish samples as a function of distance from the RGPP.

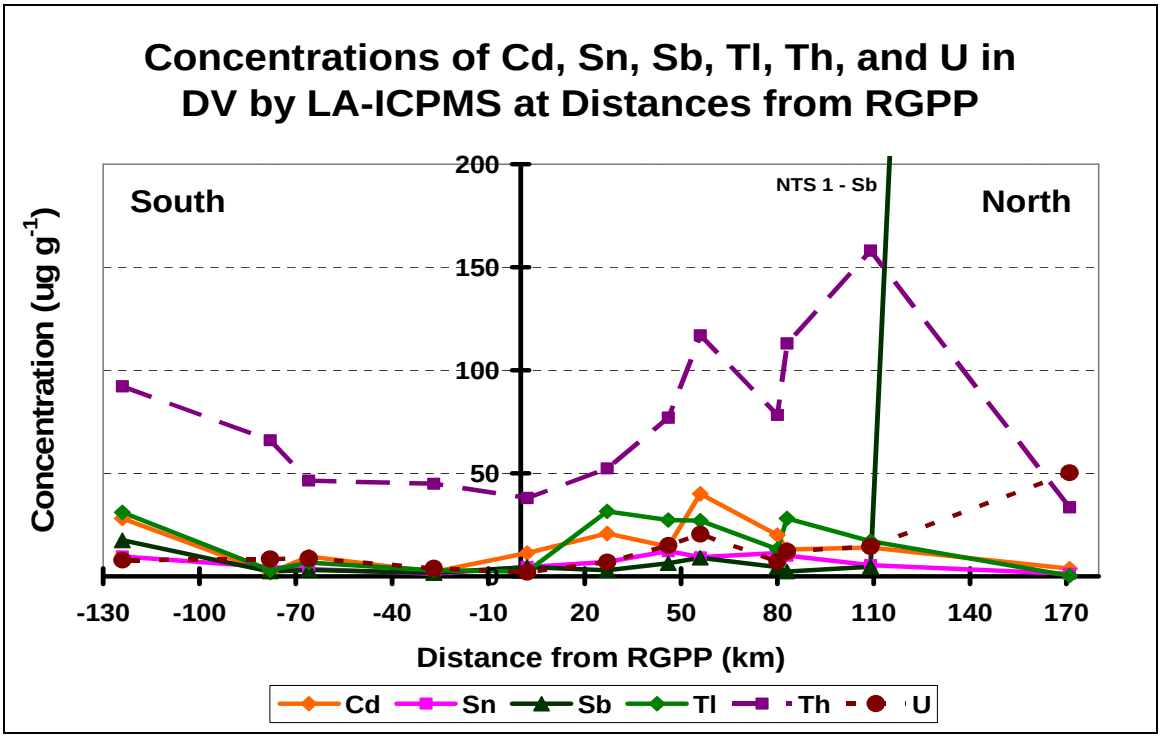

Figure 5.27. Concentrations of Cd, Sn, Sb, Tl, Th, and U by Elan LA-ICPMS analysis of desert varnish samples as a function of distance from the RGPP. The black vertical line at 110 km north of the RGPP represents the off-scale Sb concentration in NTS 1 at 2.07 x 10^3 µg·g^{-1}.

Quadrupole ICPMS Results

Varnishes collected in downwind locations from the Mohave Power Project (MPP) and the Reid Gardner Power Plant (RGPP) were stripped from the base rock with concentrated HCl. The resulting solutions were analyzed with the quadrupole ICPMS.

Moisture Content and HCl Stripping of Varnished Rocks

Prior to stripping of the varnished rocks, the moisture content (% H_2O) was determined as the average weight loss after heating the samples at 145ºC to constant weight. The % H_2O ranged from 0.01% for RGPP 6 to 0.77% for RGPP 5 (Table 5.15). The amount of stripped varnish depends on the surface area of the stripped rock and the thickness of the varnish coating. The weight of the stripped varnishes varied from 0.0011 g (0.0205 $\mu g \cdot g^{-1}$ in solution) for MPP 8 to 0.3398 g (6.5474 $\mu g \cdot g^{-1}$ in solution) for RGPP 6. During the HCl stripping, initially some effervescence was observed on the surfaces of a few of the rocks, which may indicate the presence of carbonates or other acid-reactive residues. Consequently, the weights of acid-stripped material for some samples (BKG 2 - 3 replicates, RGPP 6 - replicate 3, MPP 9 – replicate 2) were unusually high and the analytical results were not included in the final calculations. It should be noted that the geology of the substrate rock has to be considered during sample preparation. Varnishes cannot be selectively removed from some sedimentary acid-soluble rocks, like limestone ($CaCO_3$) or dolomite ($CaMg(CO_3)_2$). Similar considerations would apply to brittle or disintegrating rocks, such as soft sandstones that may lose some non-varnish material during sample preparation.

Table 5.15. Moisture content (%H_2O) and weight of stripped varnishes from desert varnish samples. All samples were analyzed in triplicate.

Sample	Weight (g)	Dry Weight (g)	Stripped Varnish (mg)	Varnish (μg·g^{-1})	% H_2O
NTS 1 1	0.9419	0.9409	4.5	0.0850	0.11
NTS 1 2	0.5261	0.5256	4.1	0.0767	0.10
NTS 1 3	3.4105	3.4043	22.5	0.4091	0.18
NTS 2 1	1.5276	1.5228	3.2	0.0600	0.31
NTS 2 2	0.4993	0.4971	4.3	0.0819	0.44
NTS 2 3	0.7546	0.7518	22.7	0.4332	0.37
NTS 3 1	1.8949	1.8897	13.1	0.2436	0.27
NTS 3 2	3.1247	3.1162	16.2	0.3039	0.27
NTS 3 3	0.6738	0.6724	38.3	0.7137	0.21
TIMET 2 1	1.5778	1.5751	67.8	1.2673	0.17
TIMET 2 2	2.4829	2.4791	65.9	1.2470	0.15
TIMET 2 3	2.0768	2.0680	15.7	0.2996	0.42
MPP 1 1	1.1994	1.1977	11.2	0.1991	0.14
MPP 1 2	0.7951	0.7938	8.7	0.1537	0.16
MPP 1 3	2.1744	2.1667	40.9	0.7475	0.35
MPP 2 1	1.2035	1.2017	2.1	0.0390	0.15
MPP 2 2	1.1732	1.1717	15.2	0.2654	0.13
MPP 2 3	0.8377	0.8359	1.7	0.0307	0.21
MPP 3 1	1.6341	1.6280	13.9	0.2567	0.37
MPP 3 2	1.0760	1.0715	5.5	0.1032	0.42
MPP 3 3	0.8207	0.8170	42.7	0.8452	0.45
MPP 4 1	3.1384	3.1336	1.3	0.0234	0.15
MPP 4 2	1.5628	1.5604	5.9	0.1111	0.15
MPP 4 3	1.5068	1.5028	6.8	0.1307	0.27
MPP 5 1	1.1996	1.1982	5.5	0.1025	0.12
MPP 5 2	1.4586	1.4566	10.1	0.1907	0.14
MPP 5 3	2.2041	2.2009	4.8	0.0914	0.15
MPP 5a 1	5.0038	4.9882	95.2	1.7964	0.31
MPP 5a 2	2.6422	2.6344	16.9	0.3183	0.30
MPP 5a 3	1.1468	1.1392	6.6	0.1239	0.66
MPP 6 1	3.3381	3.3327	8.6	0.1609	0.16
MPP 6 2	1.1723	1.1700	4.5	0.0853	0.20
MPP 6 3	1.2978	1.2963	2.5	0.0479	0.12
MPP 7 1	4.5765	4.5687	11.4	0.2192	0.17
MPP 7 2	3.6707	3.6635	10.6	0.1958	0.20
MPP 7 3	2.3725	2.3679	11.9	0.2201	0.19
MPP 8 1	3.9379	3.9296	3.0	0.0560	0.21
MPP 8 2	2.4877	2.4746	6.9	0.1293	0.53
MPP 8 3	1.5084	1.5017	1.1	0.0205	0.44
MPP 9 1	1.7848	1.7842	15.1	0.2847	0.03
MPP 9 2	5.6090	5.5910	160.4	3.0451	0.32
MPP 9 3	2.8493	2.8488	7.7	0.1483	0.02
MPP 10 1	1.6784	1.6773	12.3	0.2327	0.07
MPP 10 2	1.0685	1.0682	22.8	0.4296	0.03
MPP 10 3	4.5530	4.5503	56.5	1.0326	0.06

Table 5.15 (cont.). Moisture content (%H_2O) and weight of stripped varnishes from desert varnish samples. All samples were analyzed in triplicate.

Sample	Weight (g)	Dry Weight (g)	Stripped Varnish (mg)	Varnish ($\mu g \cdot g^{-1}$)	% H_2O
RGPP 1 1	2.1270	2.1230	4.9	0.0911	0.19
RGPP 1 2	1.4382	1.4348	4.0	0.0761	0.24
RGPP 1 3	1.7299	1.7255	3.8	0.0700	0.25
RGPP 2 1	1.2337	1.2291	2.4	0.0447	0.37
RGPP 2 2	1.5220	1.5201	6.2	0.1163	0.12
RGPP 2 3	1.7440	1.7416	2.3	0.0434	0.14
RGPP 3 1	1.6654	1.6604	12.6	0.2391	0.30
RGPP 3 2	2.9498	2.9354	171.5	3.0983	0.49
RGPP 3 3	1.1174	1.1116	22.1	0.4250	0.52
RGPP 4 1	1.8817	1.8807	140.3	2.6572	0.05
RGPP 4 2	1.6726	1.6716	68.4	1.2780	0.06
RGPP 4 3	1.8495	1.8486	62.4	1.1832	0.05
RGPP 5 1	3.4821	3.4567	21.6	0.4052	0.73
RGPP 5 2	2.8656	2.8436	9.5	0.1804	0.77
RGPP 5 3	3.4137	3.3892	9.0	0.1734	0.72
RGPP 6 1	2.2205	2.2203	8.9	0.1700	0.01
RGPP 6 2	2.6901	2.6889	3.1	0.0586	0.04
RGPP 6 3	2.0290	2.0274	339.8	6.5474	0.08
BKG 1 1	5.3692	5.3607	6.8	0.1235	0.16
BKG 1 2	2.3943	2.3895	3.1	0.0587	0.20
BKG 1 3	5.0747	5.0644	4.9	0.0895	0.20
BKG 2 1	2.5908	2.5877	275.3	5.1286	0.12
BKG 2 2	1.6658	1.6638	220.8	4.0423	0.12
BKG 2 3	2.2462	2.2428	126.8	2.4576	0.15

Semi-Quantitative ICPMS Analysis

The Elan 6100 DRC ICPMS instrument can rapidly determine 81 isotopes in a single semi-quantitative scan. Thus, initially five stripped solutions (NTS 2, TIMET 2, MPP 2, MPP 4, and RGPP 3) were "screened" with the semi-quantitative technique to quickly estimate concentrations of the elements. The following mass ranges were scanned: 6-15, 19-39, 42-210, and 230-240. The elemental responses stored by the ICPMS instrument correlated measured ion intensities with known concentrations. Figures 5.28 through 5.32 present bar graphs that relate isotope masses and signal

intensities for the analyzed elements. In addition to the major elements (Na, Mg, Si, K, Ca, Mn and Fe), all "screened" solutions show high intensities of Zn, Sr, Ba, and Pb as well as Rare Earth Elements (REE). Interestingly, Platinum Group Elements (PGE) and Re, as well as radioactive Th and U are also present in most of the samples. Thus, these elements are included in the quantitative ICPMS analyses. Silver is detected only in sample MPP 2 and was probably precipitated as silver chloride (AgCl) during sample preparation. Selenium, Os, and Hg are not detected in any solution.

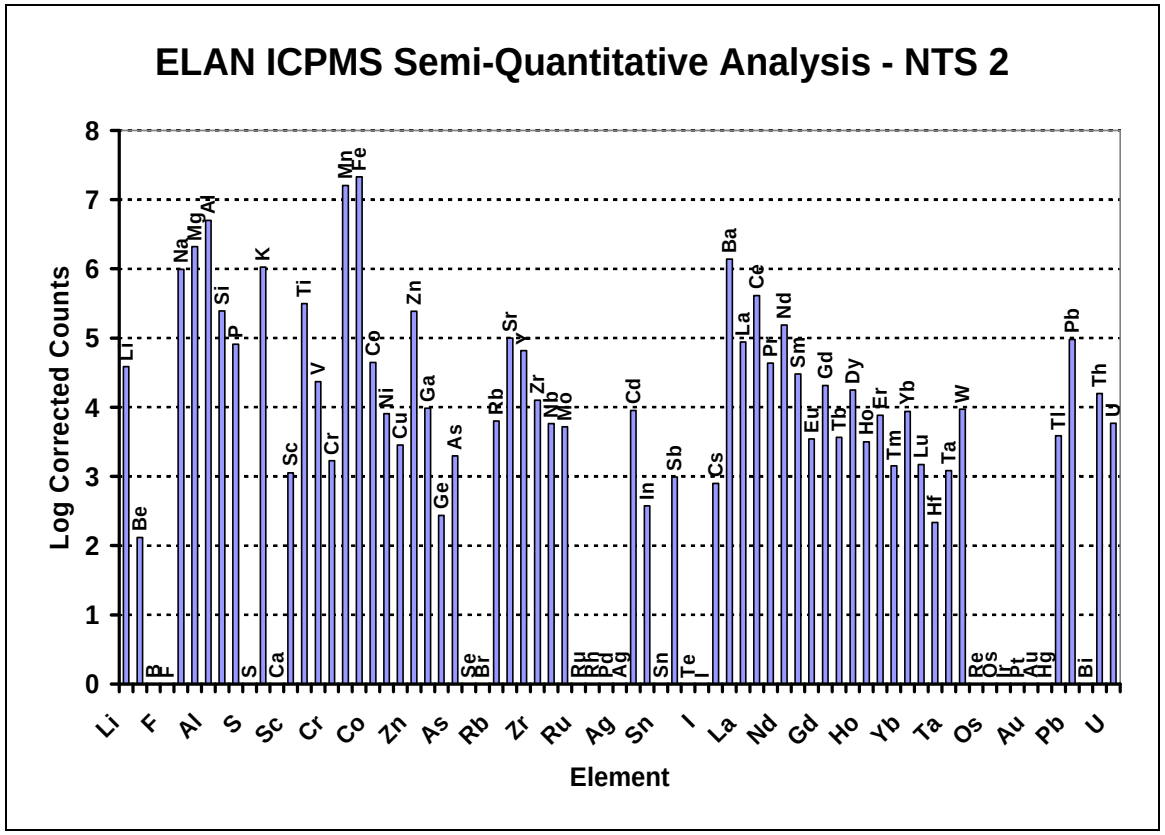

Figure 5.28. Elan 6100 DRC semi-quantitative ICPMS analysis of sample NTS 2. The corrected counts account for blank signal.

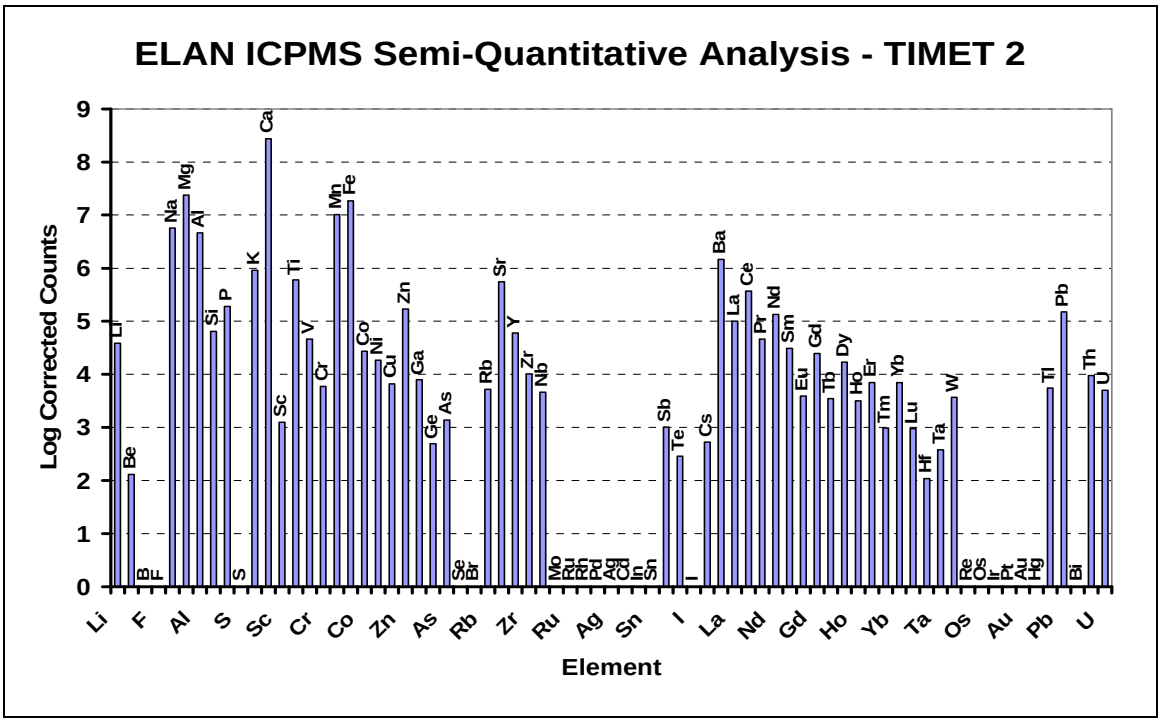

Figure 5.29. Elan 6100 DRC semi-quantitative ICPMS analysis of sample TIMET 2. The corrected counts account for blank signal.

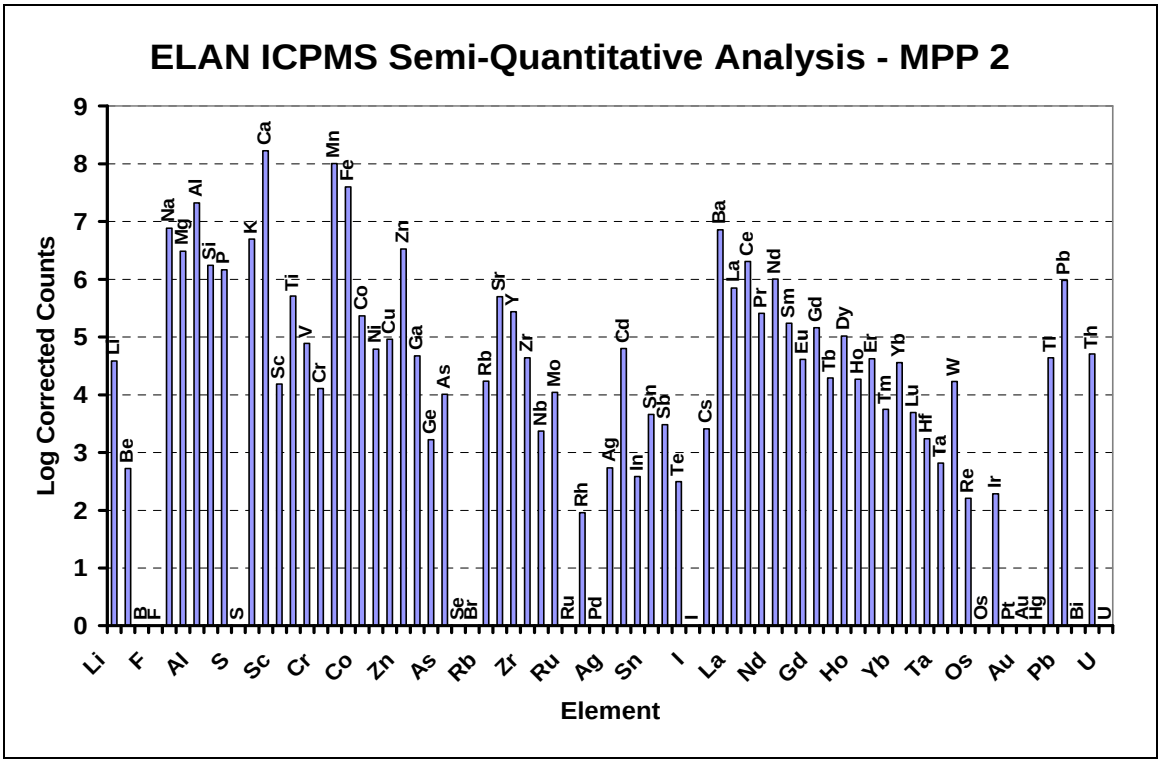

Figure 5.30. Elan 6100 DRC semi-quantitative ICPMS analysis of sample MPP 2. The corrected counts account for blank signal.

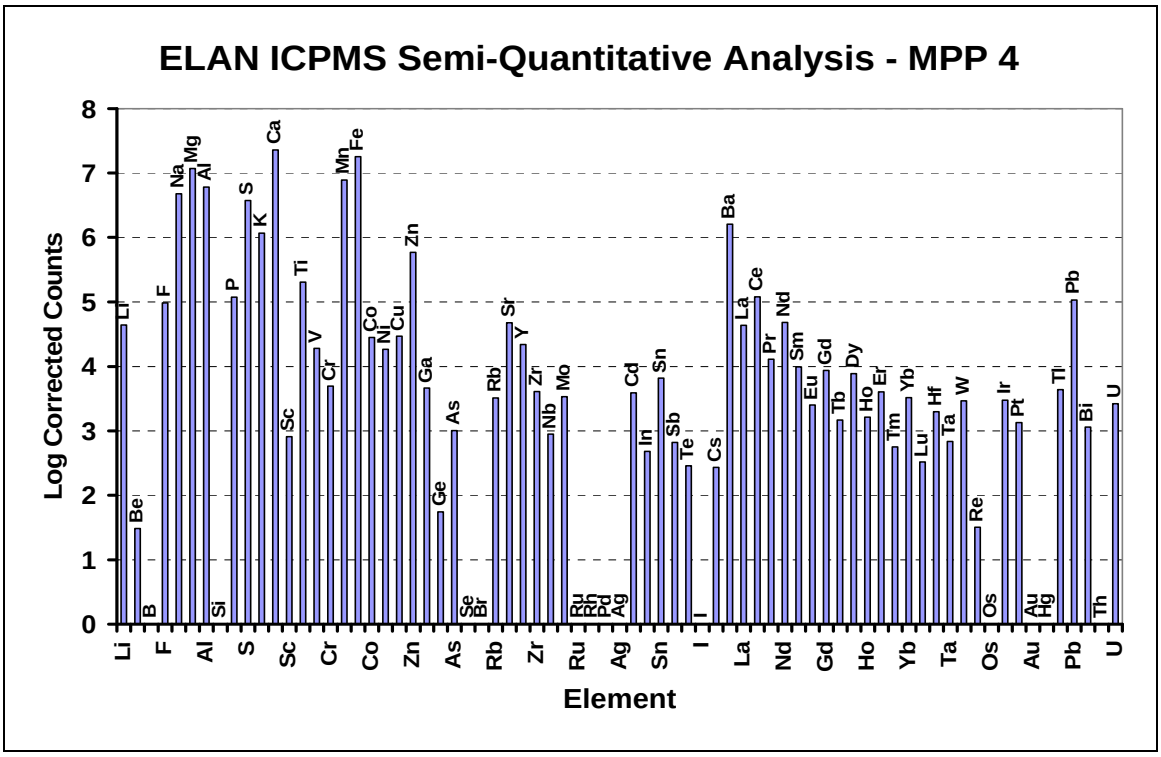

Figure 5.31. Elan 6100 DRC semi-quantitative ICPMS analysis of sample MPP 4. The corrected counts account for blank signal.

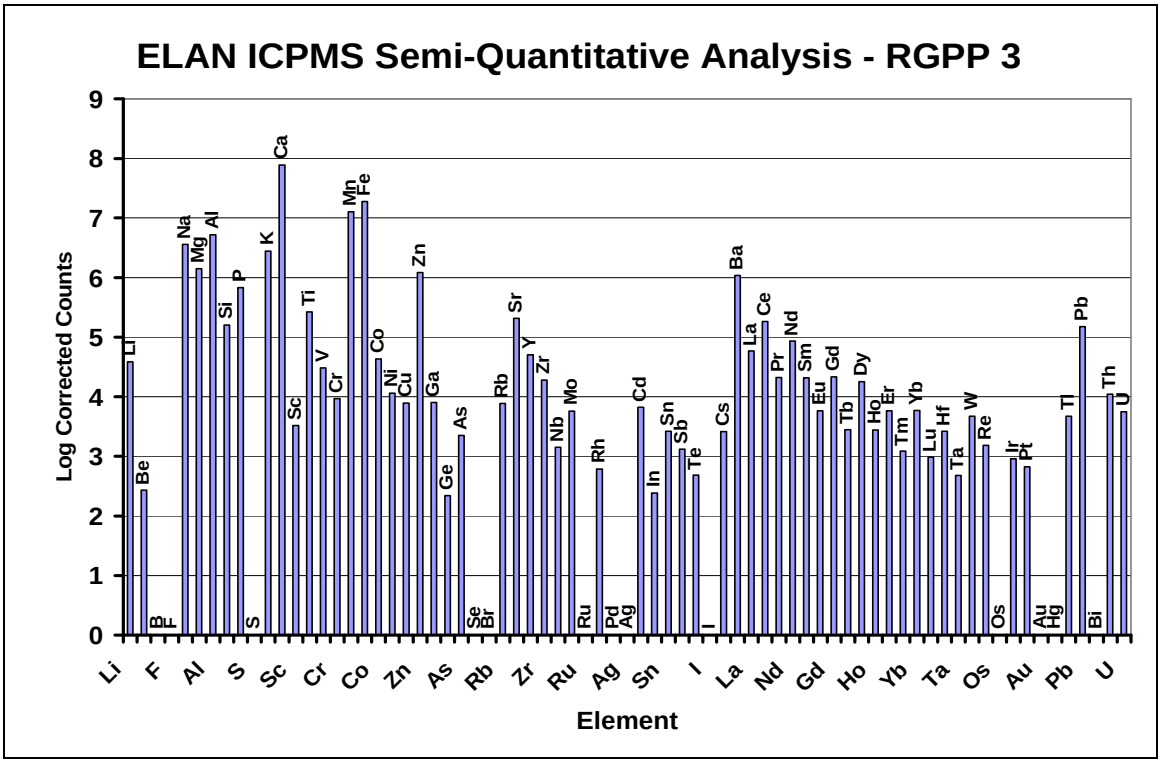

Figure 5.32. Elan 6100 DRC semi-quantitative ICPMS analysis of sample RGPP 3. The corrected counts account for blank signal.

Quantitative ICPMS Analysis

The varnish solutions resulting from HCl stripping were analyzed by quantitative ICPMS for 27 isotopes (^{9}Be, ^{51}V, ^{52}Cr, ^{59}Co, ^{60}Ni, ^{63}Cu, ^{66}Zn, ^{75}As, ^{88}Sr, ^{98}Mo, ^{102}Ru, ^{103}Rh, ^{106}Pd, ^{111}Cd, ^{118}Sn, ^{121}Sb, ^{133}Cs, ^{184}W, ^{187}Re, ^{195}Pt, ^{205}Tl, ^{206}Pb, ^{207}Pb, ^{208}Pb, ^{209}Bi, ^{232}Th, and ^{238}U). All varnish samples were stripped and analyzed in triplicate.

Method Detection Limit (MDL)

Method detection limits (MDLs) were calculated based on the replicate measurements (n=30) of water blanks and the slope of the calibration curve (3σ). The MDLs range from 0.010 µg·L^{-1} for ^{102}Ru, ^{103}Rh, ^{106}Pd, ^{133}Cs, and ^{187}Re to 0.604 µg·L^{-1} for ^{63}Cu (Figure 5.33).

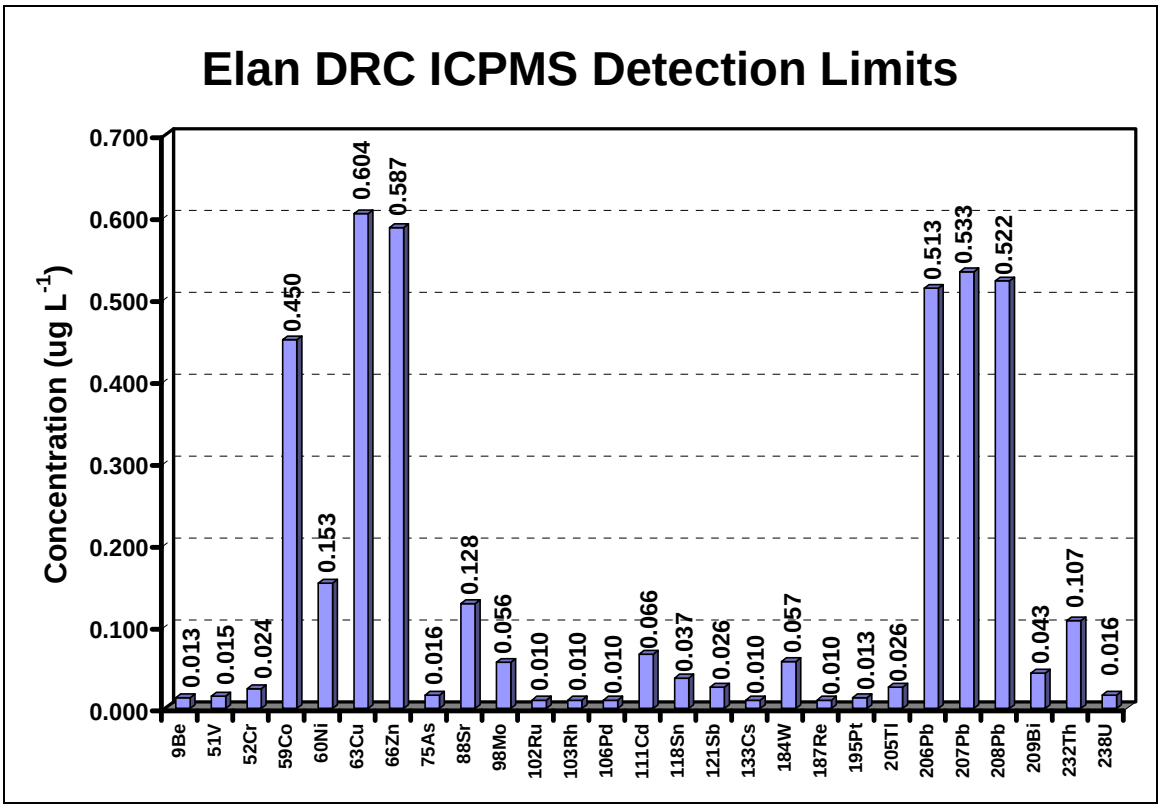

Figure 5.33. Estimated detection limits for the Elan 6100 DRC ICPMS analysis of desert varnish solutions stripped with concentrated HCl from the base rock.

Calibration Curves and QA/QC

A calibration blank and five standards (0.5, 1.0, 5.0, 10.0, 15.0 $\mu g \cdot L^{-1}$) were used for instrument calibration; the linear correlation coefficients were ≥ 0.995 for all 27 isotopes. The initial calibration verification (ICV) and continuous calibration verification (CCV) solutions were prepared from a different source than the calibration standards and were used to assess the validity of the calibration curve. The QA/QC sample frequency was 10%, with at least 90% recovery for all elements. The calibration blanks (ICB/CCB) were used to establish the analytical curve, while the preparation blanks (PB) were used to monitor for possible contamination. Memory effects and the baseline were assessed with the rinse blanks. Duplicate samples were analyzed with 5% frequency (every 20 samples) and were used to verify the analytical method precision. RPD values of less than 20% were achieved for all analytes.

Sample Data

The concentrations from the Elan DRC 6100 ICPMS analyses of 25 elements (27 isotopes) in desert varnish samples are given in Tables 5.16 through 5.37. Each result represents the average of 3 individual analyses.

Consistent with previous analyses by FPXRF and LA-ICPMS, Zn (19.1 to 5.96 x 10^3 $\mu g \cdot g^{-1}$), As (6.27 to 5.88 x 10^3 $\mu g \cdot g^{-1}$), Sr (53.2 to 6.52 x 10^3 $\mu g \cdot g^{-1}$) and Pb (26.6 to 6.53 x 10^3 $\mu g \cdot g^{-1}$), are the most abundant elements in all samples. Sample NTS 1 (Table 5.16) has very high average concentrations of and Zn (3.07 x 10^3 $\mu g \cdot g^{-1}$) and As (4.02 x 10^3 $\mu g \cdot g^{-1}$). Sample MPP 2 (Table 5.21) has very high average concentrations of V (1.30 x 10^3 $\mu g \cdot g^{-1}$), Cr (1.31 x 10^3 $\mu g \cdot g^{-1}$), Ni (1.25 x 10^3 $\mu g \cdot g^{-1}$), Zn (2.07 x 10^3 $\mu g \cdot g^{-1}$), and Pb (3.32 x 10^3 $\mu g \cdot g^{-1}$). Rhodium and ruthenium are detected only in NTS 3, MPP 1, MPP 5,

MPP 5a, and MPP 9. Rhenium is not detected in MPP 5, MPP 6, MPP 9, RGPP 1, RGPP 4, RGPP 5, RGPP 6, and BKG 1.

Figures 5.34 and 5.35 show selected elemental abundances in samples collected around MPP and RGPP normalized to estimates of the average composition of the UCC and plotted in approximate order of relative enrichment.

The MPP samples (Figure 5.34) have the following abundances of elements Sr > Pb > Zn > V > Cr > Co > Th > U > W > Mo > Ni > Cu > Sb > Be > Cd > Tl > Bi > Sn > Cs. All samples are highly enriched in V, Cr, Co, Zn, Sr, Pb, and Th. Strontium and Pb have the highest enrichment in all MPP samples, ranging from 92 to 2460 times that of the UCC for Sr and from 29 to 2020 times that of UCC for Pb. All MPP samples also show enrichment of 6 to 1690 times more than the UCC of Zn > V > Cr > Co > Th. Uranium and Mo are depleted only in TIMET 2 and W is depleted only in MPP 6. Beryllium, Ni, Cu, Cd, Sn, Sb, Cs, Tl, and Bi show variable enrichment and depletion.

The RGPP samples (Figure 5.35) show the highest enrichment of Pb > Sr > Zn > V > Co > Th > Cr, ranging from 29 to 1690 times more than the UCC for Pb, and from 2.4 to 693 times more for Cr. Nickel is depleted only in RGPP 1 and U is depleted only in TIMET 2. Sample RGPP 5 shows a high W content that could be attributed to the location of the sampling site in the W mineralization belt (Diaz, 2003). Beryllium, Cu, Mo, Cd, Sn, Sb, Cs, W, Tl, and Bi show variable enrichment and depletion.

Table 5.16. Elan DRC 6100 ICPMS data for desert varnish sample NTS 1.

	NTS 1											
	Replicate 1			Replicate 2			Replicate 3			Average		
Isotope	ppm	SD	%RSD	ppm	SD	%RSD	ppm	SD	%RSD	ppm	SD	%RSD
^{9}Be	9.70	0.46	5	10.7	0.4	4	10.0	0.2	2	10.1	0.5	5
^{51}V	504	6	1	391	2	0	745	13	2	547	181	33
^{52}Cr	73.6	1.3	2	65.2	0.7	1	176	4	2	105	62	59
^{59}Co	24.2	0.1	0	19.8	0.2	1	13.0	0.0	0	19.0	5.6	30
^{60}Ni	635	66	10	579	76	13	ND			607	40	7
^{63}Cu	64.7	1.7	3	64.7	0.5	1	28.5	1.7	6	52.6	20.9	40
^{66}Zn	5960	131	2	853	17	2	2390	76	3	3070	2620	85
^{75}As	3260	46	1	2920	9	0	5880	94	2	4020	1620	40
^{88}Sr	266	7	3	336	3	1	521	7	1	374	132	35
^{98}Mo	61.5	0.4	1	83.4	1.6	2	142	3	2	95.6	41.6	44
^{102}Ru	ND			ND			ND			NA		
^{103}Rh	ND			ND			ND			NA		
^{106}Pd	3.90	0.19	5	3.40	0.16	5	4.00	0.18	5	3.77	0.32	9
^{111}Cd	8.40	0.99	12	8.00	0.63	8	5.50	4.28	78	7.30	1.57	22
^{118}Sn	6.90	0.52	8	5.90	0.51	9	5.50	0.08	1	6.10	0.72	12
^{121}Sb	41.9	1.4	3	36.8	1.9	5	566	8	2	215	304	141
^{133}Cs	4.80	0.00	0	5.30	0.01	0	5.00	0.01	0	5.03	0.25	5
^{184}W	23.5	4.6	19	19.9	0.9	5	37.5	4.3	12	27.0	9.3	34
^{187}Re	2.40	0.04	2	2.30	0.01	0	3.00	0.01	0	2.57	0.38	15
^{195}Pt	0.500	0.046	9	0.400	0.025	6	0.500	0.042	8	0.467	0.058	12
^{205}Tl	5.90	4.21	71	2.00	0.47	23	1.00	0.18	18	2.97	2.59	87
^{206}Pb	433	11	3	316	8	2	521	13	3	423	103	24
^{207}Pb	435	17	4	321	10	3	531	11	2	429	105	25
^{208}Pb	423	20	5	308	14	5	521	19	4	417	107	26
^{209}Bi	4.40	0.89	20	4.40	0.51	12	4.50	0.06	1	4.43	0.06	1
^{232}Th	101	6	6	93.9	5.4	6	66.0	1.8	3	87.0	18.6	21
^{238}U	25.5	1.6	6	26.1	2.4	9	32.5	0.5	1	28.0	3.9	14

Each column represents average of 3 analytical runs; NA = Not Available; ND = Not Detected.

Table 5.17. Elan DRC 6100 ICPMS data for desert varnish sample NTS 2.

	NTS 2											
	Replicate 1			Replicate 2			Replicate 3			Average		
Isotope	ppm	SD	%RSD	ppm	SD	%RSD	ppm	SD	%RSD	ppm	SD	%RSD
^{9}Be	3.20	0.07	2	4.90	0.22	4	3.50	0.15	4	3.87	0.91	23
^{51}V	175	3	2	225	2	1	259	2.8	1	219	42	19
^{52}Cr	20.0	0.2	1	34.2	0.9	3	34.5	0.3	1	29.6	8.3	28
^{59}Co	76.1	1.7	2	149	7	5	139	6	4	121	39	33
^{60}Ni	199	14	7	137	4	3	169	5	3	168	31	19
^{63}Cu	43.4	2.6	6	101	10	10	76.0	4.4	6	73.4	28.8	39
^{66}Zn	853	9	1	996	27	3	891	36	4	913	74	8
^{75}As	78.0	1.4	2	166	1	1	106	1	1	117	45	39
^{88}Sr	459	10	2	276	1	0	767	18	2	500	248	50
^{98}Mo	22.7	0.5	2	33.2	0.3	1	28.0	0.4	2	28.0	5.3	19
^{102}Ru	ND			ND			ND			NA		
^{103}Rh	ND			ND			ND			NA		
^{106}Pd	2.20	0.05	2	6.60	0.2	3	7.00	0.21	3	5.27	2.66	51
^{111}Cd	10.7	0.3	3	15.1	1.1	7	12.0	7.0	59	12.6	2.3	18
^{118}Sn	4.34	0.07	2	10.9	0.7	6	5.00	0.09	2	6.75	3.61	54
^{121}Sb	1.96	0.04	2	5.40	0.10	2	6.00	0.16	3	4.45	2.18	49
^{133}Cs	2.34	0.01	1	6.60	0.01	0	5.50	0.01	0	4.81	2.21	46
^{184}W	26.2	0.4	2	48.1	5.0	10	63.5	1.8	3	45.9	18.7	41
^{187}Re	0.740	0.004	1	2.30	0.01	0	3.00	0.01	0	2.01	1.16	57
^{195}Pt	0.200	0.022	11	1.00	0.07	7	1.00	0.11	11	0.73	0.46	63
^{205}Tl	3.74	0.56	15	8.50	1.57	19	5.00	0.45	9	5.75	2.47	43
^{206}Pb	906	34	4	681	29	4	607	10	2	731	156	21
^{207}Pb	904	28	3	669	36	5	612	14	2	728	155	21
^{208}Pb	918	21	2	679	27	4	603	26	4	733	165	22
^{209}Bi	2.30	0.28	12	6.00	0.41	7	4.00	0.35	9	4.10	1.85	45
^{232}Th	305	11	4	523	17	3	490	24	5	439	117	27
^{238}U	1.90	0.12	6	18.8	2.8	15	22.0	3.5	16	14.2	10.8	76

Each column represents average of 3 analytical runs; NA = Not Available; ND = Not Detected.

Table 5.18. Elan DRC 6100 ICPMS data for desert varnish sample NTS 3.

	NTS 3											
	Replicate 1			Replicate 2			Replicate 3			Average		
Isotope	ppm	SD	%RSD	ppm	SD	%RSD	ppm	SD	%RSD	ppm	SD	%RSD
^{9}Be	2.75	0.02	1	2.50	0.02	1	2.48	0.12	5	2.58	0.15	6
^{51}V	170	1	1	177	3	2	273	6	2	207	58	28
^{52}Cr	5.70	0.15	3	7.18	0.33	5	19.5	0.2	1	10.8	7.6	70
^{59}Co	82.6	0.4	1	77.3	1.7	2	63.9	5.3	8	74.6	9.6	13
^{60}Ni	25.5	3.1	12	31.0	2.2	7	88.7	5.9	7	48.4	35.0	72
^{63}Cu	6.29	2.13	34	28.1	11.4	41	31.9	1.1	3	22.1	13.8	63
^{66}Zn	1890	47	3	1536	28	2	834	2	0	1420	537	38
^{75}As	69.8	1.1	2	74.6	1.3	2	111	2	2	85.2	22.6	27
^{88}Sr	566	7	1	626	9	1	466	5	1	552	81	15
^{98}Mo	5.68	0.36	6	5.05	0.07	1	8.77	0.10	1	6.50	1.99	31
^{102}Ru	2.33	0.12	5	2.58	0.18	7	ND			2.46	0.18	7
^{103}Rh	2.34	0.21	9	ND			ND			2.34		
^{106}Pd	17.7	2.2	13	17.6	0.6	3	4.13	0.06	2	13.1	7.8	59
^{111}Cd	5.22	0.03	1	3.66	0.04	1	5.78	0.69	12	4.89	1.10	22
^{118}Sn	0.94	0.10	10	3.68	0.30	8	4.58	0.15	3	3.07	1.90	62
^{121}Sb	ND			1.07	0.02	2	3.55	0.05	1	2.31	1.75	76
^{133}Cs	2.93	0.06	2	3.44	0.09	3	4.21	0.00	0	3.53	0.64	18
^{184}W	6.25	0.07	1	5.74	0.10	2	11.8	0.1	1	7.93	3.36	42
^{187}Re	0.350	0.009	3	0.210	0.010	5	1.65	0.01	1	0.74	0.79	108
^{195}Pt	11.2	0.42	4	7.42	0.30	4	0.45	0.03	7	6.34	5.44	86
^{205}Tl	26.8	1.7	6	20.1	0.9	5	5.71	1.00	18	17.5	10.8	61
^{206}Pb	373	15	4	331	1	0	509	11	2	405	93	23
^{207}Pb	379	9	3	330	4	1	512	13	3	407	95	23
^{208}Pb	373	5	1	327	4	1	529	34	6	410	106	26
^{209}Bi	63.4	11.4	18	29.9	1.9	6	2.85	0.25	9	32.1	30.4	95
^{232}Th	186	1	0	169	1	1	215	5	3	190	23	12
^{238}U	118	0	0	97.2	0.2	0	90.2	25.5	28	102	14	14

Each column represents average of 3 analytical runs; NA = Not Available; ND = Not Detected.

Table 5.19. Elan DRC 6100 ICPMS data for desert varnish sample TIMET 2.

	TIMET 2											
	Replicate 1			Replicate 2			Replicate 3			Average		
Isotope	ppm	SD	%RSD	ppm	SD	%RSD	ppm	SD	%RSD	ppm	SD	%RSD
^{9}Be	0.570	0.007	1	0.730	0.014	2	0.200	0.009	5	0.500	0.272	54
^{51}V	16.8	0.2	1	34.1	0.2	1	42.8	0.7	2	31.2	13.2	42
^{52}Cr	4.31	0.01	0	4.76	0.04	1	4.80	0.07	2	4.62	0.27	6
^{59}Co	22.3	0.3	1	16.5	0.2	1	5.20	0.05	1	14.7	8.7	59
^{60}Ni	9.33	0.50	5	ND			4.80	0.14	3	7.07	3.20	45
^{63}Cu	ND			ND			3.30	0.47	14	3.30		
^{66}Zn	79.7	1.7	2	114	40	35	50.9	0.1	0	81.5	31.5	39
^{75}As	7.16	0.01	0	13.5	0.20	2	9.00	0.11	1	9.89	3.26	33
^{88}Sr	857	1	0	612	10	2	302	5	2	590	278	47
^{98}Mo	1.55	0.04	2	2.52	0.06	2	0.60	0.02	3	1.56	0.96	62
^{102}Ru	ND			ND			ND			NA		
^{103}Rh	ND			ND			ND			NA		
^{106}Pd	0.700	0.033	5	0.560	0.011	2	0.200	0.005	3	0.487	0.258	53
^{111}Cd	0.150	0.016	11	0.300	0.089	30	0.300	0.019	6	0.250	0.087	35
^{118}Sn	0.450	0.010	2	0.610	0.015	2	0.200	0.004	2	0.420	0.207	49
^{121}Sb	ND			ND			0.200	0.005	3	0.200		
^{133}Cs	0.250	0.008	3	0.260	0.014	5	0.200	0.000	0	0.237	0.032	14
^{184}W	2.04	0.04	2	3.99	0.08	2	1.20	0.03	3	2.41	1.43	59
^{187}Re	ND			ND			0.100	0.000	0	0.100		
^{195}Pt	0.420	0.002	0	0.420	0.009	2	ND			0.420	0.000	0
^{205}Tl	0.590	0.040	7	0.420	0.017	4	0.400	0.053	13	0.470	0.104	22
^{206}Pb	39.0	0.2	1	100	2	2	91.3	3.5	4	76.9	33.1	43
^{207}Pb	37.8	0.3	1	103	1	1	89.9	1.3	2	76.7	34.3	45
^{208}Pb	37.8	0.7	2	102	1	1	91.1	0.3	0	76.9	34.3	45
^{209}Bi	0.460	0.006	1	0.460	0.009	2	0.100	0.010	10	0.340	0.208	61
^{232}Th	27.0	0.0	0	26.6	0.1	0	17.7	0.6	4	23.8	5.3	22
^{238}U	1.07	0.00	0	1.55	0.00	0	0.800	0.026	3	1.14	0.38	33

Each column represents average of 3 analytical runs; NA = Not Available; ND = Not Detected.

Table 5.20. Elan DRC 6100 ICPMS data for desert varnish sample MPP 1.

	MPP 1											
	Replicate 1			Replicate 2			Replicate 3			Average		
Isotope	ppm	SD	%RSD	ppm	SD	%RSD	ppm	SD	%RSD	ppm	SD	%RSD
^{9}Be	2.50	0.08	3	1.80	0.08	5	0.700	0.015	2	1.67	0.91	54
^{51}V	1060	7	1	820	12	2	187	1	1	689	451	65
^{52}Cr	44.2	0.1	0	35.1	1.0	3	18.2	0.2	1	32.5	13.2	41
^{59}Co	65.4	0.7	1	75.1	0.9	1	19.2	0.3	1	53.2	29.9	56
^{60}Ni	324	16.5	5	260	7	3	175	3	2	253	75	30
^{63}Cu	40.3	4.8	12	44.6	15.4	35	26.5	0.5	2	37.1	9.5	25
^{66}Zn	928	22	2	821	18	2	179	1	1	643	405	63
^{75}As	72.3	2.9	4	93.7	3.2	3	113	0	0	93.1	20.5	22
^{88}Sr	4671	70	2	6520	78	1	2850	46	2	4680	1830	39
^{98}Mo	4.50	0.14	3	9.20	0.17	2	1.80	0.03	2	5.17	3.74	72
^{102}Ru	0.100	0.001	1	0.200	0.000	0	0.100	0.002	2	0.133	0.058	43
^{103}Rh	0.300	0.009	3	0.500	0.016	3	0.100	0.002	2	0.300	0.200	67
^{106}Pd	2.90	0.19	6	3.00	0.14	5	0.400	0.010	3	2.10	1.47	70
^{111}Cd	3.30	1.01	31	4.40	1.21	28	1.000	0.042	4	2.90	1.73	60
^{118}Sn	2.90	0.09	3	3.40	0.10	3	0.500	0.013	3	2.27	1.55	68
^{121}Sb	1.90	0.04	2	2.50	0.06	3	1.00	0.03	3	1.80	0.75	42
^{133}Cs	4.90	0.01	0	5.10	0.01	0	1.50	0.01	1	3.83	2.02	53
^{184}W	4.40	0.12	3	6.00	0.16	3	3.40	0.29	9	4.60	1.31	29
^{187}Re	0.900	0.006	1	1.00	0.00	0	0.200	0.001	0	0.700	0.436	62
^{195}Pt	0.100	0.007	7	0.100	0.010	10	ND			0.100	0.000	0
^{205}Tl	3.50	0.17	5	4.00	0.20	5	0.600	0.029	5	2.70	1.84	68
^{206}Pb	998	12	1	2110	17	1	895	1	0	1330	674	51
^{207}Pb	1020	43	4	2110	78	4	901	9	1	1340	666	50
^{208}Pb	1050	26	3	2050	76	4	NA			1550	707	46
^{209}Bi	1.50	0.34	23	2.10	0.83	39	0.600	0.135	23	1.40	0.75	54
^{232}Th	125	2	1	100	2	2	47.9	0.8	2	90.9	39.2	43
^{238}U	7.30	0.54	7	8.10	0.66	8	3.40	0.17	5	6.27	2.51	40

Each column represents average of 3 analytical runs; NA = Not Available; ND = Not Detected.

Table 5.21. Elan DRC 6100 ICPMS data for desert varnish sample MPP 2.

	MPP 2											
	Replicate 1			Replicate 2			Replicate 3			Average		
Isotope	ppm	SD	%RSD	ppm	SD	%RSD	ppm	SD	%RSD	ppm	SD	%RSD
^{9}Be	16.9	0.9	5	13.0	0.6	4	16.3	0.7	4	15.4	2.1	14
^{51}V	1060	12	1	1150	17	2	1690	32	2	1300	341	26
^{52}Cr	923	28	3	1350	15	1	1670	27	2	1310	375	29
^{59}Co	445	12	3	407	4	1	381	23	6	411	32	8
^{60}Ni	1030	66	6	1540	82	5	1170	34	3	1250	264	21
^{63}Cu	387	43	11	852	16	2	360	19	5	533	276	52
^{66}Zn	1760	51	3	2830	57	2	1630	28	2	2070	659	32
^{75}As	569	4	1	629	13	2	586	8	1	595	31	5
^{88}Sr	1170	18	2	2140	62	3	1070	9	1	1460	591	40
^{98}Mo	31.3	0.5	2	34.0	1.0	3	39.4	1.0	3	34.9	4.1	12
^{102}Ru	ND			ND			ND			NA		
^{103}Rh	ND			ND			ND			NA		
^{106}Pd	10.3	0.4	4	6.00	0.35	6	10.4	0.9	8	8.90	2.51	28
^{111}Cd	45.4	2.3	5	30.0	1.1	4	34.2	5.9	17	36.5	8.0	22
^{118}Sn	15.6	0.4	3	10.5	0.3	3	18.2	0.6	3	14.8	3.9	27
^{121}Sb	123	2	1	52.5	0.4	1	209	2	1	128	78	61
^{133}Cs	15.1	0.0	0	12.5	0.0	0	18.2	0.0	0	15.3	2.9	19
^{184}W	111	6	5	89.0	3.4	4	148	16	11	116	30	26
^{187}Re	5.40	0.02	0	3.50	0.01	0	6.20	0.01	0	5.03	1.39	28
^{195}Pt	1.00	0.03	3	0.500	0.044	9	1.30	0.10	8	0.93	0.40	43
^{205}Tl	22.6	1.3	6	35.0	27.4	78	13.0	0.5	4	23.5	11.0	47
^{206}Pb	2910	38	1	4130	169	4	2600	96	4	3210	809	25
^{207}Pb	2880	60	2	4080	94	2	2660	32	1	3210	764	24
^{208}Pb	2960	118	4	4300	185	4	2710	68	3	3320	855	26
^{209}Bi	14.1	2.1	15	11.5	0.9	8	13.3	1.1	8	13.0	1.3	10
^{232}Th	328	3	1	369	10	3	332	8	2	343	23	7
^{238}U	45.9	6.5	14	48.5	3.4	7	42.3	15.0	36	45.6	3.1	7

Each column represents average of 3 analytical runs; NA = Not Available; ND = Not Detected.

Table 5.22. Elan DRC 6100 ICPMS data for desert varnish sample MPP 3.

	MPP 3											
	Replicate 1			Replicate 2			Replicate 3			Average		
Isotope	ppm	SD	%RSD	ppm	SD	%RSD	ppm	SD	%RSD	ppm	SD	%RSD
^{9}Be	6.88	0.10	2	4.70	0.10	2	3.40	0.06	2	4.99	1.76	35
^{51}V	196	1	1	161	6	4	138	1	1	165	29	18
^{52}Cr	35.6	0.6	2	40.0	0.8	2	33.6	0.3	1	36.4	3.3	9
^{59}Co	306	6	2	190	4	2	68.9	1.6	2	189	119	63
^{60}Ni	113	16	14	33.0	6.4	19	89.7	12.1	14	78.6	41.2	52
^{63}Cu	85.3	0.3	0	69.4	1.7	3	42.4	1.4	3	65.7	21.7	33
^{66}Zn	1430	29	2	990	40	4	290	2	1	903	575	64
^{75}As	63.1	1.4	2	29.4	1.1	4	26.3	0.9	3	39.6	20.4	52
^{88}Sr	991	3	0	441	6	1	397	5	1	610	331	54
^{98}Mo	9.65	0.12	1	5.43	0.18	3	3.40	0.1	3	6.16	3.19	52
^{102}Ru	ND			ND			ND			NA		
^{103}Rh	ND			ND			ND			NA		
^{106}Pd	7.32	0.11	2	3.28	0.13	4	1.10	0.07	6	3.90	3.16	81
^{111}Cd	5.58	0.01	0	3.80	0.08	2	2.70	0.07	3	4.03	1.45	36
^{118}Sn	4.36	0.16	4	1.81	0.10	6	1.10	0.02	2	2.42	1.71	71
^{121}Sb	1.57	0.01	1	1.37	0.03	2	0.900	0.006	1	1.28	0.34	27
^{133}Cs	3.42	0.01	0	1.81	0.05	3	1.10	0.00	0	2.11	1.19	56
^{184}W	7.41	0.13	2	5.09	0.19	4	2.90	0.28	10	5.13	2.26	44
^{187}Re	0.250	0.010	4	0.104	0.006	6	0.200	0.001	0	0.185	0.074	40
^{195}Pt	2.22	0.16	7	0.736	0.014	2	ND			1.48	1.05	71
^{205}Tl	9.84	0.13	1	4.48	0.15	3	1.90	0.15	8	5.41	4.05	75
^{206}Pb	476	5	1	369	7	2	205	1	1	350	137	39
^{207}Pb	477	8	2	366	4	1	204	5	2	349	137	39
^{208}Pb	484	13	3	364	4	1	207	3	1	352	139	40
^{209}Bi	29.2	1.3	4	17.6	1.0	5	1.10	0.04	3	16.0	14.1	88
^{232}Th	194	1	1	118	3	2	101	2	2	138	50	36
^{238}U	116	4	4	58.9	1.2	2	5.70	0.11	2	60.2	55.1	92

Each column represents average of 3 analytical runs; NA = Not Available; ND = Not Detected.

Table 5.23. Elan DRC 6100 ICPMS data for desert varnish sample MPP 4.

	MPP 4											
	Replicate 1			Replicate 2			Replicate 3			Average		
Isotope	ppm	SD	%RSD	ppm	SD	%RSD	ppm	SD	%RSD	ppm	SD	%RSD
^{9}Be	4.18	0.34	8	2.00	0.30	15	3.60	0.10	3	3.26	1.13	35
^{51}V	154	2	1	115	2	2	257	1	1	175	73	42
^{52}Cr	49.5	0.6	1	48.6	1.0	2	159	0	0	85.8	63.6	74
^{59}Co	149	2	2	90.8	1.8	2	183	4	2	141	47	33
^{60}Ni	273	14	5	175	7	4	784	20	3	411	327	80
^{63}Cu	299	13	5	260	4	2	469	3	1	343	111	32
^{66}Zn	844	9	1	450	5	1	863	13	2	719	233	32
^{75}As	63.2	0.9	1	36.9	1.2	3	84.2	2.2	3	61.4	23.7	39
^{88}Sr	371	8	2	247	1	0	343	13	4	320	65	20
^{98}Mo	7.60	0.16	2	5.90	0.12	2	8.30	0.14	2	7.27	1.23	17
^{102}Ru	ND			ND			ND			NA		
^{103}Rh	ND			ND			ND			NA		
^{106}Pd	4.26	0.16	4	3.00	0.17	6	1.80	0.05	3	3.02	1.23	41
^{111}Cd	11.1	0.6	5	8.50	2.42	29	9.00	1.13	13	9.53	1.38	14
^{118}Sn	2.22	0.13	6	4.10	0.11	3	4.20	0.16	4	3.51	1.12	32
^{121}Sb	3.92	0.10	3	2.60	0.02	1	3.00	0.03	1	3.17	0.68	21
^{133}Cs	3.68	0.00	0	4.00	0.00	0	5.10	0.01	0	4.26	0.74	17
^{184}W	7.42	0.06	1	4.70	0.02	1	5.90	0.11	2	6.01	1.36	23
^{187}Re	1.54	0.01	1	1.70	0.01	1	1.30	0.01	1	1.51	0.20	13
^{195}Pt	0.340	0.081	24	0.400	0.044	11	0.200	0.015	8	0.313	0.103	33
^{205}Tl	1.54	0.07	4	1.60	0.20	12	4.00	0.29	7	2.38	1.40	59
^{206}Pb	444	17	4	439	14	3	618	17	3	501	102	20
^{207}Pb	459	12	3	448	6	1	635	31	5	514	105	20
^{208}Pb	468	6	1	441	15	3	641	20	3	517	109	21
^{209}Bi	4.10	0.62	15	3.70	0.91	25	4.50	0.52	12	4.10	0.40	10
^{232}Th	120	13	11	73.8	1.4	2	73.5	1.2	2	88.9	26.5	30
^{238}U	8.12	0.51	6	5.90	0.26	4	8.80	0.92	10	7.61	1.52	20

Each column represents average of 3 analytical runs; NA = Not Available; ND = Not Detected.

Table 5.24. Elan DRC 6100 ICPMS data for desert varnish sample MPP 5.

	MPP 5											
	Replicate 1			Replicate 2			Replicate 3			Average		
Isotope	ppm	SD	%RSD	ppm	SD	%RSD	ppm	SD	%RSD	ppm	SD	%RSD
^{9}Be	9.45	0.42	4	9.15	0.07	1	10.6	0.7	7	9.73	0.77	8
^{51}V	403	4	1	285	6	2	428	2	1	372	76	21
^{52}Cr	28.6	0.7	3	29.8	0.7	2	30.1	0.6	2	29.5	0.8	3
^{59}Co	175	5	3	195	4	2	289	1	0	219	61	28
^{60}Ni	ND			ND			ND			NA		
^{63}Cu	NA			NA			NA			NA		
^{66}Zn	3840	307	8	1940	72	4	3840	127	3	3210	1100	34
^{75}As	170	9	5	172	1	1	222	2	1	188	30	16
^{88}Sr	708	14	2	677	17	3	435	12	3	607	149	25
^{98}Mo	15.6	0.1	1	14.7	0.3	2	32.9	0.5	1	21.1	10.2	49
^{102}Ru	1.70	0.17	10	ND		7	1.94	0.06	3	1.82	0.17	9
^{103}Rh	1.70	0.24	14	ND			ND			1.70		
^{106}Pd	6.80	0.90	13	3.70	0.12	3	5.67	0.14	2	5.39	1.57	29
^{111}Cd	1.80	1.36	76	15.5	0.7	5	24.2	1.2	5	13.8	11.3	82
^{118}Sn	18.8	0.5	3	5.06	0.39	8	19.0	1.0	6	14.3	8.0	56
^{121}Sb	65.8	2.1	3	5.20	0.51	10	NA			35.5	42.9	121
^{133}Cs	3.28	0.13	4	1.77	0.04	2	3.68	0.17	5	2.91	1.01	35
^{184}W	9.87	0.26	3	14.9	0.5	3	24.4	0.8	3	16.4	7.4	45
^{187}Re	ND			ND		0	ND			NA		
^{195}Pt	8.40	0.45	5	3.60	0.12	3	5.67	0.23	4	5.89	2.41	41
^{205}Tl	15.2	0.4	2	4.67	0.31	7	12.8	0.5	4	10.9	5.5	51
^{206}Pb	6530	46	1	1130	9	1	NA			3830	3820	100
^{207}Pb	6370	51	1	1110	16	1	NA			3740	3720	99
^{208}Pb	NA			1080	24	2	NA			1080		
^{209}Bi	7.58	0.11	1	4.07	0.09	2	27.6	1.2	5	13.1	12.7	97
^{232}Th	294	1	1	178	1	1	340	1	0	271	84	31
^{238}U	261	1	0	147	0	0	301	0	0	236	80	34

Each column represents average of 3 analytical runs; NA = Not Available; ND = Not Detected.

Table 5.25. Elan DRC 6100 ICPMS data for desert varnish sample MPP 5a.

	MPP 5a											
	Replicate 1			Replicate 2			Replicate 3			Average		
Isotope	ppm	SD	%RSD	ppm	SD	%RSD	ppm	SD	%RSD	ppm	SD	%RSD
^{9}Be	2.00	0.04	2	1.39	0.04	3	5.64	0.16	3	3.01	2.30	76
^{51}V	394	9	2	565	6	1	645	3	1	535	129	24
^{52}Cr	11.6	0.3	3	11.6	0.2	1	50.5	1.0	2	24.6	22.5	91
^{59}Co	115	3	3	84.3	0.9	1	463	8	2	221	210	95
^{60}Ni	ND			ND			ND			NA		
^{63}Cu	1.05	0.28	27	31.2	1.2	4	78.8	7.7	10	37.0	39.2	106
^{66}Zn	234	21	9	362	2	1	739	273	37	445	262	59
^{75}As	72.1	1.7	2	69.0	1.6	2	147	4	3	96	44	46
^{88}Sr	334	11	3	327	7	2	1070	18	2	577	427	74
^{98}Mo	3.60	0.17	5	1.62	0.09	6	5.50	0.35	6	3.57	1.94	54
^{102}Ru	0.500	0.023	5	ND			ND			0.500		
^{103}Rh	0.500	0.135	27	ND			ND			0.500		
^{106}Pd	2.90	0.23	8	2.17	0.06	3	4.19	0.18	4	3.09	1.02	33
^{111}Cd	2.50	0.10	4	1.45	0.06	4	4.40	0.17	4	2.78	1.50	54
^{118}Sn	11.7	0.9	8	10.6	1.5	14	17.8	1.4	8	13.4	3.9	29
^{121}Sb	7.90	0.30	4	9.25	1.24	13	10.3	1.1	10	9.15	1.20	13
^{133}Cs	ND			ND			ND			NA		
^{184}W	7.20	0.49	7	0.950	0.164	17	4.01	0.51	13	4.05	3.13	77
^{187}Re	0.050	0.005	10	ND			ND			0.050		
^{195}Pt	2.90	0.06	2	2.18	0.03	2	5.61	0.22	4	3.56	1.81	51
^{205}Tl	3.65	0.31	8	0.140	0.006	4	15.1	0.3	2	6.28	7.80	124
^{206}Pb	337	7	2	275	7	3	1320	12	1	644	586	91
^{207}Pb	335	3	1	270	4	2	1320	32	2	642	588	92
^{208}Pb	332	0	0	264	3	1	1290	26	2	629	574	91
^{209}Bi	ND			ND			ND			NA		
^{232}Th	109	1	1	127	0	0	359	1	0	198	139	70
^{238}U	78.2	0.2	0	88.2	0.2	0	222	0	0	129	80	62

Each column represents average of 3 analytical runs; NA = Not Available; ND = Not Detected.

Table 5.26. Elan DRC 6100 ICPMS data for desert varnish sample MPP 6.

	MPP 6											
	Replicate 1			Replicate 2			Replicate 3			Average		
Isotope	ppm	SD	%RSD	ppm	SD	%RSD	ppm	SD	%RSD	ppm	SD	%RSD
^{9}Be	0.30	0.01	5	0.340	0.014	4	0.400	0.068	17	0.347	0.050	15
^{51}V	408	6	1	509	4	1	471	7	1	462	51	11
^{52}Cr	270	2	1	101	3	3	86.2	0.4	1	152	102	67
^{59}Co	11.2	0.1	1	6.82	0.08	1	19.0	0.3	2	12.4	6.2	50
^{60}Ni	ND			ND			ND			NA		
^{63}Cu	ND			ND			ND			NA		
^{66}Zn	289	8	3	481	20	4	778	16	2	516	247	48
^{75}As	153	1	1	117	2	2	182	7	4	151	33	22
^{88}Sr	350	2	1	268	3	1	494	6	1	371	115	31
^{98}Mo	1.93	0.06	3	2.70	0.06	2	3.35	0.03	1	2.66	0.71	27
^{102}Ru	ND			ND			ND			NA		
^{103}Rh	ND			ND			ND			NA		
^{106}Pd	8.68	0.24	3	8.18	0.08	1	7.29	0.49	7	8.05	0.70	9
^{111}Cd	0.690	0.041	6	ND			0.960	0.063	7	0.825	0.191	23
^{118}Sn	0.360	0.011	3	0.790	0.032	4	1.01	0.02	2	0.720	0.331	46
^{121}Sb	ND			ND			ND			NA		
^{133}Cs	0.100	0.006	6	0.200	0.003	1	ND			0.150	0.071	47
^{184}W	1.70	0.11	6	0.950	0.041	4	1.90	0.03	1	1.52	0.50	33
^{187}Re	ND			ND			ND			NA		
^{195}Pt	2.15	0.02	1	4.05	0.09	2	7.21	0.13	2	4.47	2.56	57
^{205}Tl	0.390	0.004	1	0.630	0.036	6	0.740	0.019	3	0.587	0.179	31
^{206}Pb	683	12	2	230	7	3	1234	22	2	716	503	70
^{207}Pb	677	19	3	239	5	2	1246	41	3	721	505	70
^{208}Pb	663	18	3	231	5	2	1227	1	0	707	499	71
^{209}Bi	0.360	0.008	2	0.570	0.031	6	0.810	0.013	2	0.580	0.225	39
^{232}Th	488	7	2	692	1	0	755	2	0	645	139	22
^{238}U	175	0	0	313	0	0	558	1	0	349	194	56

Each column represents average from 3 analytical runs; NA = Not Available; ND = Not Detected.

Table 5.27. Elan DRC 6100 ICPMS data for desert varnish sample MPP 7.

	MPP 7											
	Replicate 1			Replicate 2			Replicate 3			Average		
Isotope	ppm	SD	%RSD	ppm	SD	%RSD	ppm	SD	%RSD	ppm	SD	%RSD
^{9}Be	5.77	0.08	1	7.97	0.13	2	7.09	0.08	1	6.94	1.11	16
^{51}V	171	4	2	386	5	1	267	1	0	275	108	39
^{52}Cr	57.6	1.3	2	113	1	1	111	2	2	93.9	31.5	34
^{59}Co	9.76	0.15	2	14.7	0.2	1	11.3	0.3	2	11.9	2.5	21
^{60}Ni	ND			ND			ND			NA		
^{63}Cu	1.20	0.01	1	1.65	0.11	7	1.43	0.11	8	1.43	0.23	16
^{66}Zn	22.9	0.2	1	38.1	16.1	42	19.1	6.8	36	26.7	10.1	38
^{75}As	34.8	1.3	4	52.9	1.6	3	37.9	0.7	2	41.9	9.7	23
^{88}Sr	364	15	4	459	4	1	309	4.32	1	377	76	20
^{98}Mo	5.17	0.30	6	6.60	0.41	6	4.87	0.37	8	5.55	0.92	17
^{102}Ru	ND			ND			ND			NA		
^{103}Rh	ND			ND			ND			NA		
^{106}Pd	2.37	0.07	3	2.65	0.13	5	7.07	0.11	2	4.03	2.64	65
^{111}Cd	7.88	0.16	2	7.02	0.15	2	7.21	0.23	3	7.37	0.45	6
^{118}Sn	0.300	0.104	35	0.320	0.104	32	0.280	0.088	31	0.300	0.020	7
^{121}Sb	0.190	0.005	3	0.260	0.009	4	0.190	0.006	3	0.213	0.040	19
^{133}Cs	ND			ND			ND			NA		
^{184}W	6.14	0.12	2	6.80	0.38	6	5.56	0.15	3	6.17	0.62	10
^{187}Re	0.060	0.013	22	ND			0.060	0.014	24	0.060	0.000	0
^{195}Pt	2.38	0.01	0	2.66	0.11	4	2.37	0.17	7	2.47	0.16	7
^{205}Tl	1.50	0.09	6	3.89	0.11	3	3.46	0.04	1	2.95	1.27	43
^{206}Pb	600	16	3	661	24	4	436	7	2	566	117	21
^{207}Pb	623	12	2	671	23	4	439	7	2	578	122	21
^{208}Pb	633	8	1	686	22	3	442	6	1	587	128	22
^{209}Bi	8.82	1.09	12	15.1	0.1	1	12.3	0.4	4	12.1	3.1	26
^{232}Th	11.7	0.1	1	17.2	0.1	0	15.5	0.0	0	14.8	2.8	19
^{238}U	4.52	0.01	0	7.33	0.01	0	9.59	0.01	0	7.15	2.54	36

Each column represents average of 3 analytical runs; NA = Not Available; ND = Not Detected.

Table 5.28. Elan DRC 6100 ICPMS data for desert varnish sample MPP 8.

	MPP 8											
	Replicate 1			Replicate 2			Replicate 3			Average		
Isotope	ppm	SD	%RSD	ppm	SD	%RSD	ppm	SD	%RSD	ppm	SD	%RSD
^{9}Be	49.4	0.2	1	20.0	0.6	3	95.4	1.2	1	55.0	38.0	69
^{51}V	605	11	2	304	2	1	1210	21	2	706	462	65
^{52}Cr	907	11	1	144	2	1	276	3	1	442	408	92
^{59}Co	52.0	0.5	1	29.5	0.2	1	107	1	1	62.9	39.9	63
^{60}Ni	ND			ND			ND			NA		
^{63}Cu	5.73	0.19	3	3.57	0.10	3	24.1	0.3	1	11.1	11.3	101
^{66}Zn	77.4	0.9	1	37.5	0.4	1	405	9	2	173	202	116
^{75}As	355	5	1	172	2	1	695	13	2	407	265	65
^{88}Sr	894	13	1	447	6	1	1620	23	1	987	592	60
^{98}Mo	43.7	2.7	6	14.5	0.2	2	71.6	1.7	2	43.3	28.6	66
^{102}Ru	ND			ND			ND			NA		
^{103}Rh	ND			ND			ND			NA		
^{106}Pd	12.4	0.6	5	5.35	0.25	5	2.37	0.05	2	6.69	5.13	77
^{111}Cd	56.4	2.1	4	25.2	0.4	2	88.4	0.8	1	56.7	31.6	56
^{118}Sn	4.13	0.46	11	0.700	0.006	1	2.42	0.10	4	2.42	1.72	71
^{121}Sb	1.11	0.01	1	0.610	0.018	3	2.04	0.08	4	1.25	0.73	58
^{133}Cs	ND			ND			ND			NA		
^{184}W	37.3	1.2	3	14.0	0.7	5	61.2	1.2	2	37.5	23.6	63
^{187}Re	0.510	0.097	19	0.110	0.014	13	ND			0.310	0.283	91
^{195}Pt	9.31	0.14	2	4.03	0.10	2	2.37	0.14	6	5.24	3.62	69
^{205}Tl	12.6	0.4	3	6.67	0.23	3	24.5	0.0	0	14.6	9.1	62
^{206}Pb	2420	10	0	1170	28	2	4620	18	0	2740	1750	64
^{207}Pb	2420	22	1	1160	12	1	4660	79	2	2750	1770	64
^{208}Pb	2450	34	1	1190	12	1	4720	76	2	2790	1790	64
^{209}Bi	60.9	2.4	4	17.6	1.3	8	66.5	3.7	6	48.3	26.8	55
^{232}Th	277	1	0	100	0	0	331	1	0	236	121	51
^{238}U	49.4	0.1	0	22.7	0.0	0	66.9	0.1	0	46.3	22.3	48

Each column represents data from 3-run analyses; NA = Not Available; ND = Not Detected.

Table 5.29. Elan DRC 6100 ICPMS data for desert varnish sample MPP 9.

	MPP 9											
	Replicate 1			Replicate 2			Replicate 3			Average		
Isotope	ppm	SD	%RSD	ppm	SD	%RSD	ppm	SD	%RSD	ppm	SD	%RSD
^{9}Be	1.91	0.06	3	NA			2.44	0.06	3	2.18	0.37	17
^{51}V	61.2	1.2	2	NA			94.4	1.7	2	77.8	23.5	30
^{52}Cr	348	1	0	NA			92.0	2.3	3	220	181	82
^{59}Co	46.8	1.2	3	NA			47.3	0.5	1	47.1	0.4	1
^{60}Ni	ND			NA			ND			NA		
^{63}Cu	ND			NA			ND			NA		
^{66}Zn	234	11	5	NA			252	3	1	243	13	5
^{75}As	26.8	0.6	2	NA			32.0	0.9	3	29.4	3.7	13
^{88}Sr	624	5	1	NA			709	9	1	667	60	9
^{98}Mo	10.3	0.2	2	NA			14.5	0.4	3	12.4	3.0	24
^{102}Ru	0.590	0.073	12	NA			ND			0.59		
^{103}Rh	0.620	0.164	26	NA			ND			0.62		
^{106}Pd	2.41	0.47	19	NA			1.15	0.04	4	1.78	0.89	50
^{111}Cd	ND			NA			ND			NA		
^{118}Sn	2.68	0.20	8	NA			1.27	0.15	12	1.98	1.00	50
^{121}Sb	ND			NA			ND			NA		
^{133}Cs	1.12	0.04	4	NA			ND			1.12		
^{184}W	4.20	0.29	7	NA			4.03	0.76	19	4.12	0.12	3
^{187}Re	ND			NA			ND			NA		
^{195}Pt	3.03	0.23	8	NA			3.49	0.05	1	3.26	0.33	10
^{205}Tl	2.14	0.12	5	NA			2.05	0.07	3	2.10	0.06	3
^{206}Pb	374	6	2	NA			530	21	4	452	110	24
^{207}Pb	383	5	1	NA			538	13	2	460	109	24
^{208}Pb	386	7	2	NA			549	3	1	467	115	25
^{209}Bi	6.78	1.0	15	NA			7.81	0.31	4	7.30	0.73	10
^{232}Th	97.0	0.5	1	NA			177	0	0	137	57	41
^{238}U	83.0	0.1	0	NA			157	0	0	120	52	44

Each column represents average of 3 analytical runs; NA = Not Available; ND = Not Detected. Replicate 2 showed effervescence during acid stripping.

Table 5.30. Elan DRC 6100 ICPMS data for desert varnish sample MPP 10.

	MPP 10											
	Replicate 1			Replicate 2			Replicate 3			Average		
Isotope	ppm	SD	%RSD	ppm	SD	%RSD	ppm	SD	%RSD	ppm	SD	%RSD
^{9}Be	4.59	0.02	0	2.07	0.01	1	0.840	0.003	0	2.50	1.91	76
^{51}V	97.0	1.1	1	24.9	0.6	2	22.4	0.6	3	48.1	42.4	88
^{52}Cr	55.5	1.4	3	14.9	0.6	4	9.63	0.25	3	26.7	25.1	94
^{59}Co	124	4	3	15.2	0.4	3	22.1	0.5	2	53.8	61.0	113
^{60}Ni	ND			ND			ND			NA		
^{63}Cu	25.6	1.1	4	7.96	0.06	1	3.92	0.38	10	12.5	11.5	92
^{66}Zn	360	14	4	161	5	3	84.0	3.3	4	202	142	71
^{75}As	338	6	2	40.9	0.9	2	58.9	1.6	3	146	167	114
^{88}Sr	421	9	2	371	9	3	492	16	3	428	60	14
^{98}Mo	10.3	0.4	4	2.21	0.11	5	0.960	0.025	3	4.49	5.08	113
^{102}Ru	ND			ND			ND			NA		
^{103}Rh	ND			ND			ND			NA		
^{106}Pd	1.49	0.09	6	0.81	0.01	2	2.01	0.03	2	1.44	0.60	42
^{111}Cd	2.50	0.03	1	1.29	0.02	1	0.630	0.010	2	NA		
^{118}Sn	25.6	1.2	5	6.96	0.37	5	1.00	0.05	5	11.2	12.8	115
^{121}Sb	10.4	0.5	5	1.19	0.04	4	1.09	0.04	4	4.22	5.33	126
^{133}Cs	ND			ND			ND			NA		
^{184}W	2.33	0.09	4	0.68	0.02	4	0.780	0.073	9	1.26	0.93	73
^{187}Re	0.060	0.013	21	ND			ND			0.060		
^{195}Pt	2.24	0.13	6	1.21	0.07	6	0.500	0.022	4	1.32	0.87	66
^{205}Tl	0.340	0.014	4	0.710	0.021	3	0.340	0.014	4	0.463	0.214	46
^{206}Pb	452	3	1	158	5	3	137	6	5	249	176	71
^{207}Pb	454	6	1	160	4	3	136	7	5	250	177	71
^{208}Pb	460	6	1	162	7	4	138	3	2	253	179	71
^{209}Bi	35.2	2.9	8	7.41	0.48	7	3.36	0.19	6	15.3	17.3	113
^{232}Th	22.5	0.0	0	6.42	0.03	0	4.71	0.04	1	11.2	9.8	88
^{238}U	9.79	0.01	0	1.47	0.00	0	1.23	0.00	0	4.16	4.87	117

Each column represents average of 3 analytical runs; NA = Not Available; ND = Not Detected.

Table 5.31. Elan DRC 6100 ICPMS data for desert varnish sample RGPP 1.

	RGPP 1											
	Replicate 1			Replicate 2			Replicate 3			Average		
Isotope	ppm	SD	%RSD	ppm	SD	%RSD	ppm	SD	%RSD	ppm	SD	%RSD
^{9}Be	0.540	0.037	7	0.770	0.032	4	0.560	0.002	0	0.623	0.127	20
^{51}V	121	1	1	157	2	1	141	1	1	140	18	13
^{52}Cr	21.8	1.2	6	39.1	0.9	2	28.3	0.6	2	29.7	8.7	29
^{59}Co	10.8	0.3	3	17.9	0.2	1	5.70	0.06	1	11.5	6.1	54
^{60}Ni	ND			ND			ND			NA		
^{63}Cu	ND			ND			ND			NA		
^{66}Zn	464	9	2	390	11	3	499	17	4	451	56	12
^{75}As	100	1	1	104	1	1	89.7	0.4	1	97.8	7.3	7
^{88}Sr	278	3	1	365	5	1	312	3	1	318	44	14
^{98}Mo	2.05	0.02	1	2.18	0.03	1	2.22	0.08	4	2.15	0.09	4
^{102}Ru	ND			ND			ND			NA		
^{103}Rh	ND			ND			ND			NA		
^{106}Pd	8.25	0.39	5	6.88	0.31	5	7.48	0.78	10	7.54	0.69	9
^{111}Cd	0.730	0.007	1	1.75	0.41	23	0.140	0.004	3	NA		
^{118}Sn	2.96	0.10	3	3.67	0.08	2	3.56	0.15	4	3.40	0.38	11
^{121}Sb	ND			ND			ND		5	NA		
^{133}Cs	0.180	0.001	1	0.220	0.004	2	0.240	0.020	8	NA		
^{184}W	1.67	0.05	3	1.87	0.03	2	1.60	0.10	6	1.71	0.14	8
^{187}Re	ND			ND			ND			NA		
^{195}Pt	4.17	0.18	4	4.54	0.38	8	4.93	0.23	5	4.55	0.38	8
^{205}Tl	13.9	0.4	3	19.4	0.3	1	15.0	0.9	6	16.1	2.9	18
^{206}Pb	1670	33	2	1740	21	1	981	36	4	1460	420	29
^{207}Pb	1700	39	2	1770	19	1	1010	19	2	1490	420	28
^{208}Pb	1690	20	1	1770	35	2	1000	8	1	1490	423	28
^{209}Bi	0.740	0.024	3	0.760	0.056	7	0.680	0.024	4	0.727	0.042	6
^{232}Th	436	2	1	488	4	1	516	3	1	480	41	8
^{238}U	310	0	0	368	0	0	397	0	0	358	44	12

Each column represents average of 3 analytical runs; NA = Not Available; ND = Not Detected.

Table 5.32. Elan DRC 6100 ICPMS data for desert varnish sample RGPP 2.

	RGPP 2											
	Replicate 1			Replicate 2			Replicate 3			Average		
Isotope	ppm	SD	%RSD	ppm	SD	%RSD	ppm	SD	%RSD	ppm	SD	%RSD
^{9}Be	1.20	0.00	0	0.080	0.005	6	0.220	0.035	16	0.50	0.61	122
^{51}V	140	1	1	58.0	0.6	1	137	2	1	112	47	42
^{52}Cr	39.5	1.3	3	16.6	0.1	1	40.7	2.1	5	32.2	13.6	42
^{59}Co	15.2	0.4	3	5.00	0.13	3	13.4	0.2	1	11.2	5.4	49
^{60}Ni	28.6	6.7	23	13.7	0.5	4	36.8	11.1	30	26.4	11.7	44
^{63}Cu	NA			NA			NA			NA		
^{66}Zn	684	17	3	90.5	1.6	2	308	6	2	361	300	83
^{75}As	92.9	4.8	5	45.4	0.1	0	91.3	1.4	2	76.5	27.0	35
^{88}Sr	538	10	2	231	8	3	587	15	3	452	193	43
^{98}Mo	0.760	0.001	0	0.600	0.005	1	1.62	0.02	1	0.99	0.55	55
^{102}Ru	ND			ND			ND			NA		
^{103}Rh	ND			ND			ND			NA		
^{106}Pd	7.81	0.10	1	3.00	0.18	6	8.04	0.31	4	6.28	2.85	45
^{111}Cd	1.21	0.00	0	ND			ND			1.21		
^{118}Sn	0.040	0.034	84	0.170	0.018	10	0.440	0.008	2	0.217	0.204	94
^{121}Sb	ND			ND			ND			NA		
^{133}Cs	ND			ND			ND			NA		
^{184}W	1.31	0.01	0	0.440	0.018	4	0.930	0.031	3	0.893	0.436	49
^{187}Re	1.19	0.00	0	ND			ND			1.19		
^{195}Pt	11.6	0.3	2	2.97	0.12	4	11.9	0.4	4	8.83	5.08	58
^{205}Tl	12.5	0.9	8	4.81	0.34	7	12.9	0.6	4	10.1	4.6	45
^{206}Pb	1310	48	4	506	4	1	1310	28	2	1040	464	45
^{207}Pb	1330	33	3	515	6	1	1300	20	2	1050	462	44
^{208}Pb	1270	30	2	506	9	2	1270	25	2	1020	441	43
^{209}Bi	ND		0	0.250	0.012	5	0.670	0.027	4	0.460	0.297	65
^{232}Th	606	1	0	235	0	0	633	1	0	491	223	45
^{238}U	562	1	0	216	0	0	578	1	0	452	205	45

Each column represents average of 3 analytical runs; NA = Not Available; ND = Not Detected.

Table 5.33. Elan DRC 6100 ICPMS data for desert varnish sample RGPP 3.

	RGPP 3											
	Replicate 1			Replicate 2			Replicate 3			Average		
Isotope	ppm	SD	%RSD	ppm	SD	%RSD	ppm	SD	%RSD	ppm	SD	%RSD
^{9}Be	1.30	0.17	13	1.00	0.05	5	1.40	0.06	4.2	1.23	0.21	17
^{51}V	28.4	0.4	1	33.6	0.5	2	28.7	0.1	0.3	30.2	2.9	10
^{52}Cr	26.8	0.6	2	18.5	0.2	1	16.9	0.1	0.8	20.7	5.3	26
^{59}Co	16.8	0.9	6	13.5	0.3	2	21.0	0.8	3.7	17.1	3.8	22
^{60}Ni	40.2	4.8	12	33.0	1.9	6	41.4	1.9	4.5	38.2	4.5	12
^{63}Cu	21.8	1.0	5	16.0	10.7	67	12.7	3.9	30.8	16.8	4.6	27
^{66}Zn	221	3	1	82.5	1.1	1	112	4	3.6	138	73	53
^{75}As	24.3	0.5	2	14.5	0.5	3	18.4	0.2	0.9	19.1	4.9	26
^{88}Sr	136	2	2	227	5	2	163	6	3.7	175	47	27
^{98}Mo	4.80	0.14	3	3.00	0.04	1	4.00	0.16	4.0	3.93	0.90	23
^{102}Ru	ND			ND			ND			NA		
^{103}Rh	ND			ND			ND			NA		
^{106}Pd	11.6	1.0	9	2.00	0.01	1	2.10	0.01	0.7	5.23	5.51	105
^{111}Cd	1.10	0.03	3	0.500	0.012	2	1.20	0.06	4.7	0.933	0.379	41
^{118}Sn	4.50	0.28	6	3.50	0.09	3	2.10	0.02	1.1	3.37	1.21	36
^{121}Sb	2.30	0.06	3	1.00	0.03	3	0.900	0.035	3.9	1.40	0.78	56
^{133}Cs	2.40	0.00	0	1.50	0.01	1	1.60	0.00	0.1	1.83	0.49	27
^{184}W	2.80	0.28	10	1.50	0.10	6	2.70	0.06	2.4	2.33	0.72	31
^{187}Re	1.30	0.03	2	0.50	0.00	1	0.600	0.003	0.5	0.800	0.436	54
^{195}Pt	0.800	0.176	22	ND			0.300	0.031	10.3	0.550	0.354	64
^{205}Tl	1.50	0.56	37	0.500	0.026	5	0.700	0.047	6.7	0.900	0.529	59
^{206}Pb	62.7	2.8	4	55.0	0.7	1	47.5	1.5	3.1	55.1	7.6	14
^{207}Pb	68.6	1.8	3	57.0	2.5	4	50.4	1.7	3.4	58.7	9.2	16
^{208}Pb	64.4	2.2	3	54.5	1.0	2	48.9	0.7	1.4	55.9	7.8	14
^{209}Bi	1.20	0.45	37	0.500	0.100	20	0.700	0.093	13.3	0.800	0.361	45
^{232}Th	91.2	1.3	1	27.5	1.8	6	25.9	1.5	5.9	48.2	37.2	77
^{238}U	3.10	0.27	9	5.00	0.15	3	3.50	1.07	30.7	3.87	1.00	26

Each column represents average of 3 analytical runs; NA = Not Available; ND = Not Detected.

Table 5.34. Elan DRC 6100 ICPMS data for desert varnish sample RGPP 4.

	RGPP 4											
	Replicate 1			Replicate 2			Replicate 3			Average		
Isotope	ppm	SD	%RSD	ppm	SD	%RSD	ppm	SD	%RSD	ppm	SD	%RSD
^{9}Be	0.200	0.012	6	0.710	0.018	3	0.460	0.028	6	0.457	0.255	56
^{51}V	9.91	0.16	2	25.5	0.4	2	15.4	0.3	2	16.9	7.9	47
^{52}Cr	6.77	0.05	1	13.6	0.1	1	6.38	0.10	2	8.90	4.04	45
^{59}Co	6.58	0.05	1	24.7	0.5	2	18.4	0.0	0	16.6	9.2	56
^{60}Ni	2.77	0.11	4	ND			7.56	0.39	5	5.17	3.39	66
^{63}Cu	NA			NA			NA			NA		
^{66}Zn	45.9	0.6	1	101	1	1	147	2	2	98.1	50.6	52
^{75}As	6.27	0.11	2	16.8	0.4	3	6.69	0.03	0	9.92	5.96	60
^{88}Sr	53.2	0.5	1	66.8	1.2	2	72.9	0.7	1	64.3	10.1	16
^{98}Mo	1.03	0.01	1	1.84	0.01	0	1.66	0.02	1	1.51	0.43	28
^{102}Ru	ND			ND			ND			NA		
^{103}Rh	ND			ND			ND			NA		
^{106}Pd	0.190	0.001	0	0.540	0.031	6	0.440	0.019	4	0.390	0.180	46
^{111}Cd	0.210	0.028	13	1.48	0.12	8	0.800	0.050	6	0.83	0.64	77
^{118}Sn	0.210	0.006	3	0.890	0.027	3	0.640	0.017	3	0.580	0.344	59
^{121}Sb	ND			0.740	0.019	3	ND			0.740		
^{133}Cs	0.120	0.000	0	0.750	0.032	4	0.270	0.001	0	0.380	0.329	87
^{184}W	0.450	0.016	4	1.25	0.02	2	1.18	0.03	3	0.96	0.44	46
^{187}Re	ND			ND			ND			NA		
^{195}Pt	0.200	0.008	4	0.400	0.022	6	0.440	0.004	1	0.347	0.129	37
^{205}Tl	0.420	0.009	2	1.02	0.03	3	0.790	0.027	3	0.743	0.303	41
^{206}Pb	28.0	0.1	1	85.5	1.8	2	112	1	1	75.3	43.0	57
^{207}Pb	27.4	0.2	1	84.8	0.8	1	110	2	2	74.1	42.4	57
^{208}Pb	26.6	0.3	1	82.1	1.0	1	107	1	1	72.0	41.3	57
^{209}Bi	0.290	0.002	1	0.600	0.020	3	0.820	0.021	3	0.570	0.266	47
^{232}Th	11.7	0.1	1	26.6	0.1	0	26.1	0.0	0	21.4	8.5	39
^{238}U	9.75	0.01	0	21.0	0.0	0	21.4	0.0	0	17.4	6.6	38

Each column represents average of 3 analytical runs; NA = Not Available; ND = Not Detected.

Table 5.35. Elan DRC 6100 ICPMS data for desert varnish sample RGPP 5.

	RGPP 5											
	Replicate 1			Replicate 2			Replicate 3			Average		
Isotope	ppm	SD	%RSD	ppm	SD	%RSD	ppm	SD	%RSD	ppm	SD	%RSD
^{9}Be	10.3	0.2	2	20.1	1.3	7	25.0	1.8	7	18.4	7.5	41
^{51}V	491	10	2	824	12	1	843	21	3	719	198	27
^{52}Cr	115	2	2	61.1	0.5	1	77.8	0.9	1	84.8	27.8	33
^{59}Co	246	5	2	302	6	2	478	8	2	342	121	35
^{60}Ni	69.2	1.8	3	189	4	2	195	5	2	151	71	47
^{63}Cu	21.6	0.3	1	ND			10.9	0.5	4	NA		
^{66}Zn	248	8	3	452	19	4	458	20	4	386	120	31
^{75}As	140	3	2	267	4	1	305	7	2	237	87	36
^{88}Sr	449	3	1	702	8	1	769	12	2	640	169	26
^{98}Mo	36.3	1.8	5	75.0	3.3	4	80.3	4.9	6	63.9	24.0	38
^{102}Ru	ND			ND			ND			NA		
^{103}Rh	ND			ND			ND			NA		
^{106}Pd	3.80	0.08	2	4.75	0.12	3	5.93	0.10	2	4.83	1.07	22
^{111}Cd	4.87	0.37	8	7.34	0.46	6	5.45	0.28	5	5.89		
^{118}Sn	3.27	0.13	4	4.19	0.44	10	3.27	0.16	5	3.58	0.53	15
^{121}Sb	56.7	0.8	1	69.4	1.0	2	89.7	2.2	3	NA		
^{133}Cs	1.58	0.03	2	1.77	0.13	8	1.84	0.08	4	NA		
^{184}W	1450	41	3	1820	89	5	1843	85	5	1700	220	13
^{187}Re	ND			ND			ND			NA		
^{195}Pt	1.28	0.05	4	2.87	0.04	1	4.54	0.20	5	2.90	1.63	56
^{205}Tl	10.1	0.7	7	22.8	1.8	8	26.3	1.7	6	19.8	8.5	43
^{206}Pb	1400	15	1	1200	16	1	1610	26	2	1400	205	15
^{207}Pb	1410	31	2	1220	4	0	1620	32	2	1420	200	14
^{208}Pb	NA		1	1240	15	1	1650	18	1	1450	290	20
^{209}Bi	4.76	0.28	6	6.42	0.18	3	6.68	0.45	7	5.95	1.04	17
^{232}Th	107	0	0	206	1	0	216	1	0	176	60	34
^{238}U	62.4	0.1	0	141	0	0	147	0	0	117	47	40

Each column represents average of 3 analytical runs; NA = Not Available; ND = Not Detected.

Table 5.36. Elan DRC 6100 ICPMS data for desert varnish sample RGPP 6.

	RGPP 6											
	Replicate 1			Replicate 2			Replicate 3			Average		
Isotope	ppm	SD	%RSD	ppm	SD	%RSD	ppm	SD	%RSD	ppm	SD	%RSD
^{9}Be	3.19	0.19	6	9.26	0.24	3	NA			6.23	4.29	69
^{51}V	68.9	0.7	1	175	2	1	NA			122	75	61
^{52}Cr	614	13	2	478	7	1	NA			546	96	18
^{59}Co	158	3	2	277	7	3	NA			218	85	39
^{60}Ni	12.1	10.4	86	ND			NA			12		
^{63}Cu	NA			NA			NA			NA		
^{66}Zn	746	21	3	3580	158	4	NA			2163	2004	93
^{75}As	87.7	1.0	1	205	2	1	NA			146	83	57
^{88}Sr	78.6	1.2	2	161	5	3	NA			120	58	49
^{98}Mo	13.8	0.2	2	33.5	1.0	3	NA			23.7	13.9	59
^{102}Ru	ND			ND			NA			NA		
^{103}Rh	ND			ND			NA			NA		
^{106}Pd	2.90	0.04	1	8.41	0.23	3	NA			5.66	3.90	69
^{111}Cd	8.90	1.07	12	12.9	4.1	32	NA			10.9		
^{118}Sn	6.67	0.19	3	25.8	0.6	2	NA			16.2	13.5	83
^{121}Sb	ND			ND			NA			NA		
^{133}Cs	1.88	0.11	6	5.45	0.22	4	NA			3.67	2.52	69
^{184}W	45.7	2.7	6	61.2	1.9	3	NA			53.4	11.0	20
^{187}Re	ND			ND			NA			NA		
^{195}Pt	1.96	0.06	3	5.69	0.13	2	NA			3.83	2.64	69
^{205}Tl	6.65	0.19	3	24.8	0.5	2	NA			15.7	12.8	82
^{206}Pb	702	15	2	1580	17	1	NA			1140	621	54
^{207}Pb	714	21	3	1610	37	2	NA			1160	633	55
^{208}Pb	729	28	4	1580	21	1	NA			1160	601	52
^{209}Bi	4.54	0.08	2	13.2	0.2	2	NA			8.86	6.11	69
^{232}Th	185	1	1	505	1	0	NA			345	226	66
^{238}U	146	0	0	425	0	0	NA			286	197	69

Each column represents average of 3 analytical runs; NA = Not Available; ND = Not Detected. Replicate 3 showed effervescence during acid stripping.

Table 5.37. Elan DRC 6100 ICPMS data for desert varnish sample BKG 1.

	BKG 1											
	Replicate 1			Replicate 2			Replicate 3			Average		
Isotope	ppm	SD	%RSD	ppm	SD	%RSD	ppm	SD	%RSD	ppm	SD	%RSD
^{9}Be	5.86	0.13	2	9.24	0.47	5	10.1	0.3	3	8.40	2.24	27
^{51}V	276	1	0	701	4	1	447	9	2	475	214	45
^{52}Cr	397	6	1	355	4	1	253	5	2	335	74	22
^{59}Co	42.0	0.5	1	253	4	2	250	5	2	182	121	67
^{60}Ni	NA			NA			NA			NA		
^{63}Cu	NA			NA			NA			NA		
^{66}Zn	1130	25	2	2250	47	2	1850	50	3	1740	568	33
^{75}As	125	2	2	177	6	3	149	3	2	150	26	18
^{88}Sr	260	8	3	378	7	2	388	7	2	342	71	21
^{98}Mo	30.2	1.6	5	43.4	2.0	5	54.8	2.8	5	42.8	12.3	29
^{102}Ru	ND			ND			ND			NA		
^{103}Rh	ND			ND			ND			NA		
^{106}Pd	3.99	0.15	4	5.59	0.32	6	5.50	0.51	9	5.03	0.90	18
^{111}Cd	1.53	0.41	27	ND			2.11	0.11	5	1.82	0.41	23
^{118}Sn	1.51	0.08	5	6.36	0.10	2	14.8	1.1	7	7.55	6.71	89
^{121}Sb	ND			ND			ND			NA		
^{133}Cs	10.4	0.6	6	10.9	0.3	3	7.14	0.55	8	9.46	2.03	21
^{184}W	43.6	2.4	6	33.9	1.0	3	109	6	5	62.2	40.9	66
^{187}Re	ND			ND			ND			NA		
^{195}Pt	2.70	0.14	5	5.68	0.12	2	3.73	0.12	3	4.04	1.51	37
^{205}Tl	6.54	0.12	2	8.89	0.34	4	3.89	0.36	9	6.44	2.50	39
^{206}Pb	381	5	1	596	11	2	697	12	2	558	162	29
^{207}Pb	397	4	1	624	9	1	736	13	2	586	173	29
^{208}Pb	392	4	1	635	11	2	722	13	2	583	171	29
^{209}Bi	4.69	0.39	8	9.87	0.59	6	4.31	0.65	15	6.29	3.11	49
^{232}Th	266	1	0	525	1	0	355	10	3	382	132	34
^{238}U	203	0	0	424	0	0	278	1	1	302	112	37

Each column represents average of 3 analytical runs; NA = Not Available; ND = Not Detected.

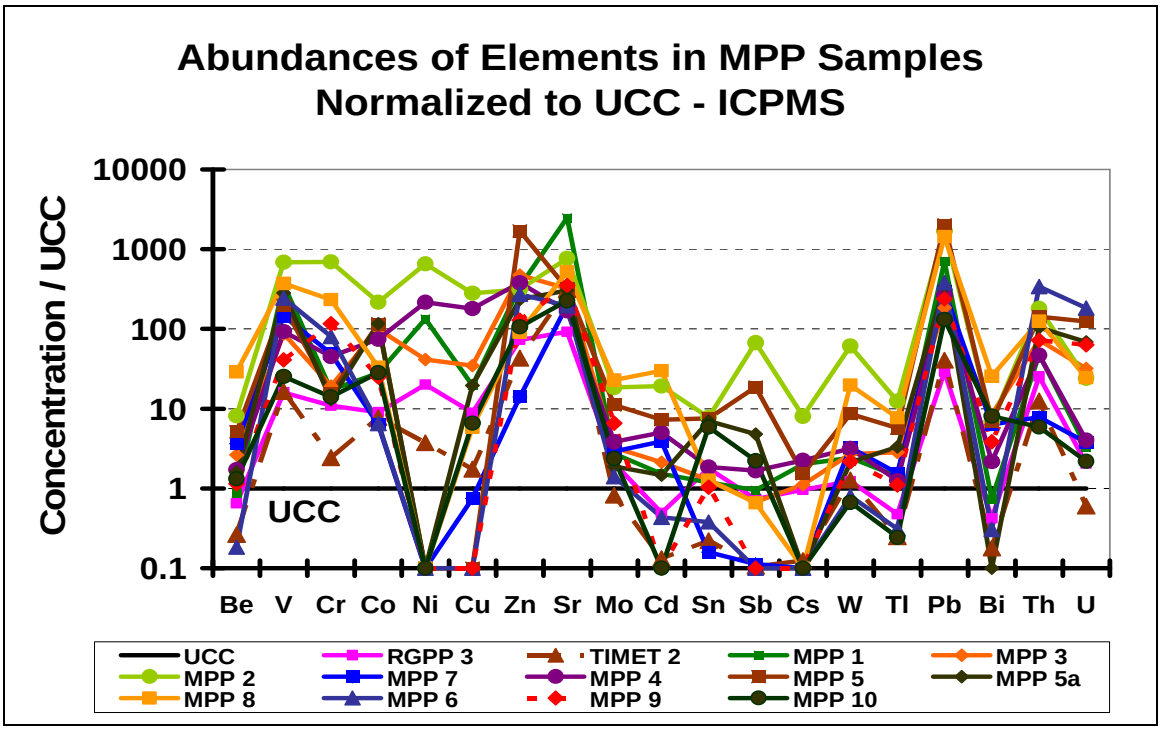

Figure 5.34. Abundances of elements by Elan DRC 6100 ICPMS analysis of varnish coatings in MPP samples normalized to the UCC. The thick black line represents the average UCC abundance (Ratio=1).

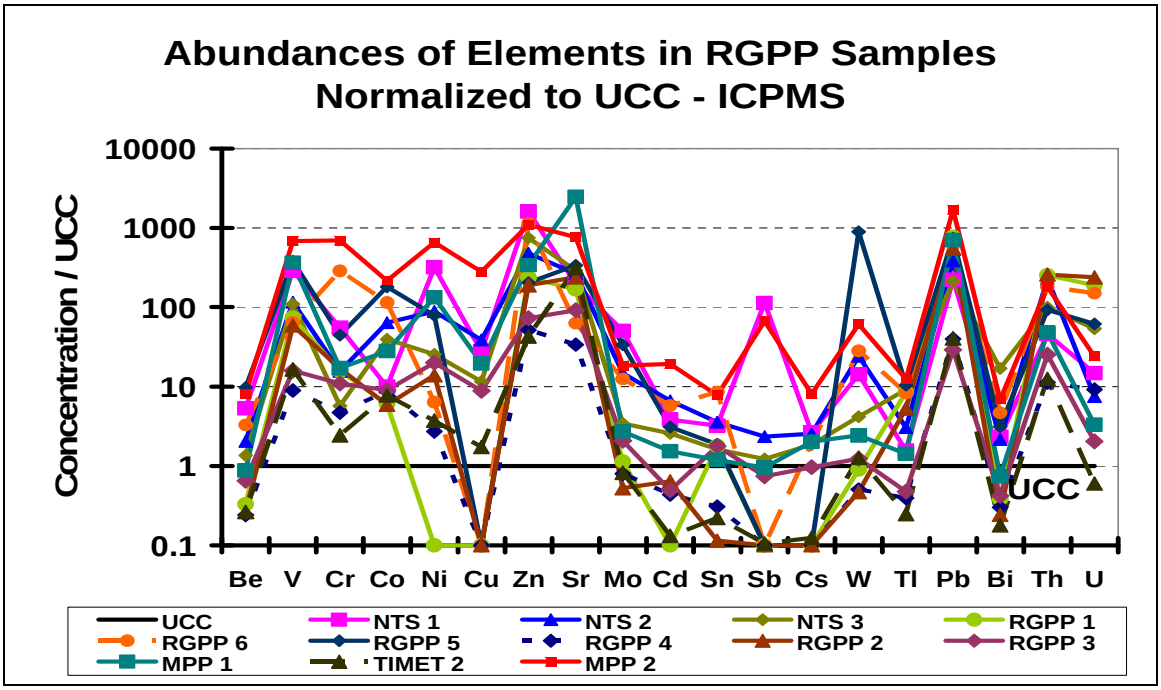

Figure 5.35. Abundances of elements by Elan DRC 6100 ICPMS analysis of varnish coatings in RGPP samples normalized to the UCC. The thick black line represents the average UCC abundance (Ratio=1).

The averages from three sampling points were calculated for each sampling location and the data were used to plot the elemental concentrations in the varnish samples as a function of the distance from the power plant (Figures 5.36 to 5.39). For each power plant, the graphs were plotted in two different groups of elements depending on the element concentrations. The first group included elements (V, Cr, Co, Ni, Cu, Zn, As, Sr, Pb, Th, and U in RGPP only) that have high desert varnish concentrations (200 to 4020 $\mu g \cdot g^{-1}$) and the second group included elements (Be, Mo, Rh, Ru, Pd, Cd, Sn, Sb, Cs, W, Re, Pt, Tl, and Bi in MPP only) with low varnish concentrations (< 150 $\mu g \cdot g^{-1}$). Similar to the XRF and the LA-ICPMS graphs, the ICPMS plots show general patterns consistent with the predictions of the Gaussian Plume model (Anderson et al., 1975; Connor et al., 1976; Wangen and Williams, 1978). The MPP plots point to two deposition areas at distances of 50 to 80 km south of the power plant and 20 to 50 km north of the power plant. Both regions with the highest elemental concentrations in desert varnish correlate with the MPP deposition areas established during summer and winter tracer release experiments during project MOHAVE (U.S. Environmental Protection Agency, 1999).

The RGPP plots display deposition areas at distances of 50 to 80 km north of the power plant and 40 to 80 km south of the power plant. Noticeably, extremely southern and northern points of the graph show increases in the concentrations of the elements. The southern point (MPP 2) is located in the deposition area of the MPP and probably includes particulate loading from both MPP and RGPP. On the other hand, the northern point (NTS 1) is located near the NTS and within the W mineralization belt, which may contribute to an increase in the concentrations of Zn, As, Mo, and Sb.

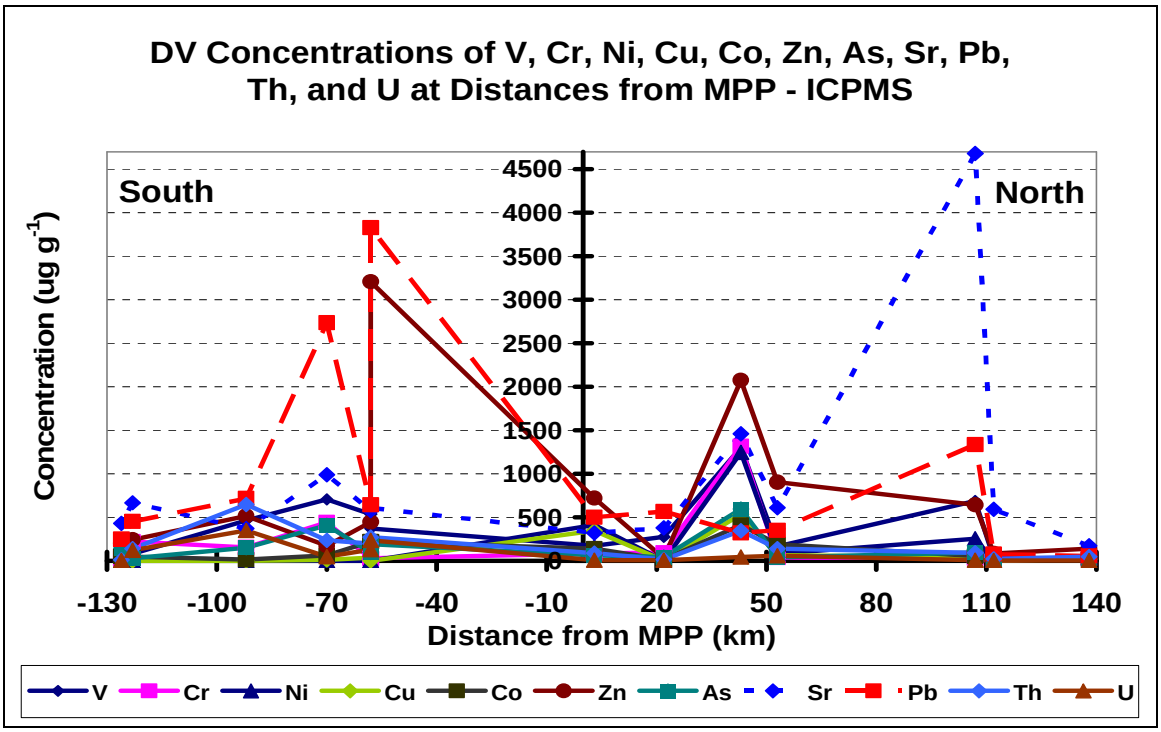

Figure 5.36. Concentrations of V, Cr, Ni, Cu, Co, Zn, As, Sr, Pb, Th and U by Elan DRC 6100 ICPMS analysis of desert varnish coatings in samples as a function of distance from MPP.

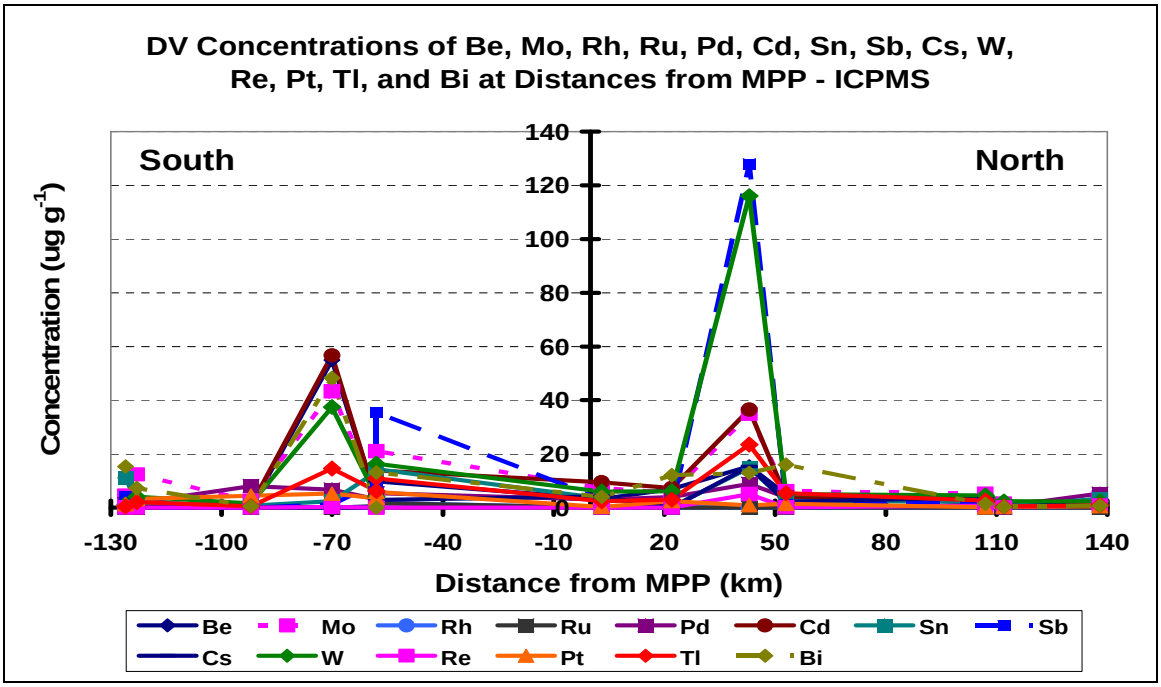

Figure 5.37. Concentrations of Be, Mo, Rh, Ru, Pd, Cd, Sn, Sb, Cs, W, Re, Pt, Tl, and Bi by Elan DRC 6100 ICPMS analysis of desert varnish coatings in samples as a function of distance from MPP.

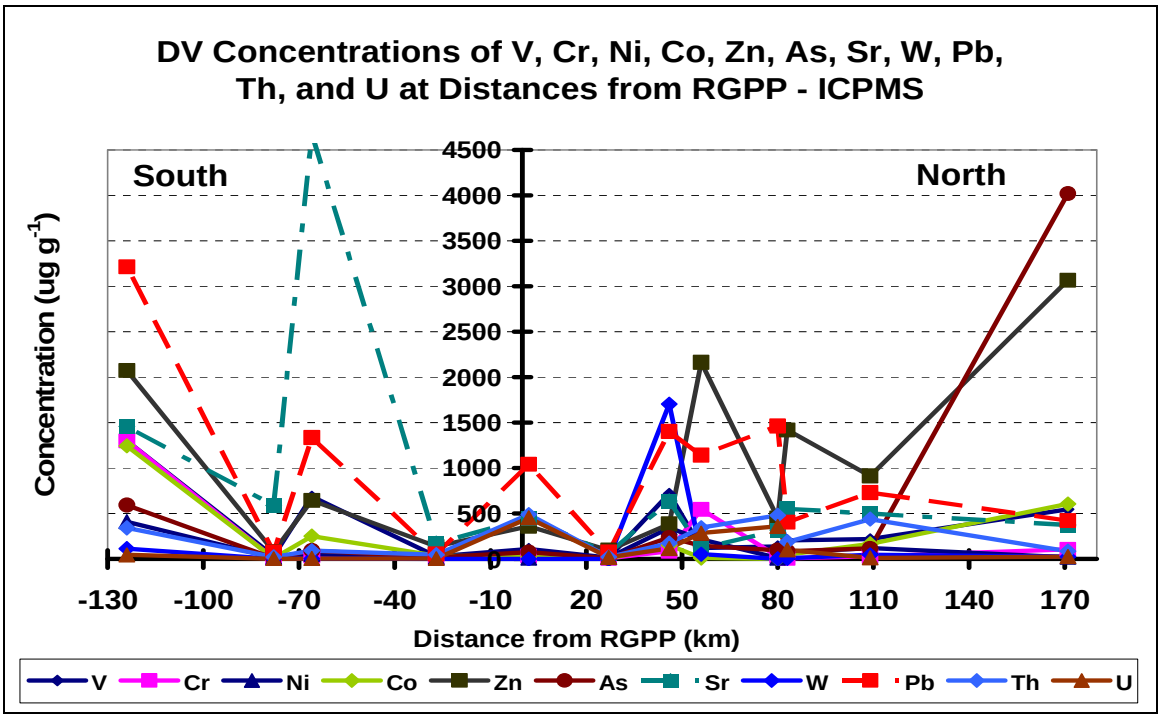

Figure 5.38. Concentrations of V, Cr, Ni, Co, Zn, As, Sr, W, Pb, Th and U by Elan DRC 6100 ICPMS analysis of desert varnish samples as a function of distance from RGPP.

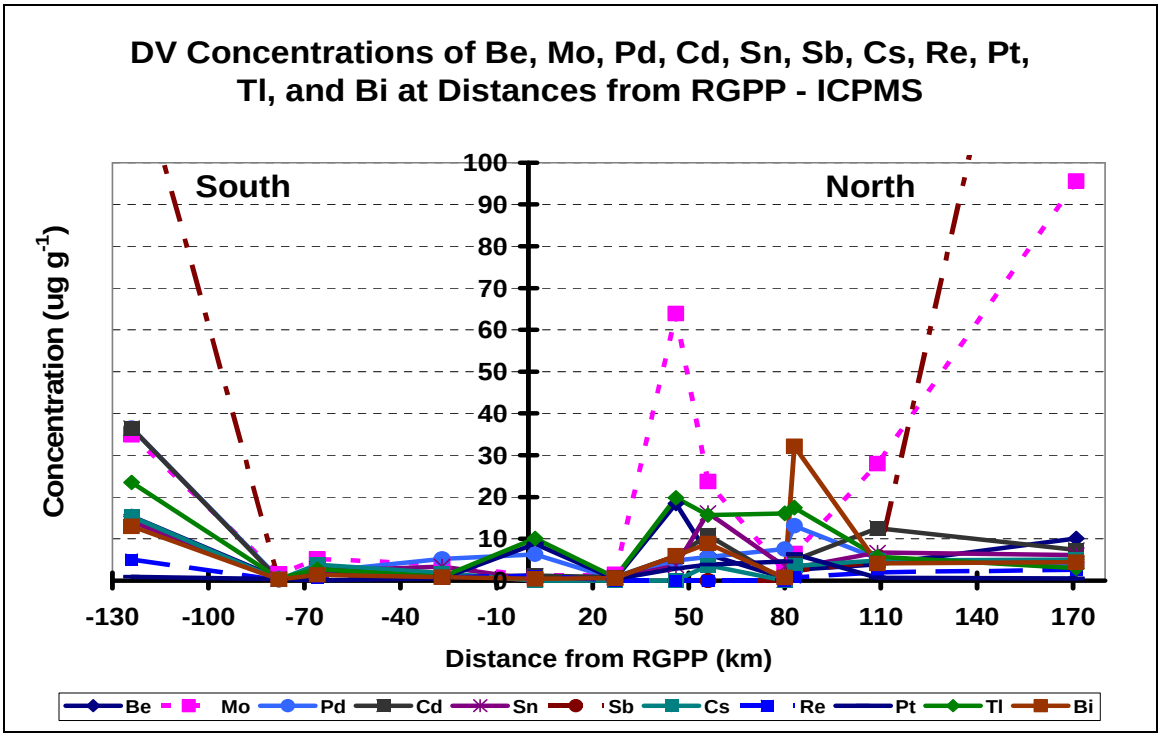

Figure 5.39. Concentrations of Be, Mo, Pd, Cd, Sn, Sb, Cs, Re, Pt, Tl, and Bi by Elan DRC 6100 ICPMS analysis of desert varnish samples as a function of distance from RGPP.

Additionally, the sampled rocks may present unique geological composition that is demonstrated in the high concentrations of As, Mo and Sb. The developed graphs confirm that all inputs of atmospheric pollution in the proximity of the investigated point source have to be considered during mapping of the deposition areas.

Other noteworthy results are presented in Figure 5.40. The concentrations of Pt and Pd are anomalously high in the varnish samples compared to their natural abundances. Mason (1958) reported crustal values of 0.005 $\mu g \cdot g^{-1}$ Pt and 0.010 $\mu g \cdot g^{-1}$ Pd, and the South African ores have platinum group elements (PGE) concentrations of 4 to10 ppm (Sharpe, 1982). The analyzed desert varnish samples have 0.10 to 8.83 $\mu g \cdot g^{-1}$ Pt and 0.49 to 13.1 $\mu g \cdot g^{-1}$ Pd, and five samples (NTS 3, MPP1, MPP 5, MPP 5a, and MPP 9) show traces of Rh and Ru. Automobiles are the likely source for the excess quantities of these metals. It has been shown that automobile catalytic converters release significant amounts of platinum and palladium to the roadside environment (Hodge and Stallard, 1988; Boutron et al., 1994). It should be noted that most of the sites sampled in this study were near roadside environments. However, the ratio of Pt/Pd reported in catalytic converters is 2.5 and the Pt/Pd ratio in the varnish samples is 0.64 ± 0.47 (Hodge et al., 1986; Cizdziel, 1998).

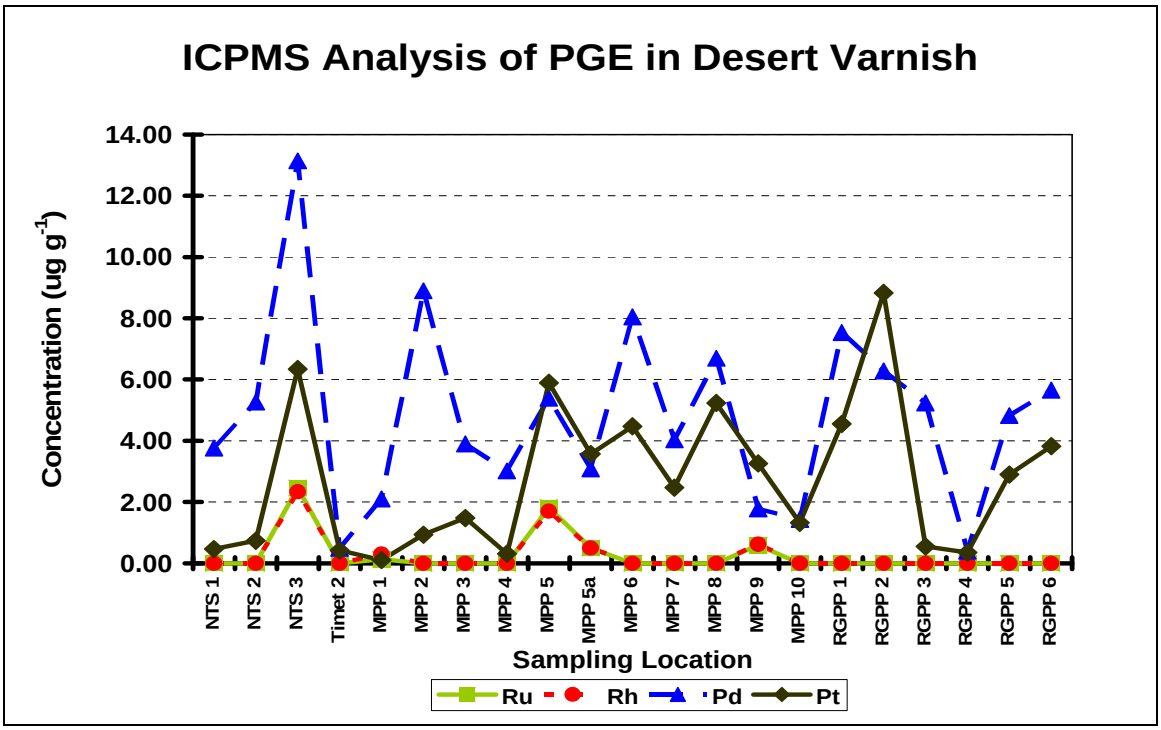

Figure 5.40. Concentrations of Ru, Rh, Pd, and Pt by Elan DRC 6100 ICPMS analysis of desert varnish samples.

Cold Vapor Atomic Absorption Hg Results

Cold vapor atomic absorption (CVAA) was used for the analysis of Hg in the solutions resulting from the HCl stripping of the desert varnish samples. All varnish samples were stripped and analyzed in triplicate.

Method Detection Limit (MDL)

The method detection limit (MDL) was calculated based on the replicate measurements (n=40) of water blanks and the slope of the calibration curve (3σ). The MDL for Hg in desert varnish samples is 0.009 $\mu g \cdot L^{-1}$.

Calibration Curve and QA/QC

A calibration blank and five standards (0.5, 1.0, 2.5, 5.0, 10.0 $\mu g \cdot L^{-1}$) were used for instrument calibration and the linear correlation coefficient was 0.9997. The ICV and

CCV solutions, prepared from different sources than the calibration standards, were used to assess the validity of the calibration curve. The QA/QC sample frequency was 10%, with recovery in a range of 90 to110 %. The calibration blanks (ICB/CCB) were used to establish the analytical curve, while the preparation blanks (PB) were used to monitor for possible contamination.

To examine the accuracy and precision of the analytical method NIST SRM 1946 Lake Superior Fish Tissue was analyzed. An excellent agreement with certified values is obtained for SRM 1946 (105 to107 %) and the duplicate RPD is 2% (Table 5.38). This gives confidence that the method is suitable for the analysis of mercury in rock varnish samples and provides very accurate and precise results.

Table 5.38. CVAA Hg results for standard reference material NIST SRM 1946. Concentrations are reported in $\mu g \cdot g^{-1}$.

Element	NIST SRM 1946							
	Found	Found	Found	Certified value	% Rec.	% Rec.	% Rec.	RPD
Hg	0.464 ± 0.019	0.453 ± 0.015	0.458 ± 0.016	0.433 ± 0.009	107	105	106	2

Found values are ± 1 SD. Certified value is ± 95% confidence limit.

Sample Data

The concentrations for CVAA analysis of Hg in desert varnish samples are given in Table 5.39. Each result represents the average of 3 individual analyses.

The average mercury concentrations from sampling points range from 0.012 $\mu g \cdot g^{-1}$ for RGPP 3 to 2.34 $\mu g \cdot g^{-1}$ for RGPP 5. Sample RGPP 6 shows the maximum individual measurement (5.21 $\mu g \cdot g^{-1}$). Mercury is not detected in replicates of NTS 1 and MPP 10. The relative standard deviation (%RSD) for individual measurements range from 0% to 57%; with the majority of the values between 1% and 5%. The relative standard

deviations (%RSD) for the average concentrations are considerably higher and range between 18% and 143%.

The average concentrations from three sampling points were plotted as a function of the distance from each power plant (Figures 5.41 and 5.42). The MPP plot shows a concentration peak at 80 km south of the power plant and another peak at 20 km north of the power plant (Figure 5.41). Both peaks with the highest Hg concentrations fall within the MPP maximum deposition areas established during summer and winter tracer release experiments during project MOHAVE (U.S. Environmental Protection Agency, 1999).

The RGPP plot displays two high concentration peaks at distances of 50 km and 117 km north and another smaller peak at about 70 km south of the power plant (Figure 5.42). The mercury deposition patterns are somewhat similar to the deposition patterns of other elements, although they are not as distinctive. This could be caused by the different chemistry of the atmospheric Hg and additional deposition mechanisms for particulate loading (Linberg and Stratton, 1998).

Combustion of coal and other fossil fuels releases mercury into the atmosphere (Clarke and Sloss, 1992; Davidson and Clarke, 1996; Danihelka et al., 2003). Due to its volatility, principal Hg emissions from power plants are in the gaseous state (Crockett and Kinnison, 1977; Wangen and Williams, 1978; Galbreath and Zygarlickie, 1996; Linberg and Stratton, 1998). In the atmosphere, Hg exists largely as gaseous Hg^0 with trace amounts of Hg^{2+} compounds (Lindqvist et al., 1991). Atmospheric Hg^{2+} compounds may be associated with particles or occur as gasses, most probably $HgCl_2$, $Hg(OH)_2$, or compounds of others halides, and are collectively called reactive gaseous mercury (RGM). These species are highly water-soluble and the water solubility strongly

influences their removal and deposition from the atmosphere (Lindberg and Stratton, 1998). Thus, the deposition of Hg is very difficult to quantify.

Mercury may be deposited by wet and dry processes to environmental surfaces. Knowledge of the speciation of atmospheric Hg is crucial for predicting its deposition and understanding its geochemical cycling. Gaseous mercury speciation measured in flue gases of coal combustion systems suggests that flue gas Hg emissions are equally divided between two oxidation states, elemental (Hg^0) and mercuric (Hg^{2+}) (Galbreath and Zygarlickie, 1996).

Several modeling studies have confirmed that the speciation of airborne Hg is crucial to the modeling of its transport and removal processes (Seigneur et al., 1994; Petersen et al., 1995). Although Hg^0 is the dominant form of atmospheric Hg, even small amounts of Hg halides ($HgCl_2$, $HgBr_2$) may control the overall deposition of Hg, since these halides could be efficiently absorbed by cloud droplets during the formation of rain and would deposit 100 times more than Hg^0 (Lindberg and Stratton, 1998). Therefore, even small amounts of reactive gaseous mercury (RGM) are important to dry Hg deposition.

RGM are highly surface-reactive species similar in behavior to gaseous HNO_3 (Anlauf et al., 1985). The reactivity of RGM plays a strong role in the removal of Hg from the atmosphere by both precipitation scavenging and dry deposition (Lindberg and Stratton, 1998; Petersen et al., 1995). Pai et al. (1997) applied an Eulerian atmospheric transport model to regional dry and wet depositions of Hg and concluded that Hg depositions are dominated by ”divalent forms of gaseous mercury”.

Table 5.39. PerkinElmer FIMS-100 CVAA Hg data for desert varnish samples.

Hg CVAA Data												
	Replicate 1			Replicate 2			Replicate 3			Average		
Sample	ppm	SD	%RSD	ppm	SD	%RSD	ppm	SD	%RSD	ppm	SD	%RSD
NTS 1	ND			0.125	0.010	8	ND			0.125		
NTS 2	5.15	0.01	0	0.902	0.013	1	0.025	0.000	2	2.03	2.74	135
NTS 3	0.185	0.028	15	0.297	0.026	9	0.138	0.001	1	0.207	0.082	40
TIMET 2	0.008	0.000	6	0.053	0.001	1	0.158	0.008	5	0.073	0.077	106
MPP 1	0.107	0.003	3	0.219	0.018	8	0.090	0.003	4	0.139	0.070	50
MPP 2	0.604	0.004	1	0.174	0.013	8	0.409	0.084	21	0.396	0.215	54
MPP 3	0.210	0.003	1	0.467	0.262	56	0.064	0.001	1	0.247	0.204	83
MPP 4	0.744	0.067	9	0.201	0.016	8	0.205	0.006	3	0.383	0.312	81
MPP 5	0.244	0.009	4	0.232	0.009	4	0.627	0.011	2	0.367	0.225	61
MPP 5a	0.023	0.000	2	0.081	0.002	3	0.453	0.014	3	0.186	0.233	126
MPP 6	0.057	0.008	14	ND			0.034	0.019	57	0.045	0.016	36
MPP 7	0.042	0.002	5	1.07	0.01	1	1.117	0.012	1	0.744	0.608	82
MPP 8	0.591	0.027	5	0.225	0.012	6	2.25	0.07	3	1.02	1.08	106
MPP 9	0.006	0.003	53	0.019	0.000	3	0.035	0.007	21	0.020	0.015	72
MPP 10	ND			ND			0.007	0.001	12	0.007		
RGPP 1	0.617	0.010	2	0.428	0.013	3	0.559	0.035	6	0.535	0.097	18
RGPP 2	0.502	0.014	3	0.367	0.015	4	0.060	0.005	8	0.310	0.227	73
RGPP 3	0.027	0.002	9	0.002	0.000	5	0.008	0.000	1	0.012	0.013	107
RGPP 4	0.082	0.001	1	0.049	0.001	1	0.124	0.001	1	0.085	0.037	44
RGPP 5	2.65	0.01	0	3.51	0.03	1	0.847	0.013	2	2.34	1.36	58
RGPP 6	0.710	0.007	1	5.21	0.02	0	0.008	0.000	5	1.98	2.82	143
BKG 1	0.302	0.019	6	0.683	0.014	2	0.308	0.015	5	0.431	0.218	51
BKG 2	0.023	0.000	1	0.014	0.000	2	0.120	0.001	1	0.052	0.059	113

Each column represents average of 3 analytical runs; NA = Not Available; ND = Not Detected.

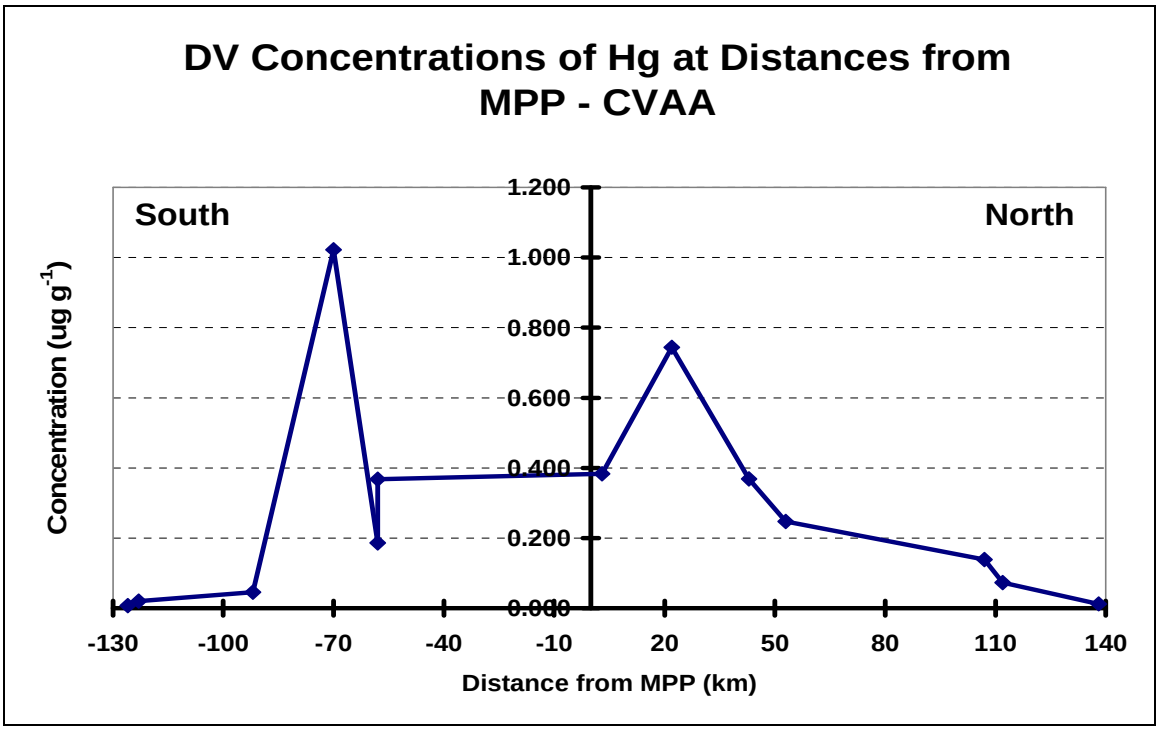

Figure 5.41. Concentration of Hg by PerkinElmer CVAA analysis of desert varnish samples as a function of distance from MPP.

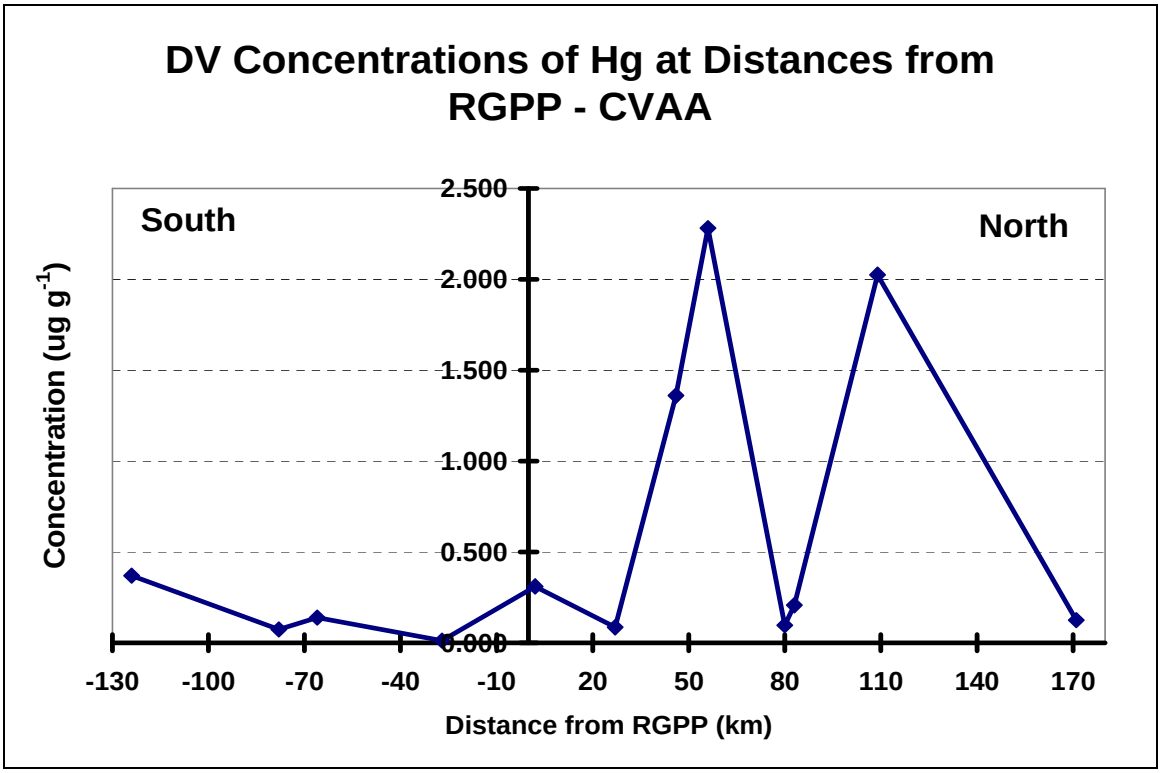

Figure 5.42. Concentration of Hg by PerkinElmer CVAA analysis of desert varnish samples as a function of distance from RGPP.

CHAPTER 6

SUMMARY, CONCLUSIONS, AND RECOMMENDATIONS

Summary of Results

The main goal of this study was to demonstrate the potential use of desert varnish as a passive environmental monitor of present and past atmospheric pollution. The results of the research supported three hypotheses: (1) rock varnish accumulates and preserves a record of airborne heavy elements and can be used as a passive environmental monitor of relatively recent events; (2) anthropogenic pollutants are deposited in the varnish and can be traced to their sources, such as ore smelters or coal–fired power plants; and (3) heavy metals can be quantified in the varnish coatings using field portable X-ray fluorescence spectroscopy (FPXRF), inductively coupled plasma mass spectroscopy (ICPMS), and laser ablation-inductively coupled plasma mass spectroscopy (LA-ICPMS).

Desert varnish samples were collected from July 2007 to March 2009 throughout the tri-state region of Nevada, California, and Arizona, in the areas surrounding four point sources of air pollution: the Nevada Test Site (NTS), Nye County, NV; the Mohave Power Project (MPP), Laughlin, NV; the Reid Gardner Power Plant (RGPP), Moapa, NV; and the Titanium Metal Corporation (TIMET), Henderson, NV. The chemical composition of rock varnishes was examined with FPXRF, LA-ICPMS, and ICPMS. Additionally, Hg was analyzed by cold vapor atomic absorption (CVAA). To examine the accuracy and precision of the analytical methods, a quality control/quality assurance (QA/QC) protocol was applied. This protocol included calibration checks, contamination and baseline assessment, as well as the analysis of replicates and standard reference materials (SRM). These applied QA/QC measures give confidence that the analytical

methods are suitable for the analysis of rock varnish samples. Additionally, the analytical techniques were optimized and evaluated.

The results from FPXRF and LA-ICPMS analyses yield concentrations of 30 elements. Sixteen elements (Ti, Cr, Mn, Fe, Co, Ni, Cu, Zn, As, Se, Rb, Sr, Zr, Mo, Hg, and Pb) were analyzed by FPXRF, and LA-ICPMS was used for the determination of 25 isotopes (^{9}Be, ^{51}V, ^{52}Cr, ^{59}Co, ^{60}Ni, ^{65}Cu, ^{66}Zn, ^{88}Sr, ^{98}Mo, ^{107}Ag, ^{111}Cd, ^{115}In, ^{118}Sn, ^{121}Sb, ^{133}Cs, ^{137}Ba, ^{184}W, ^{197}Au, ^{205}Tl, ^{206}Pb, ^{207}Pb, ^{208}Pb, ^{209}Bi, ^{232}Th, and ^{238}U).

The FPXRF data were used to estimate abundance of trace elements in the varnishes. The calculated concentration ratios of the elements in the varnished and unvarnished surfaces show that the majority of the elements have consistently higher concentrations in the varnishes. In the set of 26 varnish samples, Zn is found to be higher in 16 samples, As is higher in 13 samples, and Pb is found to be higher in 24 samples of the varnished rocks. Consistently, higher concentrations of these elements in the skyward-facing varnished surfaces indicate deposition of trace elements from the atmosphere.

The main restrictions of the XRF method include a limited number of elements that can be analyzed and relatively high detection limits. Nevertheless, this research provided strong evidence that the FPXRF method is suitable for the determination of the major varnish components and provides accurate and precise results. FPXRF proved to be a great technique for the rapid “screening” of major pollutants captured in the rock varnishes located in the areas of potential atmospheric contamination.

LA-ICPMS offers rapid and semi-quantitative *in situ* determinations of isotopes. The method also allows for spatially resolved analyses and requires no sample preparation. The challenges encountered during LA-ICPMS measurements include elemental

fractionation, limited accuracy and precision, and interferences from the substrate rock. Therefore, calibration against external, well-characterized standards is crucial during multi-element LA-ICPMS analysis. In this study, NIST glass standards were used and good agreement with the SRM certified values was obtained for most of the analytes.

Two varnish samples were initially analyzed by LA-ICPMS for eleven elements (Be, Ag, Cd, Sn, Sb, Ba, W, Tl, Pb, Th, and U). Both varnished and unvarnished surfaces were analyzed. To verify that varnished surfaces are chemically distinct from unvarnished surfaces, the null hypothesis was tested that the means of the analytical results are equal. The statistical analysis confirmed the differences in chemical composition of varnished and unvarnished surfaces. Elements that have higher concentrations in varnish coatings (Cd, Sn, Sb, Ba, W, Tl, Pb, and Th) are frequently found in fly ash emitted from coal-fired power plants. There are also significant differences in the concentrations of Cd, Sn, Sb, and Tl between skyward-facing and ground-facing varnished surfaces in samples collected near the titanium plant. These elements could originate as fugitive particulate emissions during the Ti smelting process.

The quadrupole LA-ICPMS was also used for the analysis of 25 isotopes (^{9}Be, ^{51}V, ^{52}Cr, ^{59}Co, ^{60}Ni, ^{65}Cu, ^{66}Zn, ^{88}Sr, ^{98}Mo, ^{107}Ag, ^{111}Cd, ^{115}In, ^{118}Sn, ^{121}Sb, ^{133}Cs, ^{137}Ba, ^{184}W, ^{197}Au, ^{205}Tl, ^{206}Pb, ^{207}Pb, ^{208}Pb, ^{209}Bi, ^{232}Th, and ^{238}U) in varnish coatings.

The FPXRF and LA-ICPMS results show that many trace elements (Cr, Co, Ni, Cu, Zn, As, Rb, Sr, Zr, Mo, and Pb) in the analyzed varnishes appear to be enriched relative to the upper continental crust (UCC). A few elements (As, Cd, Tl, and Pb) in the skyward-facing varnish films show extremely high enrichment, up to several hundred times more than the UCC values (Figures 6.1 and 6.2).

These results support hypothesis (1) that desert varnish can capture trace elements from the atmosphere and lock some fraction of them into the varnish matrix. Conversely, highly water-soluble elements, such as Rb and Cs, show depletion in many varnish coatings. This phenomenon suggests that atmospheric precipitation may remove these elements from the particulates adsorbed on the rock surfaces prior to their incorporation into varnishes.

Notably, elements that show the highest levels of enrichment relative to the UCC are commonly found in atmospheric emissions from coal-fired power plants (Seames and Wendt, 2000; Furimski, 2000; Martines-Tarazona and Spears, 1996; Zeng et al., 2001; Danihelka et al., 2003). Indeed, two pollution sources in this study - Mojave Power Project (MPP) and Reid Gardner Power Plant (RGPP) - are coal-fired power plants.

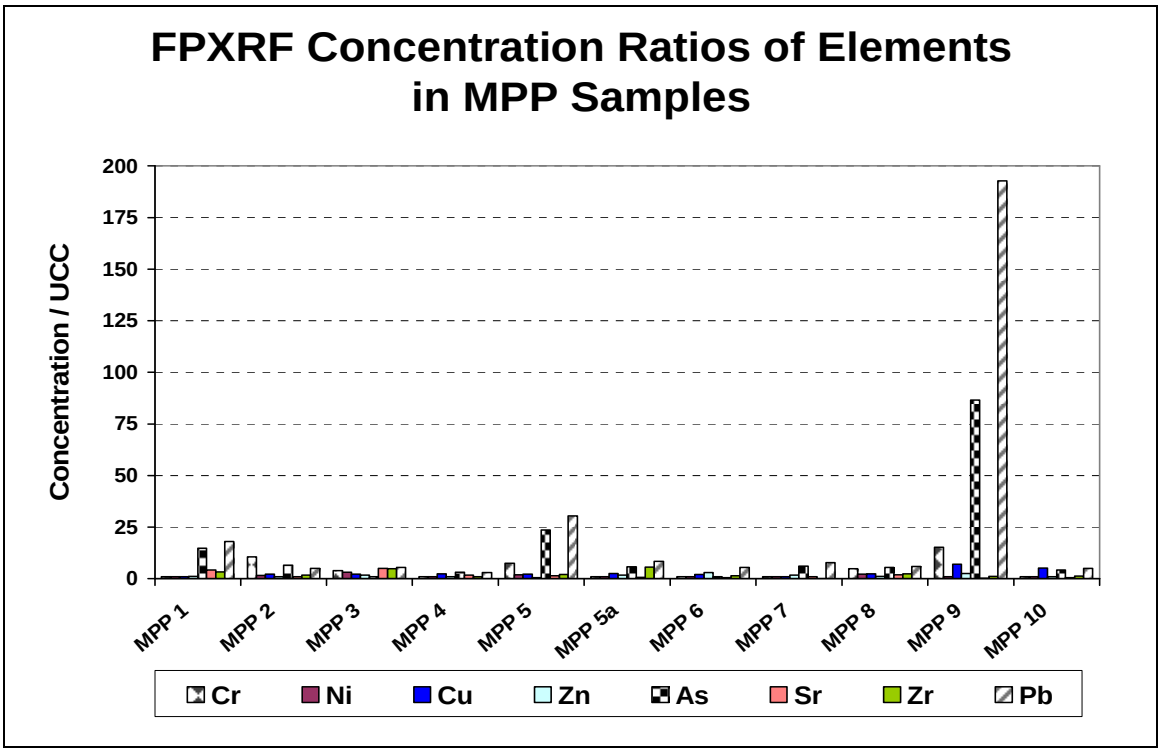

Figure 6.1. FPXRF concentration ratios of elements in MPP samples.

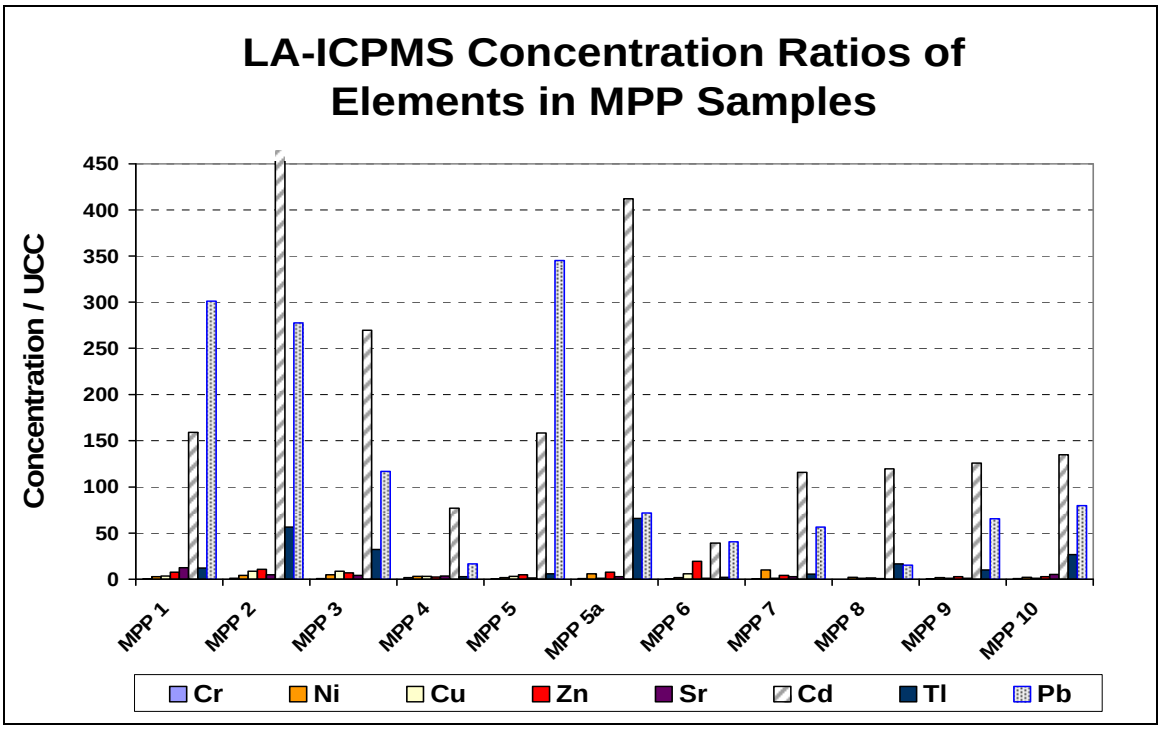

Figure 6.2. LA-ICPMS concentration ratios of elements in MPP samples.

Abundances of these elements plotted against the distance from the power plants show general patterns consistent with the predictions of the Gaussian Plume model for transport and diffusion of the pollutants. The model predicts that lower concentrations of pollutants will be observed at the point of origin followed by a maximum peak concentration and gradual decrease with distance from the source.

To confirm correlation of contamination to distance from the power plants, total concentrations of the elements in desert varnish films were determined. Triplicate samples of varnishes collected in the downwind locations from MPP and RGPP were stripped from the base rock with concentrated HCl. The resulting solutions were analyzed by quantitative ICPMS for 27 isotopes (^{9}Be, ^{51}V, ^{52}Cr, ^{59}Co, ^{60}Ni, ^{63}Cu, ^{66}Zn, ^{75}As, ^{88}Sr, ^{98}Mo, ^{102}Ru, ^{103}Rh, ^{106}Pd, ^{111}Cd, ^{118}Sn, ^{121}Sb, ^{133}Cs, ^{184}W, ^{187}Re, ^{195}Pt, ^{205}Tl, ^{206}Pb, ^{207}Pb, ^{208}Pb, ^{209}Bi, ^{232}Th, and ^{238}U); Hg was analyzed by CVAA. It should be

noted that varnishes cannot be selectively removed from acid soluble, brittle or disintegrating rocks. Therefore, maximum care and attention must be exercised during sample preparation.

The ICPMS data confirm that many trace elements are enriched relative to the upper continental crust (UCC), with Zn, Sr, and Pb showing extreme enrichment up to several thousand times more than the UCC.

The average elemental concentrations in the varnish samples were plotted as a function of the distance from each power plant. The MPP graph points to deposition areas at distances of 50 to 80 km south of the power plant and 40 to 100 km north of the power plant. Both regions with the highest concentrations very closely correlate with the MPP deposition areas established during summer and winter tracer release experiments during project MOHAVE (Figure 6.3).

The RGPP plots display deposition areas at distances of 50 to 80 km north of the power plant and 40 to 80 km south of the power plant. Noticeably, extremely southern and northern points of the graph show concentration increases. The southern point (MPP 2) is located in the deposition area of the MPP and probably includes influxes of particulates from both MPP and RGPP. On the other hand, the northern point (NTS 1) is located near the NTS and within the W mineralization belt. The sampled rocks may present unique geological composition that is demonstrated by the high abundance of As, Mo and Sb.

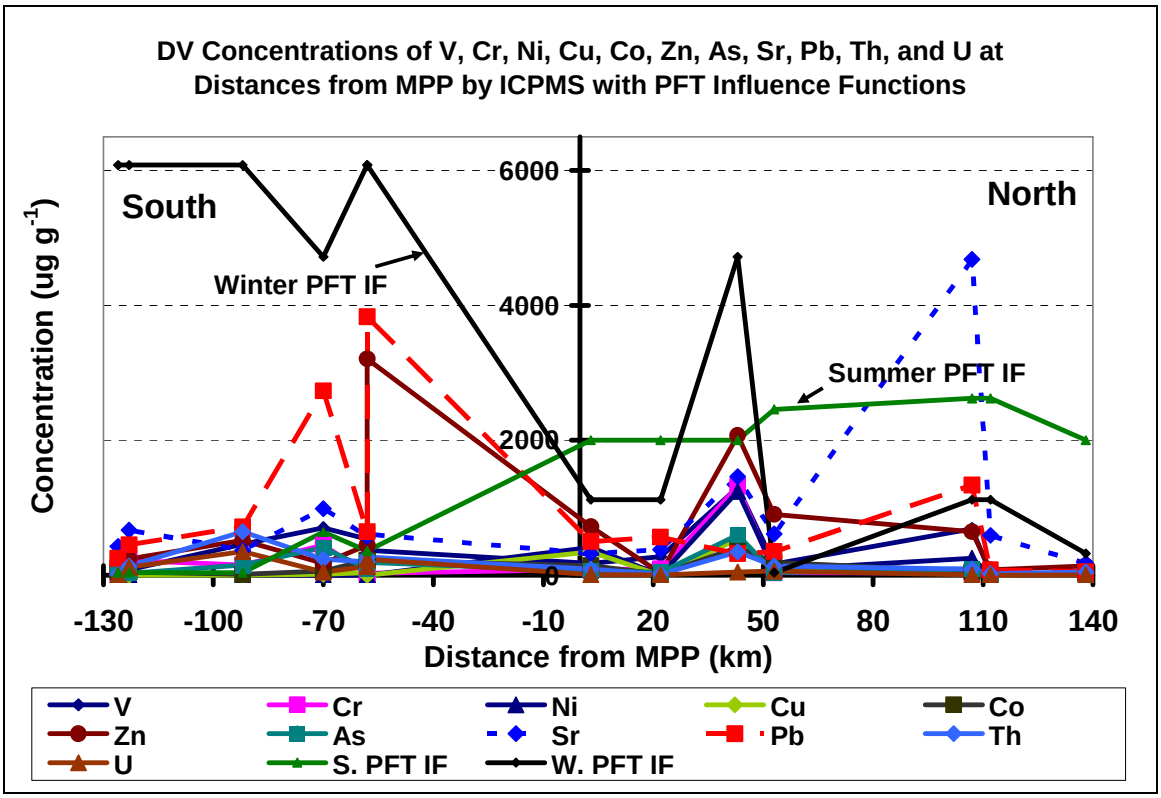

Figure 6.3. Concentrations of V, Cr, Ni, Cu, Co, Zn, As, Sr, Pb, Th and U in desert varnish coatings as a function of distance from MPP with superimposed summer and winter tracer (PFT) influence functions (IF x 2000).

Mercury analysis of the stripped solutions was performed by highly sensitive flow injection CVAA. The average Hg concentrations were plotted as a function of the distance from each power plant. The mercury deposition patterns are somewhat similar to deposition patterns of other elements, although they are not as distinctive. This could be caused by the different chemistry of the atmospheric Hg and alternate deposition mechanisms that may include wet and dry deposition of reactive gaseous mercury (RGM), in addition to particulate loading.

In summary, the observed deposition patterns of the pollutants directly point to the sources of contamination. Therefore, hypothesis (2), that anthropogenic pollutants deposited in the varnishes can be traced to their sources, is supported.

The particulate matter (PM) emissions from coal-fired power plants are typically controlled with electrostatic precipitators (ESP) or fabric filters (Crowder and Richards, 2003). These units routinely achieve 99% control efficiency. However, the finest particles in the fly ash are not removed by the pollution control equipment and are emitted with the flue gases to the atmosphere. Mercury in the flue gas exists as both gaseous and Hg reacted with the fly ash. Most of the mercury is emitted in the gaseous form (Seames and Wendt, 2000; Martines-Tarazona and Spears, 1996, Danihelka et al., 2003). Control of mercury emissions from coal-fired power plants includes capture of Hg in PM control equipment and removal of soluble Hg^{2+} compounds in wet flue gas desulfurization (FGD) systems. The selective catalytic reduction (SCR) for nitrogen oxides (NO_x) control enhances oxidation of Hg vapor in the flue gas and aids effective Hg removal by wet FGD (Richards, 1996). Additional mercury removal can be accomplished by powered activated carbon injection (PAC) with 85-95% removal efficiency (Environmental Protection Agency, 2004). However, these pollution control systems are not available commercially and Hg emissions from coal-fired power plants are the main source of atmospheric mercury pollution (Environmental Protection Agency, 2005).

The analytical data obtained during this research provided ample support for hypothesis (3), that FPXRF, LA-ICPMS, and ICPMS, as well as CVAA can be utilized in the analysis of varnish samples. Analysis of varnishes is a new field that can potentially provide records of pre-anthropogenic levels of atmospheric metals and other environmental pollutants. The proposed research provided basic knowledge of the chemical composition of varnish coatings and, thus, additional evidence to help

understand the mechanism of varnish formation. In conclusion, the results of this study will have implications 1) for mapping the distribution of some of the components of air contamination, 2) for identifying the sources of air pollution, 3) for deciphering the history of atmospheric pollution, 4) for contributing to our understanding of desert varnish formation, and 5) for applications as a prospecting tool.

Conclusions and Recommendations for Further Study

The conducted research produced preliminary data indicating the utility of rock varnish as a passive environmental monitor of relatively recent events such as atmospheric pollution from coal-fired power plants. Analysis of varnishes thus provides records of atmospheric metals and other possible environmental pollutants such as radionuclides and organic compounds. The analytical data obtained demonstrated that FPXRF, LA-ICPMS, ICPMS, and CVAA can successfully be used for the analysis of varnish samples. Even though the study provided additional knowledge of the chemical composition of varnish coatings, the origin of varnish remains a mystery. Consequently, rock varnish deserves further study as a passive environmental monitor.

Future varnish studies should focus on the implementation of a detailed plan to analyze a large number of samples from the deposition area of the point source of air pollution. The large number of samples will make it possible to distinguish a regional signal from the local noise. The obtained data suggest that Zn, As, Cd, and Pb records are the most promising. FPXRF is the best method that could easily be employed in this study. The sampling area could be expanded to determine if desert varnish may be useful in prospecting for Au and PGE. For instance, analysis of varnish samples across Nevada,

south to north, could detect higher concentrations of Au and PGE in areas in proximity to ore deposits.

Another area of study might include chemical and radiochemical measurements of the material leached from the surfaces of varnish samples collected along downwind traverses away from the NTS, other nuclear facilities, selected metal ore smelters, and coal-fired power plants. The strategy would be to map the impacted area downwind from the point sources. These studies could provide the basis for the mapping of the distribution of some of the components of air contamination.

Application of laser ablation-time of flight-inductively coupled plasma mass spectroscopy (LA-TOF-ICPMS) for the analysis of varnish samples could be beneficial for rock varnish studies. The LA-TOF-ICPMS offers rapid *in situ* determination of isotopes in selected mass regions. The isotopic ratios are specific and relate to the material's source of origin. Comparison of mass spectra of different varnishes can establish the characteristic ratio of isotopes from particular geographical areas. This spectral "fingerprint" can greatly enhance identification of the sources of air pollution.

EXHIBITS

Ratios of Elements by FPXRF Analysis

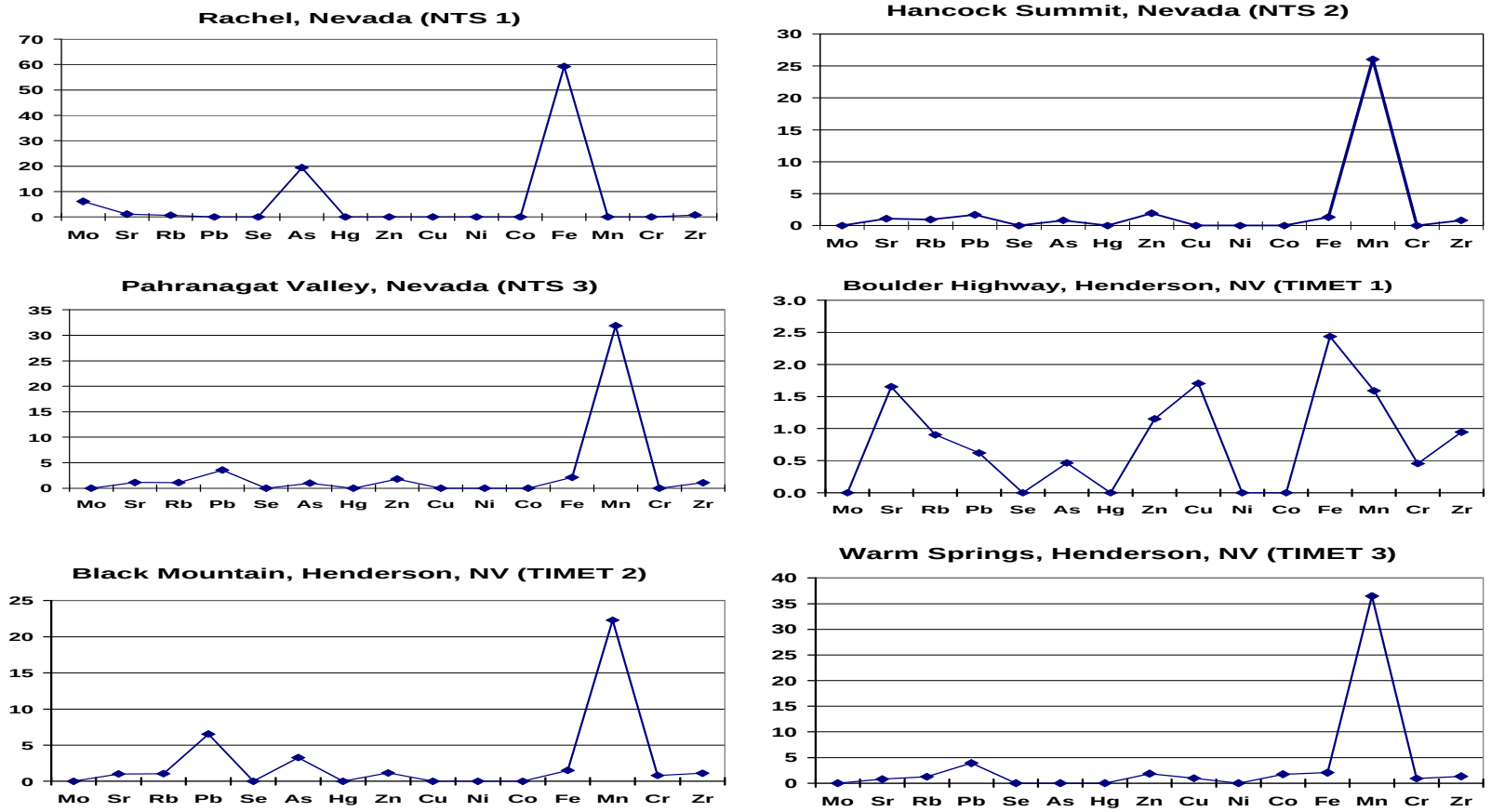

Figure E-1. Ratios of elements by FPXRF analysis (bulk mode) of samples NTS 1, NTS 2, NTS 3, TIMET 1, TIMET 2, and TIMET 3.

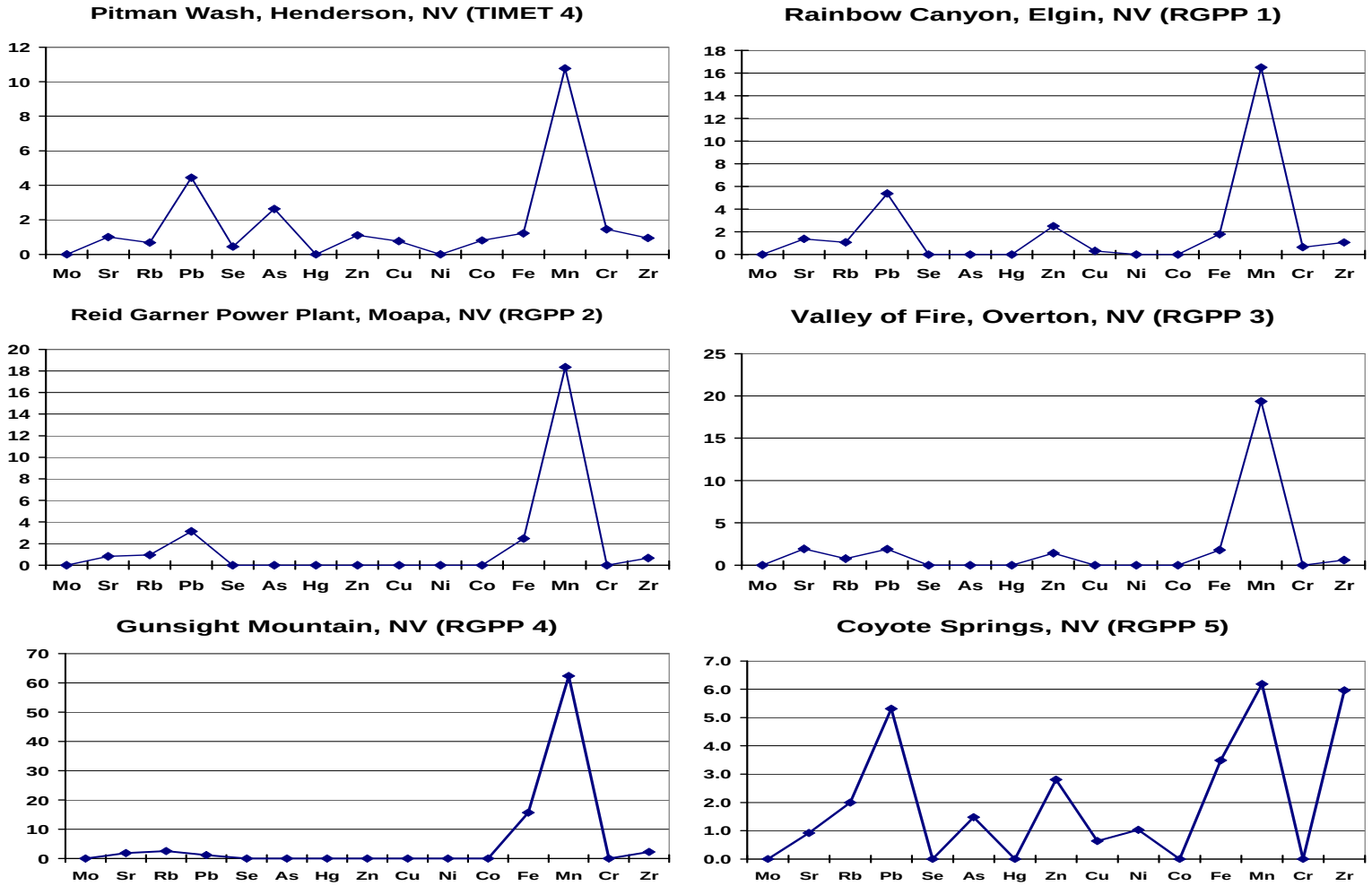

Figure E-2. Ratios of elements by FPXRF analysis (bulk analysis) of samples TIMET 4, RGPP 1, RGPP 2, RGPP 3, RGPP 4, and RGPP 5.

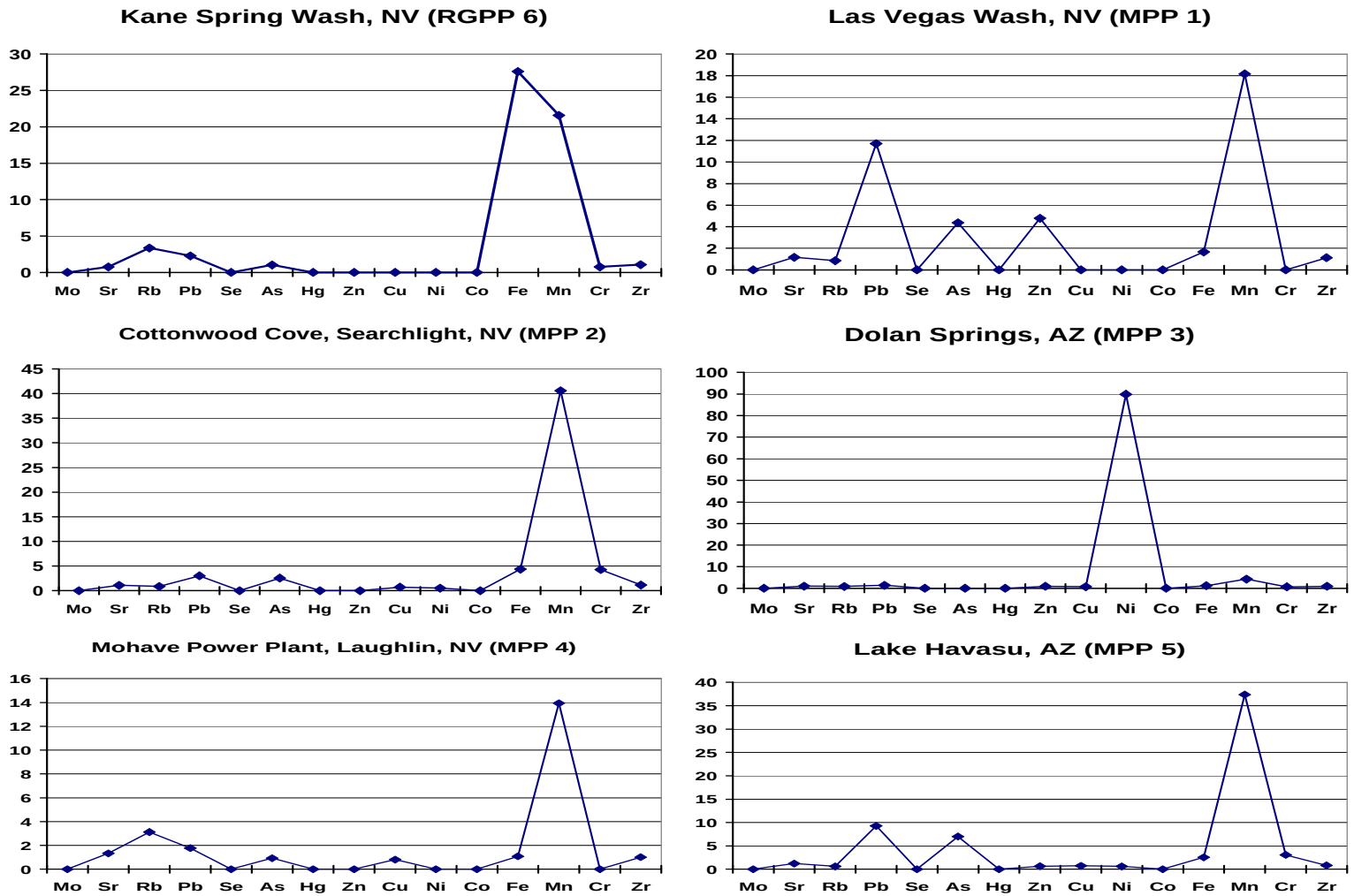

Figure E-3. Ratios of elements by FPXRF analysis (bulk analysis) of samples RGPP 6, MPP 1, MPP 2, MPP 3, MPP 4 and MPP 5.

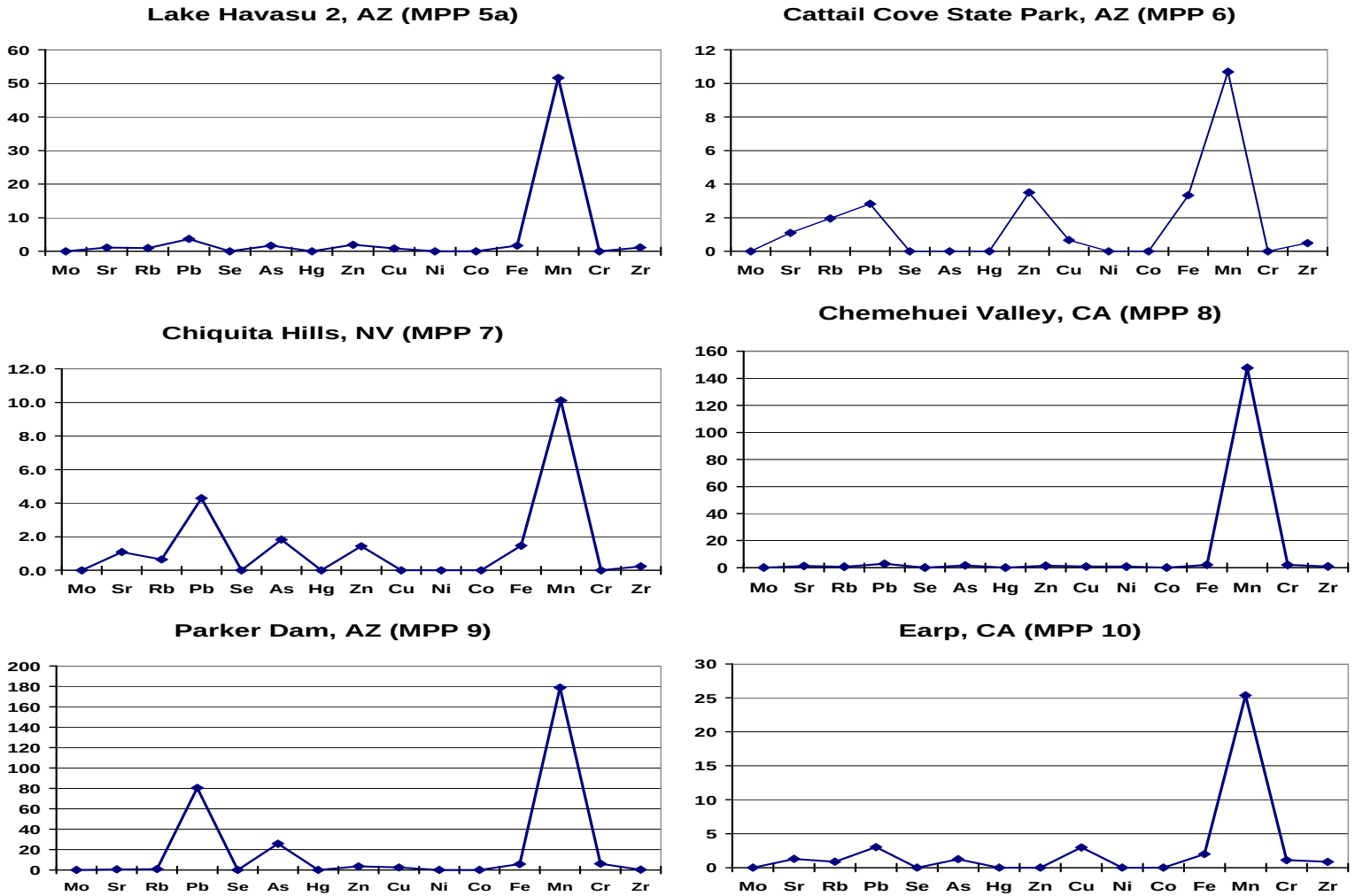

Figure E-4. Ratios of elements by FPXRF analysis (bulk analysis) of samples MPP 5a, MPP 6, MPP 7, MPP 8, MPP 9, and MPP 10.

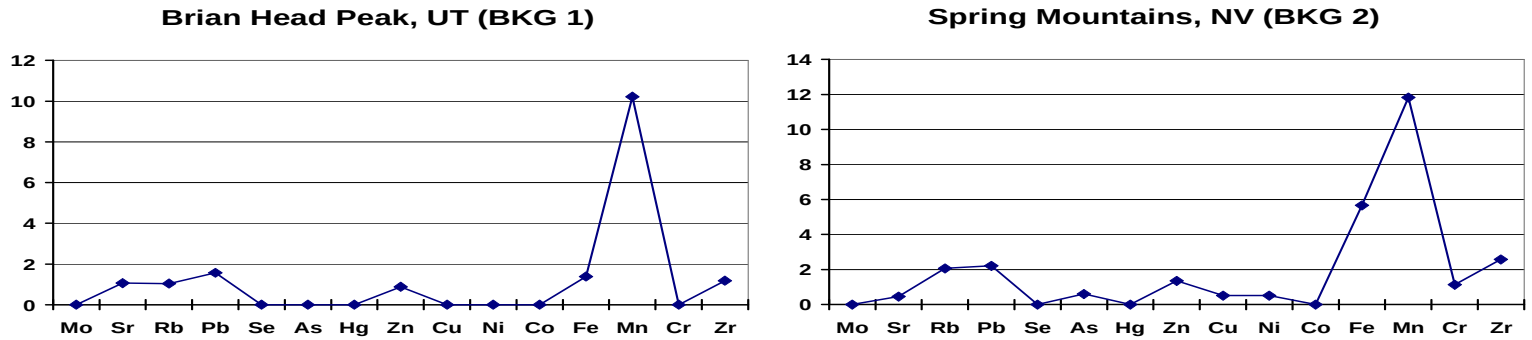

Figure E-5. Ratios of elements by FPXRF analysis (bulk analysis) of samples BKG 1 and BKG 2.

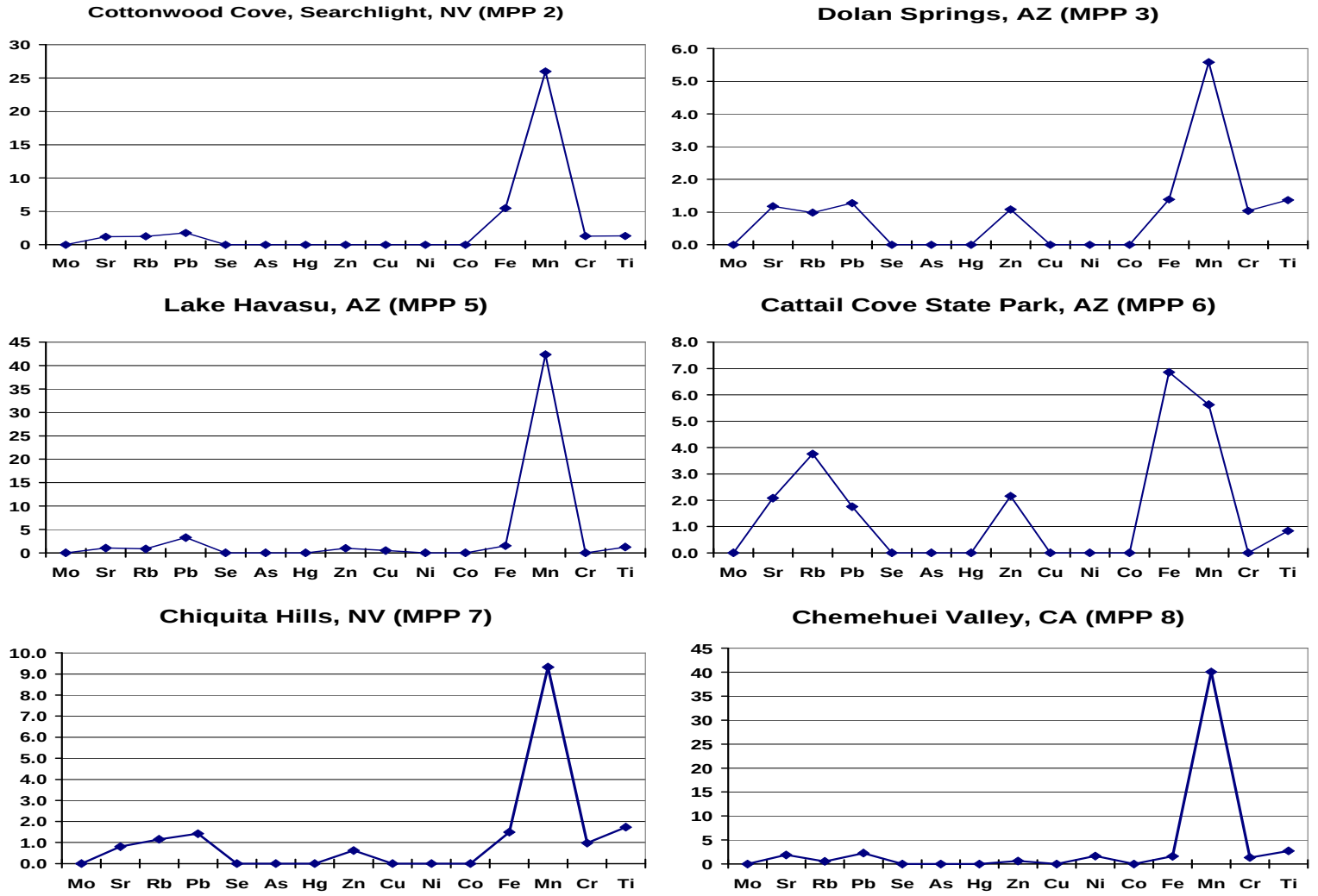

Figure E-6. Ratios of elements by FPXRF analysis (thin surface analysis) of samples MPP 2, MPP 3, MPP 5, MPP 6, MPP 7, and MPP 8.

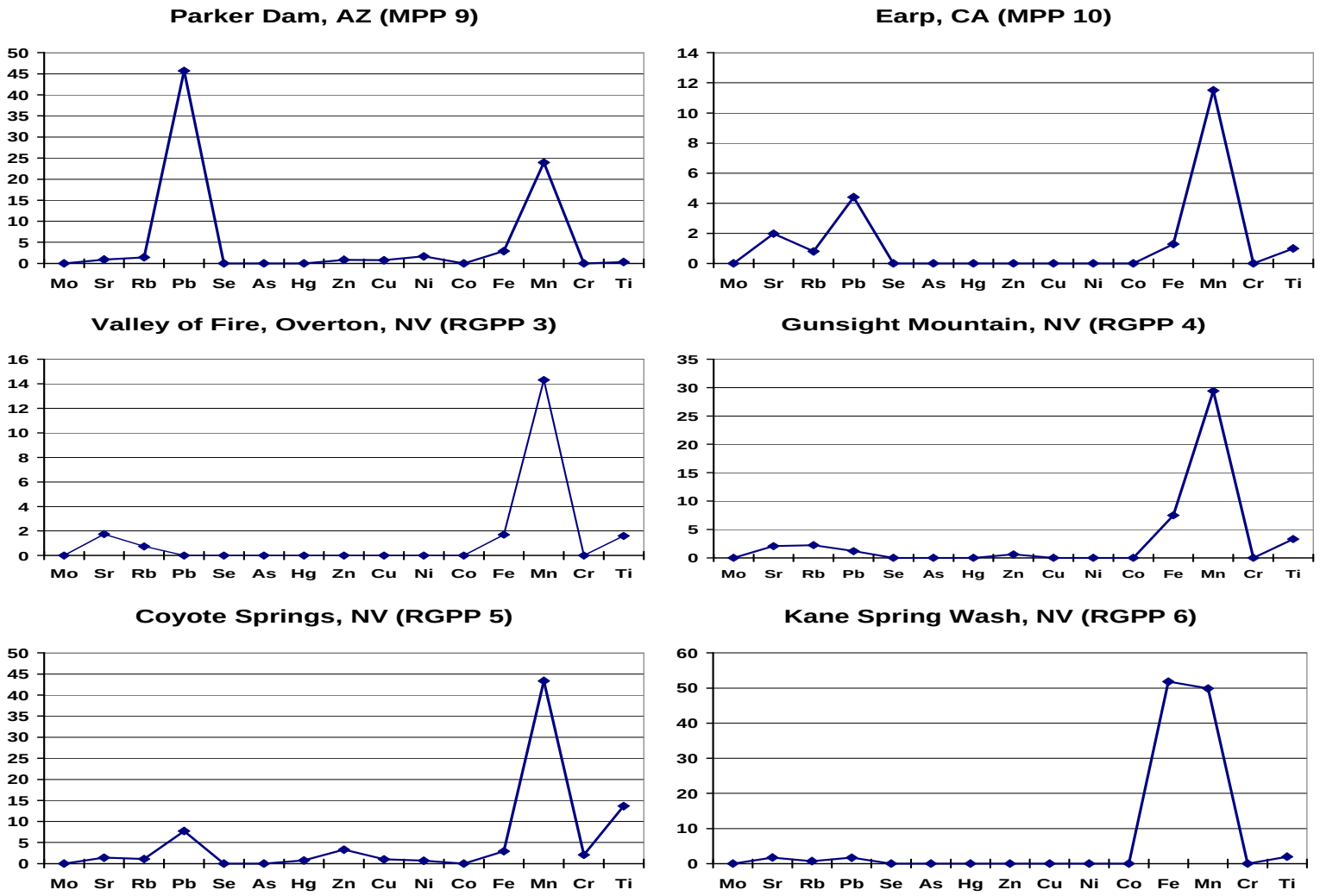

Figure E-7. Ratios of elements by FPXRF analysis (thin surface analysis) of samples MPP 9, MPP 10, RGPP 3, RGPP 4, RGPP 5, and RGPP 6.

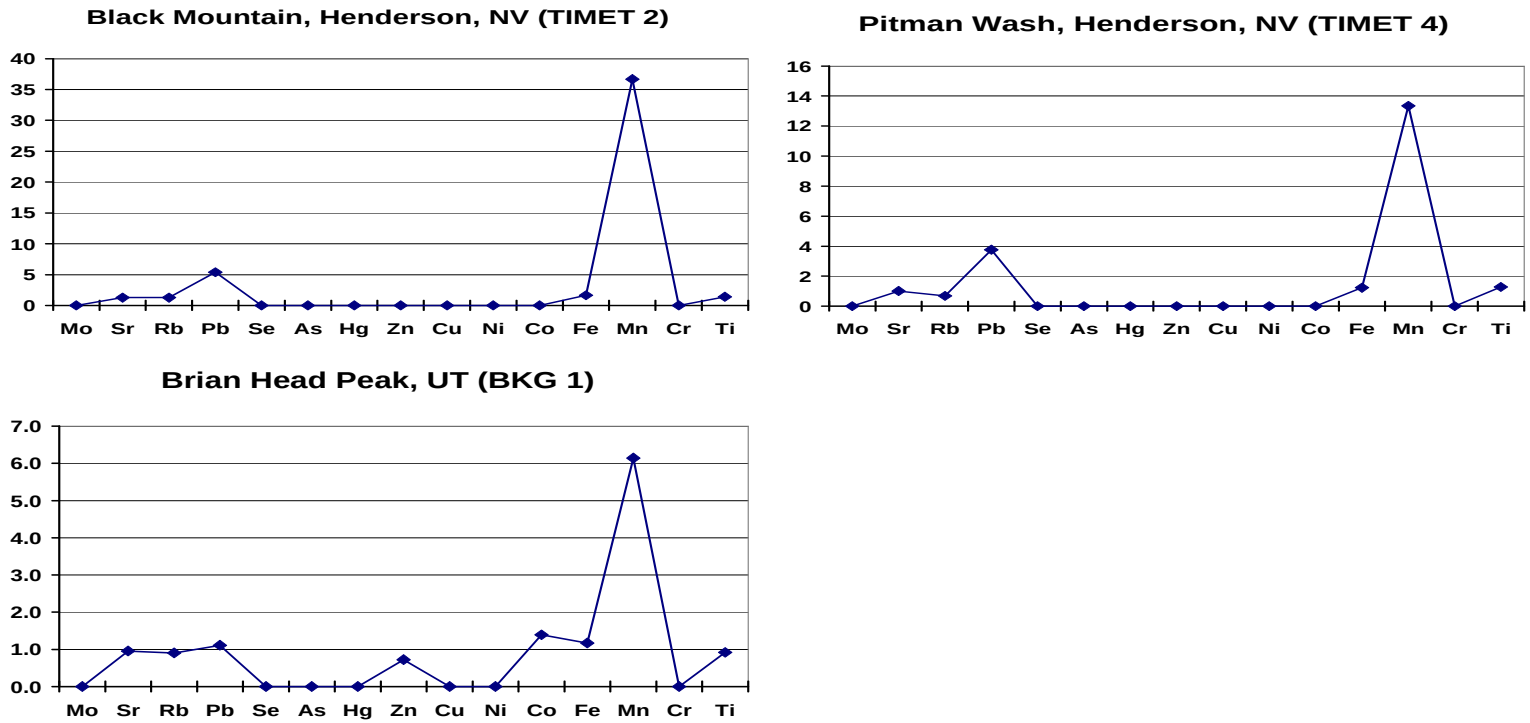

Figure E-8. Ratios of elements by FPXRF analysis (thin surface analysis) of samples TIMET 2, TIMET 4, and BKG 1.

Abundances of Elements in Varnish Samples Normalized to the UCC in Approximate Order of Increasing Abundance

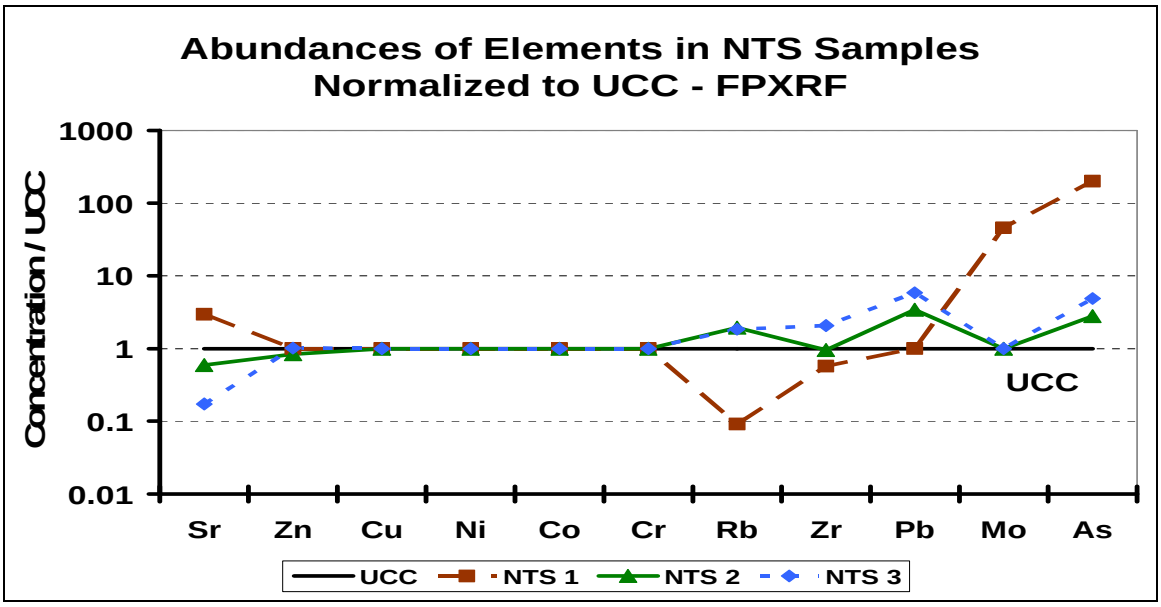

Figure E-9. Abundances of elements by FPXRF analysis of varnish coatings in NTS samples normalized to the UCC. Elements are ordered in approximate order of increasing abundance. The thick black line represents the average UCC abundance (Ratio=1).

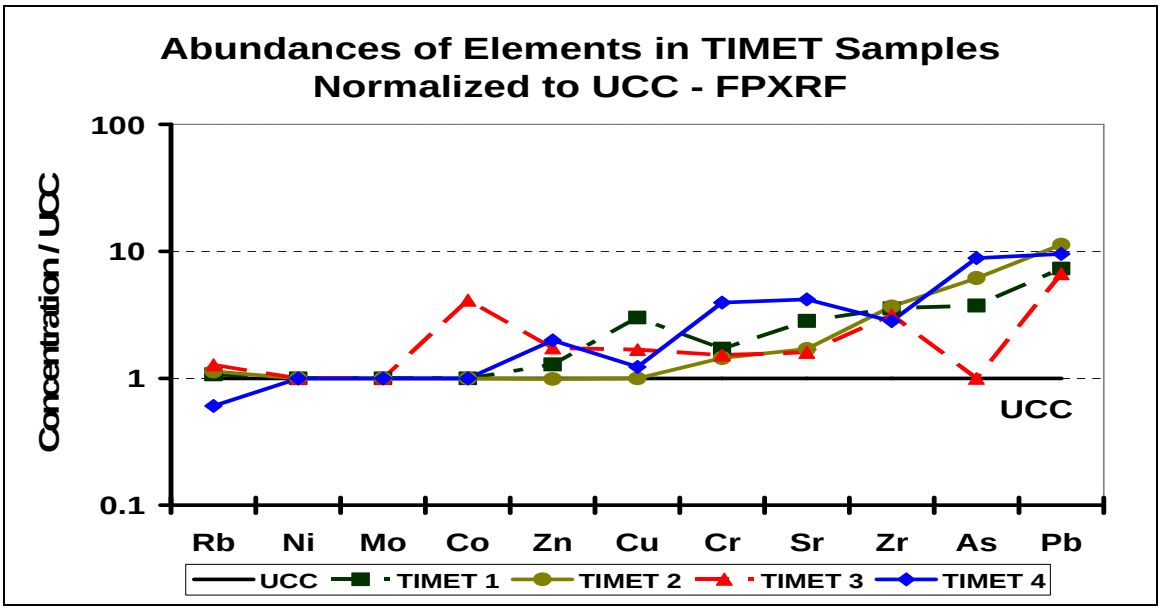

Figure E-10. Abundances of elements by FPXRF analysis of varnish coatings in TIMET samples normalized to the UCC. Elements are ordered in approximate order of increasing abundance. The thick black line represents the average UCC abundance (Ratio=1).

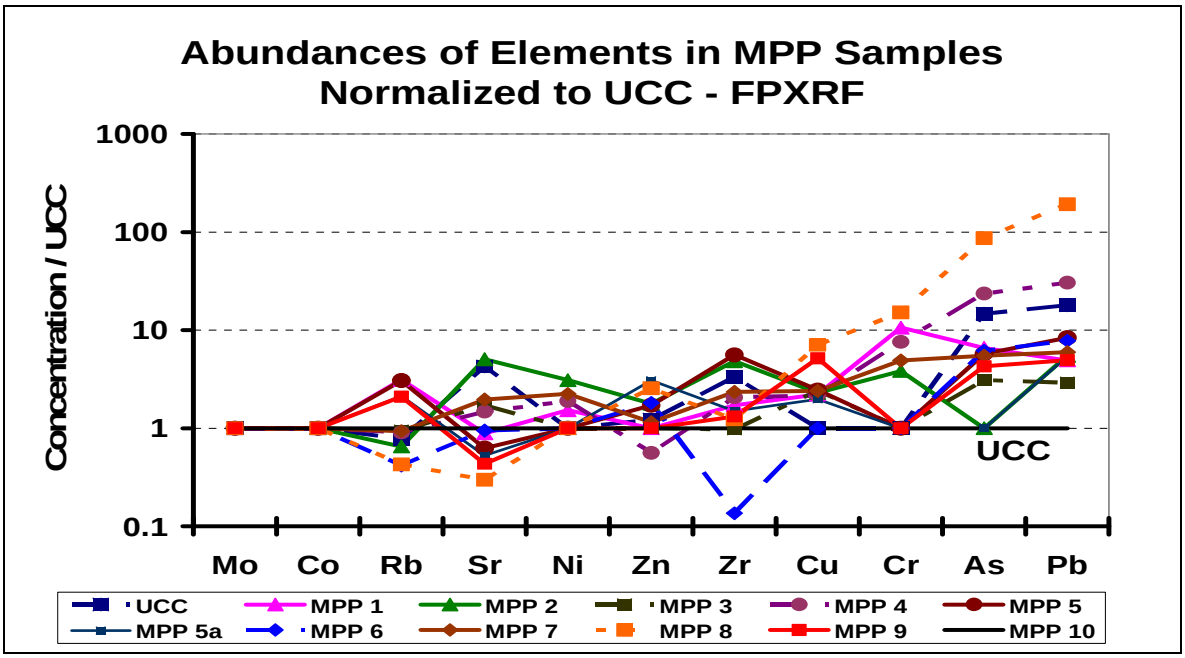

Figure E-11. Abundances of elements by FPXRF analysis of varnish coatings in MPP samples normalized to the UCC. Elements are ordered in approximate order of increasing abundance. The thick black line represents the average UCC abundance (Ratio=1).

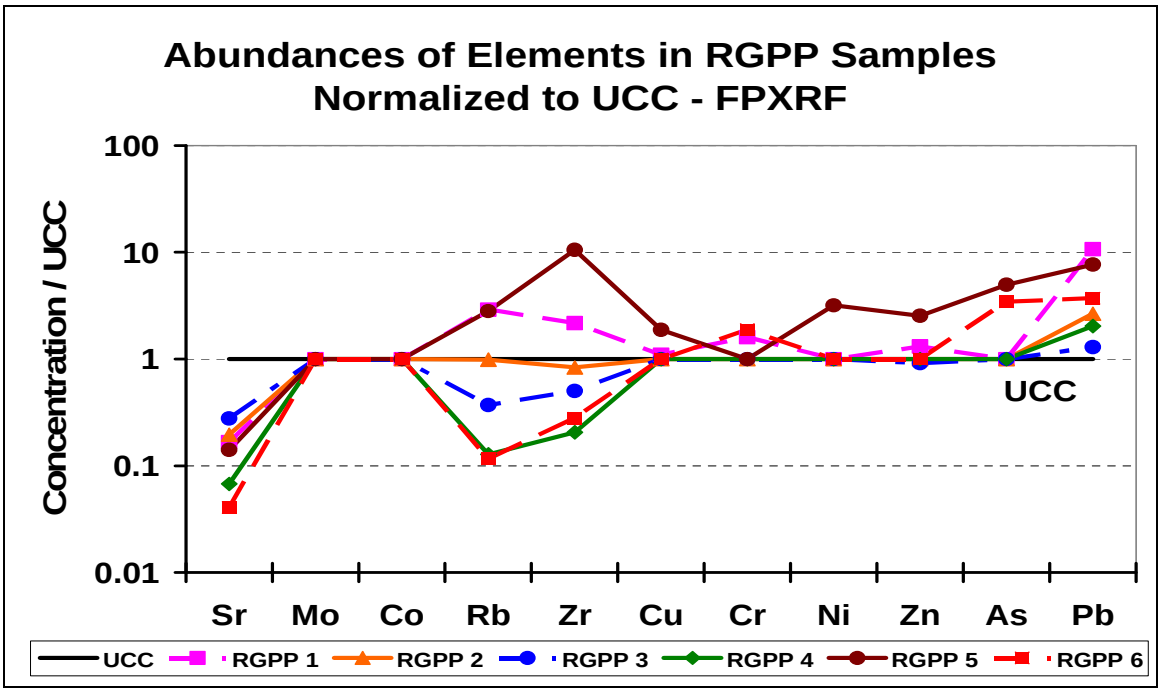

Figure E-12. Abundances of elements by FPXRF analysis of varnish coatings in RGPP samples normalized to the UCC. Elements are ordered in approximate order of increasing abundance. The thick black line represents the average UCC abundance (Ratio=1).

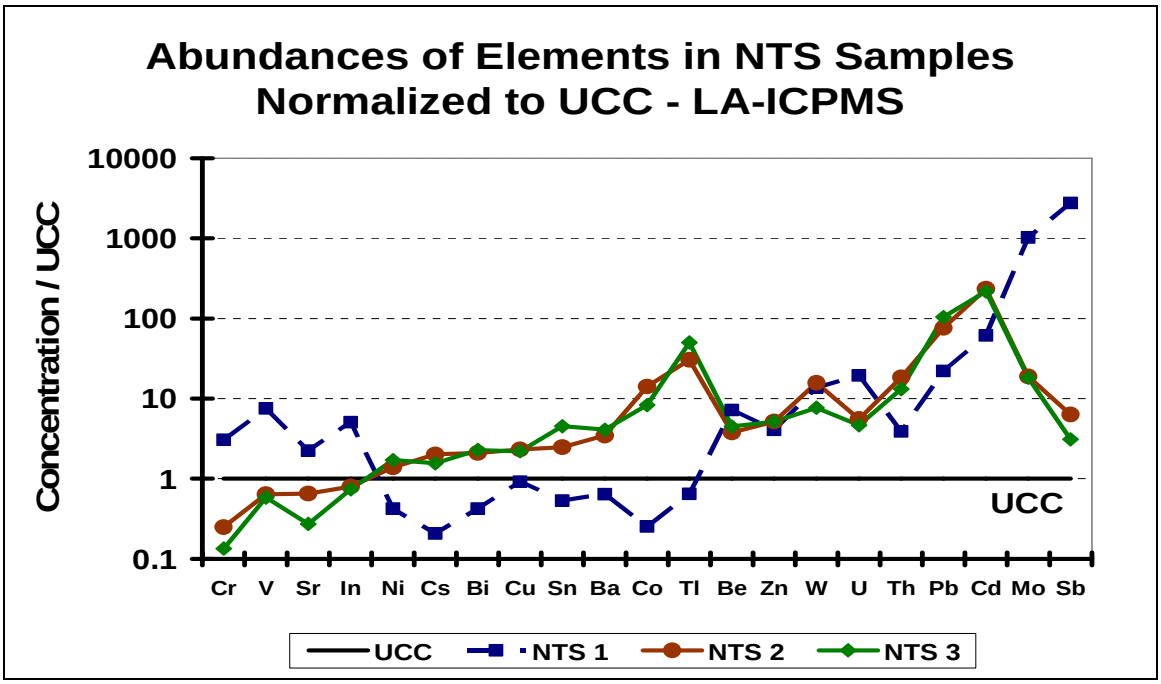

Figure E-13. Abundances of elements in the varnish coatings of NTS samples analyzed by Elan LA-ICPMS and normalized to the UCC values. Elements are ordered in approximate order of increasing abundance. The thick black line represents the average UCC abundance (Ratio=1).

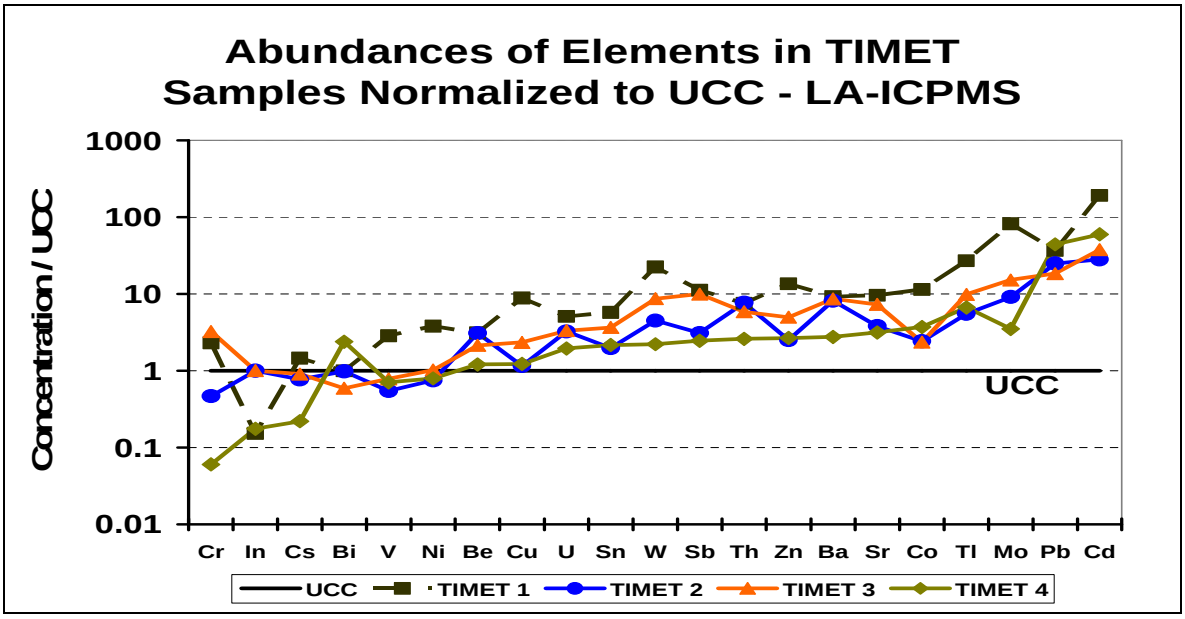

Figure E-14. Abundances of elements in the varnish coatings of TIMET samples analyzed by Elan LA-ICPMS and normalized to the UCC values. Elements are ordered in approximate order of increasing abundance. The thick black line represents the average UCC abundance (Ratio=1).

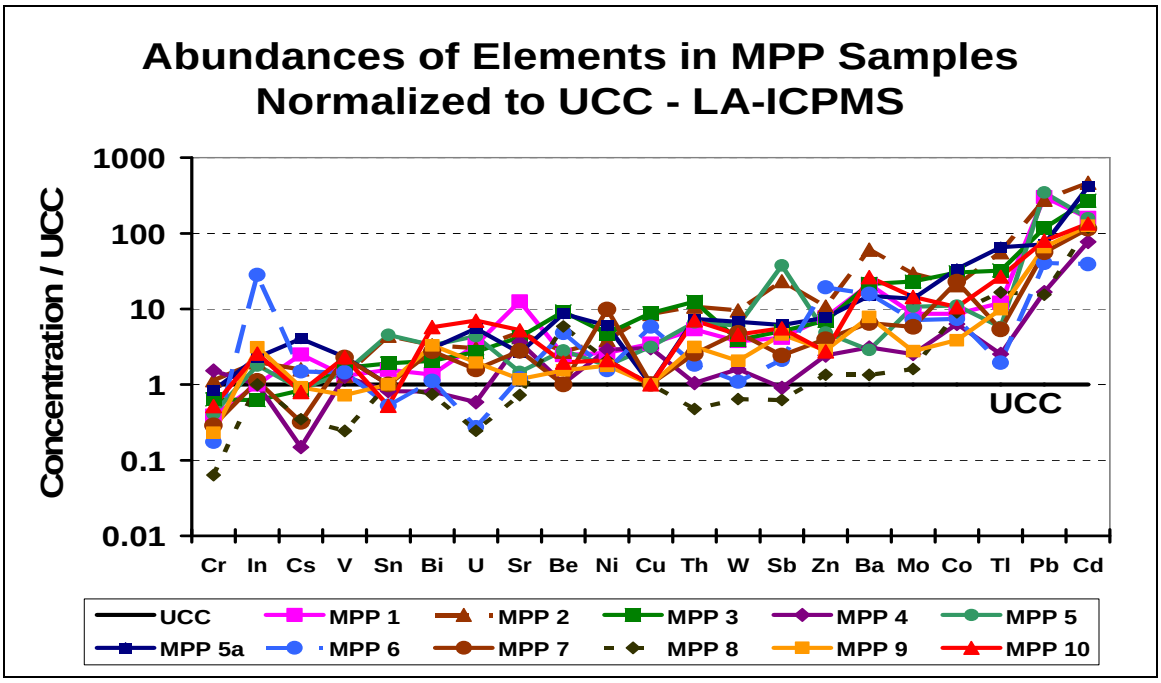

Figure E-15. Abundances of elements in the varnish coatings of MPP samples analyzed by Elan LA-ICPMS and normalized to the UCC values. Elements are ordered in approximate order of increasing abundance. The thick black line represents the average UCC abundance (Ratio=1).

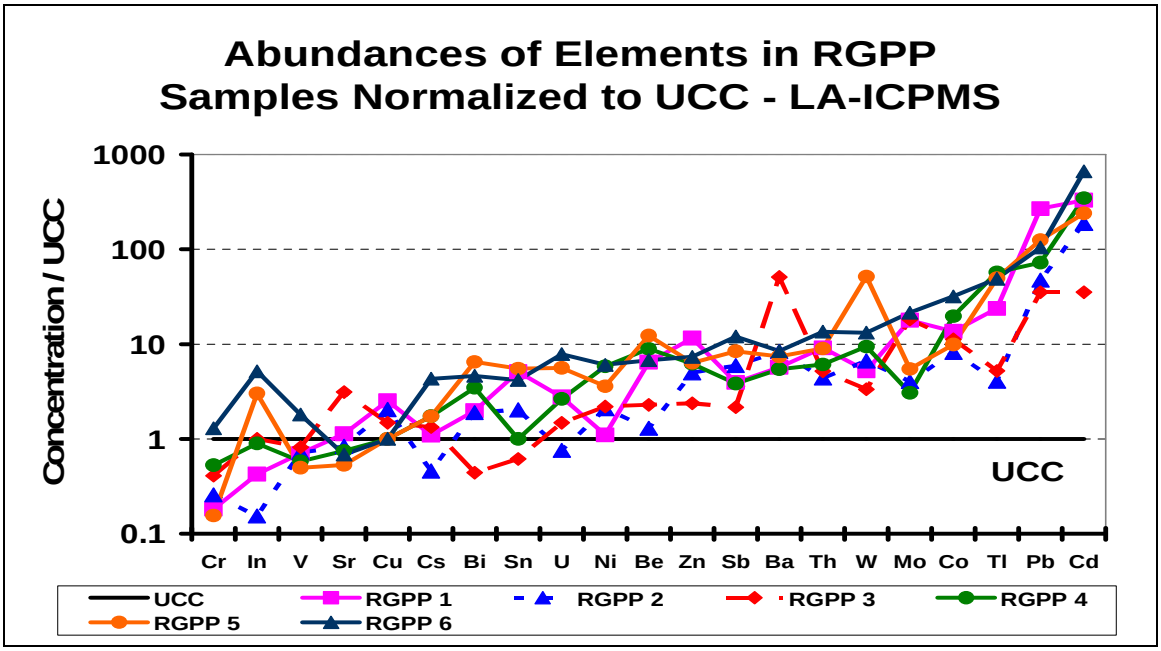

Figure E-16. Abundances of elements in the varnish coatings of RGPP samples analyzed by Elan LA-ICPMS and normalized to the UCC values. Elements are ordered in approximate order of increasing abundance. The thick black line represents the average UCC abundance (Ratio=1).

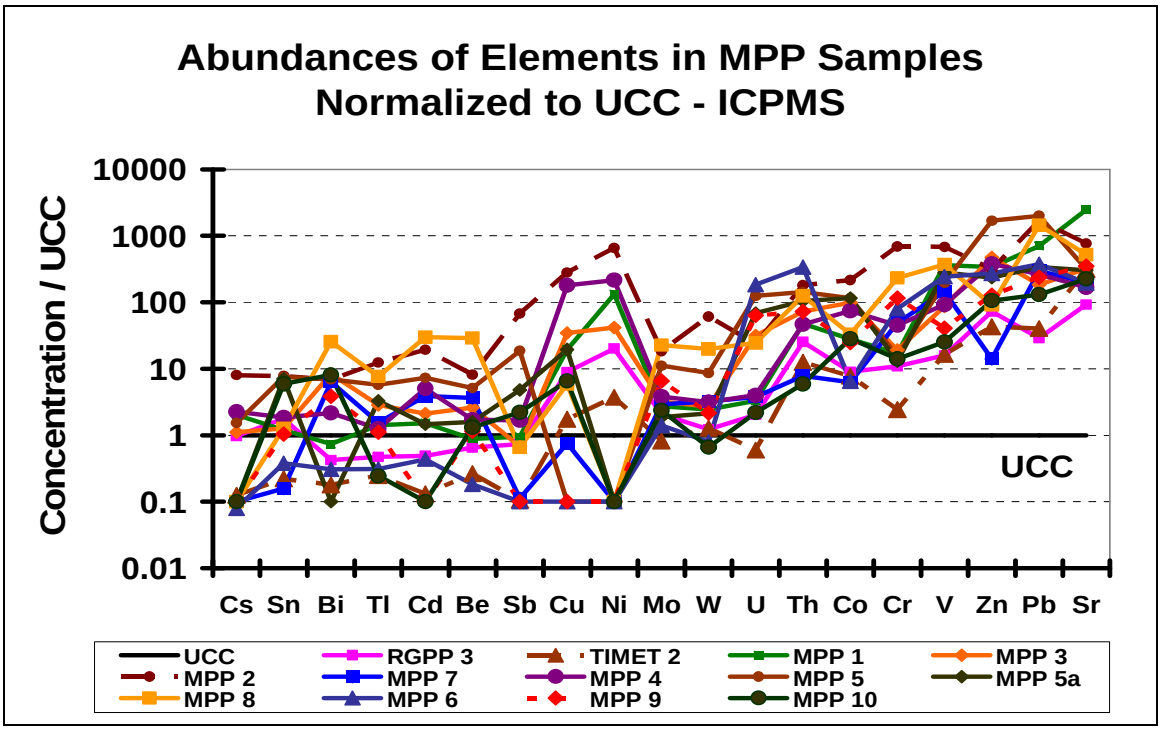

Figure E-17. Abundances of elements by Elan DRC 6100 ICPMS analysis of varnish coatings in MPP samples normalized to the UCC. The thick black line represents the average UCC abundance (Ratio=1).

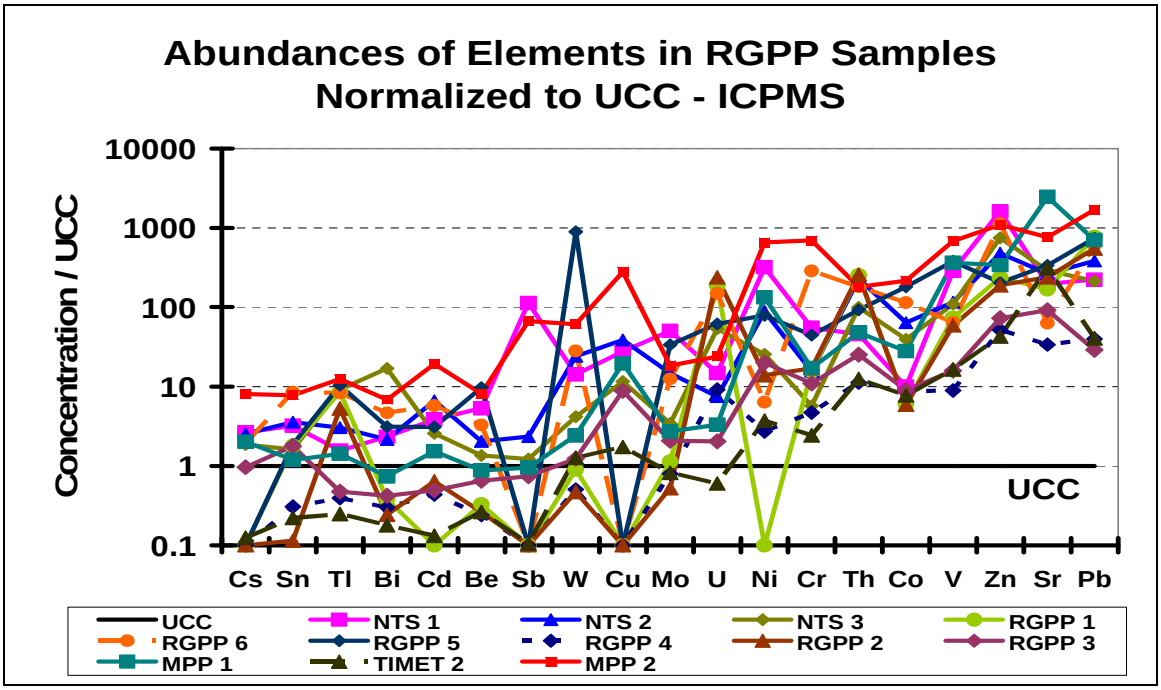

Figure E-18. Abundances of elements by Elan DRC 6100 ICPMS analysis of varnish coatings in RGPP samples normalized to the UCC. The thick black line represents the average UCC abundance (Ratio=1).

BIBLIOGRAPHY

Adams, J.B., Palmer, F., and Stanley, J.T. (1992). Rock Weathering in Deserts: Mobilization and Concentration of Ferric Iron by Microorganisms. *Geomicrobiology Journal, 10*, 99-114.

Alcock, R.E., and Jones, K.C. (1996). Dioxins in the Environment: A Review of Trend Data. *Environmental Science and Technology, 30*, 3133-3143.

Allen, C.C., Probst, L.W., Flood, B.E., Longazo, T.G., Schelbe, R.T., and Westall, F. (2004). Meridiani Planum hematitie deposits and the search for evidence of life on Mars – Iron mineralization of microorganisms in rock varnish. *Icarus 171(1)*, 20-30.

Anderson, B.M., Keith, J.R., and Connor, J.J. (1975). Antimony, Arsenic, Germanium, Lithium, Mercury, Selenium, Tin, and Zinc in Soils of the Powder River Basin. In *Geochemical Survey of the Western Coal Regions*, Second Annual Progress Report, U.S. Geological Survey Open-file Report No. 75-436, 50-57.

Anlauf, K.G., Fellin, P., and Wiebe, H.A. (1985). A comparison of three methods for measurement of atmospheric nitric acid and aerosol nitrate and ammonium. *Atmospheric Environment – Part A General Topics, 19(2)*, 325-333.

Arnaud, F., Revel-Rolland, M., Bosh, D., Winiarski, T., et al. (2004). A 300 year history of lead contamination in northern French Alps reconstructed from distant lake sediment records. *Journal of Environmental Monitoring, 2004, 6*, 448-456.

Augusto, S., Pinho, P. Branquinho, C., et al. (2004). Atmospheric Dioxin and Furan Depositon in Relation to Land and Other Pollutants: A survey with Lichens. *Journal of Atmospheric Chemistry, 49 (2004)*, 53-65.

Bacon, M.P., Brewer, P.G., Spencer, D.W., Murray, J.W., and Goddard, J. (1980). Lead-210, polonium-210, manganese and iron in the Cariaco Trench. *Deep Sea Research, 27*, 119-135.

Bailley, T. and Orndorff, R.L. (2001). SEM Analysis of Desert Varnish from Lake Lahontan Shorelines in the Eetza Range, Nevada, GSA Abstracts with Programs, 33(6), p. A-320.

Bao, H., Michalski, G.M., and Thiemens, M.H. (2001). Sulfate oxygen-17 anomalies in desert varnishes. *Geochimica et Cosmochimica Acta, 65(13)*, 2029-2036.

Barbante, C. Schwikowski, M., Doring, T., Gaggeler, H.W., Schotterer, U., Tobler, L., Van De Velde, K., and Bourton, C. (2004). Historical record of European emissions of heavy metals to the atmosphere since the 1650s from alpine snow/ice cores drilled near Monte Rosa. *Environmental Science and Technology, 38(15),* 4085-4090.

Bard, J.C. (1979). The Development of a Patination Dating Technique for Great Basin Petroglyphs Utilizing Neutron Activation and X-Ray Fluorescence Analysis. Ph.D. dissertation. University of California, Berkeley.

Bargagli, R., Monaci, F.F., Borghini, F., Bravi., F.F., and Agnorelli, C. (2002). Mosses and Lichens as biomonitors of trace metals. A comparison study on Hypnum cuperessiforme and Parmelia caperata in a former mining district in Italy. *Environmental Pollution, 124(2)*, 279-287.

Batley, G.E. (1999). Quality Assurance in Environmental Monitoring. *Marine Pollution Bulletin, 39(1-12)*, 23-31.

Battiston, G.A., Degetto, S., Gerbasi, R., and Sbrignadello, G. (1989). Determination of sediment composition and chronology as a tool for environmental impact investigation. *Marine Chemistry, 26 (2)*, 91-100.

Beaty, R.D., and Kerber, J.D. (2002). Concepts, Instrumentation, and Techniques in Atomic Absorption Spectroscopy. PerkinElmer Instruments, Norwalk, CT, 2002, pp. 4-2 – 4-4.

Bettinetti, R., Galassi, S., Falandysz, J., Camusso, M., Vignati, D.A.L. (2009). Sediment quality assessment in the Gulf of Gdansk (Baltic Sea) using complementary lines of evidence. *Environmental Management, 43(6)*, 1313-1320.

Beyer, A., Mackay, D. Matthles, M., Wania, F., and Webster, E. (2000). Assessing long-range transport potential of persistent organic pollutants. *Environmental Science and Technology, 34*, 699-703.

Bierman, P.R., and Gillespie, A.R. (1994). Evidence Suggesting That Methods of Rock-Varnish Cation-Ratio Dating Are neither Comparable nor Consistently Reliable. *Quaternary Research, 40(1994)*, 82-90.

Boening, D.W. (2000). Ecological effects, transport, and fate of mercury: a general review. *Chemosphere, 40(2000)*, 1335-1351.

Boutron, C.F., and Patterson, C.C. (1983). The occurrence of lead in Antarctic recent snow, firn deposited over the last two centuries and prehistoric ice. *Geochimica et Cosmochimica Acta, 47*, 1355-1386.

Boutron, C.F., Candelone, J.P.; and Hong, S. (1994). Past and recent changes in the large-scale tropospheric cycle of lead and other heavy metals as documented in Antarctic and Greenland snow and cores: A review. *Geochimica el Cosmochimica Acta, 58*, 3217-3225.

Boutron, C.F., Gorlach, U., Candelone, J.P.; Bolshov, M.A., and Delmas, R.J. (1991). Decrease in anthropogenic lead, cadmium and zinc in Greenland snows since the late 1960s. *Nature, 353(6340)*, 153-156.

Broecker, W.S., and Liu, T. (2001). Rock varnish: Recorder of desert wetness? *GSA Today, August 2001*, 4-10.

Brook, E. (2008). Windows on the greenhouse. *Nature, 453*, 291-292.

Bruggeman, W.A. (1982). Hydrophobic interactions in the aquatic environment. In *The Handbook of Environmental Chemistry. Reactions and Processes* Vol. 2. Part B. ed. O. Hutzinger, New York, NY.

Burgoyne, Thomas W.; Gary M. Hieftje (1996). *Mass Spectrometry Reviews, 15*, 241-259.

Calamari, D.; Bacci, E.; Focardi, S., Gaggi, C., Morosini, M., and Vighi, M. (1991). Role of plant biomass in the global environmental partitioning of chlorinated hydrocarbons. *Environmental Science and Technology, 25(8)*, 1489-1495.

Candelone, J.P.; Hong, S.; Pellone, C., and Bourton, C.F. (1995). Post-industrial revolution changes in large-scale atmospheric pollution of the Greenland snow. *Journal of Geophysical Research, 100*, 16605-16616.

Carignan, J., Simonetti, A., and Gariepy, C. (2002). Dispersal of lead in northeastern North America as recorded by epiphytic lichens. *Atmospheric Environment, 36(2002)*, 3759-3766.

Caroli, S., Alessandrelli, M., Forte, G., D'Ilio, S., Spagnoli, M., and Cresti, R. (2000). The handbook of analytical methods for trace elements as adopted by the national reference laboratories for residues. *Microchemical Journal, 67(1-3),* 381-384.

Chiarenzelli, J., Aspler, L., Dunn, C., Cousens, B., Ozarko, D., and Powis, K. (2001). Multi-element and rare earth element composition of lichens, mosses, and vascular plants from the central Barrenlands, Nanavut, Canada. *Applied Geochemistry, 16(2),* 245-270.

Christensen, J.N., Halliday, A.N., Godfrey, L.V., Hein, J.R., and Rea, D.K. (1997). Climate and ocean dynamics and the lead isotopic records in pacific ferro-manganese crusts. *Science, 227,* 913-917.

Chu, N.Y., (1971). Plutonium determination in soil by leaching and ion-exchange separation. *Analytical Chemistry, 43*, 449-452.

Cicek, A., and Koparal, A.S. (2003). The assessment of air quality and identification of pollutant sources in the Eskisehir region Turkey using Xanthoria parietina (L.) Th.Fr. (1860). *Fresenius Environmental Bulletin, 12(1),* 24-28.

Cizdziel, J.V., (1998). Plutonium Anomalies in Attic Dust and Soils at Locations Surrounding the Nevada Test Site. Ph.D. Dissertation. University of Nevada, Reno.

Clarke, L.B., and Sloss, L.L. (1992). Trace Elements-Emissions from Coal Combustion and Gasification. IEA Coal Research, London.

Condie, K.C. (1993). Chemical composition and evolution of the upper continental crust: Contrasting results from surface samples and shales. *Chemical Geology, 104(1993),* 1-37.

Connor, J.J., Anderson, B.M., Keith, J.R., and Boerngen, J.G. (1976). Soil and Grass Chemistry Near the Four Corners Power Plant. In *Geochemical Survey of the Western Energy Regions,* Third Annual Progress Report, U.S. Geological Survey Open-file Report No. 76-729, 112-120.

Cottingham, K. (2004). ICPMS: It's Elemental. *Analytical Chemistry, 76(1),* 35A-38A.

Crockett, A.B., and Kinnison, R.R. (1977). Mercury Distribution in Soil Around a Large Coal-Fired Power Plant, EPA-600/3-77-063, U.S. Environmental Protection Agency, Las Vegas, Nevada.

Crowder, J.W., and Richards, J.R. (2003). Control of Particulate Matter Emissions. Air Pollution Training Institute Course 415, Student Manual.

Czuczwa, J.M., McVeety, B.D., and Hites, R.A. (1984). Polychlorinated dibenzo-p-dioxins and dibenzofurans in sediments from Siskiwit Lake, Isle Royale. *Science, 226(4674),* 568-569.

Danihelka, P., Volna, Z., Jones, J.M., and Williams, A. (2003). Emission of trace toxic metals during pulverized fuel combustion of Czech coals. *International Journal of Energy Research, 27,* 1181-1203.

Davidson, R.M., and Clarke, L.B. (1996). Trace Elements from Coal. IEA Coal Research, London.

Delmas, R.J., and Petit, J.R. (1994). Present Antarctic aerosol composition: a memory of ice age atmospheric dust? *Geophysical Research Letters, 21(10),* 879-882.

Diaz, T., (2003). Investigating Chemical Variations in Rock Varnish from the Lahontan Range, Central Nevada. M.S. Thesis. University of Nevada, Las Vegas.

Di Leonardo, R., Vizzini, S., Bellance, A., Mazzola, A. (2009). Sedimentary record of anthropogenic contaminants (trace metals and PAHs) and organic matter in a

Mediterranean coastal area (Gulf of Palermo, Italy). *Journal of Marine Systems, 78 (1),* 136-145.

Dittrich, K. and Wennrich, R. (1990). Laser ablation and furnace techniques for sampling and detection in atomic emission spectrometry. *Fresenius' Journal of Analytical Chemistry, 337(5),* 546-550.

Dorn, R.I. (1998). *Rock Coatings*. Amsterdam: Elsevier.

Dorn, R.I., (2007). Rock varnish. In *Geochemical Sediments and Landscapes*, Blackwell, pp. 246-290.

Dorn, R.I., (2004). Desert varnish. In A.S. Goudie (Ed.) *Encyclopedia of Geomorphology*, Routledge: London (pp. 251-254).

Dorn, R.I. & Meek, N. (1995). Rapid formation of rock varnish and other rock coatings on slag deposits near Fontana. *Earth Surface Processes and Landforms, 20,* 547–560.

Dorn, R.I., and DeNiro, M.J. (1985). Stable Carbon Isotope Ratios of Rock Varnish Organic Matter: A New Paleoenvironmental Indicator. *Science, 227(4693),* 1472-1474.

Dorn, R.I., and Whitley, D.S. (1983). Cation-ratio dating of petroglyphs from the Western Great Basin, North America. *Nature, 302,* 816-818.

Dorn, R.I. (1983). Cation-Ratio Dating: A New Rock Varnish Age-Determination Technique. *Quaternary Research, 20,* 49-73.

Dorn, R.I., and Oberlander, T.M. (1981). Rock Varnish origin, characteristics, and usage. *Journal of Geomorphology, 25(4),* 420-436.

Dorn, R.I., and Oberlander, T.M. (1981). Microbial Origin of Desert Varnish. *Science, 213(4513),* 1245-1247.

Doucet, F.J., and Carignan, J. (2001). Atmospheric Pb isotopic composition and trace metal concentration as revealed by epiphytic lichens: An investigation related to two altitudinal sections in Eastern France. *Atmospheric Environment, 35(21),* 3681-3690.

Durrant, (1999). Laser ablation inductively coupled plasma mass spectrometry: achievements, problems, prospects. *Journal of Analytical Atomic Spectroscopy, 1999, 14,* 1385-1403.

Edwards, J. G. (2005, December 24). Mohave plant's closure coming: Plant loss will cost tribes jobs and cost Laughlin revenue. *Las Vegas Review-Journal*. Retrieved July 12, 2007 from http://www.reviewjournal.com.

Ehrlich, H.L. (1996). How microbes influence mineral growth and dissolution. *Chemical Geology, 132,* 5-9.

Engel, C.G., and Sharp, R.P. (1958). Chemical data on desert varnish. *Geological Society of America Bulletin, 69,* 487-518.

Fleisher, M., Liu, T., Broecker, W.S., and Moore, W. (1999). A clue regarding the origin of rock varnish. *Geophysical Research Letters, 26(1),* 103-106.

Flem, B., Larsen, R.B., Grimstvedt, A, and Mansfield, J. (2002). In situ analysis of trace elements in quartz by using laser ablation inductively plasma mass spectrometry. *Chemical Geology, 182(2002),* 237-247.

Francis, J.E., Loendorf, L.L., and Dorn, R.I., 1993. Direct radiocarbon dating and chemical analysis of Ancient Rock Paints. *Archeology and Natural Science, 1,* 127-142.

Franzen, C., Kilian, R., and Biester, H. (2004). Natural mercury enrichment in a minerogenic fen – evaluation of sources and processes. *Journal of Environmental Monitoring, 6(2004),* 466-472.

Furimski, E. (2000). Characterization of trace element emission from coal combustion by equilibrium calculations. *Fuel Processing Technology, 63,* 29-44.

Galbreath, K.C., and Zygarlickie, C.J. (1996). Mercury speciation in coal combustion and gasification flue gases. *Environmental Science and Technology, 30(8),* 818-822.

Glooschenko, W.A., Holloway, L., and Arafat, N. (1986). The use of mires in monitoring the atmospheric deposition of heavy metals. *Aquatic Botany, 25(C),* 179-190.

Goldberg, E.D., and Bertine, K.K. (2000). Beyond the Mussel Watch – New directions for monitoring marine pollution. *Estuarine, Coastal, and Shelf Science, 16(1),* 69-93.

Goldberg, E.D., Koide, M., and Hodge, V. (1983). U.S. Mussel Watch: 1977-1978 results on trace metals and radionuclides. *Science of the Total Environment, 247(2-3),* 165-174.

Green, M.C. (1999). The project MOHAVE tracer study: study design, data quality, and overview of results. *Atmospheric Environment, 33(12),* 1955-1968.

Guidotti, M., Stella, D., Owczarek, M., DeMarco, A., and De Simone, C. (2003). Lichens as polycyclic aromatic hydrocarbon bioaccumulators used in atmospheric pollution studies. *Journal of Chromatography, A, 985(1-2),* 185-190.

Halliday, A.H., Der-Chuen, L., Christensen, J.N., Rehkamper, M., Wen, Y., et al. (1998). Applications of multiple collector-ICPMS to cosmochemistry, geochemistry, and paleoceanography. *Geochimica et Cosmochimica Acta, 62(6),* 919-940.

Halsall, C., J., Lee, R.G.M., Coleman, P.J., Burnett, V., Harding-Jones, P., and Jones, K.C. (1995). PCBs in U.K. urban air. *Environmental Science and Technology, 29,* 2368-2376.

Hamelin, B., Grousset, F.E., and Sholkowitz, E.R. (1990). Pb isotopes in surficial pelagic sediments from the North Atlantic. *Geochimica et Cosmochimica Acta, 54,* 37-47.

Hayden, J. (1976). Pre-altithermal archeology in the Sierra Pinacate, Sonora, Mexico. *American Antiquity, 41,* 274-289.

Hinkley, T., and Matsumoto, A. (2001). Atmospheric regime of dust and salt through 75,000 years of Taylor Dome ice core: Refinement by measurement of major, minor, and trace metal suites. *Journal of Geophysical Research D: Atmospheres, 106(D16),* 18487-18493.

Hodge, V.F., Farmer, D.E., Diaz, T.A., and Orndorff, R.L. (2005). Prompt detection of alpha particles from ^{210}Po: another clue to the origin of rock varnish? *Journal of Environmental Radioactivity, 78(2005),* 331-342.

Hodge, V.F. and Stallard, M.O. (1988). Platinum and Palladium in Roadside Dust. *Environmental Science and Technology, 20(10),* 1060-1064.

Hodge, V.F., Stallard, M.O., Koide, M., and Goldberg, E.D. (1986). Platinum and the platinum anomaly in the marine environment. *Earth and Planetary Science Letters, 72(2-3),* 158-162.

Hong, S., Candelone, J.P., Patterson, C.C., and Boutron, C.F. (1994). Greenland ice evidence of hemispheric lead pollution two millennia ago by Greek and Roman civilizations. *Science, 265(1994),* 1841-1843.

Hooke, R. (1967). Processes on arid-region alluvial fans. *Journal of Geology, 75,* 438-460.

Hooke, R.L., Yang, H., and Weiblen, P.W. (1969). Desert varnish: an electron probe study. *Journal of Geology, 77,* 275–288.

Hu, Z. and Gao, S. (2008). Upper crustal abundances of trace elements: A revision and update. *Chemical Geology, 253(2008),* 205–221.

Humboldt, A. (1852). Personal narrative of travels to the equinoctial regions of America during the years 1799-1804. Henry Bohn, London, England.

Hungate, B., Danin, A., Pellerin, N.B., Stemmler, J., Kjellander, P., Adams, J.B., and Staley, J.T. (1987). Characterization of manganese-oxidizing (MnII → MnIV) bacteria from Negev Desert rock varnish: implications in desert varnish formation. *Canadian Journal of Microbiology, 33,* 939–943.

Jacko, R. B., and Nevendorf, D.W. (1977). Trace Metal Emission Test Results from a Number of Industrial and Municipal Point Sources. *Journal of the Air Pollution Control Association, 27(10),* 989-994.

Jaffe, R. (1991). Fate of Hydrophobic Organic Pollutants in the Aquatic Environment: A Review. *Environmental Pollution, 69 (1991),* 237-257.

Jaward, F.M., Farrar, N.J., Harner, T., Sweetman, A.J., and Jones, K.C. (2004). Passive Air Sampling of PCBs, PBDEs, and Organochlorine Pesticides Across Europe. *Environmental Science and Technology, 38,* 34-41.

Kalnicky, D.J., and Singhvi, R. (2001). Field portable XRF analysis of environmental samples. *Journal of Hazardous Materials, 83(2001),* 93-122.

Kay, J.T., Conklin, M.H., Fuller, C.C., and O'Day, P.A. (2001). Processes of nickel and cobalt uptake by a manganese oxide forming sediment in Pinal Creek, Globe Mining District, Arizona. *Environmental Science and Technology, 35,* 4719-4725.

Keith, J.R., Anderson, B.M., and Connor, J.J. (1974). Trace Metal Variations in the Powder River Basin. In *Geochemical Survey of the Western Coal Regions,* First Annual Progress Report, U.S. Geological Survey Open-file Report No. 74-250, 14-29.

Kober, B., Wessels, M., Bollhofer, A., and Mangini, A. (1999). Pb isotopes in sediments of Lake Constance, Central Europe constrain the heavy metal pathways and the pollution history of the catchment, the lake and the regional atmosphere. *Geochimica et Cosmochimica Acta, 63(9),* 1293-1303.

Koide, M., and Goldberg, E.D. (1983). Uranium isotopes in the Greenland ice-sheet. *Earth and Planetary Science Letters, 65(2),* 245-248.

Koide, M., Michel, R., Goldberg, E.D., Herron, M.M., and Langway Jr, C.C. (1982). Characterization of radioactive fallout from pre- and post-moratorium tests to polar ice caps. *Nature, 296,* 544-818.

Kovalchuk, I. and Kovalchuk, O. (2008). Transgenic plants as Sensors of Environmental Pollution Genotoxicity. *Sensors, 2008, 8,* 1539-1558.

Kramer, K.J.M. (1994). What About Quality Assurance Before Laboratory Analysis? *Marine Pollution Bulletin, 29(4-5),* 222-227.

Krauskopf, K.B. (1957). Separation of manganese from iron in sedimentary processes. *Geochimica et Cosmochimica Acta, 12(1-2),* 61-84.

Krinsley, D. (1998). Models of rock varnish formation constrained by high resolution transmission electron microscopy. *Sedimentology, 45(1998),* 711-725.

Kuhlman, K.R., Allenbach, L.B., Ball, C.L, Fusco, W.G., La Duc, et al. (2005). Enumeration, isolation, and characterization of ultraviolet (UV-C) resistant bacteria from rock varnish in the Whipple Mountains, California. *Icarus, 174 (2 SPEC. ISS.),* 585-595.

Kuhlman, K.R., Fusco, W.G., La Duc, M.T., Allenbach, L.B., et al. (2006). Diversity of Microorganisms within Rock Varnish in the Whipple Mountains, California. *Applied Environmental Microbiology, Feb. 2006,* 1708-1715.

Kylander, M.E., Weiss, D.J., and Kober, B. (2009). Two high resolution terrestrial records of atmospheric Pb deposition from New Brunswick, Canada, and Loch Laxford, Scotland. *Science of the Total Environment, 407(5),* 1644-1657.

Lakin, H.W., Hunt, C.B., Davidson, D.F., and Oda, U. (1963). Variation in Minor-Element Content of Desert Varnish. *U.S. Geological Survey Professional Paper, 475-B,* B28-B31.

Lee, M.R., and Bland, P.A. (2003). Dating climatic change in hot deserts using desert varnish on meteorite finds. *Earth and Planetary Science Letters, 206(2003),* 187-198.

Lee, J.A., and Tallis, J.H. (1973). Regional and historical aspects of lead pollution in Britain. *Nature, 245(5422),* 216-218.

Linck, G. (1900). Uber die dunkel Rinden der Gesteine der Wunsten. Jenaische Zeit. *Naturwiss, 35,* 1-8.

Lindberg, S.E. and Stratton, W.J. (1998). Atmospheric Mercury Speciation: Concentrations and Behavior of Reactive Mercury in Ambient Air. *Environmental Science and Technology, 32,* 49-57.

Lindqvist, O., Johansson, K., and Aastrup, M. (1991). Mercury in the Swedish environment – recent research on causes, consequences, and corrective methods. *Water, Air, and Soil Pollution, 55(1-2),* xi-xiii.

Liu, T., and Broecker, W.S. (2000). How fast does rock varnish grow? *Geology, 28(2),* 183-186.

Liu, T., and Broecker, W.S. (2007). Holocene rock varnish microstratigraphy and its chronometric application in the drylands of western USA. *Geomorphology, 84(2007),* 1-21.

Liu, T., and Broecker, W.S. (2008). Rock varnish microlamination dating of late Quaternary geomorphic features in the drylands of western USA. *Geomorphology, 93(3-4),* 501-523.

Liu, T., and Dorn, R.I. (1996). Understanding spatial variability in environmental changes in drylands with rock varnish microlaminations. *Annals of the Association of American Geographers 86,* 187–212.

Livett, E.A. (1988). Geochemical monitoring of atmospheric heavy metal pollution: Theory and applications. *Advanced Ecological Research, 18,* 289-297.

Lockwood, F.C., and Yousef, S. (2000). A model for the particulate matter enrichment with toxic metals in solid fuel flames. *Fuel Processing Technology, 65-66,* 439-457.

Mao, S.S., Mao, X.L., Grief.R., and Russo, R.E. (2000). Simulation of a picosecond laser ablation plasma. *Applied Physics Letters, 76(23),* 3370-3372.

Martines-Tarazona, M.R., and Spears, D.A. (1996). The fate of trace elements in bulk minerals in pulverized coal combustion in a power station. *Fuel Processing Technology, 47,* 79-92.

Mason, B. (1958). Principles of Geochemistry. 2nd edition, Wiley, New York.
Matsumoto, A., and Hinkley, T. (2001). Trace metal suites in Antarctic pre-industrial ice are consistent with emissions from quiescent degassing volcanoes worldwide. *Earth and Planetary Science Letters, 186(1),* 33-43.
Mayewski, P.A., Lyons, W.B., Spencer, M.J., Twickler, M.S., Buck, C.F., and Whitlow, S. (1990). An ice-core record of atmospheric response to anthropogenic sulphate and nitrate. *Nature, 346(6284),* 554-556.
McKeown, D.A., and Post, J.E. (2001). Characterization of manganese oxide mineralogy in rock varnish and dendrities using X-ray absorption spectroscopy. *American Mineralogy, 86*, 701-703.
Metcalf, R. (1973). A century of DDT. *Journal of Agricultural and Food Chemistry, 21(4)*, 511-519.
Miller, J.C., and Miller, J.N. (1984). Statistics for Analytical Chemistry. John Wiley & Sons, New York.
Monna, F., Lancelot, J., Croudace, I.W., Cundy, A.B., and Lewis, J.T. (1997). Pb isotopic composition of airborne particulate material from France and the southern United Kingdom: implications for Pb pollution sources in urban areas. *Environmental Science and Technology, 31*, 2277-2286.
Monna, F., Dominik, J., Loizeau, J.-Luc., Pardos, M, and Arpagaus, P. (1999). Origin and evolution of Pb in sediments of Lake Geneva (Switzerland-France). Establishing a stable Pb record. *Environmental Science and Technology, 33(17)*, 2850-2857.
Moor, H., Schlader, T. and Sturm, M. (1996). Recent changes in stable lead isotope ratios in sediments in Lake Zug, Switzerland. *Environmental Science and Technology, 30*, 2928-2933.
Moore, W.S., Liu, T., Broecker, W.S., Finkel, R.C., and Wright, A. (2001). Factors influencing ^{7}Be accumulation on rock varnish. *Geophysical Research Letters, 28(23)*, 4475-4478.
Morgan, J.J., and Stumm, W. (1965). The role of multivalent metal oxides in limnological transformations as exemplified by iron and manganese. In *Second Water Pollution Research Conference 1*. ed. Ojag. New York: Pergamon.
Namiesnik, J., and Gorecki, T. (2000). Passive sampling in environmental analysis. *LC_GC Europe, 13(9),* 678-685.
Namiesnik, J., Zabiegala, B., Kot-Wasik, A., Patryka, M. and Wasik, A. (2005). Passive sampling and/or extraction techniques in environmental analysis: a review. *Analytical and Bioanalytical Chemistry, 381*, 279-301.
Nash III, T.H. (1996). Lichen Biology, Cambridge University Press, Cambridge, pp. 303.
Nash III, T.H., and Gries, C. (1995). The response of lichens to atmospheric deposition with an emphasis on the Arctic. *Science of the Total Environment, 160-161*, 737-747.
Nevada Division of Environmental Protection. (2005, September). *Fact Sheet Reid Gardner Station, Permit NEV91022*. Retrieved June 30, 2007, from NDEP Reports Online via GPO Access: http://ndep.nv.gov/docs_04/nev91022_f05.pdf.
Nevada Division of Environmental Protection. (2007, April). *Community Involvement Plan Titanium Metal Corporation*. Retrieved September 30, 2007, from NDEP Online: http://ndep.nv.gov/bmi/docs/timet_community_involvement_plan07.pdf.

Nodelman, I.G., Pisupati, S.V., Falcone Miller, S., and Sarconi, A.W. (2000). Partitioning behavior of trace elements during pilot-scale combustion of pulverized coal and coal-water slurry fuel. *Journal of Hazardous Materials, 74*, 47-59.

Owczarek, M., Guidotti, M., Blasi, G., De Simone, C., De Marco, A., and Spadoni, M. (2001). Traffic pollution monitoring using lichens as bioaccumulators of heavy metals and polycyclic aromatic hydrocarbons. *Fresenius Environmental Bulletin, 10(1)*, 42-45.

Pai, P., Karamchandani, P., and Seigneur, C. (1997). Simulation of the regional atmospheric transport and fate of mercury using a comprehensive Eulerian model. *Atmospheric Environment, 31(17)*, 2717-2732.

Palmer, F.E., Staley, J.T., Murray, R.G.E., Counsell, T. & Adams, J.B. (1985). Identifi cation of manganese-oxidizing bacteria from desert varnish. *Geomicrobiology Journal, 4*, 343–360.

PerkinElmer, ELAN DRC II, Brochure. www.PerkinElmer.com.

Perry, R.S., and Adams, J. (1978). Desert varnish: Evidence of cyclic deposition of manganese. *Nature, 276*, 489-491.

Perry, R.S., Engel, M.H., Botta, O., and Staley, J.T. (2003). Amino Acid Analyses of Desert Varnish from the Sonoran and Mojave Deserts. *Geomicrobiology Journal, 20(5)*, 427-438.

Perry, R.S. & Kolb, V.M. (2003) Biological and organic constituents of desert varnish: Review and new hypotheses. In: Hoover, R.B. & Rozanov, A.Y. (Eds) *Instruments, Methods, and Missions for Astrobiology VII. Bellingham, WA: Society of Photo-Optical Instrumentation Engineers*, 202–217.

Perry, R.S., and Kolb, V.M. (2004). From Darwin to Mars: Desert varnish as a model for preservation of complex (bio)chemical systems. *Proceedings of SPIE – The International Society for Optical Engineering, 5163*, 202-217.

Perry, R.S., Lynne, B.Y., Sephton, M.A., Kolb, V.M., Perry C.C., and Staley, J.T. (2006). Baking black opal in the desert sun: The importance of silica in desert varnish. *Geology, 34(7)*, 537-540.

Petersen, G., Iverfeldt, A., and Munthe, J. (1995). Atmospheric mercury species over central and northern Europe. Model calculations and comparison with observations from the Nordic air and precipitation network for 1987 and 1988. *Atmospheric Environment, 29(1)*, 47-67.

Petit, J.R., Jouzel, J., Raynaud, D., Barkov, N.I., Barnola, J.M., Basile, M., et al. (1999). Climate and atmospheric history of the past 420,000 years from the Vostok ice core, Antarctica. *Nature, 399(6735)*, 429-436.

Planchon, F.A.M., Van De Velde, K., Rosman, K.J.R., Wolff, E.W., Ferrari, C.P., Boutron, C.F. (2003). One hundred fifty-year record of lead isotopes in Antarctic snow from Coats Land. *Geochimica et Cosmochimica Acta, 67(4)*, 693-708.

Potter, R.M., and Rossman, G.R. (1977). Desert Varnish: The importance of clay minerals. *Science, 196*, 1446-1448.

Potter, R.M. and Rossman, G.R. (1979). The manganese- and iron-oxide mineralogy of desert varnish. *Chemical Geology, 25*, 79-94.

Quevauvieller, P., Maier, E.A., and Griepink, B. (1995). Quality Assurance for environmental analysis. In *Quality Assurance for Environmental Analysis.* Eds Quevauvieller, P., Maier, E.A., and Griepink, P., pp 1-25, Elsevier, Amsterdam.

Renberg, I., Bindler, R., and Brannvall, M.L. (2001). Elemental relationships in rock varnish stratigraphic layers, Cima volcanic field, California: Increase in global atmospheric lead-deposition record as a chronological marker in sediment deposits in Europe. *Holocene, 11(5),* 511-516.

Reneau, S.L., Raymond, R., and Harrington, C.D. (1992). Elemental relationships in rock varnish stratigraphic layers, Cima volcanic field, California: Implications for varnish development and the interpretation of varnish chemistry. *American Journal of Science, 292,* 684-723.

Reneau, S.L. (1993). Manganese Accumulation in Rock Varnish on a Desert Piedmont, Mojave Desert, California, and Application to Evaluating Varnish Development. *Quaternary Research, 40(1993),* 309-317.

Richards, J.R. (1996). Control of Gaseous Emissions. Air Pollution Training Institute Course 413, Student Manual.

Russo, R.E., Xianglei, M., Haichen, L., Gonzales, J. and Mao, S.S. (2002). Laser ablation in analytical chemistry – a review. *Talanta, 57(2002),* 425-451.

Sarret, G., Mancenau, A., Cuny, D., Van Haluwyn, C. Derulle, S., Hazeman, J.-L., Soldo, Y., and Menthonnex, J-.J. (1998). Mechanism of lichen resistance to metallic pollution. *Environmental Science and Technology, 32(21),* 3325-3330.

Scerbo, R., Ristori, T., Possenti, L., Lampugnani, L., Barale, R., and Barghigiani, C. (2002). Lichen (Xantoria parietina) biomonitoring of trace element contamination and air quality assessment in Pisa Province (Tuscany, Italy). *Science of the Total Environment, 286(1-3),* 27-40.

Scheidegger, A., Borkovec, M., and Sticher, H. (1993). Coating of silica sand with goethite: preparation and analytical identification. *Geoderma, 58,* 43-65.

Schelbe, R.T., McDonald, G.D., Hall, J.A., and Nealson, K.H. (2005). Community structure comparison using FAME analysis of desert varnish and soil, Mojave Desert, California. *Geomicrobiology Journal 22(3-4),* 99-116.

Schintu, J.M., and Dagetto, S. (1999). Sedimentary records of heavy metals in the industrial harbour of Portovesme, Sardinia (Italy). *Science of the Total Environment, 241(1999),* 129-141.

Schwyn, B., and Neilands, B. (1987). Universal Chemical Assay for the Detection and Determination of Siderophores. *Analytical Biochemistry, 160(1987),* 47-56.

Seames, W.S., and Wendt, J.O.L. (2000). Partitioning of arsenic, selenium, and cadmium during the combustion of Pittsburgh and Illinois #6 coals in a self-sustained combustor. *Fuel Processing Technology, 63(2),* 179-196.

Seethapathy, S., Gorecki, T., and Li., X. (2008). Passive sampling in environmental analysis. *Journal of Chromatography, 1184(2008),* 234-253.

Seigneur, C., Wrobel, J., and Constantinou, E. (1994). A chemical kinetic mechanism for atmospheric inorganic mercury. *Environmental Science and Technology, 28(9),* 1589-1597.

Settle, D.M. and Patterson, C.C. (1982). Magnitudes and sources of precipitation and dry deposition fluxes of industrial and natural leads to the North Pacific at Enewetak. *Journal of Geophysical Resources, 87,* 8857-8869.

Sharpe, M.R. (1982). Noble metals in the marginal rocks of the Bushveld Complex. *Economic Geology, 77(6),* 1286-1295.

Shefsky, S. (1997). Comparing Field Portable X-Ray Fluorescence (XRF) to Laboratory Analysis of Heavy Metals in Soil. *International Symposium of Field Screening Methods for Hazardous Wastes and Toxic Chemicals*, Las Vegas, NV, 1997.

Shotyk, W., Appleby, P.G., Cheburkin, A.K., Frankhauser, A., and Kramers, J.D. (1997). Lead in three peat bog profiles, Jura Mountains, Switzerland: enrichment factors, isotope composition, and chronology of atmospheric deposition. *Water, Air, and Soil Pollution, 100,* 297-310.

Shotyk, W., Weiss, D., Appleby, P.G., Cheburkin, A.K., Frei, R., Kramers, J.D., (…), and Van Der Knaap, W.O. (1998). Atmospheric lead deposition from 12,400 to ca. 2,000 Yrs BP in a peat bog profile, Jura Mountains, Switzerland. *Science, 281(5383),* 1635-1640.

Shotyk, W., Mackenzie.A, and Norton, S. (2004). Archives of Environmental Contamination. *Journal of Environmental Monitoring, 6(5),* 417.

Silberstein, L., Siegel, B.Z., Siegel, S.M., Mukhtar, A., and Galun, M. (1996). Comparative studies of Xantoria parietina, a pollution resistant lichen, and Ramalina duriaei, a sensitive species. I. Effects of air pollution on physiological processes. *Lichenologist, 28(4),* 355-365.

Simonich, S.L., and Hites, R.A. (1994). Importance of vegetation in removing polycyclic aromatic hydrocarbons from the atmosphere. *Nature, 370(6484),* 49-51.

Smith, B.J. & Whalley, W.B. (1988). A note on the characteristics and possible origins of desert varnishes from southeast Morocco. *Earth Surface Processes and Landforms, 13,* 251–258.

Sowers, J.M. (2001). Rock varnish chronometry. In J.S. Sowers, and Lettis, W.R. (Eds.) *Quaternary Geochronology; Methods and Applications* (pp. 241-260). AGU Reference Shelf, Vol. 4.

Spahni, R., Chappellaz, J., Stocker, T.F., Loulergue, L., Hausamman, G., Kawamura, K., Fluckiger, J., and Jouzel, J. (2005). Atmospheric science: Atmospheric methane and nitrous oxide of the late Pleistocene from Antarctic Ice Cores. *Science, 310(5752),* 1317-1321.

Staley, J.T., Palmer, F. & Adams, J.B. (1982). Microcolonial fungi: common inhabitants on desert rocks? *Science 215,* 1093–1095.

Stanley, L.J., and Hites, R.A. (1991). Chlorinated Organic Contaminants in the Atmosphere. In *Organic Contaminants in the Environment: Environmental Pathways and Effects*. Jones, K.C., Ed.: Elsevier Applied Science Publishers: London and New York.

Sun, L., and Xie, Z.Q. (2001). Changes in lead concentration in Antarctic penguin droppings during the past 3000 years. *Environmental Geology, 40,* 1205-1208.

Sun, L., Yin, X.B., Liu., X.D., Zhu, R.B, Zhou, Q.X., and Wang, Y.H. (2004). A 1500-year record of Antarctic seal populations in response to climate change. *Polar Biology, 27,* 495-501.

Sun, L., Yin, X., Liu., X.B., Zhu, R., et al. (2006). A 2000-year record of mercury and ancient civilizations in seal hairs from King George Island, West Antarctica. *Science of the Total Environment, 368 (2006),* 236-247.

Taylor-George, S., Palmer, F., Stanley, J.T., Borns, D.J., Curtiss, B., and Adams, J.B. (1983). Fungi and bacteria involved in desert varnish formation. *Microbial Ecology, 9,* 227-245.

Tebo, B. M., Bargar, J.R., Clement, G.J., Gregory, J.D., Murray, K.J. (2004). Biogenic Manganese Oxides: Properties and Mechanisms of Formation. *Annual Review of Earth and Planetary Science, 2004, 32,* 287-328.

Thiagarajan, N., and Lee, C.A. (2004). Trace-element evidence for the origin of desert varnish by direct aqueous atmospheric deposition. *Earth and Planetary Science Letters, 224 (2004),* 131-141.

Torrisi, L., Caridi, F., Magarone, D., and Borrielli, A. (2008). Plasma-laser characterization by electrostatic mass quadrupole analyzer. *Nuclear Instruments and Methods in Physics Research B, 266(2008),* 308-315.

Tripp, B.W., Farrington, J.W., Goldberg, E.D., and Sericano, J. (1992). International mussel watch: The initial implementation phase [2]. *Marine Pollution Bulletin, 24(7),* 371-373.

Turner, M., Rudin, M., Cizdziel, J. and Hodge, V. (2003). Excess plutonium in soil near the Nevada Test Site, USA. *Environmental Pollution, 125(2003),* 193-203.

Urrutia, M.M., and Beveridge, T.J. (1994). Formation of fine-grained metal and silicate precipitates on a bacterial surface (Bacillus subtilis). *Chemical Geology, 116(1994),* 261-280.

U.S. Department of Energy. (1994, September). *Development of the Town Data Base: Estimates of Exposure Rates and Times of Fallout Arrival near the Nevada Test Site* (Publication No. DOE/NV-374/UC-702).

U.S. Department of Energy, 1994. United States Nuclear Tests, July 1945 through September 1992. Nevada Operations Office, DOE/NV-209-REV-14.

U.S. Environmental Protection Agency. (1999, March). *Project MOHAVE Final Report*. Retrieved June 23, 2007, from EPA Region 9 Office Reports Online via GPO Access: http://www.epa.gov/region09/air/mohave/report.html.

United States Environmental Protection Agency (2002). Guidance on Choosing a Sampling Design for Environmental Data Collection. EPA QA/G-5S. EPA/240/R-02/005, December 2002.

U.S. Environmental Protection Agency. (November, 2003). *Technical Support Document: Titanium Metal Corporation, Part 70 TSD, Source 00019*. Retrieved June 25, 2007, from EPA Reports Online via GPO Access: http://yosemite.epa.gov/R9/AIR/EPSS.NSF/735056a63c1390e08825657e0075d180/c0a3f63cddb62ef088256df60061365b!OpenDocument.

U.S. Environmental Protection Agency (2004). Control of Mercury Emissions from Coal-Fired Electric Utility Boilers. Retrieved November, 2009, from EPA Reports Online via GPO Access: http://www.epa.gov/ttn/atw/utility/hgwhitepaperfinal.pdf.

U.S. Environmental Protection Agency. (September, 2004). *Technical Support Document: The Las Vegas 8-Hour Ozone Nonattainment Area*. Retrieved June 25, 2007, from EPA Reports Online via GPO Access: http://www.epa.gov/ttn/naaqs/ozone/ozonetech/des00328.html.

U.S. Environmental Protection Agency. (March, 2005). Clean Air Mercury Rule. Retrieved November 20, 2009, from EPA Reports Online via GPO Access: http://www.epa.gov/oar/mercuryrule/basic.htm.

Van Geel, B., Bregman, R., Van Der Molen, P.C., Dupont, L.M., and Van Driel-Murray, C. (1989). Holocene raised bog deposits in the Netherlands as geochemical archives of prehistoric aerosols. *Acta Botanica Neerlandica, 38(4),* 467-476.

Vandal, G.M., Fitzgerald, W.F., Bourton, C.F., and Candelone, J.P. (1993). Variations in mercury deposition to Antarctica over the past 34,000 years. *Nature, 362*, 621-623.

VG Axiom, Thermo Elemental, Cheshire, UK. www.thermoelemental.com.

Villeneuve, J.-P., Fogelqvist, E., and Cattini, C. (1988). Lichens as bioindicators of atmospheric pollution by chlorinated hydrocarbons. *Chemosphere, 17(2),* 399-403.

Wallberg, P. and Moberg, L. (2002). Evaluation of 20 years of environmental monitoring data around Swedish nuclear installations. *Journal of Environmental Radioactivity, 63 (2002),* 117-133.

Walther, J., (1891). Die Denudation in der Wuste. Akad. Wiss: Mathematischk-Physicalische Klasse, Abh 16, pp. 435-461.

Wangen, L.E., and Williams, M.D. (1978). Elemental deposition downwind of a coal-fired power plant. *Water, Air, and Soil Pollution, 10(1978),* 33-44.

Watchman, A. (2000). A review of the history of dating rock varnishes. *Earth-Science Reviews, 49*, 261-277.

Wayne, D.M., Diaz, T.A., Fairhurst, R.J., Orndorff, R.L. and Pete, D.V. (2006). Direct major- and trace-element analyses of rock varnish by high resolution laser ablation inductively-coupled plasma mass spectrometry (LA-ICPMS). *Applied Geochemistry, 21(2006),* 1410-1431.

Weiss, D., Shotyk, W., and Kempf, O. (1999). Archives of Atmospheric Lead Pollution. *Naturwissenschaften, 86(1999),* 262-275.

Weiss, D., Boyle, A.B., Wu, J., Chavagnac, V., Michel, A., and Reuer, M.K. (2003). Spatial and temporal evolution of lead isotope ratios in the North Atlantic Ocean between 1981 and 1989. *Journal of .Geophysical Research C: Oceans, 108(10),* 4-10.

Weiss, D., Rausch, N., Mason, T.F.D., Coles, B.J., Wilkinson, J.J. Ukonmaanaho, L., Arnold, T., and Nieminen, T.M. (2007). Atmospheric deposition and isotope biogeochemistry of zinc in ombrotrophic peat. *Geochimica et Cosmochimica Acta, 71(14),* 3498-3517.

Wikipedia, the free encyclopedia. Map of Federal Lands in Southern Nevada, April 2007.

Wolff, E.W., Hutterli, M. A., and Jones, A.E. (2007). Past atmospheric composition and chemistry from ice cores - progress and prospects. *Environmental Chemistry, 4(4),* 211-216.

Wolff, E.W., and Suttie, E. D. (1994). Antarctic snow record of Southern-Hemisphere lead pollution. *Geophysical Research Letters, 21(9),* 781-784.

Wolff, E.W., Suttie, E. D., and Peel, D.A. (1999). Antarctic snow record of cadmium, copper, and zinc content during the twentieth century. *Atmospheric Environment, 33(10),* 1535-1541.

Yan, R., Gauthier, D., and Flamant, G. (2001). Volatility and chemistry of trace elements in a coal combustor. *Fuel, 80,* 2217-2226.

Yin, X., Liu., X., Sun, L., Zhu, R., et al. (2006). A 1500-year record of lead, copper, arsenic, cadmium, zinc level in Antarctic seal hairs and sediments. *Science of the Total Environment, 371 (2006),* 252-257.

Zabiegala, B., Gorecki, T., Przyk, E., and Namiesnik, J. (2002). Permeation passive sampling as a tool for the evaluation of indoor air quality. *Atmospheric Environment, 36(17),* 2907-2916.

Zabiegala, B., Gorecki, T., and Namiesnik, J. (2003). Calibration of permeation passive samplers with silicone membranes based on physicochemical properties of the analytes. *Analytical Chemistry, 75(13)*, 3182-3192.

Zachmann, D.W., and Block, R. (1994). Studies of the availability of the toxic heavy elements in soils and sediments in the vicinity of a lead smelting site (Germany). *Water, Air, and Soil Pollution, 78*, 317-334.

Zeng, T., Sarofim, A.F., and Senior, C.L. (2001). Vaporization of arsenic, selenium, and antimony during coal combustion. *Combustion and Flame, 126*, 1714-1724.

Zheng, J., Fisher, D., Blake, E., Hall, G., et al. (2006). An ultra-clean firn core from the Devon Island Ice Cap, Nunavut, Canada, retrieved using a titanium drill specially designed for trace element studies. *Journal of Environmental Monitoring, 2006, 8,* 406-413.

VITA

Graduate College
University of Nevada, Las Vegas

Piotr Nowinski

Degrees:

Bachelor of Science, Chemistry, 1988
University of Nevada, Las Vegas

Master of Science, Chemistry, 1993
University of Nevada, Las Vegas

Publications:

Nowinski, P.; and Hodge, V. Evaluation of ICP-MS/Microwave Oven Preparation for the Rapid Analysis of Ore Samples for Gold and the Platinum-Group Metals. Atomic Spectroscopy, 15/3, May/June 1994.

Hillman, D.C.; Nowinski, P.; Butler, L.C.; and Nocerino, J.M. Microwave Digestion Oven Calibration Discontinuities. American Environmental Laboratory, vol. 4, 1993.

Nowinski, P.; Dobbs, D.E.; and Hinners, T.A. Microwave-Assisted Acid Digestion of Siliceous Matrices of Incinerator Feed and Ash. EPA Method 3052.

Dissertation Title: Desert Varnish as an Indicator of Modern-Day Air Pollution in Southern Nevada

Dissertation Examination Committee:

Chairperson, Dr. Vernon F. Hodge, Ph.D.
Committee Member, Dr. Krystyna A. Stave, Ph.D.
Committee Member, Dr. Shawn Gerstenberger, Ph.D.
Graduate Faculty Representative, Dr. Moses Karakouzian, Ph.D.